University of Bath

UNIVERSITY OF BATH

PHD

The mechanics and energy economy of animal jumping and landing applied to autonomous robots

Paskins, Keith Edward

Award date:
2007

Awarding institution:
University of Bath

Link to publication

The mechanics and energy economy of animal jumping and landing applied to autonomous robots

Keith Edward Paskins

A thesis submitted for the degree of Doctor of Philosophy

University of Bath

Department of Mechanical Engineering

May 2007

UMI Number: U601883

UMI

Dissertation Publishing

ProQuest

Summary

Irregular terrain is difficult for small robots to traverse, so the research in this thesis endeavours to develop a jumping robot as a solution to this problem. Gliding is proposed as a means of reducing the landing impact forces, and potentially extending the range of each jump. The biomechanics of jumping and gliding are introduced from fundamental principles, before various examples from nature are described and contrasted. Flying squirrels glide quickly between trees by stretching out their patagia, membranous skin folds spreading between the wrists and ankles. Several hypotheses exist to explain the evolution of gliding flight in these animals. These are investigated by filming northern flying squirrels leaping across a range of short distances while measuring the corresponding take-off and landing forces. Evidence is provided that the evolution of controlled flight was most likely stimulated by the need to reduce landing impact forces. A model is proposed for the skin structure of flying squirrel patagia, which is likely to be specialised from normal mammalian skin to facilitate gliding flight and the high speed transition to other arboreal locomotion. This predicts that the skin would be thin and its stiffness highest along the length of the animal, with the behaviour more elastic perpendicularly. Uni-axial tensile test results from a single southern flying squirrel are consistent with the hypotheses. A biomimetic jumping and gliding robot, Glumper, is described which relies on a power-amplifying energy storage and catch-release mechanism. A novel, bi-stable dog clutch device was developed that enables the robot to launch itself automatically using an on-board power supply. The robot has self-deploying gliding membranes and allowance is made in the design for the adjustment of pitch to improve landing control. After testing the performance of the robot, consideration is given to its power requirement for full autonomy.

Table of Contents

Table of Contents

Acknowledgements

Firstly I would like to thank my two supervisors Dr. Adrian Bowyer and Dr. William Megill for everything they have done to help me produce this Ph.D thesis. The combination of these two contrasting personalities has provided an ideal balance, which has been crucial to my personal development as a researcher working at the boundary between the giant disciplines of Engineering and Biology. In particular I would like to thank Adrian for all the time he has given me over the past three and a half years. I shall miss our regular meetings, which have stimulated countless ideas and encouragement thanks to his seemingly infinite wisdom on all things, combined with a friendly, humble character and a great sense of humour. Likewise, it has been a privilege to work with William, a man who always knows the answer and for whom nothing is impossible. His help in setting up an international collaboration provided a launch pad for the direction of this research, and the quality of the final thesis owes much to many useful, productive discussions, and at times, thorough but constructive criticism.

I should like to warmly thank John Scheibe for all his time, help and hospitality during my stay at SouthEast Missouri State University (USA). The experimental work described in Chapter 3 of this thesis was carried out together, and he was very generous with his time and expertise during the building of equipment and throughout this study on flying squirrels. He takes great care of his colony, and his excellent knowledge of these animals and the advice he has given me throughout my research has been invaluable.

I would also like to thank the Royal Academy of Engineering, UK, whose travel grant made this particular collaborative project possible. Thanks also to Stephen Coombes in the Instrumentation Section of the Mechanical Engineering Department at the University of Bath, for his time and expertise, which were so important during the design and construction of the instrumented take-off branch used for this study. I would like to acknowledge Bijan Pashay, in the Department of Physics at SouthEast Missouri State University, who gave up many late hours on several days to help diagnose and fix some serious PCB faults that arose during the course of the experimentation in Missouri. I am additionally indebted to Nicole Augustin, in the Department of Maths at the University of Bath, for advising me on the selection and presentation of statistics in the resulting paper (published in the Journal of Experimental Biology). Additionally I would like to acknowledge Christine Bowyer for giving up an afternoon to cut and sew the robot's wings for me.

It has been a pleasure to work in the Centre for Biomimetic and Natural Technologies at the University of Bath. I have been fortunate to have several productive yet informal discussions with the leader of this group, and one of the Godfathers of research in biomimetics, Professor Julian Vincent. I would also like to thank Dr Francisco Rojo Perez, formerly a member of our research group and now at the Technical University of Madrid, for all the technical advice he gave me prior to and during the experiments of flying squirrel skin detailed in Chapter 4 of this thesis. Similarly, a big thank you must

Chapter 1

Introduction

The aim of the research described here is to design, make and test a small, autonomous and inexpensive jumping robot for traversing irregular terrain, using a low-power locally-available energy source.

1.1 Why a jumping robot?

As the size of a moving object decreases, it becomes more likely to meet an obstacle of similar or larger size than itself, and therefore it will encounter rough terrain more often. This is called the "Size-Grain Hypothesis" (Kaspari and Weiser 1999), which is defined as an "increase in environmental rugosity with decreasing body size". So a small robot, whether it walks, rolls or jumps will need the ability to cover rough terrain more frequently than a larger robot.
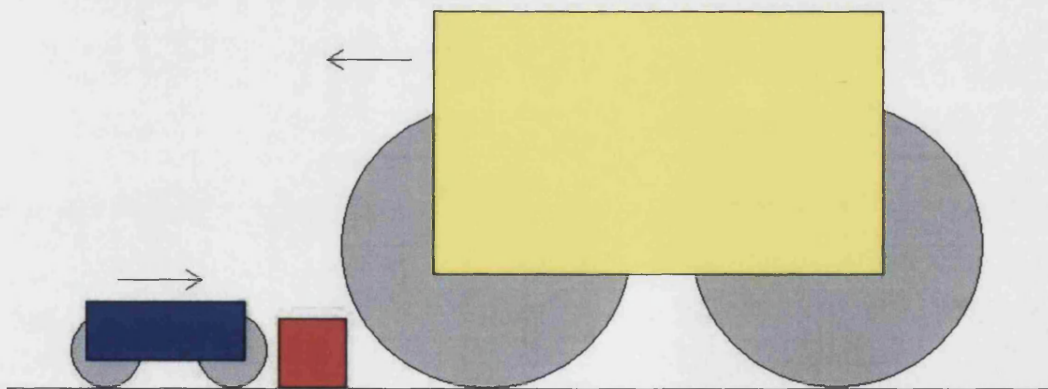
Fig. 1 – Graphical representation of the size-grain hypothesis

The majority of robot locomotion utilises wheels, which are very efficient at covering smooth terrain, but such vehicles are unable to pass obstacles of greater than half their wheel diameter. One exception is *Shrimp*, a space rover designed for improved mobility

which has its wheels mounted on high, articulating bogeys, enabling it to climb obstacles of up to twice its wheel diameter (Estier, Crausaz *et al.* 2000). Wheeled robots tend to have good manoeuvrability and could skirt around some obstacles, but others, such as a flight of stairs, walls or perimeter fences, would still halt progress completely. Walking robots are better able to cope with rough terrain, but generally rely on more complex control systems. The multiple degrees of freedom required for each leg demand several actuators to control them, meaning that the power and computational requirements are likely to be large. There are some novel 'walking' robots with very few actuators such as Rhex (Altendorfer, Moore *et al.* 2001) and Whegs™ (Quinn, Offi *et al.* 2002). The latter example has three legs rotating around the same axle, with equal angular spacing between them (120°). This design combines the simplicity of wheels with the adaptability of legs, particularly since each wheel is independently driven allowing them to align with each other when climbing. However, although legged vehicles have a surprising ability to clamber over rough terrain, they are still unlikely to get past obstacles of higher than double their leg length.

Perhaps the most effective way of travelling over rough terrain would be to fly over it. Micro-air vehicles are not hindered by obstacles on the ground, but are energetically expensive, resulting in limited power-source life (or power requirements that cannot be met continuously from the surroundings), and are hence unsuitable for some applications. The periodic nature of jumping allows time for recharging energy from the surroundings, making it a more sensible approach to designing a fully-autonomous rough-terrain robot. The inspiration for jumping robots comes from the fact that many natural organisms use jumping to traverse rough terrain. A jumping robot will be able to store energy recovered from the environment by compressing an elastic mechanism that can quickly release all the energy in one jump. This elastic energy storage is ideal for autonomous applications, because the amount of rest time is not critical and hence low power but locally available energy sources can be exploited, such as solar cells for example. The principle of solving design problems by applying ideas observed in nature is generally referred to as *biomimetics*.

1.2 Biomimetics

Looking at natural systems for inspiration is something that thinkers have been doing throughout the ages. In fact, it would be very difficult for anyone not to be influenced by what they see and know. Perhaps the earliest known record of this comes from the Chinese, who tried to make an artificial silk more than 3000 years ago (Vincent, Bogatyreva *et al.* 2006). In more recent times, the concept of copying from nature has become known by several names, such as biomimetics, bionics, biomimesis, biomimicry, biognosis and biologically-inspired design. At present there is no standard framework for biomimetic design, meaning that in order to solve a technical problem, researchers generally have to investigate any biological systems that seem appropriate in the hope of finding a good solution that can be translated to an engineering prototype. As such, biomimetics tends to happen in reverse, when engineers try to replicate some interesting natural phenomenon only after its functional principles have been discovered by a biologist. This may be about to change though, as researchers at the University of Bath are working on an ambitious project to catalogue all known biological approaches for any given required design problem (Vincent, Bogatyreva *et al.* 2006).

Sceptics of the biomimetics design methodology often cite the wheel as conclusive proof that nature doesn't always find the best solution to a problem, in this case transport. Their argument is pretty convincing: that no biological systems have axles or wheels. However, this is not quite true. The bacterial flagellum is a rigid helical structure, rotated from its base where it connects to the bacterium's body, driving the cell through liquid media as if it was a propeller. Although a controversial topic, there is apparently no doubt that the flagellum is rotated as a whole, and therefore it can be compared to the wheel and axle (Silverma.M and Simon 1974; LaBarbera 1983). However, clearly this would not have been apparent to early man, but it is conceivable that a rolling organism might have triggered the inspiration for the first wheel. Examples of these include the salamander, *Hydromantes platycephalus*, the jumping slug, *Hemphillia dromedarius* and the desert spider, *Carparachne aureoflava*. All choose to roll downhill for rapid escape in response to threat (Henschel 1990; Garcia-Paris and Deban 1995; Ovaska, Chichester *et al.* 2002). Much harder to miss might have been the Russian thistle, *Solsala tragus*, more commonly known as tumble weed. This

bush becomes more spherical as it ages, and dries and detaches from its root after death, allowing it to be carried long distances by even light winds, scattering its seeds as it rolls (Carnes 2003).

The key to a successful biomimetic design is realising at what level to imitate the natural system. Little would be gained by producing exact copies of successful organisms, but rather, by understanding the underlying mechanisms, the designer can optimise geometries and materials to match their application requirements. The main requirements set out for this research project were to investigate how and why jumping is used in nature, including considering what strategies are used to maximise range or to minimise landing impact forces or both. Above a certain size, being able to safely land a jump becomes as important as the take-off. It will be shown in Appendix 1 (page 207) that locusts occasionally land on their heads with no obvious ill-effects, whereas it is common knowledge that a cat will always attempt to orientate itself such that it can spread its impact force over all four extended limbs and its arched back (McDonald 1960). At least two deliberate strategies have evolved in order to best prepare animals larger than insects for landing. Some, such as kangaroos and rabbits, reorient themselves while in the air, enabling some of their landing energy to be stored in elastic elements of their legs and feet upon contact with the ground. This additional energy then contributes directly towards the following jump. Conversely, flying squirrels, sugar gliders and other gliding species (it will be shown in this thesis) glide to reduce their resultant landing forces. Therefore, assuming that the atmosphere is sufficient, or the intended flight speed high enough, then gliding might be considered as a means to control the jumping robot whilst it is off the ground.

Gliding increases the range of a jump, and also allows for the active selection of a landing site, in addition to more controlled impact forces on landing. An alternative method of increasing the distance travelled in a jump would have been to design a spherical robot, such that it would bounce or roll further when it hits the ground. Rolling in nature was introduced above (such as the tumbleweed example described) but there are no clear examples of organisms which actively jump into a roll. The possible exception is the jumping slug, *Hemphillia dromedarius*. Although not spherical, these slugs employ fast twitch muscles to help them quickly roll away when threatened, occasionally leaving the substrate in the process (Ovaska, Chichester *et al.* 2002).

However, the decision was taken at the outset of this research project that the 'jumping and gliding' strategy would be adopted, due to its relative prominence over 'jumping and rolling' in nature.

In the following literature review chapter, the principles of jumping and gliding will be introduced, and example animals reviewed for each. This knowledge will then be used to develop a design requirements specification list to focus the development of the robot. In an attempt to maximise the versatility of the final design, no single application has been specified for the robot, but the additional requirements associated with space exploration will deliberately be considered owing to the obvious suitability for this task. The following section will introduce the potential applications for an autonomous robot capable of traversing rough terrain.

1.3 Example Applications

A remotely operating device capable of traversing irregular or unknown substrates should have several potential applications, but becomes indispensable in scenarios where it is not possible to send a person, such as exploring distant locations in space, or searching places which could be hazardous to health. In this section, some potential applications will be introduced, although no military possibilities are considered or described because of the author's personal convictions. Although beyond the scope of this thesis, it is expected that the successful development of a jumping robot through this research project will ultimately contribute towards the introduction of jumping as an alternative gait available to other sophisticated autonomous robots, with multiple locomotor modes preparing them for every potential situation.

At the outset of this research, emphasis has been placed on autonomy, the ability of the robot to continue operating without requiring external input. This establishes a need for the robot to be capable of running from some locally-available, low-power energy resource. Nature's approach to achieving good jumping performance when limited by power capability, as introduced previously, is to amplify the available power by building up energy slowly and storing it in some way before releasing it rapidly. Details

of the various power amplification mechanism found in jumping organisms will be reviewed in Section 2.1.3 (starting on page 26). Consequently, such a fully autonomous robot will be more suited to applications where speed of operation is not important, such as space exploration. Nonetheless, a successfully-developed jumping mechanism would still be useful for other more time-dependent applications, such as search and rescue, where autonomy could be sacrificed in preference for a superior power source with limited life.

1.3.1 Search and Rescue

Search and rescue operations often utilise highly-trained dogs, which can quickly find their way over unknown terrain and have the additional advantage of their acute sense of smell. Artificial devices tend to be fragile, however, but some lightweight and fairly robust artificial noses also exist. Communication with a dog requires a handler and is clearly limited, whereas a robot could be fitted with a vision (even night-vision) system and transmitter for remote control. Mechanical devices require little or no maintenance when not in operation, in contrast to dogs which require constant attention, putting a constraint on the number that can be accommodated by one search and rescue team.

Speed is critical for search and rescue missions, with life usually dependent on success. For example, an explosion in a nuclear power station would result in leakage of dangerous radioactivity, but a swarm of scout robots capable of being remotely operated and passing over any debris should help to locate survivors. Unless large, these devices would not be able to help in moving rubble, but could be used to transmit information and reassure anyone trapped until an alternative means of extraction can be arranged. Similarly disasters which cause buildings to collapse, such as earthquakes and terrorist attacks, tend to trap people in large amounts of unstable rubble causing high risk to any people searching for trapped survivors. If jumping robots could be made small enough, it may be possible to drop them through holes in the surface to explore the hazardous voids below.

Although not specifically a search and rescue application, a similar device could also be used for obtaining scientific measurements from equally inhospitable environments, such as volcanoes, caves or large-scale pipelines requiring inspection.

1.3.2 Low cost, high volume applications

If a simple, inexpensive jumping design could be developed, this would open up new potential applications within the leisure and recreation market. The individual production cost decreases with increasing volumes in an ever improving cycle. An obvious example might be the creation of jumping toys for children, pets or perhaps executives. Full autonomy would not be necessary, and small rechargeable batteries should be ideal.

Hunting sports are increasingly becoming under pressure from animal rights protesters and many forms are being prohibited entirely. A jumping target would make range shooting more enjoyable, perhaps with a concealed pool of cheap robots jumping randomly into view from a given area. It may be possible to fit a sacrificial layer of armour to each device for protection of vital components, enabling the more sophisticated jumping mechanism to be re-fitted with new armour when necessary and reducing overall costs.

Perhaps the most valuable potential application for a swarm of inexpensive jumping robots, if such could be produced, would be the clearing of minefields. It is a highly publicised problem that armed landmines have been left throughout some of the most desolate, war-torn landscapes of the world, killing and maiming innocent people long after battles have finished. For whatever unfortunate reason, governments have not invested in making these areas safe, and it is invariably some of the world's poorest people who are affected. Sadly, however, the negative publicity has not prevented the design and use of continuously more aggressive forms of landmines in subsequent conflicts. It seems feasible that saturating these areas with small, independent robots would make them safe, with each device continuing to jump randomly about until it lands on a mine, exploding on impact.

1.3.3 Design for space

One possible and useful application for a jumping robot would be for the exploration of celestial bodies in space such as other planets, moons, or large asteroids. In the latter cases, any efficiency advantage of hopping or jumping locomotion will likely be further increased as a result of lower gravitational fields. It will be challenging, though, to build something that can repeatedly survive hard landings, particularly in the extreme conditions found on other celestial bodies such as very low temperatures. Any design intended for use in space must be of minimum mass and volume, due to the exceedingly high cost of transport. For the same reason, damage tolerance, reliability and adaptability all become essential requirements.

When considering space technology, it is important to be aware of the unique implication to the use of biomimetics as a design tool. The principals of evolution have allowed highly efficient designs to be derived in natural systems for a very specific set of conditions. Often these conditions are subject to change, such as resource availability and risk of predation, causing slightly different optimisations to dominate in future generations. Some space environments are very different to those found on earth, and so for these examples, biomimetics may be less useful. For example, if designing a jumping robot for exploration of a celestial body without an atmosphere, then there would be no advantage in enabling the device to glide. In fact, this would increase rather than decrease the resultant landing force, due to the additional mass.

1.3.3.1 Existing space robots

Very few examples of space robots have ever been successfully operated away from Earth. In all cases, designs have been kept simple, with proven technologies being preferred to any potential performance benefits owing to the huge financial (and potentially political) consequence of failure. Progress has therefore been slow, both in terms of the number of metres per day that these robots have explored, and in the development of the associated technology. A perfect example of the difficulty involved in executing planetary exploration missions is illustrated by the demise of *Beagle 2*, a

European Space Agency (ESA) explorer which was due to land on Mars on 25th December 2003. This spacecraft contained several years and millions of pounds worth of scientific equipment, and should have provided the most in-depth analysis of the Martian environment ever attempted. It was successfully ejected from Mars Express on 19th December 2003, but nothing has been heard from it since, and the mission is presumed lost.

1.4 Thesis outline

In this chapter, the need for alternative transport modes for autonomous robots has been introduced. Likewise, the principle of biomimetics has been justified as a sensible design approach for this problem, and hence the goal of this thesis has been set – to create a robot suitable for full autonomy that both jumps and glides. Finally, some example applications were suggested.

Jumping is used by many animals to escape when trapped, or in the case of kangaroos, for long distance, energy-efficient locomotion. The biomechanics of jumping will be introduced from fundamental principles in Chapter 2, before the various examples from nature are described and contrasted in the hope that the detail of their mechanisms might inspire the design phase of this research. Gliding is a simple way of extending the range of each jump, while simultaneously reducing impact forces, and this will be considered together with some more example species. The literature review continues with an overview of low-Reynolds-number, low-aspect-ratio aerodynamics and concludes by evaluating existing types of robot locomotion that have been developed for the traversal of rough terrain. As mentioned above, for example, wheeled robots generally cannot pass any obstacle of greater than half their wheel diameter.

In Chapter 3, a study is carried out on flying squirrels, seeking, through observation and the measurement of take-off and landing forces, to clarify why these animals developed their unique gliding ability and diverged evolutionarily from normal squirrels. It was expected that this study would provide useful information for the development of the robot, owing to the fact that flying squirrels regularly jump and glide while traversing an arboreal habitat which would be difficult for any robot. Experimental performance

and behavioural evidence will be presented suggesting that flight in flying squirrels may have evolved out of a need to control landing forces. Northern flying squirrels were filmed jumping from a horizontal branch to a much larger vertical pole. These were both slightly compliant (less than 1.9mm/N), and instrumented using strain gauges so that forces could be measured. Take-off and landing forces were both positively correlated with horizontal range between 0.5 and 2.5 m, (r = 0.355 and r = 0.811, P<0.05), but not significantly different to each other at each range tested. Take-off forces ranged from 1 to 10 bodyweights, and landing forces were between 3 and 10 bodyweights. Glide angles increased rapidly with horizontal range, approaching 45° at 3 m, above which they gradually decreased, suggesting that northern flying squirrels are optimised for long distance travel. Northern flying squirrels are shown to initiate full gliding posture at ranges of less than 1 m, without landing any higher than an equivalent ballistic projectile. However, this gliding posture enables them to pitch upwards, potentially stalling the wing, and spreads the landing reaction force over all four extended limbs. At steeper approach angles of close to 45°, flying squirrels were unable to pitch up sufficiently and landed forelimbs first, consequently sustaining higher impact forces.

Flying squirrels are capable of a range of transport modes, and can quickly change from one to the other. The rapid transition from gliding to climbing in particular led to the hypothesis that the skin of flying squirrels must be specialised from that of other mammals, otherwise a large gliding membrane would become a tripping hazard. This is addressed in Chapter 4, a preliminary study investigating the likely structure and composition of flying squirrel that might have evolved to facilitate their unique requirements.

In Chapter 5, all the principles learnt from the various biological examples are compiled into a design requirements specification for an autonomous robot. The design of the final, functioning robot prototype is described, which was developed so as not to prohibit space applications. Consequently, springs were preferred to elastic elements for energy storage, because the latter would become too brittle in the extreme low temperature environments of space. Power is amplified by storing energy slowly in four metal torsion springs, compressed using a heavily geared, low power motor to wind in cord around a capstan. The robot jumps only when the robot is fully compressed, which

causes a dog clutch to disengage, allowing almost instantaneous release of the capstan. A worm gear design prevents the robot from exerting torque against the motor when not powered, allowing the use of irregular energy sources such as solar power. An additional motor drives the winding mechanism quickly between the two ends of the robot, allowing it to jump upwards no matter which way up it lands. Like flying squirrels, the jumping robot developed in this thesis deploys its gliding membranes immediately during take-off, reducing detrimental mid-air rotation. Likewise, provision is made for it to be able to control its angle of attack during gliding by shifting its centre of mass, improving aerial control and potentially reducing landing forces.

The prototype weighs 0.7 kg and is able to store 21.5 joules of energy, which would enable it to jump 3.1 m vertically on Earth if it was 100% efficient. The experimental results show that the robot can raise its centre of gravity by 1.6 m on average, making it 52% efficient, with an average clearance height of approximately 1.17 m. The addition of gliding membranes reduced the total range of the robot during forward jumps, but also reduced the landing velocity and hence impact force. Experiments with flexible solar panels showed that sufficient power for autonomous jumping could be obtained by covering the wings with these solar cells and adjusting the gear ratio of the compression motor.

This thesis contains roughly equal quantities of biological and engineering research. For the benefit of readers from both disciplines some basic ideas (for example, the meanings of words like *dorsal* and *ventral*, or the equations of motion of ballistic bodies) have been explained in rather more detail than would have been needed for just one specilialism.

1.5 References – Chapter 1

ALTENDORFER, R., MOORE, N., *et al.* (2001). "RHex: A Biologically Inspired Hexapod Runner." Autonomous Robots 11(3): 207.

CARNES, J. (2003). "Immunochemical characterization of Russian thistle (Salsola kali) pollen extracts. Purification of the allergen Sal k 1." Allergy 58(11): 1152-1156.

ESTIER, T., CRAUSAZ, Y., *et al.* (2000). An innovative Space Rover with Extended Climbing Abilities. Proceedings of Space and Robotics 2000, Albuquerque, USA.

GARCIA-PARIS, M. and DEBAN, S. M. (1995). "A Novel Antipredator Mechanism in Salamanders: Rolling Escape in Hydromantes platycephalus." Journal of Herpetology **29**(1): 149-151.

HENSCHEL, J. R. (1990). "Spiders Wheel to Escape." South African journal of science **86**(3): 151-152.

KASPARI, M. and WEISER, M. D. (1999). "The size-grain hypothesis and interspecific scaling in ants." Functional Ecology **13**(13): 530-538.

LABARBERA, M. (1983). "Why the Wheels Won't Go." The American Naturalist **121**(3): 395-408.

MCDONALD, D. D. (1960). How does a cat fall on its feet? The New Scientist. **7**: 1647-1649.

OVASKA, K., CHICHESTER, L., *et al.* (2002). "Anatomy of the dromedary jumping-slug, Hemphillia dromedarius Branson, 1972 (Gastropoda : Stylommatophora : Arionidae), with new distributional records." **116**(3): 89-94.

QUINN, R. D., OFFI, J. T., KINGSLEY, D. A. and RITZMANN, R. E. (2002). Improved mobility through abstracted biological principles. IEEE/RSJ International Conference on Intelligent Robots and System, Lausanne, Switzerland.

SILVERMA.M and SIMON, M. (1974). "Flagellar Rotation and Mechanism of Bacterial Motility." Nature **249**(5452): 73-74.

VINCENT, J., BOGATYREVA, O., *et al.* (2006). "Biomimetics: its practice and theory." Journal of The Royal Society Interface **3**(9): 471-482.

Chapter 2

Literature Review

This review will attempt to give a thorough overview of each of the three main themes within this Thesis: jumping, gliding and robots, in turn. Jumping is introduced with a look at the biomechanical principles behind it, including take-off techniques. Two distinct jumping strategies are found in nature, 'Pause and Leap' and 'Continuous Hopping'. These are introduced and then many specific biological examples are discussed within these categories. Finally, gliding is formally reviewed, beginning with the underlying aerodynamic principles. Biological examples are then considered from each of the five classifications of vertebrates. More detail is then given of low-Reynolds-number, low-aspect-ratio aerodynamics and within this context, rigid and flexible wings are compared. Finally, this literature review concludes with a look at the current status of robotic locomotion in general, before focussing on some of the jumping and hopping robots that have so far been developed. Micro air vehicles are also considered.

2.1 Jumping

2.1.1 Biomechanics of jumping

In order to jump, an animal needs to generate a rapid acceleration of its body mass away from the ground substrate, causing it to leave the surface entirely. It is only necessary for a portion of the mass to be accelerated, so long as this is travelling fast enough for the conservation of momentum to carry the remainder of the mass with it. Fig. 2 shows this idea modelled as a spring and mass system, and, if the spring became rigid after take-off, conservation of momentum equations would give:

$$MV_1 = (M + m)V_2$$

Since the basic principle is always the same, the best jumping performance can be achieved by maximising V_1 and the ratio of M to m.
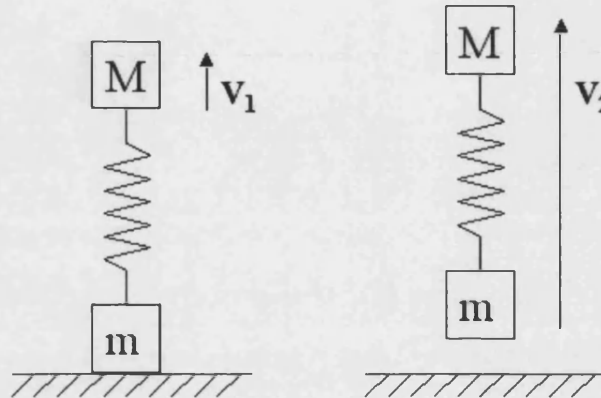
Fig. 2 – Sketch showing the mechanics of the jump

In order for a system to achieve its largest jump, it needs to produce the maximum possible energy in a single event. In nature, active muscles are the most common means of initiating locomotion. These have the ability to contract or generate tension and if they do both simultaneously, can perform mechanical work. (Bennet-Clark 1976)

Neglecting air resistance, the maximum energy that the animal can produce will be converted directly into kinetic energy:

$$K.E. = \frac{1}{2} mv^2$$

Where m is the mass of the animal, and v is its take-off velocity. The kinematic equations for calculating the maximum height and range of ballistic projectiles ignoring wind resistance are well known.

Peak height:
$$h = \frac{(v \sin \theta)^2}{2g}$$

And maximum range:

$$x = v^2 \frac{\sin 2\theta}{g}$$

Where g is the acceleration due to gravity and θ is the take-off angle. These equations and all subsequent kinematic equations can be found in any elementary physics text book.

It is clear from Equation 4 that the maximum horizontal range is achieved when the take-off angle is 45°. Likewise, in order to maximise the height of a jump, the ideal take-off angle is 90°. By combining either Equation 3 or Equation 4 with Equation 2, we see that both the maximum height h, and the maximum range x, are proportional to the energy produced by the muscle divided by the total mass. Therefore, by assuming that the work done by a muscle is proportional to its mass (Gabriel 1984), then the jumping performance is directly dependent on the percentage of the body that is muscle directly involved in the jump. It follows then that if the proportion of the body mass made up of jumping muscle is consistent, and neglecting other factors such as air resistance, all animals should in theory be able to jump to the same height independent of their size. However, Henry Bennet-Clark (1976) suggests that larger animals are limited by energy availability, where as the performance of smaller animals is limited by high power requirements. Looking first at this latter point, the energy required for a jump is usually applied to the ground through extension or rotation of the legs, and the take-off force can only act while these are in contact with the ground. Therefore, the length of the leg also has a direct influence on jumping performance, and in order to improve this many insects and other small animals use 'biological catapults' - energy storage mechanisms - as a means of generating higher power from their muscles. The proof that shorter leg length requires higher power actuation is demonstrated below.

The equation for an accelerating body is:

$$v^2 = u^2 + 2as$$

where u is the initial velocity, a is the acceleration and s is the distance through which it is accelerating (the leg length). Therefore, from equations 3 and 4 again, we can see that the height and range will improve directly with increased leg length. The power output can be related to either energy or force using the standard equations, 6 and 7 below:

$$P = \frac{Energy}{time}$$

<div align="right">Equation 6</div>

$$P = Fv = mav$$

<div align="right">Equation 7</div>

Therefore, for an animal jumping from rest, equations 5 and 7 can be combined to give:

$$P = \frac{mv^3}{2s}$$

<div align="right">Equation 8</div>

Hence, the smaller the leg length, the higher the specific power requirement to reach a given take-off velocity, and therefore range and height.

Muscles have been shown many times (one example being via physiological measurements on tree-frog legs - Peplowski and Marsh, 1997) to have a limited power output, proportional to the maximum speed at which they can operate. However, with decreasing size, power becomes more important than energy to jumping performance, warranting the need for amplification. Catapults are a good example of a power amplifier, because they can launch a missile much faster than it is possible to move a human arm, even though that is where the energy comes from. Work is done by the operator's arm muscle to stretch the elastic part of the catapult, which stores this energy until it's released, recoiling much more rapidly than it was loaded. Therefore the power output is greater than the power input (Alexander 2003).

For maximum agility, the mass of the skeleton shouldn't be too high, leading to a trade-off with structural strength. It is obviously in the best interests of the animal to keep any jumping forces well within the safe limits of its skeletal material (Bennet-Clark 1976). Lindstedt, Reich et al. (2002) discuss that the highest forces relative to energetic cost are achieved by eccentric contractions (when an actively contracting muscle is lengthened due to external forces). This property, in combination with the location of

tendons (tensile elastic elements), enables additional performance to be gained from using a counter-movement prior to jumping. Elastic strain energy is stored during the initial eccentric contraction, which is then recovered and added to the mechanical work generated during the subsequent shortening of the muscle (Lindstedt, Reich *et al.* 2002). This behaviour is adopted by many animals, including humans, for improved jumping performance.

Any animal that displays increasing jump distances with increasing size is likely to be employing an energy storage mechanism (Gabriel 1984). It shall be shown in the next section that some insects employ the compression of the material *resillin*, which has a low Young's modulus but a high energy storage capacity of more than 2 Jg^{-1} (a value superior to spring steel), and a very fast and almost 100% recovery. Others, in contrast, store energy in the bending of skeletal elements.

The *isometric force* of a muscle can be defined as the tension generated by contracting a muscle that is restricted such that its length cannot change. Jumping requires high power output and it has been shown that when a muscle works at maximum power, the highest force that it can deliver is only one third of the isometric force (Bennet-Clark 1976). However, if an animal generates the power required by storing energy in a spring-like element, it can be assumed that Hooke's law applies so the output force can be said to be:

$$F = \frac{1}{2}kx$$

Here the spring constant, k is equivalent to the isometric force of the muscle when the strain, x is at the full isometric extension. This means that by not operating at its maximum power, the muscle is actually able to deliver one half of the total isometric force to the energy storage mechanism rather than one third. Therefore, by minimising the losses and mass of such a power amplification system, up to 50% more energy is available for jumping using energy storage than from direct actuation. With increasing size, it becomes harder to keep the mass of such a system low enough to make use of this effect, explaining the trend that larger animals have all evolved with direct actuation (as opposed to spring storage) as the primary means of jumping.

2.1.2 Take-off Techniques

Whatever the original reason for the development of their jumping ability, animals tend to utilise all their resources, and so it is likely that the jumping gait will be employed for alternative purposes. Maximising the height or range of a jump is something that will be learnt naturally through experience, although it could be innate too in some animals. The optimum strategies for high and long jumps by humans were modelled by Alexander (1990). His model supported the strategies already employed by athletes in these two sporting disciplines. This is that for high jumpers, it is best to run up with a low centre of mass and set down the take-off foot at a shallow angle of about 45°. By contrast, long jumpers need to maximise their speed during the run up, and set their leg at a steeper angle. Alexander's model was later developed to more accurately represent muscle and tendon properties in order to investigate the action of knee extensor muscles during long jumps (Seyfarth, Friedrichs *et al.* 1999; Seyfarth, Blickhan *et al.* 2000). In the first of two separate papers, Seyfarth (1999) demonstrates that increasing the touch-down velocity of the take-off leg results in a higher vertical momentum and hence improves the range. The conclusions drawn from the later paper were that jumping performance improves with increasing muscle strength but is insensitive to changes in the speed of the muscle or compliance of the tendon. The leg extensor muscles are highly stretched during take-off and Seyfarth also shows that by arranging elastic elements in series with this muscle, the duration of this lengthening and dissipation can be increased, resulting in enhanced eccentric forces and hence improved jumping ability.

2.1.3 Biological approaches to jumping

The Biomechanics section above demonstrated why size is an important influencing factor on the way in which an animal will jump. Animals jump to escape predators, capture food, and in some cases (such as rabbits and kangaroos) it is the favoured method of locomotion. There are two distinct patterns that can be observed. Locusts, for example, travel using single jumps followed by a rest period to recharge and re-orientate (Bennet-Clark 1975). This can be categorised as the 'pause and leap' method and is

common in insects and other small animals such as frogs. The alternative approach is continuous hopping, where energy is recovered during the landing and used in the following jump, a technique employed by kangaroos in order for them to travel large distances across open country (Alexander 1975). For general locomotion, one would expect that the animal would attempt to get maximum performance by using the optimum take-off angle for example, whereas rapid acceleration is most critical when jumping is used primarily as an escape mechanism. In this section, examples of jumpers from both categories are reviewed.

Nature evolves to make the best of the tools and materials that it has, and jumping is a useful type of locomotion that has been optimised by many animals, of all sizes. The dog, for example, manages to generate extra energy for jumping by employing counter-movements in combination with its already powerful leg musculature, such that the elastic extensors of the ankle, knee and hip are stretched prior to shortening. The muscle loading is such that the peak force occurs at the start of the impulse and falls as the animal accelerates, hence producing a high-energy output from a single contraction (Alexander 1974). In human beings, improved performance is achieved by swinging the arms simultaneously with jumping, increasing the amount of momentum in the direction of the jump (Ashby and Heegaard 2002).

2.1.3.1 Pause and leap

Within this broad category are all of the insect jumpers, perhaps due to the higher level of control sophistication required for continuous hopping to be energetically advantageous. Owing to their small size, insect leg length is limited and in addition, they are more affected by air resistance so power amplification is essential for jumping. As a result, many different specialisations have evolved in insects to enable effective jumping, some of which have even developed so far as to hinder simple walking (Bennet-Clark 1977). Three broadly defining categories of catapult mechanisms, bi-stable designs and flippers will be introduced below, with example insects described for each. It will be shown that larger animals, which employ direct actuation of muscles in order to jump, are also able to amplify this power generated to improve their jumping.

2.1.3.1.1 Catapult jumping mechanisms

Maximising relative leg length is advantageous to jumping performance irrespective of scale. This increases the work done during take-off, which is the product of muscle force and the distance through which it is exerted (equivalent to the leg length). Many of the best insect jumpers have greatly enlarged jumping limbs. The *metathoracic* legs of grasshoppers and locusts, for example, are only actually used for jumping and are very much larger than the other pairs of legs (primarily used for walking and stability). It was shown by Bennett-Clark (1975) that locusts are able to achieve a high jumping impulse by moving these legs at a velocity much higher than is possible for the muscles to work at by pre-loading energy into a quick release mechanism. Energy is stored in the bending of specialised sclerotised tanned cuticle, such as the semi-lunar processes (the half-moon shaped pieces in the knee joint – as shown in Fig. 3), by the contraction of the large extensor tibiae muscles of the two metathoracic legs. As the tibia rotates in towards the femur, the extensor tendons are stretched until a catch locks into place (Bennet-Clark 1975). This catch is engaged only when the leg is fully flexed, when the strap-like flexor tendon is relaxed. To understand how this works, this tendon can be considered as a belt, which when in tension, runs smoothly over the slippery top surface of Heitler's lump as the leg rotates. This flexor tendon belt bifuricates into strands at the distal end, (nearest to the knee joint), which are connected to either side of the tibia. This leaves a pocket of tissue in the middle of the resulting fork, which naturally becomes hooked around the wrong side of Heitler's lump when the tendon is fully relaxed (at full leg flexion). In this position, considerable extensor tension can be developed without the tibia being able to move. The locust can then release this catch whenever it needs to by relaxing separate, smaller flexor muscles (Brown 1967; Heitler 1974; Bennet-Clark 1975).
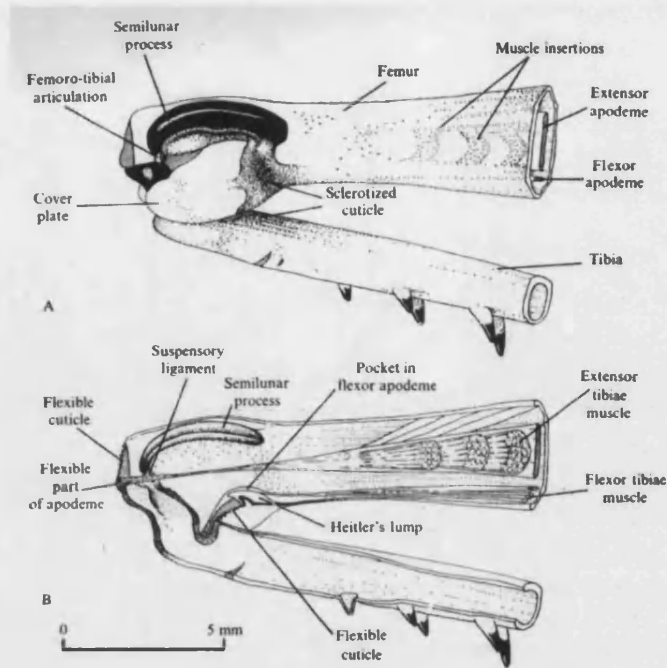
Fig. 3 – Physiology of locust leg

Diagram A shows the external anatomy with the hatched regions representing flexible cuticle. The tibia is suspended from the distal end of the semilunar process, heavily sclerotised tanned cuticle with a half-moon shape that provides some of the energy storage, attached by flexible cuticle to enable articulation. Diagram B shows the simplified internal anatomy of the leg including the pocket in the flexor tendon which is naturally pulled down around Heitler's lump when the tibia is in the fully flexed position. This acts as a catch which enables additional extensor tension to be developed, and it is held in place by the small, flexor tibiae muscle until it's relaxed for take-off. (Bennet-Clark 1975).

Bennet-Clark showed that each metathoracic leg contains less than 4 mg for energy storage, but can store the equivalent energy to 70 mg of muscle (1975). Meanwhile, thanks to suitable geometry, these legs are able to achieve almost constant acceleration (and hence force) throughout the impulse. This has two benefits. Firstly, it minimises the peak force that the skeletal elements must be able to safely absorb, thus allowing them to operate at closer to their structural limits, which in turn enables more energy to be safely stored. Secondly, the chance of the leg losing contact with the substrate before all the energy has been exerted is greatly reduced, which might otherwise occur at the point of peak force. Such optimisation would seem highly relevant to the design of a jumping robot.

Bush crickets are also in the order *Orthoptera*, and, like locusts and grasshoppers, are able to jump well as a result of their long hind legs, which in this case are more than four times the length of the front legs. However, Burrows and Morris (2003) show that the jumping mechanisms are not identical. In crickets, an initial full flexion of the hind

legs is not required, and the semi-lunar processes are not bent at all during the course of the jump.

A closely-related insect to the locust is the false stick insect, *Prosarthria teretrirostris,* which uncharacteristically for a stick insect is able to jump and kick. Although it mostly looks and behaves like a real stick insect, it has hind legs that are up to 2.5 times as long as the front or middle legs, which give rise to a similar jumping style to the orthopterans (locusts and grasshoppers). However, an additional feature of interest in this study is that this insect stores 7% of its jumping energy transiently in the bending of its skeletal structure (i.e. not in its legs). This partially compensates for its inability to store energy in the semi-lunar process, which is significantly less developed than in locusts (Burrows and Wolf 2002).

Work by Bennet-Clark (1967) and an extensive study of the flea by Rothschild *et al.* (1975) showed that the secret to its impressive jumping ability was the rapid release of stored energy (Bennet-Clark and Lucey 1967). The pre-loading takes place prior to a jump as the flea crouches down with the coxa, femur and tibia (on the third pair of legs) all tightly folded together, and parallel, forming an 'N' shape. This compresses a large pad of the rubber-like material, resilin, in the *pleural arch* (see Fig. 4) and also gives the flea maximum possible leg extension in the jump. The compressed resilin stores energy, and is held in place by a *coxal catch*, which is only released at the initiation of the jump by a rapid twitch of the *trochantal depressor* muscle. Leverage from the *depressor apodeme* tendon acts simultaneously with the resilin to cause the *trochanter* and *femur* to rotate around their hinges and accelerate upwards in the process. This acceleration is very rapid, and continuously increasing while force continues to be exerted through the tibia and its relatively powerful spines against the substrate (Rothschild 1975). This is the optimum force profile for ensuring that the flea does not leave the substrate until all the force has been exerted through it.
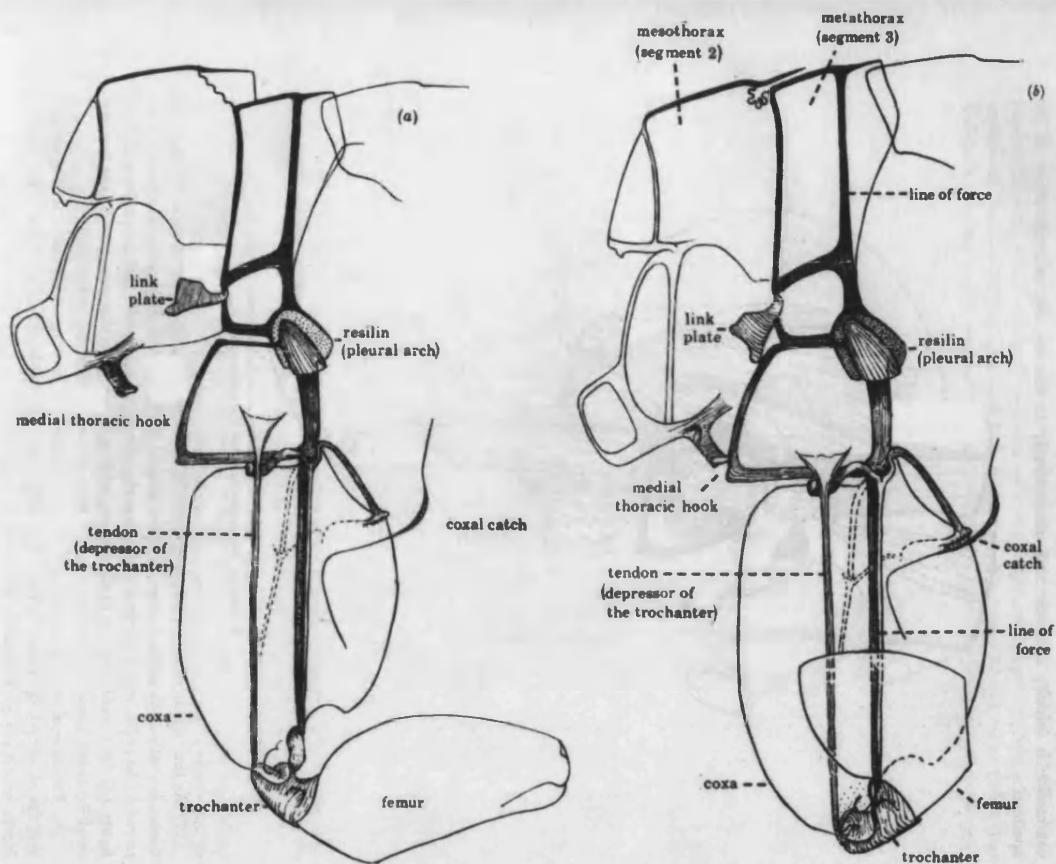
Fig. 4 – Diagram showing the elastic storage mechanism for jumping in the flea.
(Rothschild 1975)

a) is a sketch of the lateral view of a flea in the relaxed state, and b) is the same diagram shown with the femur raised ready for jumping. This compresses the resilin pad along the line of force in the pleural arch, while simultaneously extending the tendon labelled 'depressor of trochanter'. The link plate is also rotated bringing the meso- and metathoracic segments 2 and 3 into line, and partly engaging the medial thoracic hook. The location of the coxal catch, which holds the system in place prior to jumping, is also shown.

The performance of the flea relative to its body length is very impressive, but the design would not work if scaled to a significantly larger size. Any increase in length during such scaling increases the volume as the cube, and hence the mass would quickly become too large for jumping due to the mechanics and the structural and energy storage properties of the materials involved. Froghoppers (also known as Spittlebugs) actually exceed the 'height jumped relative to body length' of a flea (Burrows 2003). In the process, they exert a force of 414 times their body weight due to the very rapid (less than a millisecond) rotation and extension of their relatively short hind legs. Burrows suggests that this energy is once again stored in resilin, possibly also storing some in an extra large tendon. The hind legs are not used in normal walking, but rather are just dragged along behind the insect. However, they are always cocked and ready for an

escape jump thanks to a locking mechanism and some huge jumping muscles necessary to overcome it. Leafhoppers are very similar to froghoppers, although no literature currently exists on their jumping ability. Consequently some high-speed camera experiments were carried out by the author for comparison. It was demonstrated in these experiments (see Appendix 1 on page 207) that leafhoppers are capable of generating similarly rapid accelerations during take-off to those reported for froghoppers.

Bristletails, *Petrobius,* jump using two mechanisms employed independently. The main propulsive force comes from a very rapid tail beat lasting 2-8 ms, induced by a relaxing of the dorsal abdominal muscles, which straightens and forces the ventral surface of the abdomen against the ground. Energy is stored during the slower loading of this tail, hence its inclusion in the catapults section. It could otherwise equally have been reviewed in the upcoming "flips" section because during the rotation of the tail, the bristletail also swings the head and front end of the body (where the majority of the mass is) upwards, thus raising its centre of gravity even higher. This second movement can considerably influence the direction of the jump depending on its exact timing relative to the initial tail beat. In order for the tail beat to reach such high speeds, normal musculature alone is insufficient. However, no catch mechanism has been found and it is proposed that the catapult action depends on the dynamic balance between dorsal longitudinal muscles and deep oblique muscle (Evans 1975).

One of the fastest animal mechanisms ever recorded is that of the strike of trap-jaw ants, *Odontomachus bauri,* which occasionally propel themselves away from danger using their jaws. These ants can close their large mandibles at speeds ranging from 35 to 64 ms^{-1}. The speed and consequent force exerted (which can exceed 300 bodyweights) allows these ants to utilise their jaws for distinct purposes, such as capturing prey and ejecting intruders from their nest. By angling their heads towards a hard substrate, their strike becomes an escape mechanism as it has enough power to propel them rapidly away from danger. These high speeds are actually achieved using slower, higher force muscles (with relatively longer *sarcomere* lengths, a concept explained in Section 2.1.3.1.4 on page 35) compared to the jaws of other similarly sized ants. These powerful muscles are required to open the jaws, storing energy in the bending of cuticular elements, apodemes, and in the closer muscle itself as they do so until a catch mechanism engages. When the ant chooses to strike, a smaller, highly specialised

trigger muscle unlocks the catch, rapidly releasing the stored energy to accelerate the mandible (Gronenberg, Tautz *et al.* 1993; Gronenberg 1995; Paul 2001).

2.1.3.1.2 Bi-stable jumping mechanisms

When Springtails jump, their entire body rotates as they travel through the air. This is due to the location of their springing organ, the *manubrium*, which rapidly unfurls from a position directly under the centre of gravity at the posterior end of their abdomen. The *manubrium* is a bi-stable mechanism, meaning that it is stable in both the flexed or extended positions but not in between. As a result, standard relatively slow muscle contraction (which appears to flex the entire body of the springtail) is enough to force the manubrium into the unstable position, but it rotates very rapidly to get through to the more stable, extended position, thrusting the springtail forwards in the process (Brackenbury and Hunt 1993).
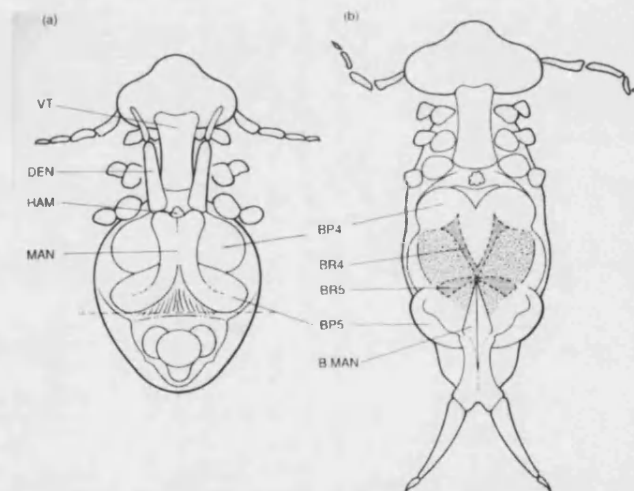
Fig. 5 – Ventral view of the Springtail jumping mechanism shown in the folded position (a), and open (b).

The click beetle usually makes its jump from an upside down position (lying on its back). It starts by arching its back as an initial counter movement, before rapidly jack-knifing its body upwards at the joint between the prothorax and mesothorax. This process of arching pre-loads energy into the skeletal structure of the beetle, and the system is then held in the ready state by friction from a peg (see Fig. 6). The release of the peg causes the violent reverse in body curvature due to its bi-stable nature, moving

the position of the centre of gravity rapidly upwards giving the momentum required for the beetle to leave the ground (Evans 1972; Evans 1973).
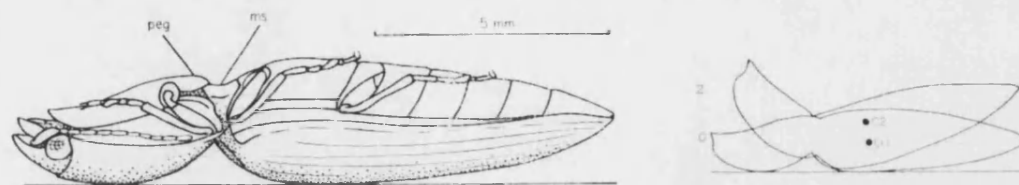
Fig. 6 – The click-beetle lies on its back to initiate a jump.
Diagram taken from Evans' paper (1972).

2.1.3.1.3 Flip jumping mechanisms

This category includes all the insect jumpers which have developed alternative ways of power amplification for jumping to the catapult and bistable ideas described previously. One that doesn't seem to employ any such mechanism, for example, is the jumping millipede, which still manages to jump quite successfully even without any large muscular jumping legs. It turns its head and the first few segments forward to grip the substrate, whilst the rest of the legs run forward, forming a vertical loop. Eventually the front of the millipede is overtaken forcing it upwards, and with it much of the mass of the insect, resulting in complete separation from the ground. It lands with its body in a U-shape, before falling onto its side and very quickly swinging its head forward and commencing running again for a short distance before the next jump (Evans 1973).

The winged stick insect *Sipyloidea sp.* is also able to jump, but using a quite different mechanism to the false stick insect, described in the Catapults Section above. In this case jumping is initiated is by the insect rapidly swinging its abdomen simultaneously with the extension of its middle and hind legs (Burrows and Morris 2002).

The Mediterranean fruit-fly larva is, like any other fly larva, a soft-bodied organism without legs that relies on hydraulic-based locomotion. Generally, such organisms are only able to crawl slowly around, but during the most vulnerable stage of its development, this maggot is able to escape its ant predators and reach speeds of up to $0.5 ms^{-1}$ by leaving the ground. Initially, it rolls itself up and hooks its mouthparts onto

its posterior cuticle, before contracting its helical muscles to create tension in the body wall. Eventually the system starts to become unstable, somewhat resembling a bent sausage-shaped balloon, before a final wave of muscle contraction travelling from the back to the front of the maggot disengages the mouth hooks. Recoil from the elastic strain energy stored in the cuticle is then enough to thrust the tail towards the substrate and the head away from it, launching the fruit fly larva into the air (Maitland 1992).
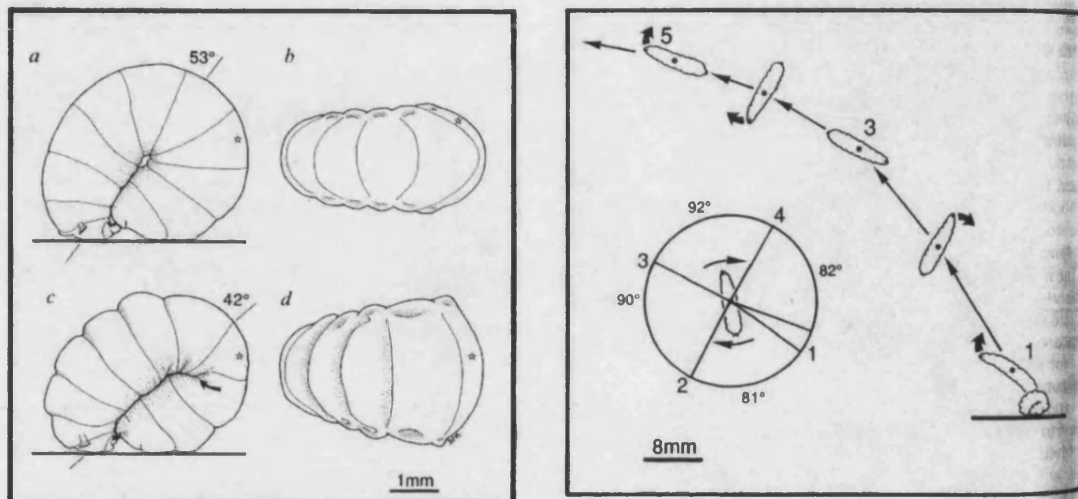
Fig. 7 – Diagrams showing how the fruit-fly larva is able to jump
The left hand diagram shows how it rolls itself up and hooks its mouthparts onto its posterior cuticle before tensing the muscles in its body wall. The system becomes unstable, allowing the larvae to release it, and the elastic recoil sends it spinning into the air as shown on the right hand diagram.

2.1.3.1.4 Direct actuation jumping mechanisms

Frogs and toads have evolved to have large powerful hind-limbs, which allow them to jump far or swim fast when under threat. However, results from several studies show that muscle power alone is not sufficient to explain the excellent jumping performance achieved (Marsh and Johnalder 1994; Peplowski and Marsh 1997; Wilson, Franklin *et al.* 2000). Isolated frog muscle has been mechanically tested to determine the amount of power that can be produced by contraction, and this is significantly less than the power (calculated from ballistic equations) necessary to project a frog a given distance and height. As an example, Cuban tree frogs (*Osteopilus septentrionalis*) can execute jumps requiring peak instantaneous muscle powers more than seven times higher than can be

generated by their hindlimb muscles (Peplowski and Marsh 1997). Yet, unlike the catapult and bi-stable jumpers described earlier, no clear catch mechanism to release an energy storage device has yet been found in frogs.
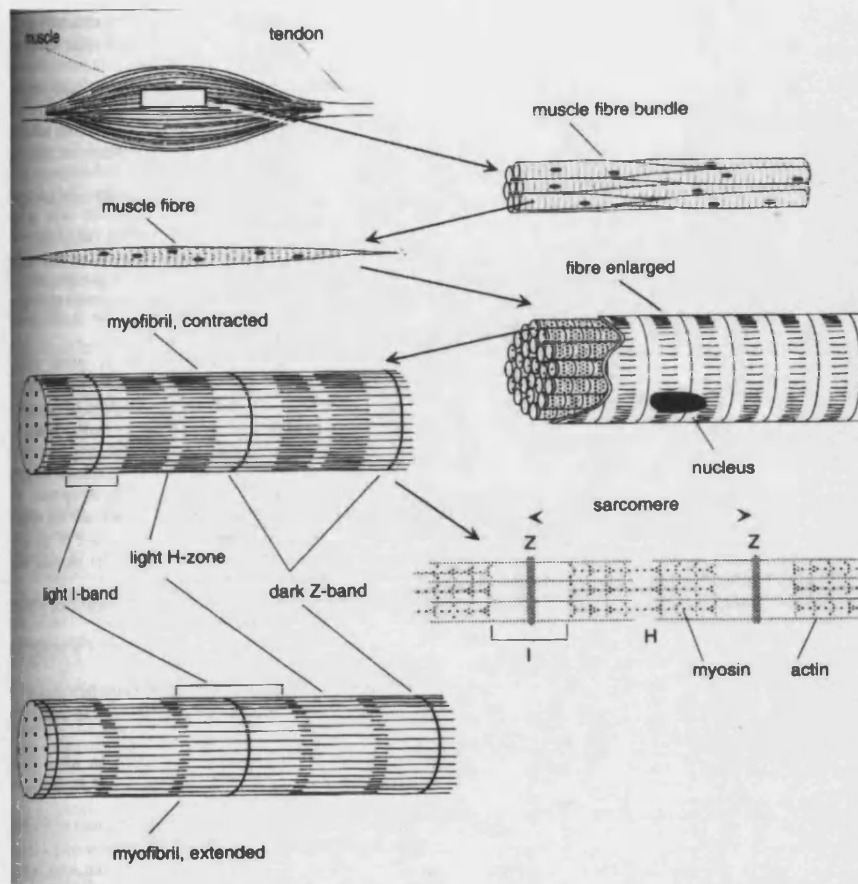
Fig. 8 – Exploded view of a muscle showing the sarcomere length
(Larousse 1995)

It has been shown that frogs are optimised for jumping, because the design of the length of the leg muscles relative to the positions of the joints means that the output force remains constant during the shortening. In contrast, for animals that generate cyclical movements (such as fish swimming), the muscle force declines progressively during shortening to allow the subsequent extension to initiate with little resistance (Lutz and Rome 1994). The muscle fibres operate at the optimal shortening velocities, and over the range of *sarcomere* lengths where most tension is generated. (The Sarcomere length determines the amount of myofilament overlap in each muscle fibre, and is labelled in the exploded diagram of a muscle, Fig. 8) (Lutz and Rome 1996). Roberts and Marsh (2003) modelled the system, and concluded that work output and peak power output can be improved by adding an elastic element in series with the muscle. This elastic

mechanism also allows muscles to generate accelerations, force and velocity trajectories that are not possible from standard muscle contractions. They also improved the performance of their model by arranging an effective mechanical advantage (EMA) of the muscle that increases continually throughout the contraction. It is suggested that this acts as an inertial catch, such that energy is stored in the series elastic element at the beginning of the jump allowing the delayed release of energy at increased power in the advanced stages of the take-off (Roberts and Marsh 2003).
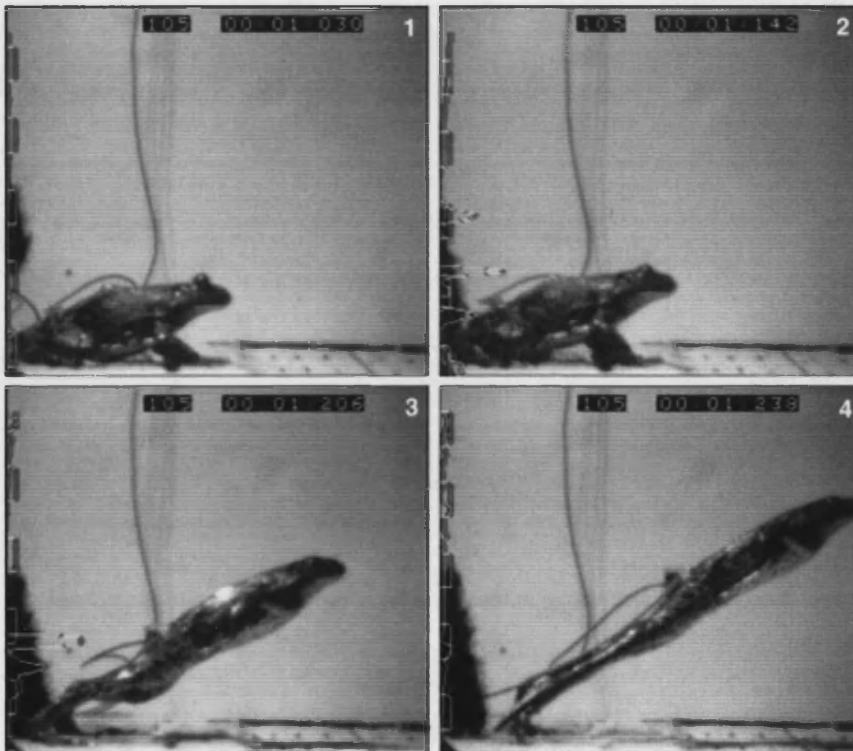
Fig. 9 – Four frames from a high-speed video sequence of a frog jump.
Frame 2 depicts the point where half of the *plantaris* muscle *fascicle* shortening has occurred (Roberts and Marsh 2003).

Useful from the perspective of building a jumping robot is some research by Kargo *et al.* (2002). They simulated experimental models of frogs, and in particular investigated the possible actions of the different skeletal joints. They found that a unique extra degree of freedom in the knee, allowing internal rotation between the tibia and the fibula was crucial to bringing the frog's feet under the body and hence enabling maximal jump distances. The relative position of the foot that the force acts through to the main body will therefore be an important design consideration for any jumping robot.

Bushbabies, *Galago senegalensis,* have excellent jumping ability and a vertical jump was observed by Hall-Craggs in 1965 of 2.25 m, approximately 6 times the body length of the individual. This would be impossible without some power amplification mechanism. Prior to jumping, energy is stored initially during a counter-movement as the bushbabies crouch down and the hip extends. As the animal begins to squat jump, further tension loading of the large muscle-tendon complex in the thigh continues after knee-extension has begun and is held until the moment of peak power requirement. Only then, for the last 13 ms of push-off, are the knee-extensors suddenly released such that all of the stored energy in the system is released simultaneously (Aerts 1998).

Dogs and horses are other good examples of direct-actuation jumping. Alexander (1974) showed that the principal extensor muscles in the hip were being contracted to shorten continuously throughout the take-off of a jumping dog. In contrast, the extensor muscles of the knee and ankle are stretched first during the take-off, and are then able to do more work as they shorten. He concludes that most of the energy storage is in tendon. Tendon is a highly elastic material, primarily made from a type I collagen (Puxkandl, Zizak *et al.* 2002), and it is capable of storing more energy relative to its weight than muscle.

In quadrupeds, both the fore and hind limbs are used to generate the work required for a given jump. Research on horses has shown that although the forelimbs create a larger impulse on the ground, it is the final push-off from the hind limbs that is most critical to a successful jump (Dutto, Hoyt *et al.* 2004). The joints of the hind limbs were also shown to be absorbing power overall for the first 40% of the ground contact, with the animal able to accelerate continually for the remainder of the take-off primarily thanks to a late burst of energy from the *metatarsophalangeal* (MP) joints. The MP joints, also known as fetlock joints, are below the horse's ankle and there is not a large muscle mass acting across them. Instead they are controlled by tendons, and it was proposed that elastic energy is stored here and released optimally late in the jump. Horses also employ energy storage when galloping, which enables them to move their legs faster than the maximum operating speed of the controlling muscles (Wilson, Watson *et al.* 2003). This is achieved by the storage of energy elastically in the extended biceps muscles, releasing a burst of energy to increase the power of protraction.

Parry (1959) shows that a very different example of a direct-actuation jumping mechanism is employed by saltacid spiders. It is suggested that the spiders manage to convert an applied hydraulic force (from *haemocoelic* blood pressure) into a rapid extension of their fourth pair of legs (Parry 1959). These spiders are also capable of accurate targeting, and can vary both the magnitude and velocity of their take-off (Hill 2001).
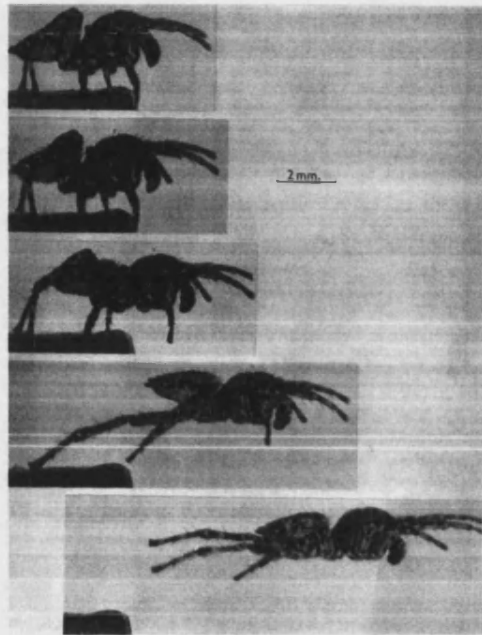
Fig. 10 – Take-off image sequence of a Saltacid spider (Parry 1959).

2.1.3.1.5 Power amplification mechanisms not used for jumping

There are other elastic storage mechanisms found in nature that are not used for jumping. For example, the Mantis shrimp, *Odontodactylus scyllarus,* is able to smash the shell of its prey by amplifying the power of its punch. It delivers a punch approximately 2-3 cm from its body in just 3 ms, thanks to high energy storage and release in its saddle-shaped exoskeletal spring and lever mechanism. The saddle, modelled as an orange spring in Fig. 11, is compressed slowly by muscles until a catch is engaged. When released, the two pivot points (shown as a red point and a white point in part c of Fig. 11) are forced to rotate in opposite directions as the spring rapidly

extends, considerably amplifying the force owing to the massive leverage (Patek, Korff *et al.* 2004).
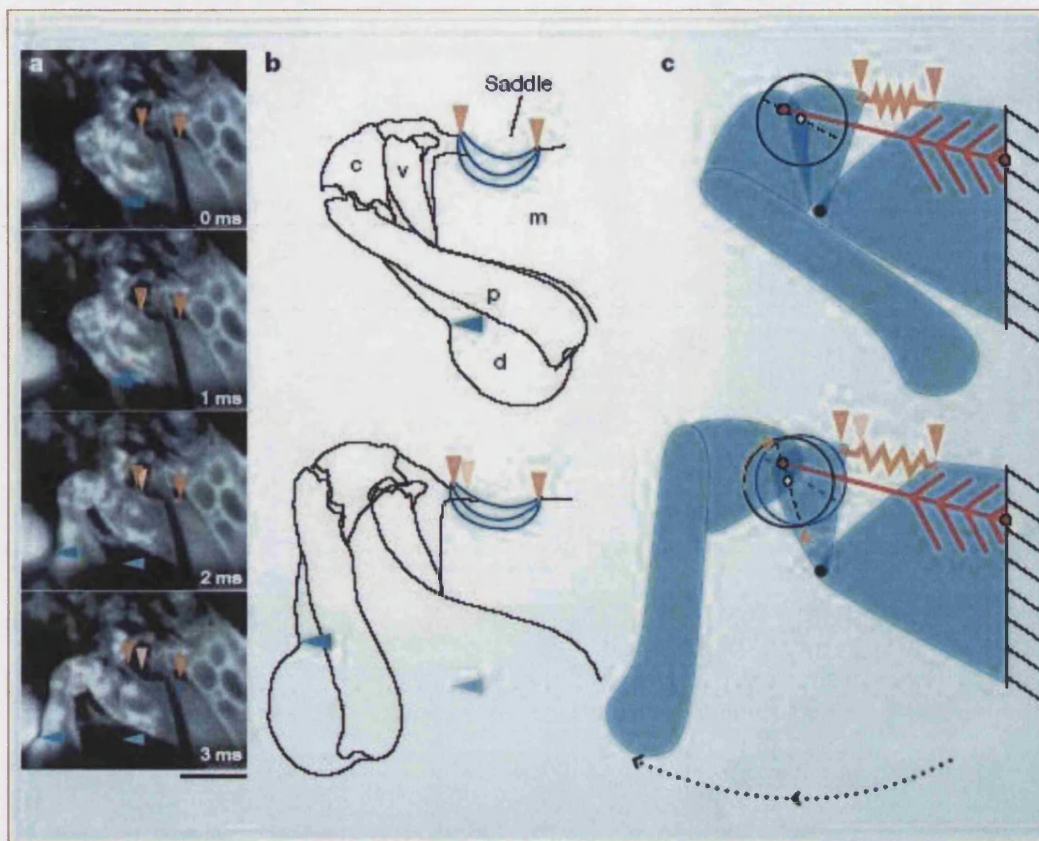
Fig. 11 – Mantis shrimp punch mechanism.
a, high-speed camera images, b, a sketch of the saddle-shaped elastic storage mechanism, and c, a mechanical model of the system. Here, the red point marks the attachment point of the rigid link between the punching arm and the body, which causes it to rotate sharply around the white point marking its centre of rotation. (Patek, Korff *et al.* 2004).

A chameleon's tongue also accelerates at a faster rate than could be achieved by muscle alone. Researchers have dissected chameleon tongues revealing an elastic collagen tissue sandwiched between the tongue bone and the accelerator muscle. They have discovered that this collagen structure is the biological catapult that propels the tongue tip in much the same way a bow delivers an arrow (de Groot and van Leeuwen 2004).

2.1.3.2 Hopping

Hopping refers to the repeated jumping used by some animals as a general means of locomotion. The smallest animals known to adopt this motion are kangaroo rats. This

apparent size limit may be related to the fact that as mass decreases, so the potential terminal velocity decreases, and hence there is less landing energy to retrieve. It is also fair to say that insects have simpler nervous systems and are therefore less able to control their landing. However, the point should be made that frogs have relatively quite sophisticated brains and yet often do not control their landing. Kangaroos provide the best example of hopping in nature, and can jump up to 13 m in a single hop and travel at nearly 65 km/h. The morphology of the kangaroo has clearly developed to improve its hopping locomotion, with its large hind limbs and feet relative to much smaller forelimbs, and a large tail that it can use as a counterbalance. When walking, at speeds less than about 6 km/h, kangaroos have very organised changes of gait between using the forelimbs, tail or hind limbs as supports. At higher speeds, they begin to bounce on their hind limbs, and remarkably, require less oxygen (and hence are using less energy) as speed increases to an optimum (Dawson 1973). This cruising tends to have a frequency of 2.5 hops per second, with each hop ranging from 0.7 – 6 m at a peak height of about 0.5 m (Bennet-Clark 1976). The reason for this is due to a very efficient storage of energy in their long Achilles tendons, which behave like springs and can store and release up to 70% of the energy from the previous jump. The hopping gait also leads to a better overall jumping performance, just in the same way that human beings are able to jump higher and further from a running rather than a standing start (Alexander 1974).
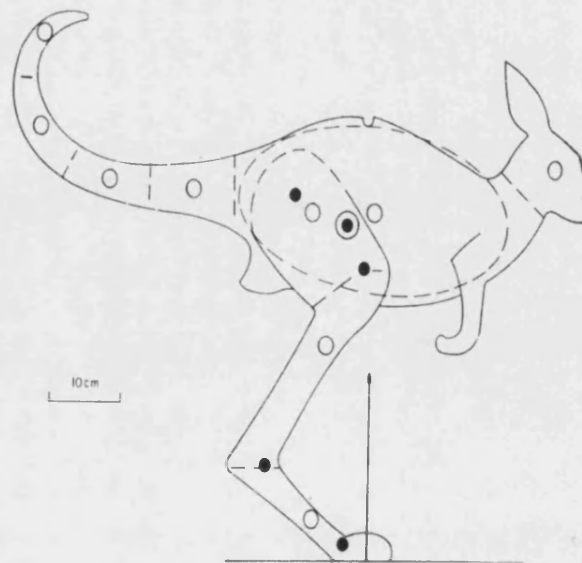
Fig. 12 – Outline drawing of a kangaroo at the moment when the force exerted on the ground is vertical (Alexander 1975).

Biewener *et al.* (2004) used surgical techniques to directly measure the forces and length variation in the tendons of wallabies during locomotion in the hopping gait. They observed that while the foot was in contact with the ground, the length of the major muscles remained almost constant with the tendons instead stretching and recoiling like springs (Biewener, McGowan *et al.* 2004). The frequency at which a kangaroo hops influences the maximum vertical displacement reached at the mid-point of each bounce. It is the slower, flat trajectories that are preferred giving the animal superior range with each hop and resulting in a longer contact duration with the ground, which is directly proportional to the ground reaction force (Blickhan 1989).

Some research has suggested that morphology favouring elastic energy recovery limits an animal's potential for mechanical power generation (Biewener 1998; Daley and Biewener 2003). However, yellow-footed wallabies were shown to generate substantial amounts of power, sometimes even in excess of the maximum capability of vertebrate skeletal muscle (McGowan, Baudinette *et al.* 2005). Rock wallabies approach high jumps at a steady velocity and with a relatively low angle of attack (45°-55°), a similar style to that of human high jumpers. The main difference in strategy for high jumping compared with normal hopping is that the leg stiffness almost doubles. The result is that more of the horizontal kinetic energy input into the jump can be converted directly into vertical kinetic energy.

Energy recovery is not just restricted to animals that hop continuously. In large animals, such as the dog, elastic elements of the leg are able to absorb much of the impact on landing (Alexander 1974). Most of the elastic energy is stored in tendons, which then contribute work towards the next movement.

In summary, two jumping patterns have been reviewed in this chapter, 'pause and leap' jumping or 'continuous hopping'. Continuous hopping has enabled some animals to recycle energy from each landing in a sequence of jumps, which requires a more sophisticated level of control than is necessary for the 'pause and leap' jumpers. Power amplification has been shown to be essential for smaller animals, but it is also usefully employed by larger animals such as horses. This generally relies on the pre-loading of energy into a catapult-like catch-release mechanism capable of a very high-speed action. In locusts and fleas, physical catch-release mechanisms can be observed, whereas power

amplification in larger jumping animals seems to rely on temporal catches, achieved through optimal usage of their specific biomechanical arrangements.

2.2 Gliding

2.2.1 Principles of Gliding Flight

Gliding is generally defined as unpowered flight. Given enough initial altitude, a free-falling object will eventually reach equilibrium, where the force generated by air resistance against its body is equal to its weight. At this point, it will no longer accelerate, continuing to fall at its terminal velocity. Any asymmetric body will experience the two perpendicular forces of *lift* and *drag* against it when moving through a fluid, where drag is a force against the direction of motion. Equilibrium is reached when the resultant of the lift and drag forces acting on the falling body are equal to its weight, as shown in Fig. 13.
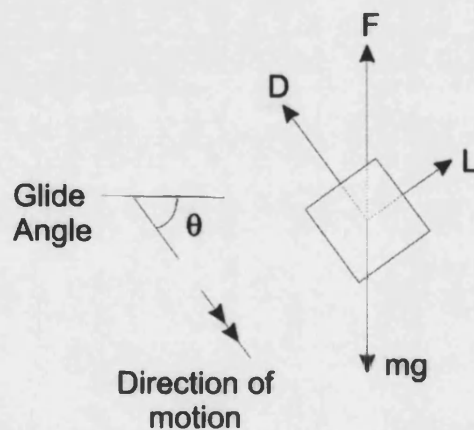
Fig. 13 – Free body diagram showing that the resultant of the lift (L) and drag (D) forces, F, must be equal to its weight (m×g) at equilibrium.

The angle of descent or *glide angle* (labelled θ in Fig. 13) can then be determined from the ratio of lift to drag forces by simple trigonometry as shown in Equation 10:

Lift to Drag ratio,

$$\frac{L}{D} = \frac{1}{\tan\theta}$$

Equation 10

In literature on aerial locomotion in animals, a generally accepted convention uses the Lift to Drag ratio to make the distinction between gliding and parachuting (Oliver 1951; Rayner 1991). Where L/D <1, the descent is at less than 45° to the vertical and this is defined as parachuting. An animal can be said to glide, therefore, only if it can achieve shallower descents (at angles of less than 45° to the horizontal, where L/D >1).

Shape is important in determining the amount of lift that an aerofoil will generate in a stream of air, as is the *angle of attack*, which is the relative angle of the aerofoil to the airflow. Both of these things were important discoveries at the turn of the 19th century by George Cayley. In what could be described as an early example of biomimetics, his work was inspired by watching birds gliding with their wings fixed in one position, and by examining the body-shape of the trout, which offers minimum resistance when swimming through water (Anderson 1978). Many years later, biomimetics was also the key to the next major advancement in aerofoil design. Otto Lilienthal studied the structure of bird's wings through dissections, and experimented with his findings to refine Cayley's cambered aerofoil towards the now familiar asymmetrical shape shown in Fig. 14.
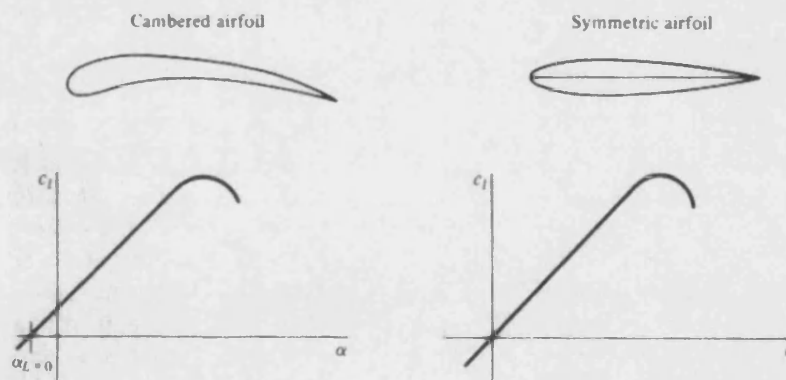
Fig. 14 – The approximate cross-sectional shapes of a cambered and a symmetrical aerofoil. Beneath are drawn their respective graphs for the coefficient of lift C_l against angle of attack, a. The cambered aerofoil can generate lift at negative angles of attack. (Anderson 1978)

In order to understand why shape is so important to the amount of lift generated by a surface, this review will briefly describe some basic aerodynamic principles. Except where stated, much of this long established theory was taken from the following book, *Introduction to flight its engineering and history* (Anderson 1978), which provides a

well-structured introduction to the topic. Consider the air flow around the cambered aerofoil in Fig. 14. Streams of air molecules striking the front of the aerofoil (the leading edge) will be forced to flow either underneath or over the top of it. Due to its cambered shape, air molecules flowing over the top surface of the aerofoil have to travel further than the equivalent stream following the flatter under-surface. As a result, they travel faster. At this point, it is necessary to digress slightly further to introduce Bernoulli's theorem.

Bernoulli did some experiments with airflow through a Venturi tube, which narrows to a *throat* in the middle as shown in Fig. 15. If a crowd of people were to walk down a passageway of this shape, they would naturally slow down and become more densely packed at the throat. However, Bernoulli discovered that the reverse is true for air. The velocity of the air is higher as it travels through the throat, and the pressure decreases. Consequently, he developed his theorem, fundamental to all aerodynamics, which states: *At any two points along the same streamline in a non-viscous, incompressible fluid in steady flow, the sum of the pressure, the kinetic energy per unit volume, and the potential energy per unit volume has the same value* (Anderson 1978).
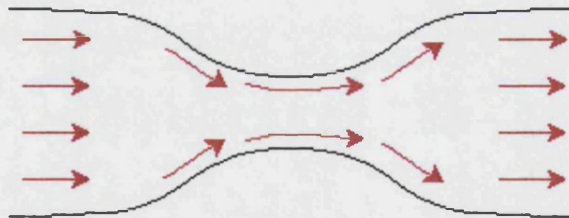
Fig. 15 – Diagram of a Venturi tube, in which air speeds up to get through the throat.

The consequence of the air flow being faster on the top surface of the wing is that the pressure is lower than that underneath – the aerofoil acts like half a Venturi tube with the other half open to the surroundings. This pressure gradient causes a force upwards in the aerofoil and is often referred to as *negative pressure*. Some lift is also generated by the positive pressure of the airflow striking the slightly cambered underside of the wing. Another consequence of positive pressure beneath a wing and negative pressure above it, is that air will inevitably spill up over the wing tips. The resultant vortices cause an *induced* drag in addition to the *friction* drag introduced earlier. It follows then, that as *aspect ratio* (A.R, the ratio of wing length or *span* to its width or *chord*) increases, the

effect of this induced drag decreases. It is likely that for this reason, gliding birds (discussed in Section 2.2.2, page 47) tend to have high aspect ratio wings (Savile 1962; Norberg 1990).

Increasing the angle of attack of an aerofoil in relation to the air flow causes an increase in the amount of lift produced as shown in Fig. 14 and Fig. 16. The relationship is linear until the wing stalls causing a rapid decrease in lift. Stalling is caused by *flow separation*, where due to the viscosity of the air and the skin friction of the wing, the air flow over the top surface of the aerofoil becomes detached and does not reach the trailing edge. This is also sketched in Fig. 16. This alters the *pressure distribution* around the wing such that the total lift is much lower, and the drag force much larger. The relationship between lift coefficient and the angle of attack depends to some extent on the cross-sectional shape of the wing. Fig. 14 demonstrates that the cambered aerofoil design is able to generate lift even at negative angles of attack.
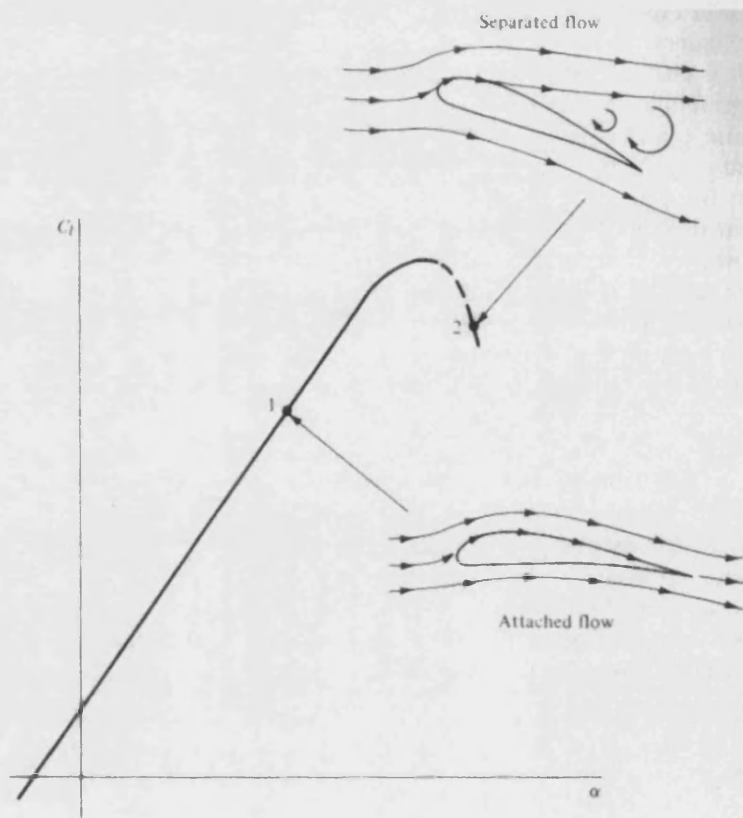
Fig. 16 – Graph of Lift coefficient against angle of attack for a cambered aerofoil, which peaks when the wing stalls. This is due to flow separation, as shown by the streamlines in separate diagrams of attached and separated flow (Anderson 1978).

Flow separation, and hence stall, is not just dependent on angle of attack, but will also occur when the air flow over the wing drops below a critical velocity. In order to glide more slowly, an increased wing area is required (Norberg 1990). The flow separation can also be postponed by adding slots to the wings. The air speed increases as it is forced through the slots, generating a jet of faster flowing air along the top surface of the wing (Savile 1962).

2.2.2 Gliding in nature

Gliding has been adopted as a means of locomotion by several species in five of the vertebrate classes. These classes are birds, fish, amphibians, reptiles and mammals, and certain examples from each are described below.

2.2.2.1 Birds

Birds generally flap their wings in order to generate the required lift for flight. The frequency with which they beat their wings is inversely proportional to their size, with the smallest examples, hummingbirds, flapping their wings at between 50 and 200 Hz (Tobalske, Altshuler *et al.* 2004). At the other end of the spectrum, some of the largest birds only use flapping intermittently to maintain a high enough speed for gliding with their large wings in a fixed position. This gliding in birds is usually referred to as *soaring*. Due to the high flight speeds and large wing areas required, soaring tends to be adopted by birds living in suitably sparse environments, such as mountains, deserts, plains and coasts. Vultures, *Catharsis aura*, birds of prey and many seabirds such as albatrosses, Diomedeidae, and gannets and boobies, Sulidae, are all examples of soaring birds, each having characteristic high aspect ratios. The best glide ratios (L/D) for birds of prey are 15:1 and 10:1 for vultures. The wandering albatross, *Diomedea exulans*, weighs around 9 kg and can achieve glide ratios of 23:1 (Norberg 1990).

In habitats where large aspect ratio is not advantageous, bird wings are smaller but have extensive slotting. This enables them to be able to generate extra lift and travel more

slowly without stalling (as described in section 2.2.1 on Page 43). Flexion of their wings allows birds to reduce their wing area and accelerate quickly, but at the expense of altitude. The success of birds is testament to the design of feathers. These have exceptional strength to weight ratio and resilience, whilst still permitting flexibility where required. The shape of the feathers allows the birds to manipulate the wingtips in flight, and open and close slots for superior control. However, feathers give birds yet another aerodynamic advantage by being several times more porous to downward moving air than upward through the wing. As a result, air is drawn through the top surface of the wing and released underneath during flight. Air flow over the wing which would otherwise be turbulent due to skin friction is more laminar because it's effectively flowing over a layer of air molecules (being sucked through the wing). This mechanism of reducing skin friction drag also used in the aircraft industry and is known as *Boundary Layer Control* (Savile 1962).

2.2.2.2 Fish

Flapping flight has been observed in two species of fish; the butterfly fish (*Pantadon*) and the flying hatchet fish (*Gasteropelecus, Carnegiella*) are able to beat their pectoral fins owing to relatively well-developed pectoral muscles (Davenport 1994). However, this review will focus on Exocoetidae, commonly referred to as flying fish, which have developed many specialisations towards gliding during their evolution.

There are two main types of exocoetid flying fish, two-winged and four-winged. Both have greatly enlarged pectoral fins, which are used to generate lift when held out of the water. The four-winged variety, *cyanopterus*, also have enlarged pelvic fins which contribute lift but also function as stabilisers in much the same way as the tail of an aircraft. These fins cannot be folded and are also required for swimming, so high aspect ratios are not possible but they are further specialised for flight in that the top surface is very smooth, with all the structural ribs placed on the lower surface (Breder 1930). Flying fish have a cigar shaped body with a flattened ventral surface which promotes extra lift during gliding. They also have a distinctive, asymmetrical hypocercal tail, the lower lobe being much longer and stiffened. This allows the fish to taxi across the surface of the water with its wings spread and almost all of its body above the water

level, propelling itself by oscillating the small piece of fin still in the water. The fish can therefore fly much faster, and it is thought that the enlarged, wing-like fins evolved to support this as an escape mechanism rather than specifically to allow gliding away from the water (Davenport 2003). Flight is energetically expensive for the fish, so it is not thought that it has developed to save energy in travelling long distances (Davenport 1994). Another reason for this is hypothesis is that when not taxiing, the position of the centre of mass in two-winged flying fish, *exocoetus*, is such that it naturally wants to pitch upwards and stall. The enlarged pelvic fins of the four-winged flying fish compensate for this, and are likely more recently developed.
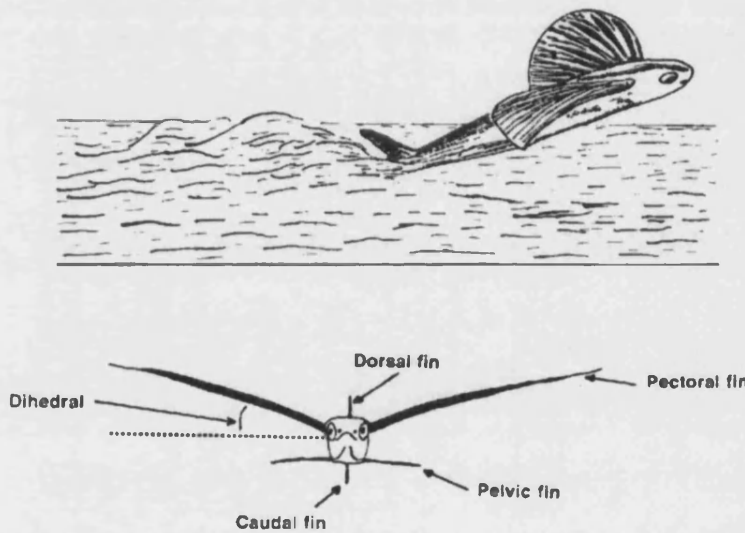
Fig. 17 – Lateral sketch of a cypselurid (four-winged) flying fish taxiing, with a front view of its gliding position below, demonstrating the relative positions of all the fins (Davenport 1994).

The ability to accelerate away from danger very quickly and leave the water entirely before re-submerging somewhere else is clearly a useful response to threat, although it is much more effective at night when the predator cannot follow the prey's shadow. The typical behavioural pattern of flying fish is as follows. They swim at high speed (approximately 10 ms^{-1} or 20-30 body lengths per second) keeping their fins close to their body immediately prior to take-off, leaving the water at about 30°. Momentarily, the entire fish is out of the water, before the base of the tail fin re-enters and beats rapidly (50-70 strokes per second) during the taxi phase. After this they pitch upwards and leave the water entirely, gliding on their wings which are positioned in a slight *dihedral* (V-shape) for superior stability but at the expense of lift. A common

misconception is that Exocoetidae flap their wings, because of the noise they make during flight. However, the whole fish is actually rolling from side to side around its longitudinal axis at high frequency. This means that as one wing tilts upwards, the other is tilting downwards, ruling out flapping flight (Breder 1930). It has also been demonstrated that flying fish will almost always fly into the wind. At heights of below 0.5 m from the water, it has been shown that the flying fish take advantage of *ground effect,* the generation of extra lift due to the proximity of the wings to the water's surface (Davenport 1994). They can reach heights in the region of 8 m above sea level and travel up to 300 m in 30 s in a single jump by repeated taxiing. Controlled re-entry is possible because flying fish draw their pelvic fins forwards at the end of flight, maximising drag like air brakes on an aircraft.

Another specialisation of these flying fish are their eyes, which are large and the cornea has a flattened pyramidal shape to allow focus in both water and air. (The usual curved cornea of most fish species would result in short-sightedness in air). Additionally, the head of the flying fish has an inverted triangular shape when viewed from the front, optimised for looking down at the water during gliding. Unlike other gliders, body size varies a great deal within species, ranging from juveniles of a few cm, to examples close to 40 cm in length. The wing loading (weight per unit area of wing surface) is comparable to that of birds and bats, and in the case of the largest flying fish, similar to that of cormorants or pelicans (Davenport 1992).

2.2.2.3 Amphibians

Among amphibians, only frogs have been shown to exhibit aerial locomotion. However, this would be classified as parachuting rather than gliding because the glide angle is steeper than 45°. The Malayan frog, *Rhacophorus nigropalmatus*, has lateral flaps of skin on its limbs and long, fully webbed toes. The ability of a frog to parachute was shown to be primarily behavioural in a study by Cott (1926). He compared a Brazilian tree frog, *Hyla* venuosa, with two comparable European frogs, a common terrestrial frog, *Rana temporaria*, and a tree frog, *Hyla arborea*. The Brazilian frog was dropped from 43.7 m and always managed to stretch its limbs out to the side and keep its belly downward, parachuting to land at a point 27.4 m away from the vertical line. The

European frogs, however, were frantic during their vertical fall, turning over and over and landing hard (Oliver 1951). At the time of writing, no data exists to quantify by how much this unique morphology is able to reduce the landing impact forces of the flying frogs. Emerson and Koehl (1990), experimented with models of the flying frog in a wind tunnel, and concluded that their evolution was directed more towards improving manoeuvrability than maximising horizontal range. This is contrary to the observation by Savile (1962) that steering capability would be of little use because the frog is short-sighted.
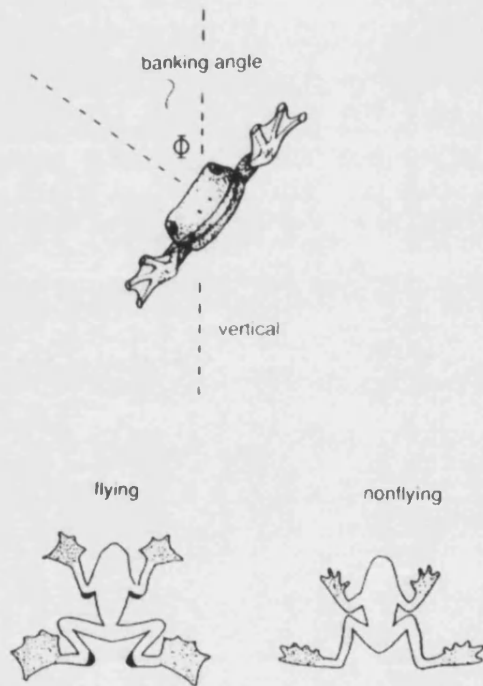
Fig. 18 – Front view of a flying frog performing a banking manoeuvre, followed by top views of a flying frog with its webbed appendages positioned for flying and nonflying locomotion (Emerson and Koehl 1990).

2.2.2.4 Reptiles

The most famous gliding reptile is undoubtedly the gliding lizard, Draco, with its dragon-like appearance when the wings are deployed and its long tail. Fig. 19 shows both a dorsal and a ventral sketch of Draco, which - like many other gliders - is found in the forests of South East Asia.
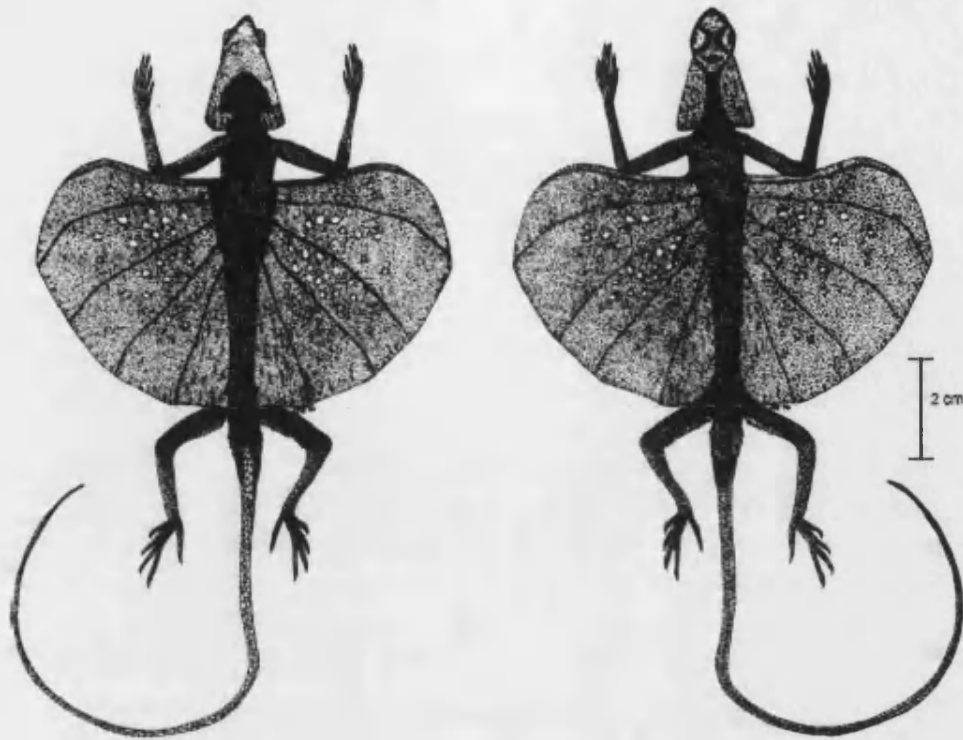
Fig. 19 - Dorsal and ventral views of Draco (Shine 1998).

An example glide trajectory for a large, *Draco fimbriatus* (mass 21.6 g), and a small species of Draco, *Draco melanopogon* (mass 2.95 g) are shown in Fig. 20 (McGuire and Dudley 2005). Both examples are clearly gliding (the glide angle is shallower than 45°), but the smaller of the two species is able to achieve superior performance.
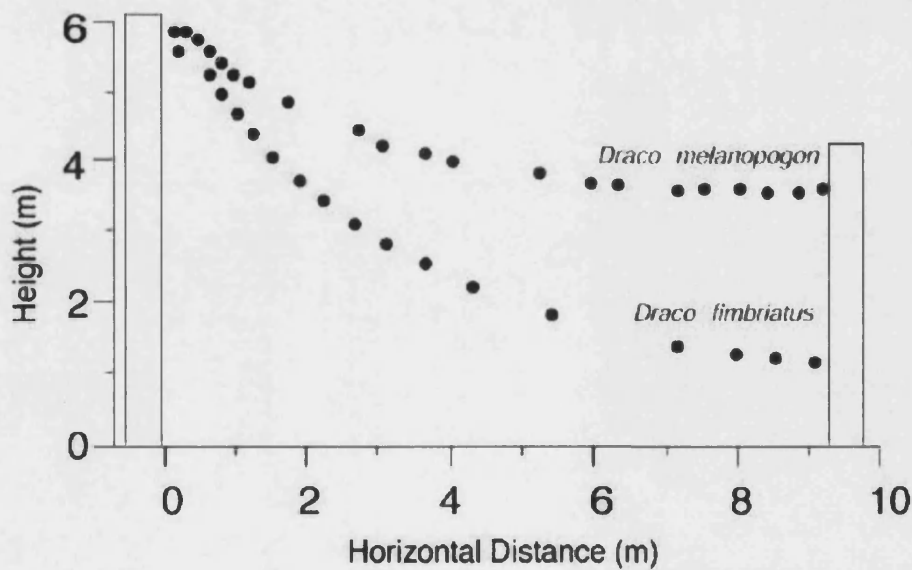
Fig. 20 – Example glides for a large, *Draco fimbriatus* (mass 21.6 g), and a small species of Draco, *Draco melanopogon* (mass 2.95 g) taken from McGuire (2005).

Most of the world's specialist gliders live in either South or Southeast Asia, the latter being home to a small group of tree snakes that remarkably choose to glide. They take-off by rapidly uncoiling themselves from a branch, and then flatten their entire body into a characteristic s-shape as shown in Fig. 21. This presumably maximises their surface area for lift generation, enabling them to glide to the ground or another tree to avoid predators, or chase aerial prey. In tests from a take-off branch of height 9.62 m, the flying snake, *Chrysopelea paradisi,* reached a minimum glide angle of 28±10° (Socha, O'Dempsey *et al.* 2005).
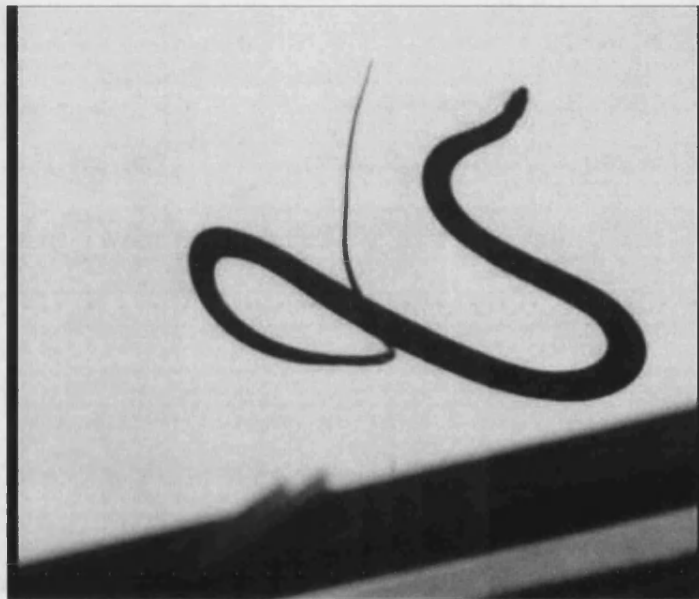
Fig. 21 – Flying snake gliding in its distinctive s-shaped posture and flattened body, viewed from below. This picture was taken from www.flyingsnake.org .

2.2.2.5 Mammals

The only mammals capable of flapping flight are bats, which are not as sophisticated as birds, and hence tend to be small, slow flyers. Red squirrels are able to parachute in much the same way as the gliding frogs, by stretching their legs out and holding them steady, maximising the surface area resisting the fall. It is believed that this behaviour is a pre-cursor to the evolution of true patagia, as found on flying squirrels and many other similar mammals such as colugos and flying oposums (Savile 1962). The patagia is a larger and more developed piece of skin attached between the wrists and ankles, and

enables these mammals to glide at shallow angles, and also make impressive manoeuvres such as 180° turns. For these reasons, and because flying squirrels have evolved great versatility in locomotory mode (being able to walk, run, climb, jump and glide), they have been selected for further study here. In addition, northern flying squirrels often weigh over 200g, and similar species in South East Asia (such as the Colugo, and Japanese Giant Flying Squirrels) are much larger and heavier, so a robot designed using the same principles should be able to carry a reasonable payload and not run into any problems with scaling. In the following chapter, (Chapter 3, on page 81), experimental work will be described giving the initial reason for their divergence from non-gliding squirrels. Afterwards, their patagia will be investigated to see if this is noticeably different from normal mammalian skin (Chapter 4, page 111).

2.2.3 Low Reynolds Number, Low Aspect Ratio Aerodynamics

In comparison with high-speed passenger planes, birds, gliding animals and micro-air-vehicles (MAVs) are operating at low Reynolds numbers, (normally less than 2×10^5). Reynolds number is an important dimensionless value, calculated from the density (ρ), viscosity (μ) and relative velocity (V) of a fluid in freestream conditions, and the local distance along the surface of interest (x) as shown in Equation 11 (Anderson 1978).

$$\mathrm{Re}_x = \frac{\rho_\infty V_\infty x}{\mu_\infty}$$

Equation 11

Classical aerodynamic theory is accurate for high Reynolds numbers in the region of 1×10^7, but has been found to be inadequate for dealing with low aspect ratio wings (A.R < 2) at low Reynolds numbers (Torres and Mueller 2004). A robot that jumps into a glide will not reach very high speeds, and hence low Reynolds number aerodynamic theory applies. Therefore it is necessary to review this area, which after some brief interest early in the twentieth century has only recently begun to receive much attention with the introduction of MAVs. The performance, such as maximum lift to drag ratio, of standard aerofoil shapes has been shown to be vastly reduced at low Reynolds numbers,

primarily due to laminar boundary-layer separation (Pelletier and Mueller 2000). The free shear layer does not normally change to turbulent flow in time to reattach to the aerofoil surface and as soon as this separation point reaches the leading edge, the wing is stalled (Mueller and DeLaurier 2003).

Low aspect ratio has some potential advantages, such as the ability to fly more slowly without stalling, and a more useful internal volume. Structural strength and impact tolerance are also superior. The main disadvantage is the much larger induced drag, caused by air leaking over the much larger wingtip. Original work by Zimmerman (1935) showed that the performance of low aspect ratio wings was highly dependent on planiform shape, that is, the top view of the aerofoil. This work was extended by Torres and Mueller (2004), who experimented with the planiform shapes drawn in Fig. 22. The most efficient shape for aspect ratios of less than 1 was the inverse Zimmerman at high angles of attack. In other conditions, the elliptical shape produced more favourable performance.

Fig. 22 – Low aspect ratio planiform shapes tested by Torres and Mueller (2004)at low Reynolds numbers. In this diagram, the top surface of the shapes is the leading edge.

Torres and Mueller (2004) have also shown that the linear relationship between coefficient of lift and angle of attack no longer applies at aspect ratios below 1.5. Here the wing can be seen to have two sources of lift, linear and non-linear. The former is the

lift considered previously, created by circulation around the aerofoil, and the non-linear lift is created when the wing-tip vortices form cells of low-pressure on the top surface. As a result, there is a non-linear increase in lift with angle of attack, allowing flight at much higher angles of attack before stalling. The location of the centre of lift was shown to move towards the rear of the wing with increasing angle of attack.

Present knowledge suggests that at low Reynolds numbers, low aspect ratio wings can fly more slowly without stalling and are inherently more stable. However, they are strongly disadvantaged by the need to fly at high angle of attack in order to achieve acceptable lift/drag performance (Mueller and DeLaurier 2003).

2.2.3.1 Rigid vs. Flexible Wings

At low angles of attack (below 6°) flexible wings do not generate as much lift as rigid equivalents. At 15°, the lift coefficient is still 2% lower, but the flexible wing generates a lift to drag ratio 1.5% larger due to the high frequency vibrations produced. This vibration causes an effective shape change with a beneficial increase in effective camber, but a reduced overall angle of attack. With careful optimisation, flexible wings have the potential to outperform rigid wings at low aspect ratio and Reynolds number (Shyy 2005).

2.3 Robots

2.3.1 Overview of Exploratory Robots

The size-grain hypothesis was introduced in the previous chapter, explaining that as robot size decreases, the relatively size of obstacles in its surroundings increases. This is particularly relevant to wheeled robots, which although simple to control, struggle to cope with irregular terrain because they can only drive over objects of up to half their

wheel diameter. Some intelligent designs have managed to improve this performance, the best known at the time of writing being the SHRIMP 'high mobility wheeled rover' shown in Fig. 23 (Estier, Crausaz *et al.* 2000). This is able to pass obstacles of up to twice its wheel diameter and even climb stairs thanks to an independently driven front wheel on an articulating front fork. This fork has spring suspension to ensure optimal ground contact, and will simply rise up and over any obstacle smaller than twice its wheel diameter. All the wheels are driven, and the two bogeys on each side have deliberately high ground clearance to prevent grounding.
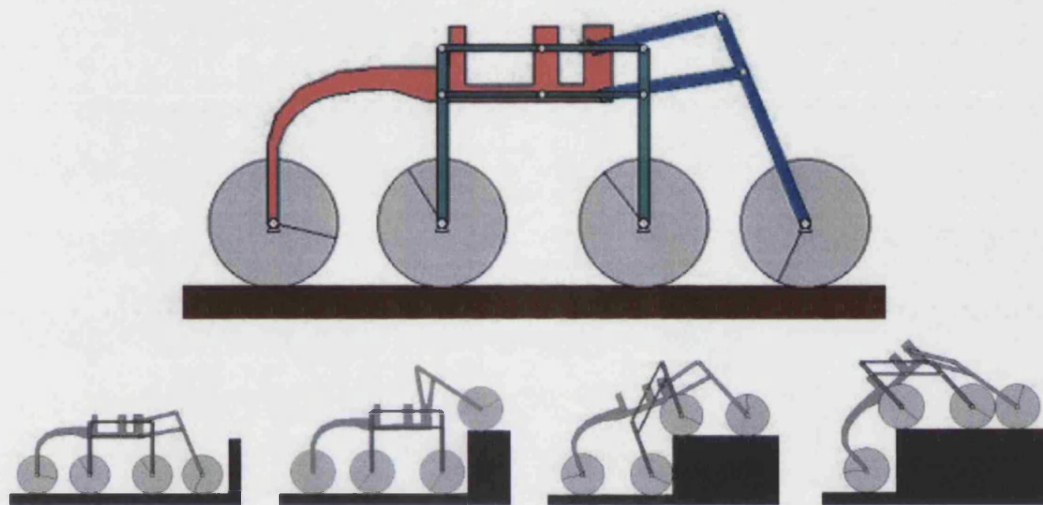
Fig. 23 – Side view of the 6 wheeled rover, SHRIMP, designed at the Autonomous Systems Lab at the Ecole Polytechnique Federale de Lausanne. The front of the robot is the blue articulated wheel. Below is a sequence of images demonstrating how it manages to pass obstacles of more than its wheel diameter (Estier 2000).

Walking robots are generally more successful than those with wheels when travelling over rough terrain for the same reason that all terrestrial vertebrates (except snakes) have legs. Body pitches can be used to swing the front legs up high and onto the top of a surface, dragging the remaining legs up behind them. However, traditional walking robots have been difficult to control due to the use of separate actuators for each leg and others for pitching moments. Much effort has been spent in reducing the number of actuators in such robots, for weight reduction amongst other things. One such example is the K2T Inc. crab robot, which uses a drive chain of clutches and cables to control 17 joints with 5 motors (Quinn 2002). Following on from these, the Whegs[TM] series of robots use just 1 drive motor. Whegs, or wheel-legs are driven like wheels, but consist of three equally spaced, compliant leg spokes. Two and three axled versions have been

built, and are able to move quickly over irregular ground. When encountering large obstacles, passive gait adaptation is achieved by a compliant drive mechanism, allowing the two front whegs to synchronise and hence reach further up and hopefully over the obstruction (Schroer 2004).
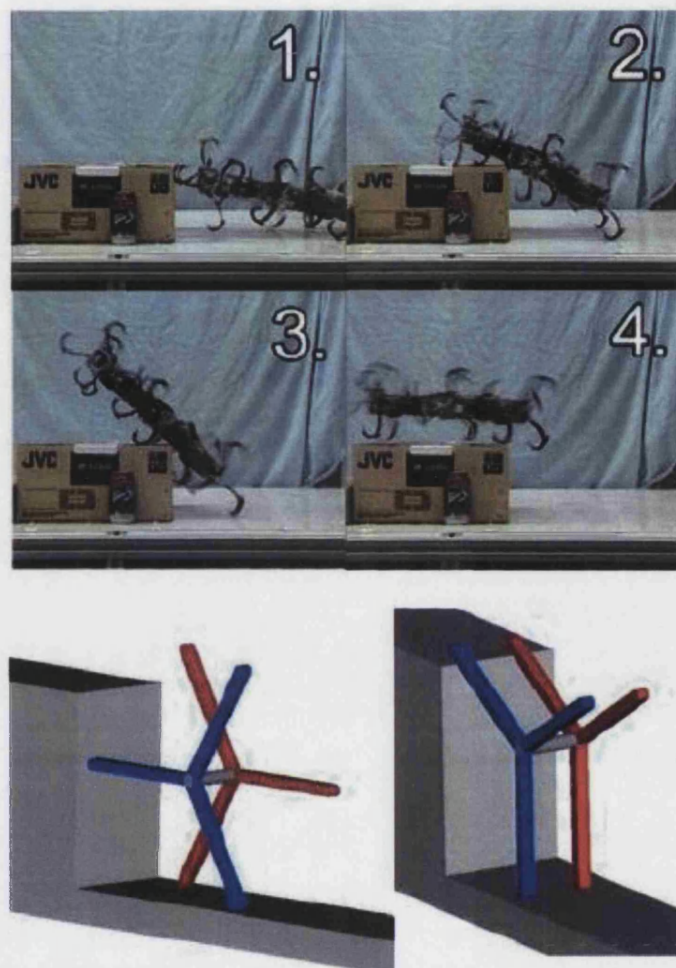
Fig. 24 – Top: Sequence of images showing the Whegs VP robot climbing an obstacle 7 inches high. Bottom: Diagram showing how compliance in the drive of the whegs allows for superior climbing performance (Schroer 2004).

The locomotion of walking robots resembles that of some insects, such as cockroaches. However, there is still a maximum size of obstacle which they can successfully get over, and this is dependent on the leg length. Many insects are also equipped with an alternative locomotory mechanisms, such as sticky feet for climbing vertical walls or walking upside down, wings for powered flight or a jumping mechanism. Jumping mechanisms were introduced in some detail in section 2.1.3 of this thesis (beginning on page 26). Recently, jumping has been introduced to some robots as an alternative means

of locomotion over rough terrain; examples are described in the following section. Another obvious solution to the rough ground problem is to fly over it, and many small flying robots, (micro air vehicles: MAVs) have been developed, which will be discussed in Section 2.3.3, on page 70. Finally, the latest planetary exploration robots to be successfully operated away from Earth will be introduced in Section 2.3.4 (page 73).

2.3.2 Jumping Robots

Although kangaroos and most of the jumping insects reviewed in this thesis have two jumping legs, they are not used independently in this gait and so for robotic design the system should still be considered as a monopod. Very few robots have been developed that can jump, with the majority of research effort in this area focussing on the complex stability control required for a device to make successive hops. At the time of writing, all of the projects reviewed have investigated one-legged models of jumping, whether the robot be designed to pause and leap or hop around continuously. Of course, the only possible way for a monopod to move around is by jumping. The robots will be classified as either 'pause and leap' or 'continuous hopping', depending on which of these two jumping strategies found in nature that they more closely resemble.

2.3.2.1 'Pause and Leap' robots

2.3.2.1.1 JPL Hopper

The most sophisticated robotic jumper to date is probably the 'Minimally actuated hopping rover for exploration of celestial bodies' built in collaboration with NASA in the Jet Propulsion Laboratories (JPL) at the California Institute of Technology (Hale 2000). Its designers experimented with alternative jumping mechanisms, with the underlying goal of minimising the number of actuators. They showed that it was possible to use a single actuator to control both the jumping and directional operations, as well as being able to pan an on-board camera. In the final design, the energy for

jumping was stored in the tension of a steel tension spring, mounted in a 6-bar linkage geared mechanism.
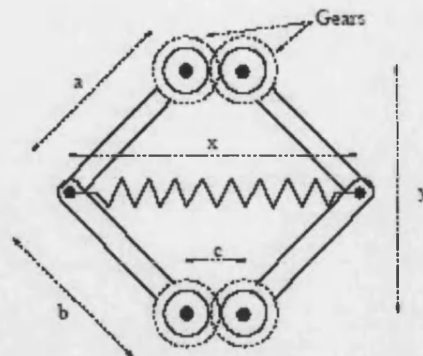
Fig. 25 –Sketch showing the mounting of the steel tension spring horizontally within a 6-bar linkage mechanism in the JPL hopper. (Hale 2000)

The reason for the design of this linkage is to produce a steady build up of leg thrust with increasing leg extension, which reduces the chance of premature lift-off (after which all further stored energy in the system is wasted). This robot was designed for space applications, and as such, the actual jumping performance on earth is unexceptional. However, the vertical height reached of 0.9 m, and the consequent horizontal range of 2.0 m would both be improved if jumping was taking place on a planet or moon with a lower gravitational field. Additionally, the final design shown does seem to have a second actuator for the self-righting mechanism (Hale 2000; Burdick and Fiorini 2003).
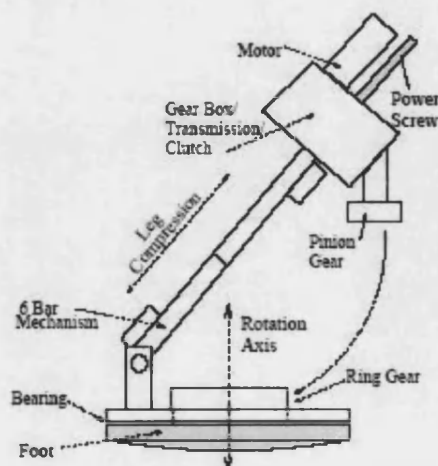
Fig. 26 – Schematic drawing of the JPL hopper. This is a single-actuator jumping robot with mass concentrated in the motor and transmission, which is compressed from the top right to the bottom left of this figure. Take-off angle is determined by rotation of this whole mechanism relative to the foot. (Hale 2000)

2.3.2.1.2 Monopod

Another robot to store energy in metal coil-springs (this time in compression), Monopod was developed by Allison (2002) at the University of Utah in order to compete in three events at the 2002 Robo-Olympics: the high jump, long jump and obstacle course. The spring is compressed by driving a ball-screw mechanism with an integral clutch allowing rapid release of this relatively massive element upward and away from the foot. This robot does not need to be remote controlled as it is complete with a controlling microprocessor, all the necessary sensors and an onboard power source. This robot weighed 2.4 kg, but was still able to achieve a range of 30.5 cm while reaching a maximum vertical height of 51 cm in the process.
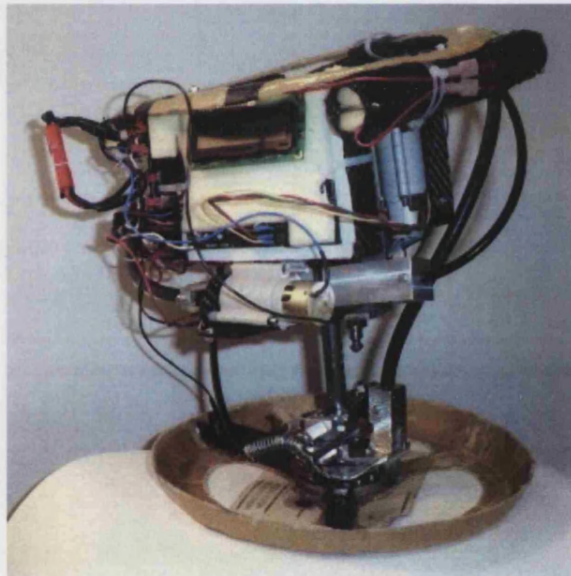
Fig. 27 - Monopod Jumping Robot (Picture courtesy of James Allison)

2.3.2.1.3 Jumping mini-Whegs

A third robot to store its energy in a metal coil-spring (in tension) is Jumping Mini-Whegs^{TM} (Fig. 28). This robot is particularly versatile because jumping is an additional transport mode to the walking wheel concept of the Whegs series of robots, as introduced previously in this chapter. These allow it to move quickly over smooth ground, but it can also get over larger obstacles thanks to its jumping apparatus. A motor closes the four-bar linkage shown in Fig. 28, causing the coil spring to extend.

This is then released automatically when the spring reaches full extension. The current evolution of this design weighs 191 g, and is able to reach a peak jump height of 19 cm. It is also possible to steer the whegs at the front of the robot (like car wheels) to achieve direction control during either form of locomotion.
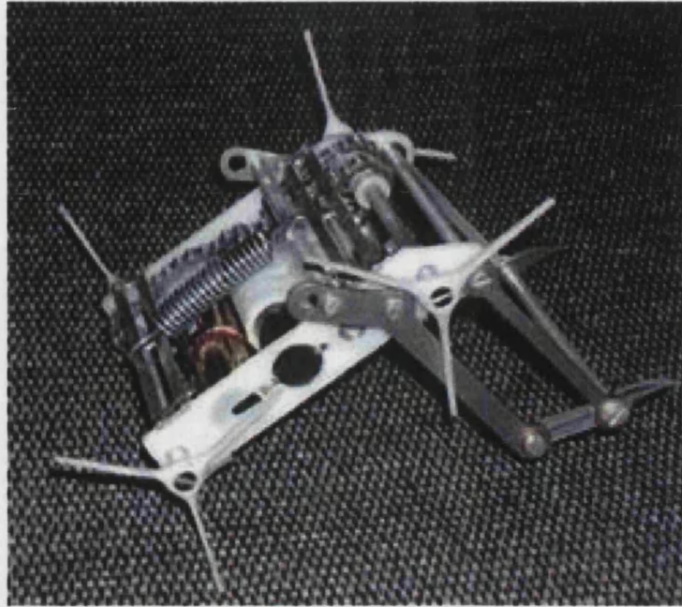
Fig. 28 – Jumping Mini-WhegsTM. Picture copyright of Case Western Reserve Universtiy (2006).

2.3.2.1.4 Scout robot

Another jumping robot that adopts the 'pause and leap' strategy was built as a design solution to the tricky problem in robotics of climbing stairs. Stairs provide a difficult challenge to robots that are intended for search and rescue in hazardous urban environments. Stoeter and Papanikolopoulos (2005) investigated ways of closing the control loop to allow miniature scout robots to be fully autonomous in this application. A 12 cm long cylindrical robot was built with toothed wheels at each end, which stores energy by bending a sprung metal foot for jumping (Fig. 29). Despite its small size, it is able to carry a camera and analogue video transmitter, but with an average staircase having 13 stairs it is a slow climber due to the time required to winch the foot in. (This mechanism is not described in the paper, but it is presumably the traditional winch design of a wire - attached at one end to the foot - being wound around a motorised pulley.) Servomotors automatically control the launch angle of the robot, which deliberately positions itself a distance back from the step equivalent to half of its horizontal range, such that it will be at the peak of its trajectory as it reaches the step

(Stoeter and Papanikolopoulos 2005). It can successfully climb most staircases owing to a peak jump height capability of 30 cm.
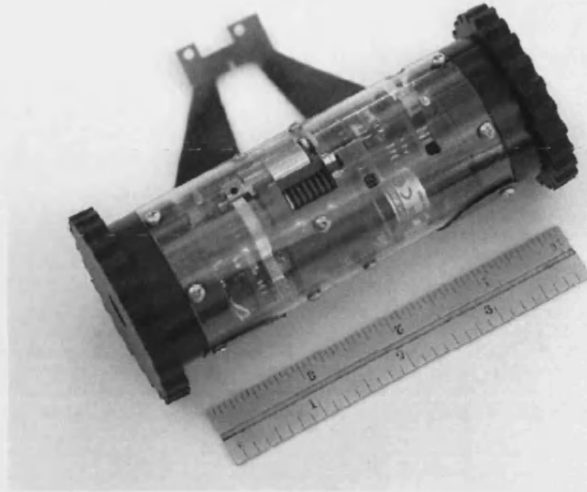
Fig. 29 – Scout robot (Picture courtesy of University of Minnesota)

2.3.2.1.5 Deformable jumping robot

So far all the jumping robots reviewed have been able to jump by storing energy slowly in the bending of spring metal, and releasing it rapidly to amplify the power. To date, only one jumping robot has been developed which stores energy in an elastomer, which was developed at Ritsumeikan University in Japan and will be referred to in this thesis as Deformable. This circular robot (40 mm diameter) is made up of shape memory alloys (SMA), which can be contracted by applying appropriate voltages to one half of its actuators, causing it to buckle and storing energy in its rubber shell. Extending these SMA actuators again causes the rubber wheel to quickly return to its original form and the resultant shift in centre of mass causes it to leave the ground, reaching a peak clearance height of 8 cm (Fig. 30). However, the application of this technology is so far limited given that it only weighs 3 g but requires a much heavier cable tether to supply the necessary voltage to the SMA actuators.
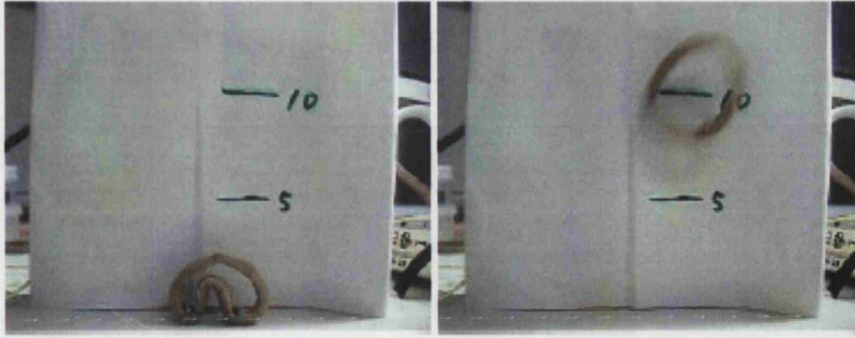
Fig. 30 – Deformable jumping robot reaching a clearance height of approximately 8 cm. (courtesy of Ritsumeikan University, Japan).

2.3.2.1.6 Sandia hopper

The US Sandia National Laboratory have developed a 'hopper' that is powered by the combustion of hydrocarbons that fire a piston into the ground to generate the take-off force (Fig. 31). Like the above NASA robot, this is a 'pause and leap' jumper, trying to maximise its jump energy, but then hitting the ground in an uncontrolled landing and self-righting afterwards. It is entirely contained inside a small, plastic shell and shaped something like the children's toy Weeble®, so that it naturally rights itself after each jump. In this position, the piston points towards the ground but slightly askew from the vertical. This means that directional control can be achieved by rotating these internal mechanisms according to a compass. The combustion chamber then fires, the piston punches the ground, and the hopper leaps. The performance claimed for this robot is a jump height of just under 1m, and that a full tank of gas (approx 20 grams of fuel) is enough for the jumper to travel up to five miles. The versatility of this design is demonstrated by the fact that an alternative version can be made to jump 3 to 5 metres in the air, by combusting a larger volume of fuel for each jump. The advantage of this combustion design comes from the high energy density of hydrocarbons, which are compatible with small size applications and allow much higher jumps to be achieved than would be possible with simpler mechanical spring systems. However, even though planetary exploration is suggested as a possible application, no mention is given to the fact that the fuel requires an oxygen based atmosphere to burn. An oxidizing agent could be used as fuel in a reducing atmosphere however, or an explosive in an inert

atmosphere or vacuum, but the life of these robots is limited by the finite amount of fuel in the tank (German 2000).

Fig. 31 – Photo of the working part of the Sandia hopper. This is mounted in a hemispherical shell which is weighted like a Weeble® toy to ensure that the piston always fires downwards for jumping.

2.3.2.1.7 Airhopper

The other jumping robot to store its energy for jumping in a fluid is Airhopper (Tokyo Institute of Technology), which relies on the expansion of compressed air to rapidly fill and extend pneumatic cylinders. Each leg is made up of a four bar linkage and driven by two individual pneumatic cylinders (Fig. 32). This robot was designed to be use in earthquake search and rescue operations, and is able to clear a height of 68 cm even though it weighs 20 kg, far heavier than any of the other jumping robots reviewed (Kikuchi, Ota *et al.* 2003).
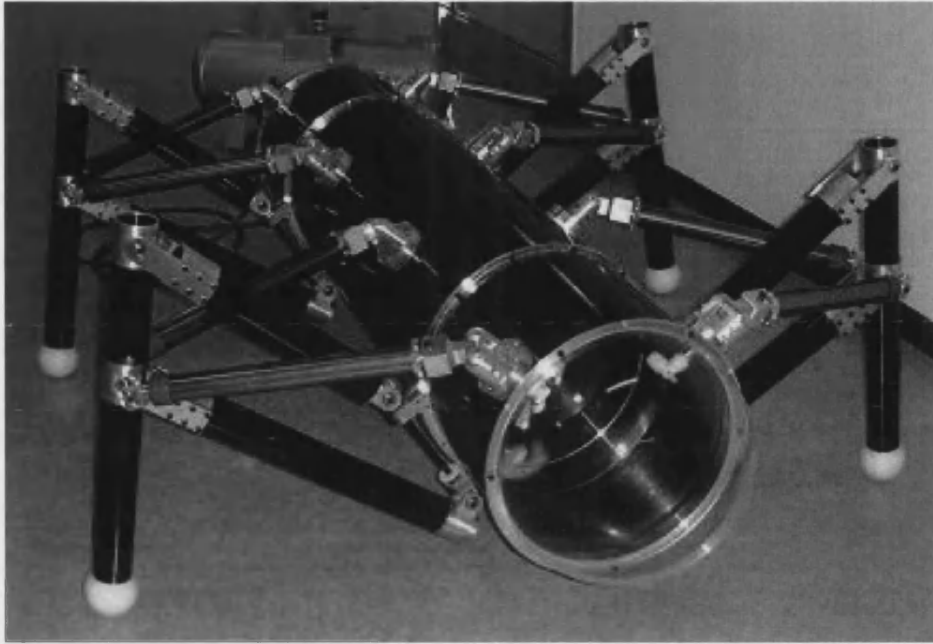
Fig. 32 – Airhopper jumping robot. Photo courtesy of the Tokyo Institute of Technology, Japan.

2.3.2.1.8 Pendulum

The final 'pause and leap' style jumping robot studied at the time of writing this thesis jumps by rapidly swinging a pendulum, and so is in some way comparable to the 'flip' jumpers discussed in Section 2.1.3.1.3, page 34. Fig. 33 shows a sketch of this robot, which sits on a flat foot, and has a pendulum arm mounted at the top of a central pole. A servo motor swings the pendulum which causes the whole structure, (720 g), to leave the ground by 6 cm. A similar robot successfully employed multiple counter-rotating pendulums to climb some small steps. However, it should be noted that the pendulum robots did not have their power sources onboard, and had no control over their direction (Hayashi and Tsujio 2001).
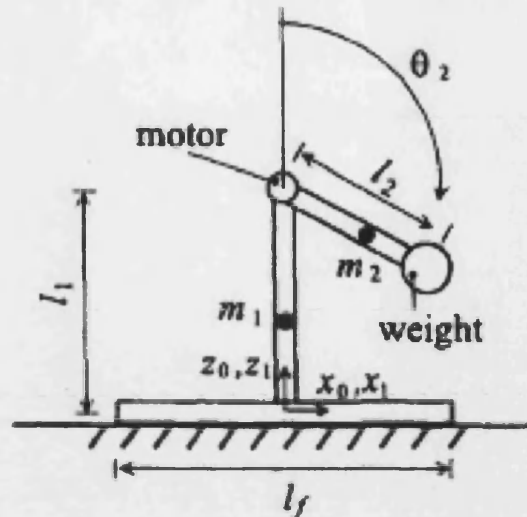
Fig. 33 – Pendulum driven jumping machine (Hayashi and Tsujio 2001)

2.3.2.2 Hopping robots

Some research has been carried out that looks into robots that hop continuously, rather than pausing and leaping. The advantage of this system is that the mass is not such a critical issue, allowing more batteries to be mounted on-board. Alexander (1990) shows that running animals can save energy and reduce unwanted heat production by bouncing along on springs, principally the tendons (Alexander 1990). Further energy savings are made from the use of return springs that halt the legs at the end point of the swing, and by using compliance in the feet. Fig. 34 shows how return springs would look on a hypothetical robot. All of these ideas could be applied in robotics, but so far most of these projects seem to have focussed on the complex stability-control operation required for balance. This means that for every hop in the sequence, the centre of mass and the position of the leg must be accurately controlled during flight ready for impact (De Man; Zeglin 1998; Kuswadi, Ohnishi *et al.* 2003; Vermeulen 2003). As a result, none of the machines are fully autonomous, with some needing help starting and others requiring external power supplies, etc. The Kuswadi design, for a specific example, resembles a pogo stick but requires an umbilical power cable to allow pneumatic actuation to be employed. In its current state it is only able to rotate around a central axle due to a rigid linkage designed to keep the robot upright.
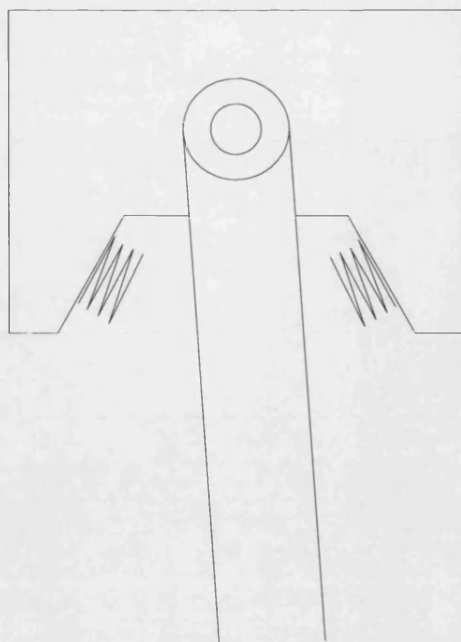
Fig. 34 - Diagram showing how return springs might be used to help maintain the swinging of a leg in a hypothetical robot.

The design of a monopod robot for continuous and stable forward hopping requires accurate control of the leg angle. It is therefore necessary to maximise the ratio of body inertia to leg inertia in order to reduce body pitching during the leg swing, because only the relative angle between the body and the leg can be actuated. As a consequence of this, and a need to keep the overall mass of the system as low as possible, most of the hopping robots look very similar: a horizontally long body with the mass concentrated at the ends, as in Fig. 36 (Gregorio 1994). This weighs 15 kg and a tethered running speed of 1.2 ms^{-1} is reported.
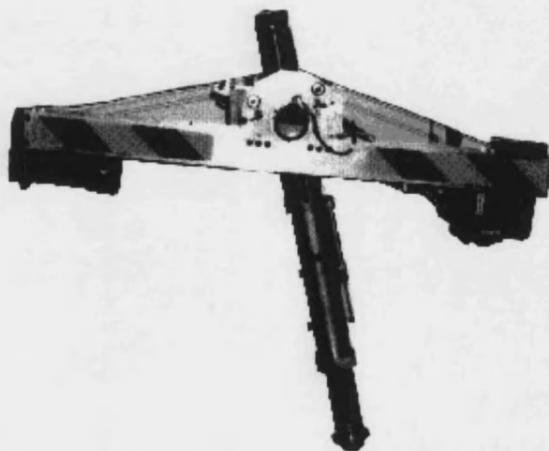
Fig. 6 - Photograph of an example hopping robot, which typically comprise of a single leg supporting a horizontally orientated body. This example is called Prismatic Planar Hopping Robot and was developed in the Department of Mechanical Engineering at McGill University, Montreal, Canada. (Gregorio 1994).

Another such hopping robot is the 3D Bow Leg Hopper, which takes advantage of a flexible, arc-shape leg to store energy from each landing as it hops continuously. The centre of mass is right above the leg for accurate control of the body with limited actuation. The robot uses feedback from distance sensors and gyroscopes to control servo motors that move counterweights in order to actively balance the body during flight (Zeglin 1998). Experiments with this robot mounted on a boom as shown in Fig. 35 reported recovery of 70% of its energy between successive hops reaching a peak height of 50 cm. The total mass of this machine was 4 kg including 3 kg of ballast boom weight and a running speed of 1 ms^{-1} has been achieved.
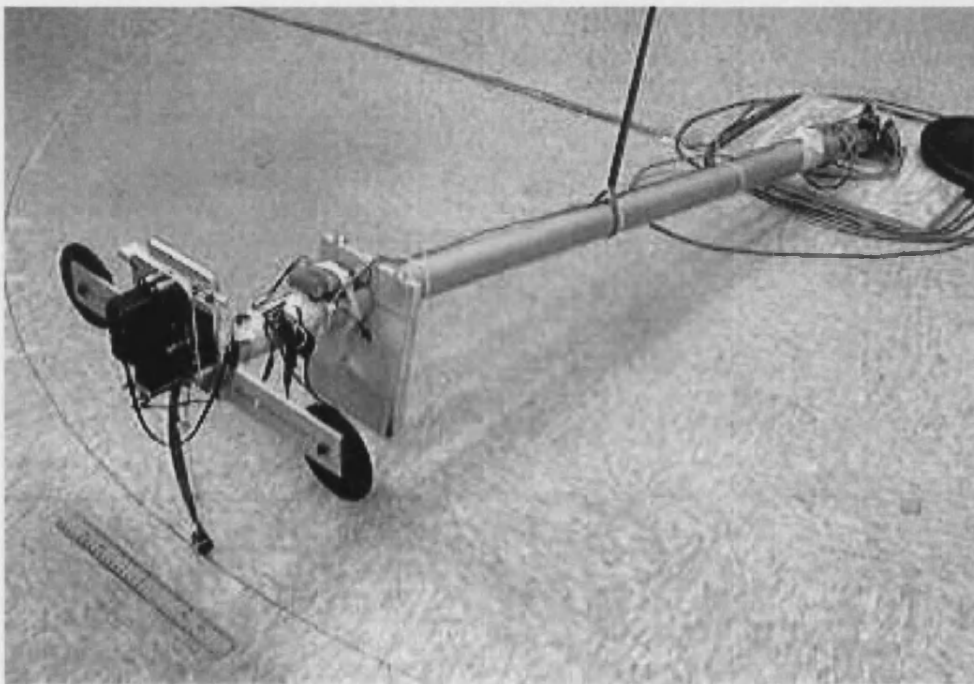
Fig. 35 – The bow leg hopper. (Zeglin 1998).

Massachusetts Institute of Technology's Uniroo is a hopping robot has been been based closely on the kangaroo (see Fig. 5). Unlike many of the other hopping robots, *Uniroo* is not symmetrical, and has a heavy, articulated leg (as opposed to having linear actuation). A further difference is that the hip is offset from the centre of mass and it has a tail, which is constrained to one degree of freedom. A natural looking pitching was observed during locomotion as a result of the heavy leg swinging between strides. The total weight was 6.6 kg and some of the resulting kinetic energy was successfully recovered from each landing thanks to coil springs mounted in the ankles. Forward

velocities of up to 1.8 ms^{-1} were achieved during the experimentation, faster than the other two hopping robots introduced (Zeglin 1993).

Fig. 36 – MIT's Uniroo hopping robot (courtesy Massachusetts Institute of Technology).

2.3.3 Micro Air Vehicles

The surface detail of the irregular terrain to be traversed will influence the precise orientation of the robot foot immediately prior to take-off. Pause and leap jumping robots should be able to compensate for this by adjusting their take-off angle accordingly but this might prove difficult for a hopping robot bouncing along at high speed. Likewise, the viscosity of the surface or areas of liquid could pose problems for a jumping robot that might require careful path planning to avoid. The performance of a micro air vehicle, however, is not dependent on the quality of the substrate it is flying over.

The flight of MAVs occurs at low Reynolds numbers, and increasingly also uses low aspect ratio wings. Section 2.2.3 describes low-aspect-ratio, low Reynolds number aerodynamic theory, and can be found on Page 54. Current MAV designs can be separated into three distinct categories: Firstly, there are traditional fixed wing planes, which generate lift when propelled through the air as described in the aerodynamic theory in section 2.2.1 on Page 43. Some effort has been put into trying to recreate flapping flight, commonly found in birds and insects, in MAVs but with only limited success. Finally, there are ornithopters with rotating wings, which generate both thrust and lift.

Fig. 37 shows a sketch of five fixed-wing MAVs drawn approximately to scale, where the wingspans of the *Sender* and *Dragon Eye* are just over a metre. This image, and much of the information presented from this paragraph was published in a review paper by Mueller and DeLaurier (2003). Credit should be given for the inspiration of many of these designs to initial development by generations of model aircraft hobbyists. The Sender was designed with the intention of full autonomy, with an onboard global positioning system (GPS). Such autonomy was never achieved, but it could fly at a cruising speed of 90 km/h for up to 2 hours, powered electrically. The Dragon Eye, currently being manufactured by Aero Vironment Inc. and BAI Aerosystems is also powered electrically, and can fly for 30 – 60 minutes at 65 km/h. This vehicle successfully controls its own flight using GPS for navigation, and can also carry a payload such as camera. The high-speeds required by these larger MAVs in order to fly hinders their usefulness for exploration of clustered environments, such as a forest. The MITE 2 is smaller, also electric, and can fly at 30 km/h carrying a useful payload with its wingspan of 36 cm. The Black Widow, developed by Aero Vironment Inc. is one of the smallest MAVs that can carry a useful payload. It has an un-laden weight of 80 g, and a wingspan of 15.2 cm. It is able to fly at 50 km/h whilst carrying a colour video camera and transmitter for 30 minutes before its batteries run out.

Equally small, but with a mass of just 40g, is the flexible winged MAV developed at the University of Florida. All the examples discussed so far have had rigid wings. The advantage of the flexible wing is its superior adaptation to stall but it can also change shape which makes it more agile. Powered electrically, it can fly at speeds between 20 and 40 km/h for about 15 minutes, carrying both a camera and transmitter (Shyy 2005).
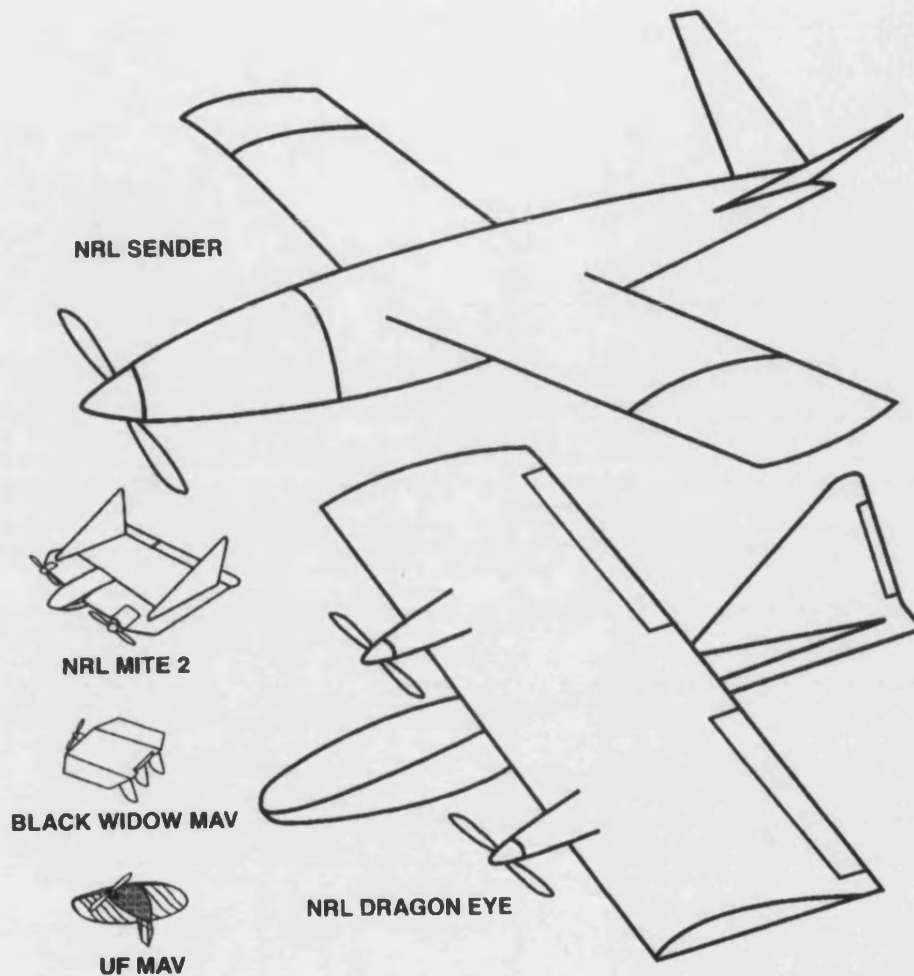
Fig. 37 – Sketches of some MAVs drawn approximately to scale, where the wingspans of the Sender and Dragon Eye are just over a metre. The smallest is a flexible winged MAV developed at the University of Florida, with a 15.2cm span. (Mueller and DeLaurier 2003)

Two Ornithopters that have been flown successfully are the Harris/DeLaurier and the *MicroBat*. Only the former is able to carry a payload of up to 227 g, and its reciprocating engine rotates its wings at 3 Hz, enabling 3 minutes of flight at 55 km/h. The MicroBat weighs in at just 12 g and hence it can fly much slower, just 20 km/h. The frequency of revolutions is 12 Hz, but the electric power source can only maintain flight for 6 minutes and the throttle, elevator and rudder are all manually controlled. These ornithopters highlight one of the main problems with the MAV concept, which is that they have high power consumption, restricting their use in fully autonomous exploration applications.

2.3.4 Planetary exploration rovers
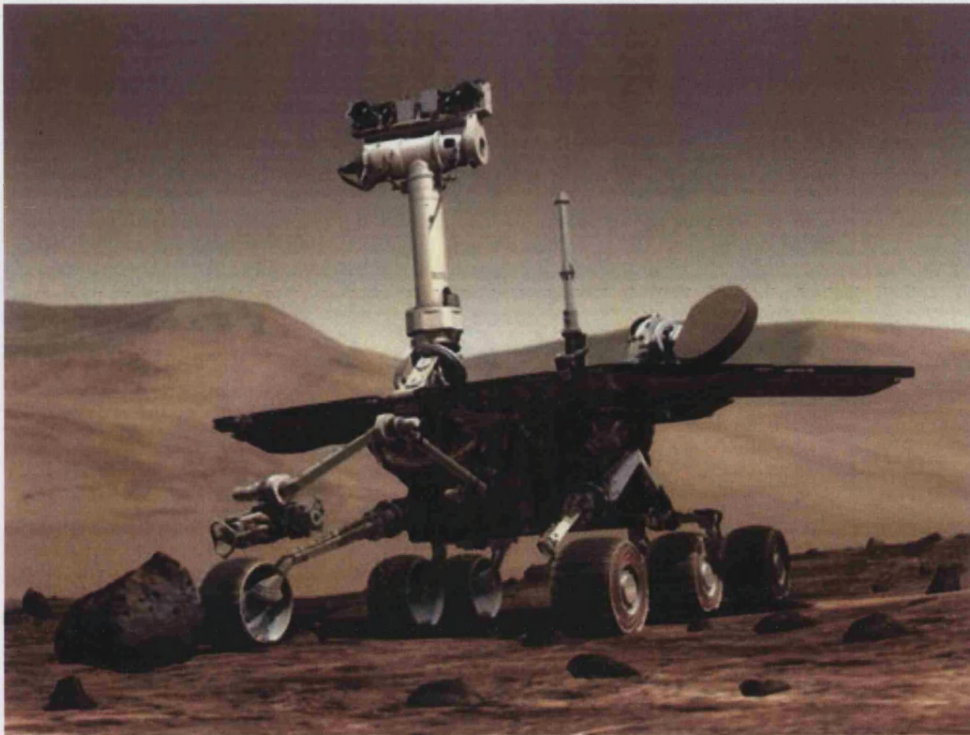
Fig. 38 – An artist impression of how the exploration rovers, Spirit and Opportunity would look like on Mars. Courtesy NASA/JPL-Caltech

The only planetary exploration robots operating at the time of writing this thesis were built by NASA (National Aeronautics and Space Administration, USA), who successfully landed two rovers, Spirit and Opportunity onto Mars in January 2004. These identical six-wheeled buggies are 1.6 m long, and were deliberately landed on opposite sides of the Red Planet, with their primary objective to look for geological evidence that Mars once had enough water to support life (Fig. 38). These Rovers are powered by large arrays of high performance solar panels, storing electrical energy in two 8-amp-hour lithium batteries. Early in their life, these arrays were able to produce about 900 watt-hours of energy per Martian day, or sol. (This is about 40 minutes longer than an Earth day). Both Spirit and Opportunity have surpassed their life expectancy, and by strategically driving them through solar-rich areas, the panels are still providing up to 410 watt-hours per Martian sol. However, this power requirement inevitably limits the potential area which can be explored, something that was already limited by the speed of the robots. Since its landing, Spirit has recorded a wheel odometry of 6896 m in 1087 sols, which is not quite the same as total distance travelled which would assume no loss of traction. Some wheel slip is highly likely on the sandy Martian surface, but

even if ignored, this rover has only managed to travel 6.3 m per sol. Opportunity has managed slightly better, travelling 9918 m in 1068 sols at an average of 9.3 m / sol (NASA 2007). The implication of this slow rate of progress for planetary exploration becomes more apparent when it is remembered that such wheeled rovers must manoeuvre around any obstacle larger than their own wheel diameter. There is certainly room for improvement in the design of robot locomotion for space applications, and so it is worthwhile considering as a potential application for the jumping robot to be developed in this research.

2.4 References – Chapter 2

AERTS, P. (1998). "Vertical jumping in Galago senegalensis: the quest for an obligate mechanical power amplifier." Philosophical Transactions of the Royal Society of London Series B-Biological Sciences 353(1375): 1607-1620.

ALEXANDER, R. M. (1974). "The mechanics of jumping by a dog (Canis familiaris)." Journal of Zoology 173: 549-573.

ALEXANDER, R. M. (1990). "3 Uses for Springs in Legged Locomotion." International Journal of Robotics Research 9(2): 53-61.

ALEXANDER, R. M. (2003). Function of Elastomeric Proteins in Animals. Elastomeric proteins: structures, biomechanical properties and biological roles. P. R. T. Shewry, A.S. Bailey, A.J. Cambridge, Cambridge University Press.

ALEXANDER, R. M. V., A. (1975). "The Mechanics of hopping by kangaroos (Macropodidae)." Journal of Zoology 177: 265-303.

ALLISON, J. (2002). "Monopod Jumping Robot." Retrieved 4 May 2006, 2006, from http://www-personal.umich.edu/~jtalliso/Design/Design2.html.

ANDERSON, J. D. (1978). Introduction to flight its engineering and history. New York, McGraw-Hill, Inc.

ASHBY, B. M. and HEEGAARD, J. H. (2002). "Role of arm motion in the standing long jump." Journal of Biomechanics 35(12): 1631-1637.

BENNET-CLARK, H. C. (1975). "The energetics of the jump of the locust Schistocerca Gregaria." Journal of Experimental Biology 63: 53-83.

BENNET-CLARK, H. C. (1976). Energy Storage in jumping animals. Perspectives in experimental biology. P. Spencer Davies. Oxford, Pergamon Press: 467-479.

BENNET-CLARK, H. C. (1977). Scale Effects in Jumping Animals. Scale Effects in Animal Locomotion. T. J. Pedley. London, Academic Press: 185-201.

BENNET-CLARK, H. C. and LUCEY, E. C. A. (1967). "The jump of the flea: a study of the energetics and a model of the mechanism." Journal of Experimental Biology 47: 59-76.

BIEWENER, A. A. (1998). "Muscle function in vivo: A comparison of muscles used for elastic energy savings versus muscles used to generate mechanical power." American Zoologist 38(4): 703-717.

BIEWENER, A. A., MCGOWAN, C., CARD, G. M. and BAUDINETTE, R. V. (2004). "Dynamics of leg muscle function in tammar wallabies (M-eugenii) during level versus incline hopping." Journal of Experimental Biology 207(2): 211-223.

BLICKHAN, R. (1989). "The Spring Mass Model for Running and Hopping." Journal of Biomechanics 22(11-12): 1217-1227.

BRACKENBURY, J. and HUNT, H. (1993). "Jumping in Springtails - Mechanism and Dynamics." Journal of Zoology 229: 217-236.

BREDER, C. (1930). "On the structural specialization of flying fishes from the standpoint of aerodynamics." Copeia 4: 114-121.

BROWN, R. H. J. (1967). "Mechanism of locust jumping." Nature 214: 939.

BURDICK, J. and FIORINI, P. (2003). "Minimalist jumping robots for celestial exploration." International Journal of Robotics Research 22(7-8): 653-674.

BURROWS, M. (2003). "Froghopper insects leap to new heights." Nature 424: 509.

BURROWS, M. and MORRIS, O. (2002). "Jumping in a winged stick insect." Journal of Experimental Biology 205(16): 2399-2412.

BURROWS, M. and MORRIS, O. (2003). "Jumping and kicking in bush crickets." Journal of Experimental Biology 206(6): 1035-1049.

BURROWS, M. and WOLF, H. (2002). "Jumping and kicking in the false stick insect Prosarthria teretrirostris: kinematics and motor control." Journal of Experimental Biology 205(11): 1519-1530.

COTT, H. (1926). "Observations on the life-habits of some batrachians and reptiles from the lower Amazon: and a note on some mammals from Marajó Island." Proc. Zool. Soc. 2: 1159-1178.

DALEY, M. A. and BIEWENER, A. A. (2003). "Muscle force-length dynamics during level versus incline locomotion: a comparison of in vivo performance of two guinea fowl ankle extensors." Journal Of Experimental Biology 206(17): 2941-2958.

DAVENPORT, J. (1992). "Wing-Loading, Stability And Morphometric Relationships In Flying Fish (Exocoetidae) From The North-Eastern Atlantic." **72**(1): 25-39.

DAVENPORT, J. (1994). "How And Why Do Flying Fish Fly." **4**(2): 184-214.

DAVENPORT, J. (2003). "Allometric constraints on stability and maximum size in flying fishes: implications for their evolution." **62**(2): 455-463.

DAWSON, T. J. H., A.J. (1973). "Energy cost of locomotion in kangaroos." Nature **206**: 313-314.

DE GROOT, J. H. and VAN LEEUWEN, J. L. (2004). "Evidence for an elastic projection mechanism in the chameleon tongue." Proceedings of the Royal Society of London Series B-Biological Sciences **271**(1540): 761-770.

DE MAN, H. L., D. VERMEULEN, J. Design and control of a robot with one articulated leg for locomotion on irregular terrain.

DUTTO, D. J., HOYT, D. F., *et al.* (2004). "Moments and power generated by the horse (Equus caballus) hind limb during jumping." J Exp Biol **207**(4): 667-674.

EMERSON, S. B. and KOEHL, M. A. R. (1990). "The Interaction Of Behavioral And Morphological Change In The Evolution Of A Novel Locomotor Type - Flying Frogs." **44**(8): 1931-1946.

ESTIER, T., CRAUSAZ, Y., *et al.* (2000). An innovative Space Rover with Extended Climbing Abilities. Proceedings of Space and Robotics 2000, Albuquerque, USA.

ESTIER, T. C., Y. MERMINOD, B. LAURIA, M. PIGUET, R. SIEWART, R. (2000). An Innovative Space Rover with Extended Climbing Abilities. Space and Robotics 2000, Albuquerque, USA.

EVANS, M. E. G. (1972). "The jump of the click beetle (Coleoptera, Elateridae) - a preliminary study." Journal of Zoology **167**: 319-336.

EVANS, M. E. G. (1973). "The jump of the click beetle (Coleoptera : Elateridae) - energetics and mechanics." Journal of Zoology **169**: 181-194.

EVANS, M. E. G. (1975). "The jump of Petrobius (Thysanura, Machilidae)." Journal of Zoology **176**: 49-65.

EVANS, M. E. G. B., J.G. (1973). "A jumping millipede." Nature **246**: 427-428.

GABRIEL, J. M. (1984). "The Effect of Animal Design on Jumping Performance." Journal of Zoology **204**(DEC): 533-539.

GERMAN, J. (2000). "Hop to it: Sandia hoppers leapfrog conventional wisdom about robot mobility." Retrieved 18/05/05, from *http://www.sandia.gov/LabNews/LN10-20-00/hop_story.html*.

GREGORIO, P. A., M. BUEHLER, M. (1994). Experiments with an Electrically Actuated Planar Hopping Robot. Lecture Notes in Control and Information Sciences 200. T. Y. a. F. Miyazaki. Springer Verlag: 269-281.

GRONENBERG, W. (1995). "The Fast Mandible Strike in the Trap-Jaw Ant Odontomachus .1. Temporal Properties and Morphological-Characteristics." Journal of Comparative Physiology a-Sensory Neural and Behavioral Physiology 176(3): 391-398.

GRONENBERG, W., TAUTZ, J. and HOLLDOBLER, B. (1993). "Fast Trap Jaws and Giant-Neurons in the Ant Odontomachus." Science 262(5133): 561-563.

HALE, E. S., NATHAN. BURDICK, JOEL (2000). A Minimally Actuated Hopping rover for Exploration of Celestial Bodies. IEEE International Conference on Robotics and Automation, California Institute of Technology.

HAYASHI, R. and TSUJIO, S. (2001). "High-performance Jumping Movements by Pendulum-type Jumping Machines." Proceedings of the IEEE/RSJ - International Conference on Intelligent Robots and Systems: 722-727.

HEITLER, W. J. (1974). "The Locust Jump. Specialisations of the Metathoracic Femoral-Tibial Joint." J. Comp. Physiol. 89: 93-104.

HILL, D. E. (2001). Targeted Jumps by Salticid Spiders (Aranea, Salticidae, *Phidippus*).

KIKUCHI, F., OTA, Y. and HIROSE, S. (2003). "Basic Performance Experiments for Jumping Quadruped." Proceedings of the 2003 IEEE/RSJ International Conference on Intelligent Robots and Systems: 3378-3383.

KUSWADI, S., OHNISHI, A., *et al.* (2003). "A one linear actuator hopping robot: modeling and control." Advanced Robotics 17(8): 709-737.

LABORATORY, B. I. R. (2006). Mini-Whegs™ Robots, Case Western Reserve University.

LAROUSSE (1995). Dictionary of Science and Technology.

LINDSTEDT, S. L., REICH, T. E., KEIM, P. and LASTAYO, P. C. (2002). "Do muscles function as adaptable locomotor springs?" Journal of Experimental Biology 205(15): 2211-2216.

LUTZ, G. J. and ROME, L. C. (1994). "Built For Jumping - The Design Of The Frog Muscular System." Science 263(5145): 370-372.

LUTZ, G. J. and ROME, L. C. (1996). "Muscle function during jumping in frogs .2. Mechanical properties of muscle: Implications for system design." American Journal Of Physiology-Cell Physiology 40(2): C571-C578.

MAITLAND, D. P. (1992). "Locomotion by jumping in the Mediterranean fruit-fly larva *Ceratitis capitata*." Nature 355: 159-161.

MARSH, R. L. and JOHNALDER, H. B. (1994). "Jumping Performance of Hylid Frogs Measured with High-Speed Cine Film." Journal of Experimental Biology **188**: 131-141.

MCGOWAN, C. P., BAUDINETTE, R. V., USHERWOOD, J. R. and BIEWENER, A. A. (2005). "The mechanics of jumping versus steady hopping in yellow-footed rock wallabies." J Exp Biol **208**(14): 2741-2751.

MCGUIRE, J. A. and DUDLEY, R. (2005). "The cost of living large: Comparative gliding performance in flying lizards (Agamidae : Draco)." American Naturalist **166**(1): 93-106.

MUELLER, T. J. and DELAURIER, J. D. (2003). "Aerodynamics of small vehicles." Annual Review Of Fluid Mechanics **35**: 89-111.

NASA. (2007). "Mission update." Retrieved 30/01, 2007, from *http://marsrovers.nasa.gov/mission/status_opportunity.html* *http://marsrovers.nasa.gov/mission/status_spirit.html*.

NORBERG, U. M. (1990). Gliding Flight. Vertebrate Flight: Mechanics, Physiology, Morphology, Ecology and Evolution: 65-75.

OLIVER, J. (1951). "Gliding in Amphibians and Reptiles." The American Naturalist **85**: 171-176.

PARRY, D. A. B., R.H.J (1959). "The jumping mechanism of Saltacid Spiders." Journal of Experimental Biology **36**(4): 654-664.

PATEK, S. N., KORFF, W. L. and CALDWELL, R. L. (2004). "Biomechanics: Deadly strike mechanism of a mantis shrimp - This shrimp packs a punch powerful enough to smash its prey's shell underwater." Nature **428**(6985): 819-820.

PAUL, J. (2001). "Mandible movements in ants." Comparative Biochemistry and Physiology a-Molecular and Integrative Physiology **131**(1): 7-20.

PELLETIER, A. and MUELLER, T. J. (2000). "Low Reynolds number aerodynamics of low-aspect-ratio, thin/flat/cambered-plate wings." **37**(5): 825-832.

PEPLOWSKI, M. M. and MARSH, R. L. (1997). "Work and power output in the hindlimb muscles of Cuban tree frogs Osteopilus septentrionalis during jumping." Journal of Experimental Biology **200**(22): 2861-2870.

PUXKANDL, R., ZIZAK, I., et al. (2002). "Viscoelastic properties of collagen: synchrotron radiation investigations and structural model." Philosophical Transactions of the Royal Society of London Series B-Biological Sciences **357**(1418): 191-197.

QUINN, R. D., KINGSLEY, D.A., OFFI, J.T. AND RITZMANN, R.E. (2002). Improved Mobility Through Abstracted Biological Principles. IEEE Int. Conf. On Intelligent Robots and Systems (IROS'02), Lausanne, Switzerland.

RAYNER, J. M. V. (1991). "On The Aerodynamics Of Animal Flight In Ground Effect." 334(1269): 119-128.

ROBERTS, T. J. and MARSH, R. L. (2003). "Probing the limits to muscle-powered accelerations: lessons from jumping bullfrogs." J Exp Biol 206(15): 2567-2580.

ROTHSCHILD, M. S., J. PARKER, K. NEVILLE, C. AND STERNBERG, S. (1975). "The jumping mechanism of Xenopsylla cheopis." Philosophical Transactions of the Royal Society of London B. Biological Sciences 271(914): 457-520.

SAVILE, D. (1962). "Gliding and flight in the vertebrates." American Zoologist 2: 161-166.

SCHROER, R. T., BOGGESS, M.J., BACHMANN, R.J., QUINN, R.D., AND RITZMANN, R.E. (2004). Comparing Cockroach and Whegs Robot Body Motions. IEEE Conference on Robotics and Automation (ICRA '04), New Orleans, USA.

SEYFARTH, A., BLICKHAN, R. and VAN LEEUWEN, J. (2000). "Optimum take-off techniques and muscle design for long jump." J Exp Biol 203(4): 741-750.

SEYFARTH, A., FRIEDRICHS, A., WANK, V. and BLICKHAN, R. (1999). "Dynamics of the long jump." Journal of Biomechanics 32(12): 1259-1267.

SHINE, R., JS KEOGH, P DOUGHTY, H GIRAGOSSYAN (1998). "Costs of reproduction and the evolution of sexual dimorphism in a "flying lizard" Draco melanopogon (Agamidae)." Journal of Zoology 246: 203-213.

SHYY, W. I., PETER. VIIERU, DRAGOS. (2005). "Membrane Wing-Based Micro Air Vehicles." Applied Mechanics Reviews 58: 283-301.

SOCHA, J. J., O'DEMPSEY, T. and LABARBERA, M. (2005). "A 3-D kinematic analysis of gliding in a flying snake, Chrysopelea paradisi." J Exp Biol 208(10): 1817-1833.

STOETER, S. A. and PAPANIKOLOPOULOS, N. (2005). "Autonomous stair-climbing with miniature jumping robots." Ieee Transactions on Systems Man and Cybernetics Part B- Cybernetics 35(2): 313-325.

TOBALSKE, B. W., ALTSHULER, D. L. and POWERS, D. R. (2004). "Take-off mechanics in hummingbirds (Trochilidae)." 207(8): 1345-1352.

TORRES, G. E. and MUELLER, T. J. (2004). "Low-aspect-ratio wing aerodynamics at low reynolds numbers." AIAA 42(5): 865-873.

VERMEULEN, J. L., D. VERRELST, B. (2003). "Control of foot placement, forward velocity and body orientation of a one-legged hopping robot." Robotica 21: 45-57.

WILSON, A. M., WATSON, J. C. and LICHTWARK, G. A. (2003). "Biomechanics: A catapult action for rapid limb protraction." Nature 421(6918): 35-36.

WILSON, R. S., FRANKLIN, C. E. and JAMES, R. S. (2000). "Allometric scaling relationships of jumping performance in the striped marsh frog Limnodynastes peronii." J Exp Biol **203**(12): 1937-1946.

ZEGLIN, B. B. A. G. (1998). The Bow Leg Hopping Robot. IEEE Intl. Conf. on Robotics and Automation.

ZEGLIN, G. J. (1993). "Uniroo." Retrieved 18/05/05, from *http://www.ai.mit.edu/projects/leglab/robots/uniroo/uniroo.html*.

Chapter 3

Take-off and landing forces and the evolution of controlled gliding in northern flying squirrels (*Glaucomys sabrinus*)

At the outset of this research, it was decided that examination of animal jumping and landing should provide the basis of a robot design for traversing irregular and unfamiliar terrain. Of all the animals considered during the literature review, Flying squirrels seemed most worthy of additional investigation – in part due to a lack of present literature explaining the reason for the evolution of their unique gliding capabilities. Flying squirrels, like all gliding mammals, can utilise many forms of locomotion, including bounding, jumping, gliding and climbing. Any robot that could rely on such a range of transport modes, and particularly the ability to climb, would clearly be well suited to rough terrain exploration. However, a fully autonomous robot for use in space applications, for example, has the additional, important consideration of energy economy. Where time is not a constraint, jumping allows energy to be stored very slowly, allowing even the most patchy power resource eventually to prime the jumping mechanism, which amplifies the power in a quick release jump. Once airborne, gliding could potentially extend range, and should simultaneously reduce landing impact force at no additional cost. Therefore, it was decided that the research effort into both flying squirrels, and the design of an autonomous robot, should focus on jumping and gliding. This chapter has also been published as a paper in the Journal of Experimental Biology (Paskins, Bowyer *et al.* 2007).

3.1 INTRODUCTION TO STUDY

Gliding mammals can generally be found in large forest habitats, and are particularly prominent in the South Eastern Asian rainforests. An interesting ecological fact is that the spacing between trees in these forests is significantly more distant than in the other

rainforests of the world. This seems to have favoured the evolution of gliders rather than animals with prehensile tails, such as monkeys which prevail in Africa and South America. There are also two gliding mammal species in North America, northern flying squirrels, *Glaucomys sabrinus*, and southern flying squirrels, *Glaucomys volans*. Flying squirrels can certainly be considered to be a successful species, tending to live up to 50% longer than their less aerodynamically sophisticated cousins. They are capable of fast arboreal transport in often steep areas of woodland which provides a difficult environment for other animals to traverse.

There are three principal hypotheses to explain the divergence of flying squirrels from other types of squirrel. The first, suggested by Norberg (1985), is that gliding may have evolved as a means of reducing the energetic cost of foraging. The squirrel can jump and glide from one tree to the next, enabling it to cover greater distances within the canopy more quickly than would be possible by climbing down and moving across the forest floor. Scheibe *et al.* (2006) suggested that rather than reducing cost of transport, gliding may offer a means of foraging over a larger area in a certain time, making them better able to exploit a patchy food resource than non-gliders of similar size. The third hypothesis is that gliding evolved primarily as an escape mechanism (Scheibe, Figgs *et al.* 1990; Keith, Scheibe *et al.* 2000). Tree squirrels react to disturbances by moving to the opposite side of their tree, whereas flying squirrels climb upwards and then glide to another tree. However, Scheibe and Robins (1998) also noted that this behaviour may increase susceptibility to attack from their most likely predator, owls. A fourth hypothesis is proposed: that the *patagia*, the flexible membranes which squirrels stretch by fully extending their forelimbs and hind limbs, evolved to reduce or control landing forces. Evidence to support this comes from work by Caple *et al.* (1983) who calculated that increasing the amount of lift available to a body from 0 to 5% would not noticeably lengthen the jump nor allow much turning, but would give the animal significantly improved control around the pitch and roll axes. Norberg (1985) argued that although this is true if the lift to drag ratio is unaltered, if the incremental increase was in the aspect ratio (a lengthening of the wings), then the range would in fact increase proportionally and so this should not be disregarded. Of course, none of these four hypotheses are mutually exclusive.

This chapter will investigate these hypotheses through experimental determination of the performance and behaviour of these animals. By measuring take-off and landing forces, it is proposed to quantify the advantage flying squirrels can achieve as a result of their unique morphology. The outcome of these measurements will be directly affected by substrate compliance. The majority of previous studies measuring ground reaction forces used rigid force measuring devices, while Demes *et al.* (1999) and Bonser (1999) investigated the effects of substrate compliance on ground reaction forces. The former found that take-off forces were higher than landing forces when testing seven primate species of varying body sizes using compliant apparatus, contradicting previous studies based on rigid platforms. Some of the take-off force is used in bending the compliant branch before toe-off, whereas the reaction force on landing is damped as the substrate yields in the direction of motion, allowing more time for deceleration. Likewise, Bonser (1999) showed that the magnitude of landing forces for starlings was lower than their take-off forces. He proposed both that the birds used their wings to decelerate during landing, and that additional energy is dissipated in deflecting their compliant perch during take-off.

In arboreal locomotion, flying squirrels must generate higher take-off forces when jumping from narrow (and hence compliant) tree branches, and encounter their highest impact forces when landing on rigid tree trunks. Compliant substrates have been instrumented for this study, and so take-off forces are expected to exceed landing forces over short distances. At higher ranges, the squirrels will have accelerated due to gravity and their landing force will likely increase unless the squirrel can use its morphology to slow itself aerodynamically. Therefore the hypothesis that gliding in the squirrel evolved primarily to enable aerodynamic control of its landing speed can be rejected if measured landing forces continually rise at high ranges.

It is possible for animals to utilise stored elastic energy within a branch by timing their take-off with its motion. However, Demes (1995) did not find primates to take advantage of this, which supports Alexander's (1991) proposition that they would not intentionally recover this energy. Therefore flying squirrels are not expected to take advantage of the recoil of the instrumented branch in this study either. However, they have been observed using a bounding gait before launching with both fore and hind feet together at the end of a platform just before take-off (Keith, Scheibe *et al.* 2000). It is

probable that this bounding is used to maximise take-off velocity and hence increase range.

The northern flying squirrel (*Glaucomys sabrinus*) is the larger of two species of North American flying squirrel, although still much smaller than some species found in S.E Asia (Ando and Shiraishi 1993). Flight is made possible by the presence of patagia, a morphological feature which has evolved independently several times in vertebrates, the earliest known being from the Mesozoic era (Meng, Hu *et al.* 2006). By manipulating their limbs, flying squirrels are able to actively modify the shape of this lift-generating surface during flight. Thorington and Heaney (1981) compared body proportions of flying squirrels with tree squirrels to determine what morphological changes might be attributed to gliding. Increased leg length allows more energy to be expended during take-off, offering superior horizontal range. In comparison with other similar-sized squirrels, the forelimbs of flying squirrels are significantly longer, a trait which has almost certainly evolved to improve aerodynamics during gliding (Essner 2002). This is further improved by the *styliform* cartilage, a flexible projection from the wrist held upward from the rest of the lift surface during gliding. This combines with the *manus* (or hand, which points ventrally towards the mid-line of the squirrel) to form a wing-tip very similar to a NASA designed winglet as shown by Thorington *et al.* (1998), who proposed that it reduces induced drag by diffusing and directing vortices away from the patagia. Smaller flying squirrels tend to have greater manoeuvrability and agility, whereas the larger species must glide faster to achieve the same glide ratio.

3.2 MATERIALS AND METHODS

3.2.1 Animals

Study animals came from a laboratory colony of northern flying squirrels housed in the Department of Biology at Southeast Missouri State University. Two young females and a young male were chosen because they were consistent performers in previous kinematic work. All animals were born in the same week and were approximately 27 months old. The mass, wing span and wing area of each animal is given in Table 1. Other members of the colony were required for other projects and were not available. The colony had been maintained on a diet of pecans, walnuts, sunflower seeds, mushrooms and birdseed in a large, temperature-controlled room (20°C) for five years. The room is on a continuous 12 hour light/dark cycle. There are various branches and sufficient space for jumping and gliding to take place. Initially, measurements were made in the squirrel lab, but longer glides were measured in a 7 m x 14 m x 7 m barn on the university farm.

3.2.2 Apparatus

As flying squirrels often land on tree trunks, allowing vertical variation in contact point, a vertical landing pole was used, based on the design of Demes *et al.* (Demes, Jungers *et al.* 1995; Demes, Jungers *et al.* 1996; Demes, Fleagle *et al.* 1999). The squirrels were acclimated to it for several months prior to experimentation and used it regularly. It was constructed in two pieces: a 1.52 m long PVC tube (114 mm DIA) covered in carpet and marked at 10 cm intervals (for calibration and image analysis), mounted 80 cm of the way up a 2.41 m long galvanised steel tube (23 mm DIA). A concrete base secured this steel tube which had four strain gauges (FLA-2-11-3L, TML, Tokyo, Japan) equally spaced around its circumference and aligned vertically (Fig. 39). A half-bridge circuit was used for each tension/compression pair so that force parallel and perpendicular to the squirrel's direction of motion could be determined. The compliance of the pole was

measured to be 1.5 mm/N at the free end, gradually decreasing down the pole, reducing to 0.2 mm/N close to the fixed end and the resonant frequency was 2.2 Hz.
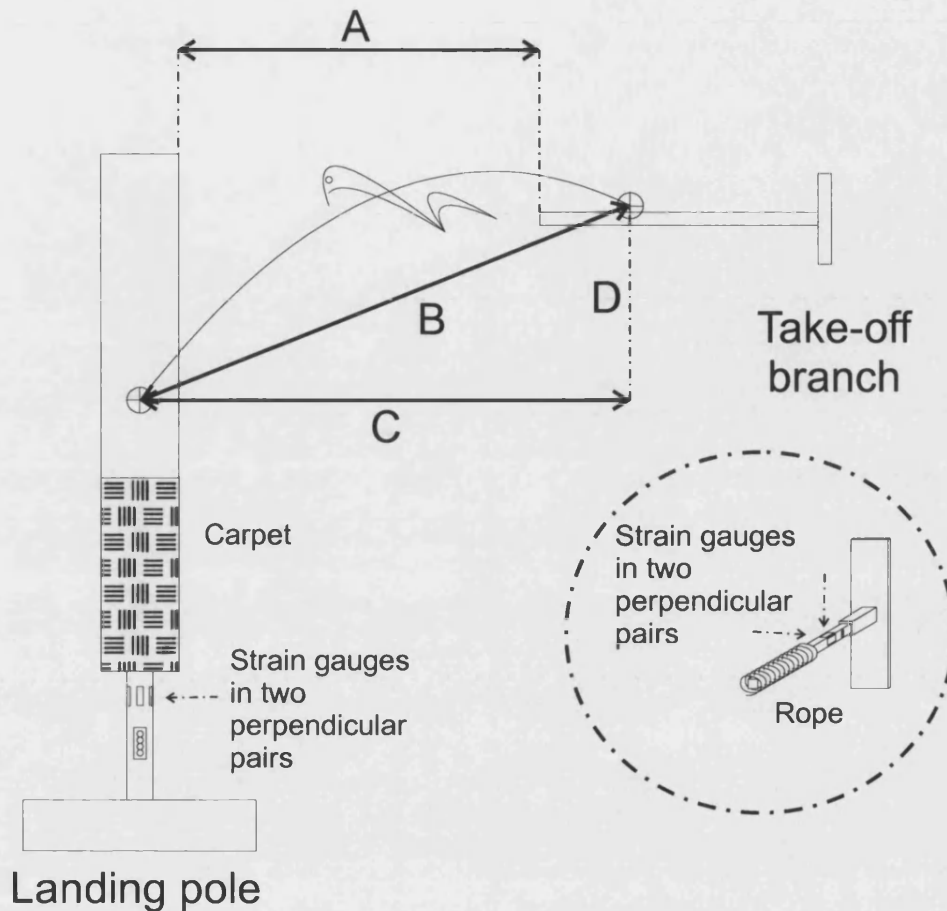
Fig. 39 – A diagram of the experimental set-up, showing the instrumentation used to measure take-off and landing forces including the carpet-covered landing pole, the rope-covered take-off branch and the location of the strain gauge pairs on each. Also shown are the measurements used to analyse the results, relative to an approximate squirrel trajectory: A – The controlled horizontal distance between the end of the take-off branch and the vertical landing pole, B – The total distance covered in the glide calculated from the exact horizontal distance (C) and the drop (D).

For the take-off branch, a horizontal cantilevered beam was designed to mimic a tree branch because Vernes (2001) observed that northern flying squirrels predominantly launched from a crouched, horizontal position. Four standard linear strain gauges (CEA-13-240UZ-120, Vishay, Basingstoke - UK) were mounted in 2 pairs, 50 mm from the fixed end of the 10 mm square aluminium bar (Fig. 39) and connected in a half-bridge circuit. Alignment was simplified because the chosen gauge width was almost as large as the 10mm width of the aluminium bar, but not critical because any cross-talk was eliminated during calibration. The aluminium branch was covered by tightly wound rope to simulate the surface of a tree branch. The strain gauges were protected using polystyrene foam, which was itself covered by plastic. A length of 4 x 9 cm timber was

fixed vertically to the wall, and drilled with mounting holes every 10 cm to allow height adjustment of the launch branch. The design of the branch was such that the compliance was similar to that of the landing pole, measured to be 1.9 mm/N at the free end and decreasing as would be expected towards 0.0 mm/N at the fixed end. The resonant frequency of the take-off branch was 17.3 Hz. The signal output from the strain gauges on both instruments were amplified using AD524 chips or equivalent and the sampling rate was 250 Hz. There was no need to acclimatise the squirrels to the take-off pole as – unlike the landing pole – they had no choice over whether or not to use it.

3.2.3 Experimental Design

The take-off branch was raised as the experimental range increased such that the angle between the tip of the branch and the base of the landing pole remained consistent at approximately 55°. This experimental design was chosen because it was not possible to set-up short jumps at high altitudes with the equipment and in the locations available, and the squirrels were unable to reach the landing pole unless given sufficient starting height. Animals were released individually onto the instrumented branch and responded by running along the branch, usually pausing and then leaping to the instrumented landing pole. The horizontal range was increased progressively in 0.5 m increments above a minimum of 0.5 m to ensure the capture of the leap to glide transition point below which squirrels merely leap around, and above which the flying squirrels achieve aerodynamic advantage over other types of squirrel. Analysing this range of arboreal locomotion was considered to be more critical for investigating the initial divergence of flying squirrels.

Three digital video cameras (Canon GL2, Sony TRV 108, and Panasonic NV-DS55B) were used to film jumps. The first was positioned to capture take-off angle, the second to capture lateral landing angle and the third to capture a ventral view of landing. In the large squirrel barn it was not possible to mount a camera level horizontally with the take-off branch, so the resultant images represent frames perpendicular from the known camera angle. A minor trigonometric correction was therefore employed. Horizontal measurements were unaffected but it was necessary to adjust all vertical distances by dividing them by the cosine of the projection angle between the camera and the branch.

3.2.4 Calibration

With strain gauges, large changes in the external environment are potentially significant, so a record of temperature was kept using two I-buttons (Maxim Integrated Products, California), fixed to the top and bottom of the 4 x 9 cm timber stud respectively. These recorded temperature every hour. This daily verification of calibration was particularly important because testing was carried out in two contrasting environments; a temperature-controlled laboratory, and a hot and humid metal barn.

Only the landing forces were measured by converting the output from strain gauges into force, for which a static calibration was performed daily by applying forces to different points along the pole. Resultant steady signals were used to draw calibration graphs that established the force constant, k, where $F = kx$, F is force (N) and x is the measured strain signal (V). Forces equivalent to between 1 and 10 bodyweights were applied producing good linearity across the full range of marking points on the pole. (On average, the square of the Pearson product moment correlation coefficient, $r^2 = 1.00$ in line and 0.99 transverse to the expected direction of motion.) Position of the animal along the instrumented poles was taken into account and a linear equation allowed the correct calibration to be used at any point. The cross-talk magnitudes were 13% and 17% accordingly for parallel and transverse forces. Cross-talk, in this context, is the unwanted output signal measured on one pair of strain gauges for a force applied perpendicularly. The frequency response of the equipment was sufficient to measure impulses generated by the squirrels. The effect of temperature on the calibration was found to be unimportant, as although it varied considerably between the two test areas, calibration graphs remained consistent throughout the study.

3.2.5 Results processing

Although both could measure force in two directions, neither the take-off branch, nor the landing pole were capable of measuring forces along their long axes. To overcome this limitation, video footage from laterally positioned cameras was recorded to determine the angle of action of the force, which allowed the force vector to be resolved in 3D from the two measured force components. This was an acceptable procedure for the landing forces because the squirrels were arriving at angles perpendicular to the

pole. For the median data point at medium range, 1.5 m, a trigonometric calculation showed that a 5° shift in measured landing angle would cause a 10% change in the resultant force. During take-off the squirrels were consistent in their behaviour, always choosing to move towards the free end of the branch and jump away in the same direction. However, the resulting shallow take-off angles mean that a 5° measurement error leads to an unacceptable 39% change to the median resultant force at 1.5 m. Hence, resultant take-off forces had to be calculated by integrating the output from the strain gauges with respect to time, so that measured take-off velocity could be used to determine the acceleration. This was multiplied by the known mass of each flying squirrel for all jumps to calculate the resultant force. The frame rate of the lateral take-off camera was 30 fps so an estimate of velocity between the first two consecutive frames after toe-off could be obtained by measuring the change in position of the centre of mass. The resultant force calculated by this method is the total force required to accelerate the squirrel to its actual take-off velocity based on its known acceleration profile. This method does not take into account losses caused by deforming the branch, but is completely independent of the accuracy in measurement of take-off angle.

The video records were digitised using edge-detection software which tracked the outline of the squirrel in each frame of a sequence of images from the laterally positioned camera (LabView – National Instruments, Austin TX). The tail was deliberately excluded from this outline, because it constitutes only a small percentage of the total weight of the animal and was often dorsally flattened and moving at high velocity outside the plane of the images. The centre of the region enclosed by the lateral outline of the squirrel was used as an approximation for its centre of mass and could be tracked from frame to frame, enabling both the landing point on the pole, and the angle of impact to be determined. Hence the resultant reaction force for each landing squirrel could be calculated.

To measure the take-off angle of the squirrel, principal components analysis was applied in the LabView squirrel tracking program to find the best-fitting ellipse to the outline detected in each frame. The take-off angle was taken to be the angle between the major axis of this ellipse and the axis of the branch in the final frame before toe-off. This program was also used to estimate the change in pitch during the landing sequence shown in Fig. 40. Another program was written in NI Labview to determine the wing

span and wing area of each squirrel from ventral images of a glide. Lateral images were used in conjunction with these to ensure that only frames in which the squirrels were in plane with a calibration bar were used for these measurements.
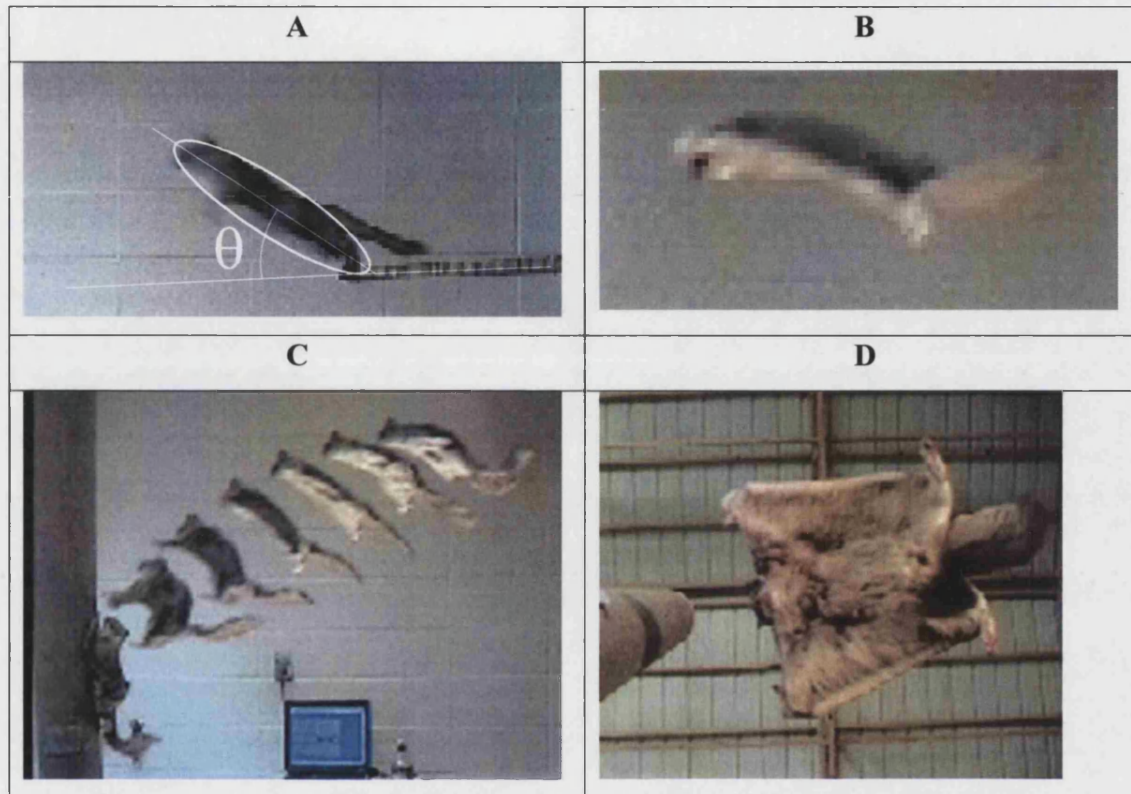
Fig. 40 – Video stills of the squirrels in the three postures observed. A shows the forelimbs being abducted prior to the hind limbs leaving the substrate during take-off, and how the take-off angle, θ, is calculated as the angle between the branch and the major axis of the best-fitting ellipse to the squirrel (excluding its tail). B shows normal gliding flight, C shows the landing from the side and D shows a ventral view landing on the pole on the left. In C, the last few frames of a landing sequence have been superimposed onto one image to demonstrate the landing behaviour, although the penultimate frame had to be omitted for clarity. In this short, 1m jump, the squirrel initially pitches upwards and flattens its body and tail against the direction of motion. Immediately prior to landing, the head is tilted backwards while the limbs are all pushed forwards with the tail simultaneously rotated back so that it is parallel with the ground.

A calculation was performed to determine the percentage of bodyweight supported during each measured glide, relative to the equivalent ballistic trajectory (that is the trajectory of an object with the same take-off velocity and angle subject to no drag or lift). For a simple free-falling mass, the gravitational force acting downwards is opposed by any lift generated. The resultant force acting on the body is hence:

$$F = ma = mg - L$$

<div align="right">Equation 12</div>

Where m = mass (kg), a = resultant acceleration (ms^{-2}), g is gravitational acceleration (9.814 ms^{-2}) and L is the lift force (N). The percentage weight supported is simply this lift force divided by the animal weight. Measured take-off angle, θ, velocity, v (ms^{-1}), and jump duration, t (s), are sufficient to calculate the vertical drop, y (m), from the resultant acceleration using the standard kinematic equation below:

$$y = (v\sin\theta)t - \frac{1}{2}at^2$$

<div align="right">Equation 13</div>

Therefore, by combining Equation 12 and Equation 13 an expression can be derived for the overall lift force generated during the glide:

$$L = m(g - (\frac{2tv\sin\theta - y}{t^2}))$$

<div align="right">Equation 14</div>

3.2.6 Jumps observed, General Mixed Model, and other statistics

Table 1 shows the number of jumps of each animal at each range specified, for the 79 take-offs and 53 corresponding landings measured. No landing force data was obtained for the shortest range jumps of 0.5 m, but with this exception, all measured take-off forces have a corresponding landing force. Only one squirrel, young female 1, performed in the barn but it did not leap to the force pole at distances greater than 2.5 m, landing instead on the ground beyond the instrumented pole. This was the only animal to perform at all ranges tested. Unfortunately, young female 2 only cooperated at 0.5, 1 and 1.5 m and the young male at 0.5 and 1 m. Owing to the number of missing data points, the typical multivariate ANOVA could not be applied to this data, and so a *general mixed model* (Krueger and Tian 2004) was applied to both take-off and landing forces, with range as a fixed factor and squirrel ID a random factor. Unless otherwise stated, all correlation statistics use Pearson's product moment correlation.

3.3 RESULTS

Video stills from the lateral camera illustrate the consistent take-off, gliding and landing postures of the squirrels (Fig. 40). During take-offs, the forelimbs were abducted prior to toe-off enabling the squirrel to immediately adopt gliding posture. During gliding all limbs were abducted creating a cambered wing surface held at a small positive angle of attack. The tail was dorsally flattened, presumably to generate lift. Prior to landing, the squirrel pitched upwards keeping its body and tail in line and flattened against the direction of motion. Immediately prior to landing, the head tilted backwards while the limbs were all pushed forwards with the tail simultaneously rotated back so that it was parallel with the ground. In the example landing sequence (Fig. 40), the pitch angle of the body changed from approximately 22.5° relative to the horizontal, towards 90° immediately prior to landing.

Squirrel ID	Wing Span (cm)	Wing Area (cm²)	Leap distance (m)	Mass on day of testing (g)	Take-off force (in units of bodyweight)			Landing force (in units of bodyweight)		
					Count	Mean	Standard Deviation	Count	Mean	Standard Deviation
Young female 1	28.0	511	0.5	272	9	3.70	1.99	-	-	-
			1	274	6	4.64	1.17	6	3.47	.37
			1.5	267	10	4.36	1.64	10	4.88	.35
			2	256.5*	7	5.57	1.53	7	7.58	.96
			2.5	256.5*	5	5.91	1.49	5	6.16	.54
Young female 2	27.5	500	0.5	200	8	2.56	1.28	-	-	-
			1	201	10	5.21	2.47	10	3.56	.30
			1.5	198	11	3.30	1.70	11	4.28	.21
Young male	25.9	554	0.5	259	9	3.38	0.96	-	-	-
			1	260	4	6.97	1.23	4	3.79	.44

Table 1 – Summary table of all the measured forces generated by northern flying squirrels during leaping and landing. There are 79 take-offs but only 53 corresponding landings because no landing force data was obtained for the shortest range jumps of 0.5 m. Only one individual, young female 1, performed in the barn but it would not land on the force pole at distances greater than 2.5 m. Unfortunately, for reasons beyond our control, young female 2 only cooperated at 0.5, 1 and 1.5 m and the young male at 0.5 and 1 m.
* indicates that the squirrels seemed to lose a considerable percentage of their weight before testing at this distance. The reason for this is unknown but it could have been caused by the change of environment as these tests were carried out in a barn, which was very hot and humid compared to the temperature-controlled lab.

In the barn, the squirrels tended to have a steeper approach and did not pitch up very much prior to landing. The head still tilted backwards but the tail was rotated forwards towards the vertical. As a consequence of the lower angle of attack, the forelimbs contacted the pole first causing the body to rotate around rapidly onto the hind limbs

due to the conversion of linear to angular momentum. Occasionally the tail was cambered such that the inside of the curve faced the landing pole. In some jumps, the squirrels were clearly banking or turning in the penultimate frames to correct misalignment with the pole and in one instance, a subject landed on the side of the pole. As it was simple to calculate the forces for these jumps too, these results were included in our analysis.
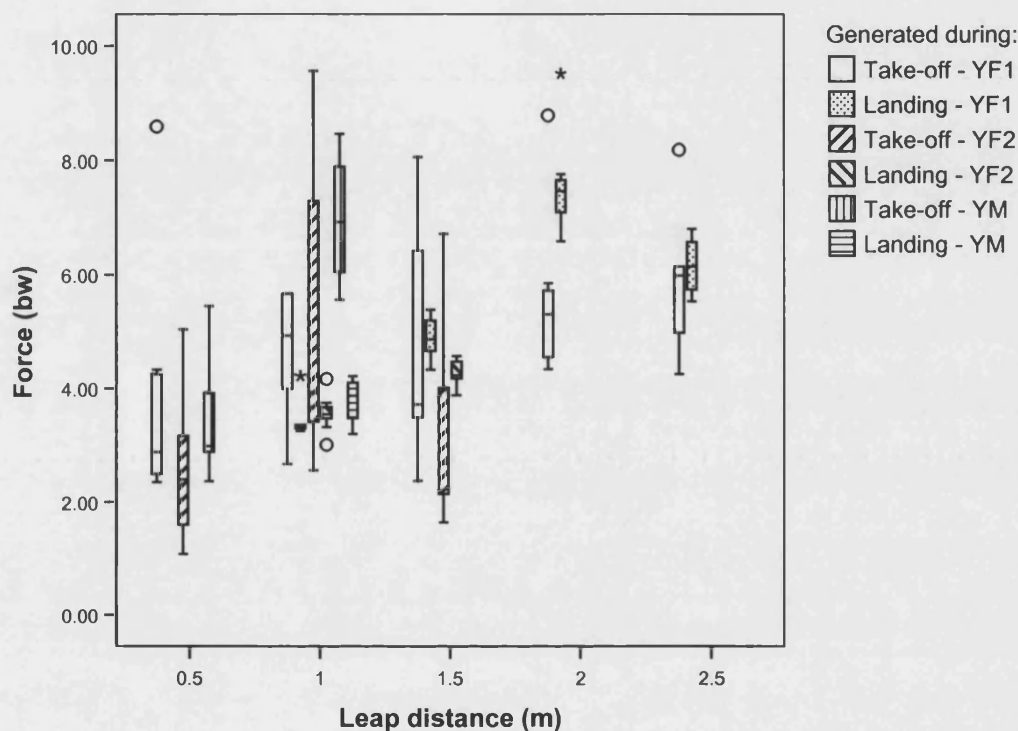
Fig. 41 – A box plot directly comparing the landing forces with the corresponding take-off forces for three of the flying squirrels (young females 1 and 2, and young male) at each horizontal range (from the end of the take-off branch to the landing pole). The stars and circles show values that were outside the interquartile range, the former being statistically significantly far away.

A summary of take-off and landing forces recorded as a multiple of bodyweight is shown in Table 1. There was considerable variation between take-off and landing forces measured for each squirrel at each distance. Take-off forces normalised by body weight increased significantly with leap distance (Fig. 41; $r = 0.323$, $p = 0.004$). The same box plot also shows the positive correlation between landing forces and horizontal range ($r = 0.816$, $p < 0.001$).

The general mixed model introduced above provides statistical verification that normalised take-off forces were significantly dependent on range ($F_{5, 11.5} = 45.182$, $p < 0.001$) but not squirrel identity, ($p = 0.602$). Likewise, landing forces were dependent on range ($F_{4, 9.5} = 409.341$, $p < 0.001$) but independent of the particular squirrel ($p =$

0.548). The means and 95% confidence intervals produced by the mixed model are plotted in Fig. 42.
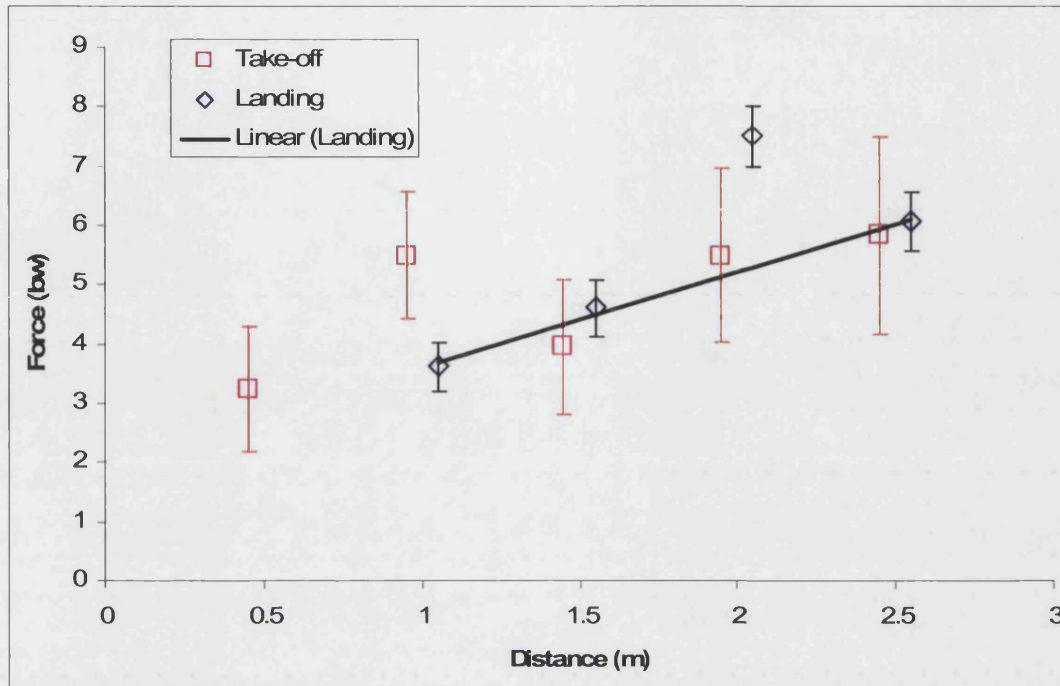
Fig. 42 – A graph showing the output from the mixed model statistics of mean take-off and landing forces at each horizontal range. The error bars represent the 95% confidence intervals. By ignoring the few jumps at 2m, when the squirrel consistently landed at the more rigid base of the pole, the square of the Pearson product moment correlation coefficient (the r-squared value) improves from 0.61 to 0.99.

All landing and take-off forces are not correlated to one another ($r = 0.094$, $p = 0.507$). A paired sample t-test comparing landing force with its corresponding take-off force for each jump was not statistically significant ($t_{51} = 0.374$, $p = 0.710$). The standard deviations of the mean forces for each animal at each distance are shown in Table 1. Standard deviation in take-off forces at each range is clearly larger than that for landing forces. Excluding the 0.5 m range, for which there is no landing force data, the standard deviation ranges from 1.37 to 6.10 units of bodyweights for take-off force, compared with only 0.04 to 0.92 bw for landing.

Landing force is positively correlated with angle of descent ($r = 0.740$, $p < 0.001$).

The outputs from all strain gauges were recorded simultaneously enabling the duration of each glide to be measured. There is, unsurprisingly, a strong positive correlation ($r = 0.923$, $p < 0.001$) between glide distance and glide duration. Mean glide velocity based on the linear distance from take-off to landing position and not the actual trajectory, was

strongly positively correlated ($r= 0.951$, $p < 0.001$) with horizontal range. This reached 4.5 ms^{-1} across a horizontal range of 2.5 m.

Fig. 43 – Graph of the average take-off angle for each individual flying squirrel as a function of the horizontal distance travelled in the jump (labelled C in Fig. 3). This implies that the squirrels are planning ahead which in turn may imply that they are considering their landing.

Average take-off angle for each squirrel at each distance was negatively correlated with range (Fig. 43; $r = -0.684$, $p < 0.001$).

Fig. 44 shows the percentage of bodyweight supported by lift during gliding, as a function of horizontal range. The average value for each squirrel at each range is plotted against horizontal range and the error bars represent plus and minus one standard deviation. At ranges of 1.5 m and above, the squirrel was able to support the equivalent of approximately 40% of its weight by gliding, but none when jumping only 1 m or less. The advantage gained by gliding increases with range ($r = 0.609$, $p < 0.001$).
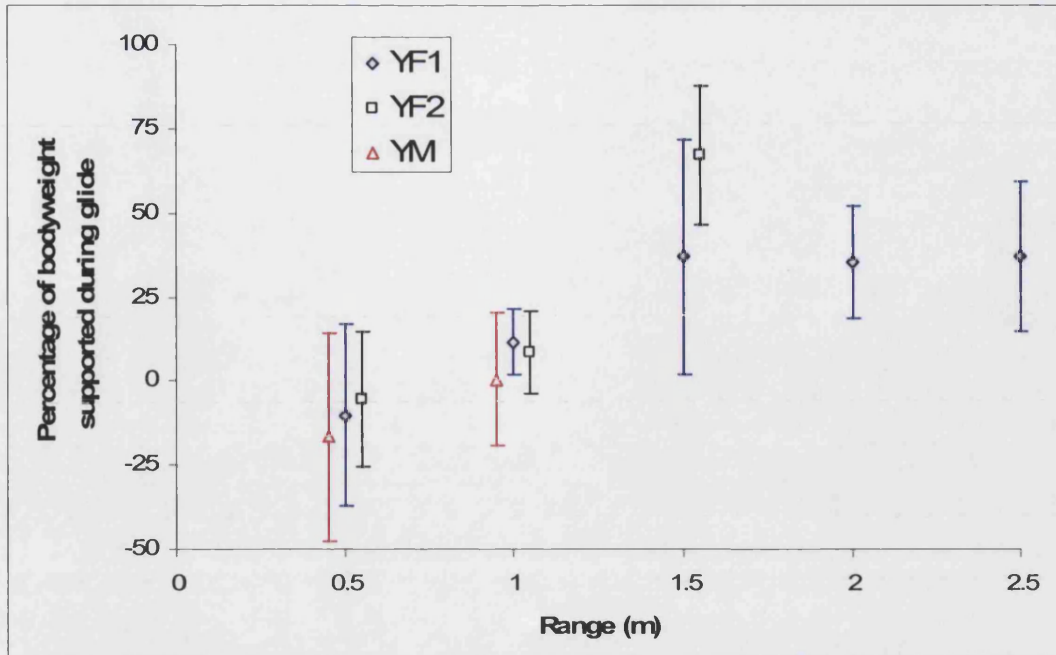
Fig. 44 – Graph of the percentage of bodyweight supported by lift during gliding as a function of horizontal range. Data points are average values for each squirrel at each range and the error bars represent plus and minus one standard deviation.

Landing force was found to be significantly correlated to the position of impact on the pole ($r = -0.713$, $p < 0.001$).

Glide angles increased steeply with horizontal range until they reached approximately 45° beyond 2.5 m, (Fig. 45), the angle at which gliding is distinguished from parachuting, after which they gradually improve as seen by a strong, negative correlation between the 17 longest jumps ($r = -0.816$, $p < 0.001$). At this point, only one animal was still performing but it did not land on the pole, and instead glided past it and landed on the floor.
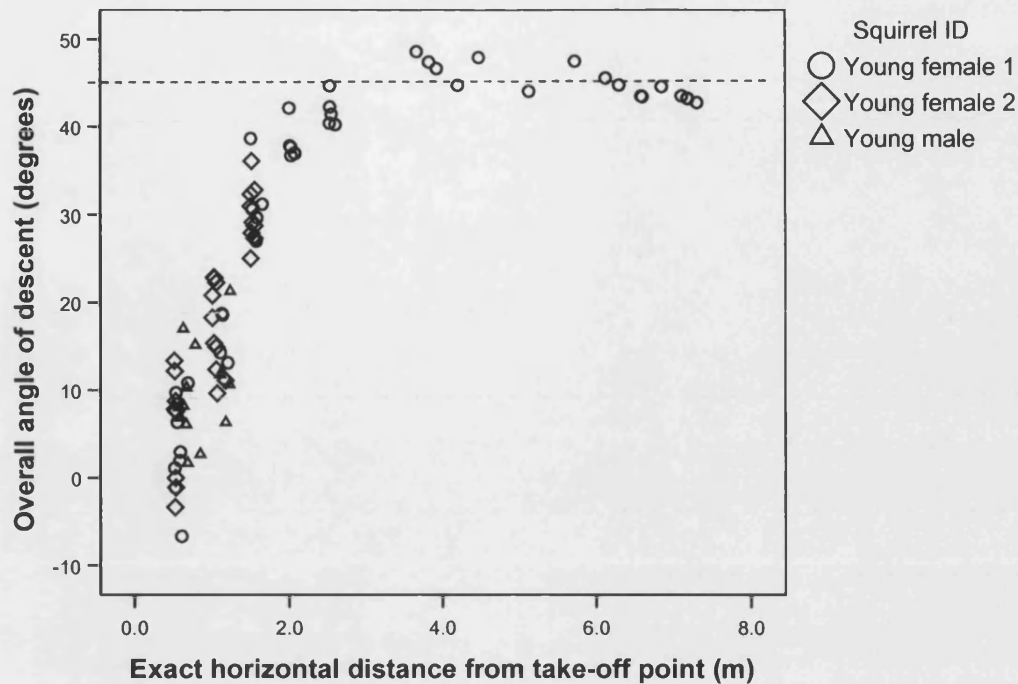
Fig. 45 – Scatter plot showing how the glide angle increases with horizontal range until it reaches approximately 45°, represented by a dashed line, after which the glide ratio begins to improve slightly. High take-off angles and limited time spent in the air are the factors responsible for the low vales of glide angle across low ranges. Glide angle is strongly negatively correlated with range above 4 m ($r = -0.816$, $p<0.001$) where higher glide speeds enable northern flying squirrels to exhibit superior lift to drag ratios.

3.4 DISCUSSION

In this study, take-off and landing forces were measured for northern flying squirrels traversing various distances between compliant substrates. Extensive analysis of video of their movements was also carried out. The results provide more insight into the evolution of gliding in these mammals. And observations are linked, where possible, to the following four hypotheses for the divergence from other tree squirrels:

1. To reduce energetic cost of foraging.
2. To maximise the potential foraging area in a given time without thought to transport cost.
3. To improve predation escape capability.
4. To enable superior control of landing.

Take-off, landing and gliding performance are discussed separately.

3.4.1 Take-off

Flying squirrels generated take-off forces ranging from 1.08 to 9.57 bodyweights. The amount of force was proportional to the distance the animal travelled (Fig. 41). It is logical that squirrels generate a larger take-off force to go further, as ballistic theory dictates they require a higher velocity in order to cover the distance. However, there must be a maximum force the squirrel can generate. The results presented here suggest this might be approximately 10 bodyweights, which is equivalent to occasional high jump forces at shorter ranges. (These occasional jumps support the idea that flying squirrels jump more forcefully when startled, incidentally.)

The highest take-off angle recorded was 35° and this occurred at the shortest range of 0.5m, which was short enough that landing position was often higher than take-off position. Take-off angle decreased as range of the jump increased (Fig. 43) but this may have been influenced by a confounding factor, the height of the branch. With sufficient height the animal can afford a shallower take-off angle, allowing it to generate a higher horizontal velocity. According to ballistic theory, in order to maximise range the optimum take-off angle from the ground is 45°. However, this has been shown to decrease as the relative height of the take-off point increases, and it can be determined from equation below (Linthorne 2001):

$$R = \frac{v^2 \sin 2\theta}{2g} \left[1 + \left(1 + \frac{2gh}{v^2 \sin^2 \theta} \right)^{1/2} \right]$$

Equation 15

Where R is the horizontal range of the projectile, v is the velocity at take-off, θ is the take-off angle, g is gravitational acceleration and h is the height difference between launch and landing. Therefore, using the experimental data, it was possible to compare the average take-off angle adopted by the squirrel with the optimum value for the corresponding average vertical drop, as shown in below:

Take-off and landing forces and the evolution of controlled gliding in northern flying squirrels
(Glaucomys sabrinus)

Horizontal Range (m)	Average measured vertical drop (m)	Average measured take-off angle (degrees)	Calculated optimum take-off angle (degrees)
0.5	0.04	26.4	44
1.0	0.31	20.2	38
1.5	0.89	16.0	27
2.0	1.56	15.2	23
2.5	2.28	12.7	21

Table 2 – Table showing the average measured take-off angle adopted by young female 1 at all horizontal ranges tested, together with the calculated optimum value for the corresponding average vertical drop.

At every range tested, this flying squirrel was adopting a take-off angle considerably lower than the calculated optimum value calculated, approximately 60% (SD = 4.5%). However, the optimum value is based on ballistic theory, and does not take lift or drag into account, and Fig. 44 demonstrates that the study animals were capable of generating lift equivalent to 40% of their bodyweight. Therefore it is quite possible that the flying squirrels in this study were deliberately adopting optimum take-off angles for maximum range.

Overall velocities of the squirrels increased with range. The animals usually ran and jumped immediately after release onto the branch, but occasionally it was necessary to startle them. It is unknown if the apparent levelling off of glide angle that was observed for longer jumps is a general trend because results could not be obtained for longer leaps.

3.4.2 Gliding performance

Squirrels used lower glide angles in the lab, but angles near 45° (parachuting) for the longer ranges of 2 m and above in the barn. This may have been a behavioural change due to unfamiliarity, and is based on only one squirrel at these ranges. In a study describing the kinematics of two southern flying squirrels, Glaucomys volans, glides from both animals were shorter and significantly steeper after moving to a new test arena (Bishop 2006). Here, however, measured glide angles improved with increasing range (Fig. 45) and are comparable with similar distance results from two field studies of northern flying squirrels (Vernes 2001; Scheibe, Smith et al. 2006), so it is more

likely a consequence of the need for this species (the larger of the two North American species) to reach a higher velocity before it is able to exhibit superior aerodynamic performance. Average glide velocities measured in this study increased with range as would be expected. Observations of the Japanese giant flying squirrel on long glides (Ando and Shiraishi 1993) sometimes showed an initial steep descent with the glide angle decreasing with increasing velocity, until both became constant. Likewise, Vernes (2001) observed that northern flying squirrels dropped steeply prior to gliding, and often even managed to gain altitude slightly, just before landing. The squirrels in this study may have initiated a similar behaviour, but the possible ranges were too short for the effect to be noticed. This would help to explain why field observations of northern flying squirrels have reported significantly better glide ratios. Scheibe *et al.* (2006) in Alaska, USA, evaluated 168 glides from 82 different squirrels with mean glide distances of 12.46 m and 14.39 m in successive years, and corresponding mean glide angles were 41.31° and 36.31°. Vernes (2001) reports a mean angle of descent of just 26.8° for glides which were longer, averaging 16.4 m. Gliding behaviour is therefore likely to be optimised for significantly longer ranges than were possible in this study.

Flying squirrels use their patagium as a low-aspect-ratio wing, which has good aerodynamic stability at the relatively low speeds involved, generating lift at high angles of attack of up around 40 degrees without stalling (Torres and Mueller 2004). This shape allows the squirrel to overcome any detrimental rotational momentum that it might have generated during take-off. In the present study, forelimbs were always protracted and abducted before the hind limbs left the substrate, allowing the angular momentum produced to be transmitted directly to the branch, even over the shortest leaps of just 0.5 m. Although the wrists and elbows are still flexed at this point, Essner (2000) argued that this behaviour enabled the squirrel to begin gliding earlier, resulting in a flatter trajectory with more immediate manoeuvrability and control. Gliding performance of each squirrel was quantified by calculating the percentage of its bodyweight supported during each glide, which showed that flying squirrels exploited their unique morphology to generate lift at ranges greater than 1.5 m (Fig. 44). However, these values were negative over 0.5 m implying that the squirrels generated down-force. It could be that the combination of steep take-off angles with immediate initiation of gliding results in their large patagial surface area working against the squirrels on these steeper take-off angles. Alternatively the estimate for the percentage

bodyweight supported could be slightly conservative. In any case, it has been established that the transition from leaping to gliding occurs at a horizontal range of between 1 m and 1.5 m for northern flying squirrels. They are not able to benefit from gliding over distances of less than 1 m, so although the resultant glide angles may appear to be superior at these ranges, this is only a consequence of the higher take-off angles and limited time in the air.

3.4.3 Landing

Landing forces varied between 3.01 and 9.52 times bodyweight. The impact force on the landing pole was proportional to the range of the leap. This is expected because the measured gliding velocity increased with horizontal distance, reflecting the effects of gravitational acceleration.

The correlation of measured landing force with the contact position of the animal on the pole is due to the compliance decreasing towards the fixed end. Higher forces were experienced by squirrels landing lower down on the pole where it was relatively stiffer and did not deflect so far. This is inevitable because the kinetic energy of the squirrel becomes the product of reaction force and deceleration distance – proportional to the deflection of the pole given that leg length remains constant. This has an important implication for the use of compliant substrates when quantifying forces for comparison. Ideally, only forces measured at points of equal compliance should be compared directly, or there should be a random scattering of landing positions. This was the case for the present results, with the exception of the 2 m range, at which the squirrel consistently landed at the base of the pole. The reason for this is unknown, because the angle between the base of the landing pole and the tip of the take-off branch was consistent at 55° for all ranges. However, by removing the data from the 2 m range (7 data points out of 53), a strong linear relationship can be observed between the means of the other 46 jumps where more compliance was available, Fig. 42. The square of the Pearson product moment correlation coefficient (the r-squared value) improves from 0.61 to 0.99 when the 2 m data is ignored. Such a good linear fit means that the flying squirrels adopt a consistent landing technique. On stiffer substrates, a similar but steeper, linear increase in landing force with range would be expected.

Over short leaping distances, take-off forces are not significantly different from landing forces (Fig. 41; t-test). This fits with the expectation (see Section 3.1, page 81) that landing forces would not be higher than take-off forces on compliant substrates, as they are on rigid platforms (Demes, Jungers *et al.* 1995).

Landing force was correlated with angle of descent, suggesting the squirrels are better able to absorb landing impacts with a flatter approach. Some of the impact force is likely absorbed as a result of the consistent landing posture observed, which it seems the squirrels were unable to accomplish with steeper approaches. During shallower glides the squirrels are able to increase their drag force by transforming the patagia and distichous tail from a cambered surface with low angle of attack, high lift and low drag, to a more parachute-like surface orientated against the direction of motion. Additionally, this posture enabled the squirrel to absorb the remaining impact forces more evenly over its four extended limbs on contact. Aerodynamically, the flying squirrel has a low aspect ratio (close to 1) and glides at low speed so an angle of attack in excess of 40° would be required for it to stall in flight (Torres and Mueller 2004). The squirrel has additional aerodynamic implications associated with its morphology, such as its fur, so it is not possible to measure whether or not they are actually stalling from the video footage. However, it is clear from the example landing sequence shown in Fig. 40 that the pitch angle of the body has increased to effectively 90° immediately prior to landing, supporting the theory that they deliberately stall themselves (Alexander 1995).

Caple *et al.* (1983) state that the vector sum of angular momentum must be conserved during any mid-air movement of a body with no lift or drag. Although flying squirrels will also be able to generate some external force from their patagium, this could help explain the origin of some of the consistent landing movements observed. For example, the rotations of the head and tail backwards would directly counteract the thrusting of the limbs ventrally although it is equally likely that the head tilt may be for defence against accidental impact. A falling cat also uses counter-rotations in order to right itself when falling from an upside down position (McDonald 1960). Calculations by Caple *et al.* (1983) also show that some of the morphological features of flying squirrels, such as long forelimbs with dense, distally located mass (hands and feet) and a lightweight tail that can produce lift are optimisations for controlling pitch and roll. The results show

that the squirrels were able to reduce landing forces by pitching upwards as they approach, and it is this behaviour that may have applied selective pressure to these morphological features rather than the desire to maximise glide range, which increases negligibly in comparison. Increasing forelimb length allows the landing energy to be absorbed over a larger distance. Likewise, the flexed back on impact should further reduce the peak landing force. A falling cat also tries to land with its back arched and all four limbs outstretched towards the ground (McDonald 1960).

Unfortunately the squirrels could not be persuaded to land on the pole above the relatively small horizontal range of 2.5 m, compared to their normal arboreal glide distances (Vernes 2001; Scheibe, Smith *et al.* 2006). They chose instead to deliberately manoeuvre past the landing pole and land on the floor. It is possible that the squirrels may have a sense for a maximum speed at which they can safely or comfortably land on a stiff or unknown substrate for a given approach angle. Glide angles achieved at ranges between 3 and 6 m exceeded 45° (Fig. 45), which would normally be defined as parachuting rather than gliding (Oliver 1951), and so it is speculated that this is likely to be the most difficult distance for northern flying squirrels to land. The steeper approach angles inhibit their ability to pitch up and absorb the landing across all four limbs simultaneously, and there is more energy to dissipate due to the inevitable increase in velocity with range. Velocity continues to increase above the proposed awkward range but this also improves the flying squirrel's aerodynamic ability, allowing a progressive improvement in approach angle and consequent landing posture. It is likely that these animals would try to avoid making hard landings on tree trunks at this unfavourable range. Vernes (2001) reported that in 21% of his 100 glides observed, northern flying squirrels landed on the ground or in dense undergrowth. The other landings were on trees and it should be noted that the mean glide distance was much higher in the Vernes study than in this research. Likewise, Scheibe *et al.* (2006) noted that sometimes squirrels released onto a tree trunk at breast height did not climb and glide, choosing instead to jump to the ground and run to a nearby tree. Future experimental designs should consider that northern flying squirrels might be more likely to land on an instrumented pole positioned at a high rather than medium horizontal distance from the take-off position, but this would necessitate an arena allowing sufficient take-off height.

The equation for the linear relationship between landing force and range on the compliant part of the pole is shown on Fig. 42 and can be used to predict the landing force at longer ranges than were measured. However, the squirrels would not keep accelerating indefinitely during long glides, but rather their speed would stabilise as they approach terminal velocity. Scheibe *et al.* (2006) reported maximum glide velocities of close to 12 ms^{-1} although the weighted means were 6.26 ms^{-1} and 8.11 ms^{-1} in two consecutive years. These values are much higher than the highest observed speed of 4.5 ms^{-1} although this was measured across a relatively much shorter horizontal glide distance. With more time in the air, squirrels must be able to control their trajectories, otherwise they would be subject to extremely high impact forces. Depending on substrate compliance, the equation from Fig. 42 can be used to calculate that squirrels trying to land an ordinary 16 m glide would be subject to impact forces of upwards of 28 body weights if they did not slow themselves, perhaps by pitching up and employing air braking.

3.4.4 Evolution of gliding

Hypothesis 1 that gliding developed to reduce the energetic cost of foraging supposes that the squirrels' primary objective should be to maximise range in every jump while minimising the loss in altitude. It was shown that the individuals in this study consistently used take-off angles of approximately 60% of the calculated optimum value for a ballistic projectile. Therefore it is quite possible that these flying squirrels were employing optimum take-off angles when the effect of lift and drag is considered. As expected, the advantage gained by gliding increases with range. This vertical advantage achieved relative to the ballistic trajectory enables flying squirrels to reach trees beyond normal jumping range, or reduces the amount of climbing required after a glide is completed, thus saving energy. Range-reducing aerial manoeuvres were frequently observed, but these alone are insufficient evidence to reject the energetic cost of transport cost hypothesis.

If gliding evolved to maximise the foraging area that could be reached in a given time, as proposed by **Hypothesis 2**, then the squirrels would be expected to glide at high velocities. It has been shown here that velocity increases with range, and flying squirrels

can generate higher lift forces when travelling further, so the hypothesis that gliding is an optimisation to maximise speed and potential foraging area cannot be rejected.

Hypothesis 3 is that gliding evolved primarily to facilitate escape from predation. One might expect that an escaping squirrel would jump horizontally, or downwards given sufficient altitude, in order to ensure that it did not decelerate due to gravity. Bonser (1996) proposed that starlings may deliberately vary take-off trajectory for predator avoidance, but the present study shows a negative correlation of the take-off angle with range, suggesting that during this experimentation at least, flying squirrels choose a take-off trajectory to suit their intended destination. Caple *et al.* (1983) stated that all gliders pre-select a landing site, which must be large enough to allow some vertical variation in the contact point. Vernes (2001) also observed that flying squirrels appeared to think about their intended flight path before launching and the present study gives no evidence to suggest otherwise. Given that the squirrels seem to exhibit this behaviour even during the jumps which were initiated by startling, it seems unlikely that gliding evolved primarily for escape, at least not from high-speed chases.

The ability to make sudden aerial direction changes could potentially help to lose a predator. However, Scheibe (1990) reports that their most likely aerial predator is the owl, and it is unlikely that such sophisticated fliers would be troubled by the relatively clumsy swerving squirrel.

Hypothesis 4 relates the development of flight to the control of landing. Even at the comparatively short ranges in this study, direction changes were seen being introduced, perhaps aided by the observed rapid beating of the tail from side to side. Additionally, last-second manoeuvres were observed, such as banking and using the tail as a rudder, implying that flying squirrels are able to make precise adjustments to improve their landing. As range increases, any error in take-off trajectory would become more significant without aerial control; in this case squirrels could face serious consequences for misjudging long leaps at the top of the forest canopy.

Flying squirrels choose to initiate a full gliding posture even though they do not produce significant lift during glides of less than a metre, suggesting that this behaviour is innate. It might be that the squirrel is simply throwing its arms out conveniently widely

for rapid rotation of the joint in order to gain forward momentum during take-off. They do exhibit a consistent landing behaviour at these distances, with the gliding posture enabling them to pitch upwards as they approach and spread the landing reaction force over all limbs. It is likely that the squirrels deliberately stall themselves by this quick increase of their angle of attack immediately prior to landing.

Landing control of pitch and roll improves much more rapidly than range for the same incremental improvements in forelimb length and tail surface area. Increasing forelimb length simultaneously reduces the landing force further by increasing the deceleration distance. Landing force was correlated with angle of descent, suggesting flying squirrels were unable to pitch up sufficiently to execute the evenly-distributed four-limbed landings when approaching steeply, demonstrating the utility of aerial control in longer jumps. The final argument is that without reducing the impact force through postural control prior to landing, northern flying squirrels would have to sustain impact forces of upwards of 28 bw.

Evolution of gliding in flying squirrels has undoubtedly reduced their energetic cost of transport, while improving potential foraging area and response to predation, but this thesis concludes that the selective pressure for their divergence from tree squirrels might have been the improvement of landing control.

3.5 CONCLUSIONS AND IMPLICATIONS TO JUMPING ROBOT

Take-off and landing forces generated by northern flying squirrels are both positively correlated with horizontal range, at least up to 2.5 m. The maximum take-off force measured was 9.57 bodyweights, although the squirrels would occasionally produce close to this force when jumping only short distances, most likely a natural behavioural response to alarm. Take-off forces were not significantly different to the corresponding landing forces on these similarly compliant substrates. They are able gliders, abducting all limbs to create a wing-like surface which is held at a low angle of attack for maximum lift/drag ratio. Glide angle increased rapidly with horizontal range up to approximately 4 m, before progressively improving suggesting that gliding in northern flying squirrels is optimised for significantly longer ranges than were possible in this study.

Any compliant force measuring device will likely have some variation in its compliance along its length. In the case of a cantilever beam, this begins to behave more like a rigid instrument towards its fixed end. Valuable comparisons can only be made between forces measured at known points of equal compliance. If this is not possible, then sample sizes should be chosen to ensure a random scattering of landing positions.

In order to draw solid evolutionary conclusions it would have been preferable to obtain equivalent data for a sequence of species from non-gliding genera, such as grey squirrels (Sciurus), through to the most highly developed forms such as the Japanese giant flying squirrel (Petaurista). This was not possible, but Glaucomys was viewed as a valid compromise because it is a relatively primitive gliding squirrel (Johnson-Murray 1977). The hypothesis that gliding evolved in flying squirrels to reduce the energetic cost of transport could not be rejected, although the study animals were observed to make aerial manoeuvres occasionally, which would result in a lower landing position. The flying squirrels in this study did not attempt to make either unplanned or deliberately unpredictable take-offs, casting doubt on the theory that gliding might improve predatory escape response.

Gliding might have evolved to maximise the foraging area that could be reached in a given time. High glide speeds were measured and this velocity increases with range, but the development of improved landing control is a necessary consequence of faster flight. Evidence is provided that if northern flying squirrels could not slow themselves aerodynamically from terminal velocity, prior to landing, they would have to be able to sustain impact forces of upwards of 28 bw. Flying squirrels seem to innately adopt a gliding posture on take-off, even during leaps of less than a metre when no vertical advantage is gained, but this leaves them better prepared for aerial control. At these low distances, a consistent landing strategy was exhibited by flying squirrels allowing the impact force to be spread over all four limbs and their arched back, thanks to a dramatic pitch upwards immediately prior to contact with the pole. This rapid increase of their angle of attack immediately prior to landing is likely a behaviour evolved to enable rapid deceleration by stalling, although this would have greater effect at high speeds. Therefore, the major conclusion from this chapter is that at divergence, small glide producing surfaces were developing in flying squirrels allowing mid-air adjustments in pitch and roll, and improving their resilience during high speed arboreal transport.

The implications of these conclusions to the development of a jumping robot are that integrating gliding should certainly be considered as a means to both control landing orientation and reduce impact force. Flying squirrels start to extend their patagia during take-off, before their hind limbs leave the substrate, and so the robot might also benefit from extending some kind of gliding membrane during the jump cycle. Attempting to deploy once airborne could cause detrimental mid-air rotations, where as incorporation into the jump mechanism utilises already amplified power from its otherwise low grade energy. In order to reduce their landing forces, flying squirrels attempt to control their angle of attack such that their membranous wing is parallel to the landing surface. A robot that jumps into a glide would likely also benefit from some kind of pitch control, to prevent it from nose-diving, (in which case the membranes would only accelerate it due to their additional mass and the comparative lack of drag). In the same way, it could potentially orientate itself so as to store some of its kinetic energy on landing, reducing the total impact force, although this should not be a requirement. This study also showed that sufficient forward speed is important for a glider. This carries an implication for the take-off angle of the jumping robot being developed.

3.6 References – Chapter 3

ALEXANDER, R. M. (1991). "Elastic mechanisms in primate locomotion." Z. Morph. Anthropol. **78**: 315-320.

ALEXANDER, R. M. (1995). How Animals Move, Maris Multimedia, Discovery Communications, Inc.

ANDO, M. and SHIRAISHI, S. (1993). "Gliding flight in the Japanese giant flying squirrel Petaurista leucogenys." Journal of the Mammalogical Society of Japan **18**(1): 19-32.

BISHOP, K. L. (2006). "The relationship between 3-D kinematics and gliding performance in the southern flying squirrel, Glaucomys volans." Journal Of Experimental Biology **209**(4): 689-701.

BONSER, R. H. C. (1999). "Branching out in locomotion: The mechanics of perch use in birds and primates." Journal Of Experimental Biology **202**(11): 1459-1463.

BONSER, R. H. C. and RAYNER, J. M. V. (1996). "Measuring leg thrust forces in the common starling." Journal Of Experimental Biology **199**(2): 435-439.

CAPLE, G., BALDA, R. P. and WILLIS, W. R. (1983). "The Physics Of Leaping Animals And The Evolution Of Pre-Flight." The American Naturalist **121**(4): 455-476.

DEMES, B., FLEAGLE, J. G. and JUNGERS, W. L. (1999). "Takeoff and landing forces of leaping strepsirhine primates." Journal of Human Evolution **37**(2): 279-292.

DEMES, B., JUNGERS, W. L., et al. (1996). "Body size and leaping kinematics in Malagasy vertical clingers and leapers." Journal of Human Evolution **31**(4): 367-388.

DEMES, B., JUNGERS, W. L., GROSS, T. S. and FLEAGLE, J. G. (1995). "Kinetics of Leaping Primates." American Journal of Physical Anthropology **96**(PT 4): 419-429.

ESSNER, R. L. (2000). "Comparison of takeoff kinematics in gliding and nongliding squirrels." American Zoologist **40**(6): 1010-1011.

ESSNER, R. L. (2002). "Three-dimensional launch kinematics in leaping, parachuting and gliding squirrels." Journal of Experimental Biology **205**(16): 2469-2477.

JOHNSON-MURRAY, J. L. (1977). "Myology of the gliding membranes of some petauristine rodents (Genera: Glaucomys, Pteromys, Petinomys, and Petaurista) " Journal of Mammalogy **58**(3): 374-384.

KEITH, M. M., SCHEIBE, J. S. and HENDERSHOTT, A. J. (2000). Launch Dynamics in Glaucomys Volans. The Biology of Gliding Mammals. R. Goldingay and J. S. Scheibe. Germany, Filander Press: 185-198.

KRUEGER, C. and TIAN, L. (2004). "A Comparison of the General Linear Mixed Model and Repeated Measures ANOVA Using a Dataset with Multiple Missing Data Points." Biological research for nursing 6(2): 151-157.

LINTHORNE, N. P. (2001). "Optimum release angle in the shot put." Journal of Sports Sciences 19: 359-372.

MCDONALD, D. D. (1960). How does a cat fall on its feet? The New Scientist. 7: 1647-1649.

MENG, J., HU, Y., et al. (2006). "A Mesozoic gliding mammal from northeastern China." Nature 444(7121): 889-893.

NORBERG, U. M. (1985). "Evolution of Vertebrate Flight - an Aerodynamic Model for the Transition from Gliding to Active Flight." American Naturalist 126(3): 303-327.

OLIVER, J. (1951). "Gliding in Amphibians and Reptiles." The American Naturalist 85: 171-176.

PASKINS, K. E., BOWYER, A., MEGILL, W. M. and AND SCHEIBE, J. S. (2007). "Takeoff and landing forces and the evolution of controlled gliding in northern flying squirrels (Glaucomys sabrinus)." J Exp Biol 210(8): 1413-1423.

SCHEIBE, J. S., FIGGS, D. and HEILAND, J. (1990). "Morphological Attributes of Gliding Rodents a Preliminary Analysis." Transactions of the Missouri Academy of Science 24: 49-56.

SCHEIBE, J. S. and ROBINS, J. H. (1998). Morphological and performance attributes of gliding mammals. In Ecology and Evolutionary Biology of Tree Squirrels. M.A.Steele, J.F.Merritt and D.A.Zegers. Martinsville, VA., Virginia Museum of Natural History: 131-144.

SCHEIBE, J. S., SMITH, W. P., BASSHAM, J. and MAGNESS, D. (2006). "Locomotor performance and cost of transport in the northern flying squirrel Glaucomys sabrinus." Acta Theriologica 51(2): 169-178.

THORINGTON, R. W., DARROW, K. and ANDERSON, C. G. (1998). "Wing tip anatomy and aerodynamics in flying squirrels." Journal of Mammalogy 79(1): 245-250.

THORINGTON, R. W. and HEANEY, L. R. (1981). "Body Proportions and Gliding Adaptations of Flying Squirrels (Petauristinae)." Journal of Mammalogy 62(1): 101-114.

TORRES, G. E. and MUELLER, T. J. (2004). "Low-aspect-ratio wing aerodynamics at low reynolds numbers." AIAA 42(5): 865-873.

VERNES, K. (2001). "Gliding performance of the northern flying squirrel (Glaucomys sabrinus) in mature mixed forest of eastern Canada." Journal of Mammalogy 82(4): 1026-1033.

Chapter 4

Functional attributes of flying squirrel skin – A preliminary study

The study of Northern Flying Squirrels in the previous Chapter concluded that the unique aerial capabilities of these animals developed primarily to control their landing posture for impact force reduction, potentially to enable faster arboreal travel. This morphology simultaneously extends the range of the jump at little or no additional energetic cost, and an equivalent means of landing preparation became a design requirement for the jumping robot in development for this Ph.D research project. This chapter will seek to further inspire this design by considering how the gliding membranes (patagia) of flying squirrels are specialised to facilitate the transition between the various transport modes available to these animals.

4.1 Introduction

Gliding has evolved as a means of enhancing arboreal locomotion in a very similar, yet independent way in several mammal and marsupial species. Flying squirrels, colugos and flying oposums all have patagia, a larger and more developed piece of skin attached between the wrists and ankles, which they choose to stretch when jumping from a tree by fully abducting their limbs. The consequent large surface area of this skin enables them to glide at shallow angles, and also make impressive aerial manoeuvres such as 180° turns (Savile 1962). However, there is a compromise between maximising the surface area of the skin available for aerial locomotion, while not impeding normal arboreal locomotion such as running up, down and around tree-trunks. Flying squirrels are adept at both kinds of locomotion, with their skin apparently held elastically in folds tight against their bodies during climbing (personal observation). Johnson-Murray (1977) speculates that the patagium is pulled towards the body by contraction of *humerodorsalis* and *flexor carpi ulnaris* musculature.

Fig. 46 illustrates some of the terminology used throughout this chapter to describe the directional properties of flying squirrel skin.
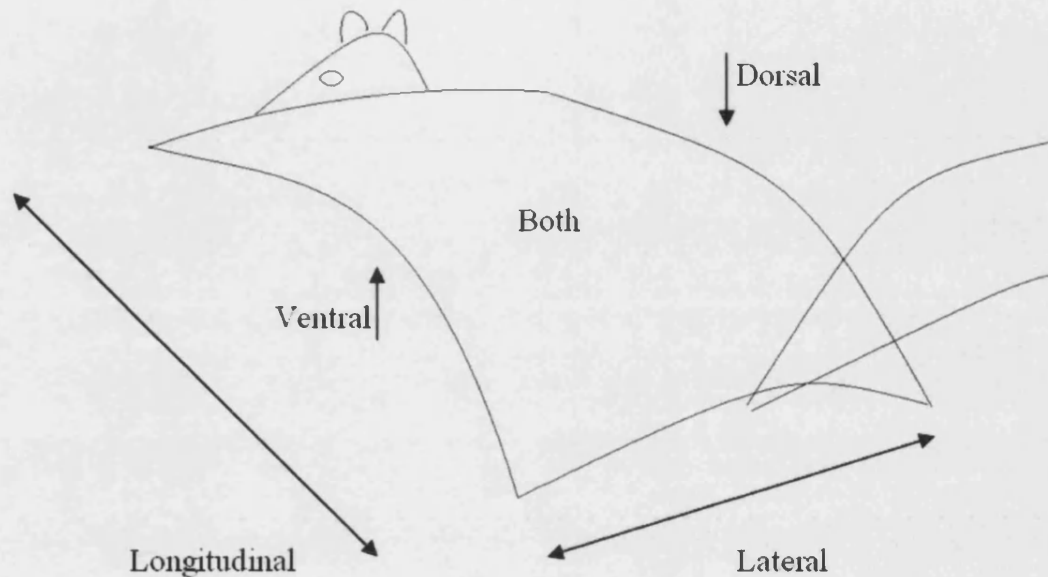
Fig. 46 – Diagrammatic representation of a Southern flying squirrel detailing the biological terms used in this chapter relating to the position and orientation of its skin.

4.1.1 Desirable material properties for flying squirrel patagia

During their normal arboreal locomotion, flying squirrels frequently land on tree trunks then immediately climb upwards towards the top before taking off again to continue their journey. It was discussed in the previous chapter that flying squirrels rapidly abduct their forelimbs into the gliding posture during take-off. Consequently, their patagia must be able to stretch quickly to enable rapid, momentum-producing arm swing on take-off and also retract quickly on landing so as not to be a trip hazard during subsequent walking or bounding. Puncture resistance is another desirable property for flying squirrel skin, due to their being nocturnal and travelling at high velocity, making numerous landings on trees dotted with small snags and other irregularities. In addition, their own claws are necessarily sharp to ensure good purchase on vertical substrates, increasing the risk of accidental skin tearing, which would be difficult to avoid in the event of a fight between squirrels. Therefore damage tolerance is essential in both the

ability to heal quickly, and in the potential to continue gliding and foraging successfully after injury without continuously reopening any wound. Ideally the gliding membrane would still be as lightweight as possible, reducing the animal's total mass and thus improving glide ratio. At the same time, this wing should be capable of sustaining high wing loading, with a reasonable element of safety margin. This is particularly important for females during pregnancy, which must carry more weight while also needing to forage more than usual.

During a normal glide, flying squirrels hold their membrane out at a positive angle of attack and with some camber (when viewed in profile), as shown by a simplified model in Fig. 47. This means that the ventral skin is subjected to positive pressure while the dorsal skin is under negative pressure. At low angles of attack, which minimises drag, it is this negative pressure which produces the majority of the lift force. The steeper the angle of descent, the more important positive pressure becomes, as the drag created makes up more and more of the total lift force.
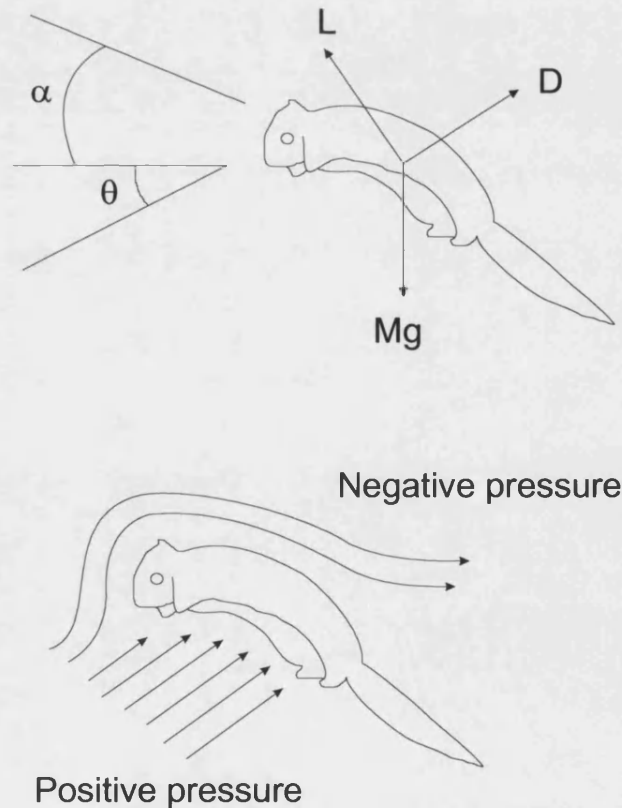
Fig. 47 – Simplified model of a flying squirrel, viewed laterally during normal gliding at an angle of attack, α, and a descent angle, θ. The lower half of the diagram shows how positive pressure acts on its ventral skin, while the dorsal surface is subjected to negative pressure. To clarify, negative pressure refers to a lower pressure than that of the surrounding air, and positive pressure refers to higher pressure.

It is possible to draw a parallel here between a flying squirrel and a sailing boat. When sailing into the wind, a horizontal lift force is generated by the stiff camber produced on the mainsail, the resultant shape being similar to that of an aerofoil. Therefore, when designing main sails, high stiffness is vital to improving speed and the angle to which the boat can sail relative to the on-coming wind (It is not possible to sail directly into the wind – see Fig. 48). Therefore for flying squirrels to be able to glide quickly, at a low angle of attack, they would also want to be able to form their patagia into a stiff, cambered aerofoil shape. Hence, as for the close-hauled sail, high longitudinal stiffness would be a desirable mechanical property for their patagial skin. This would allow the flying squirrel to accurately control the precise camber of its wing with small movements of its limbs either forwards or backwards.

WIND

UPWIND SAILING
(CLOSE HAULED)

BEAM REACHING

DOWNWIND SAILING
(RUNNING)
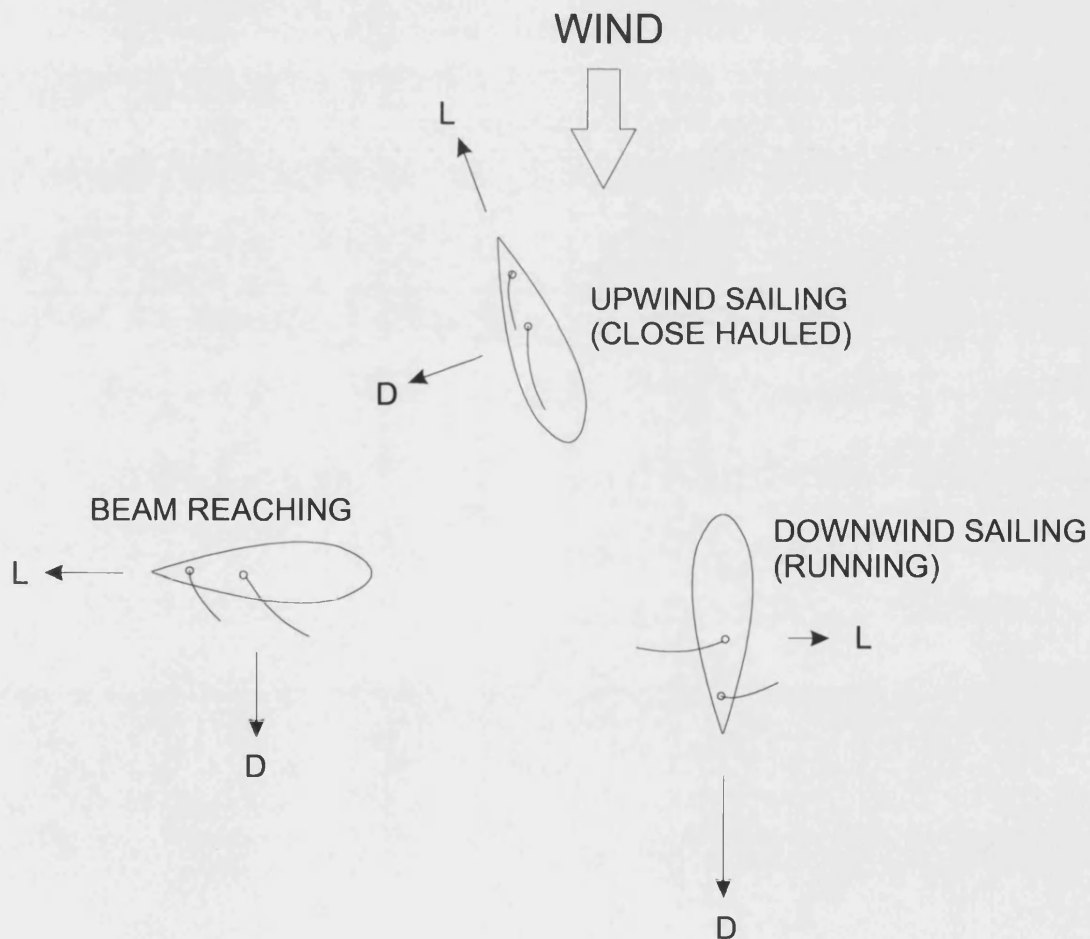
Fig. 48 – Diagram showing how the lift and drag forces become relatively more important for propelling sailing boats depending on wind direction.

There is a compromise between the stiffness and strength of a sail – the stiffer something is, the less able it is to absorb high stresses by stretching and hence it is more prone to tearing. When sailing downwind (the wind blows from behind the boat) where drag force rather than lift is what drives the boat forwards, a spinnaker sail gives best performance. If the spinnaker was made of high stiffness material like a mainsail, much of the wind would spill over its sides and the frequent flapping would increase the likelihood of tearing. However, reducing stiffness permits higher tear strength while catching more wind, in much the same way as a parachute works. It was shown in the previous chapter that flying squirrels deliberately pitch up immediately prior to landing, and hence more closely resemble a running spinnaker than a close-hauled mainsail during this phase of the locomotion. However, a compromise is therefore required, as it was discussed previously that high longitudinal stiffness would be desirable for gliding at low angle of attack during the main phase of flight. Assuming that their patagia had high longitudinal stiffness required for this close-hauled phase, it would therefore be advantageous for the skin to be much more compliant in the lateral direction for improved air braking performance, and damage tolerance. A more deformable surface of the patagia may also help to reduce induced drag (caused by air spilling up over the wing-tips due to the pressure gradient described).

Hundreds of years of sail making have taught that sails can be improved by using thicker materials where the loads are highest (Whidden and Levitt 1990). More recently, computer generated stress maps have been used to demonstrate that mainsail loads are highest on the *leading edge*, the edge of the sail that the wind reaches first, while spinnaker loads radiate from the corners (Lasher, Sonnenmeier *et al.* 2005). Seams aligned to the load are used both to add strength, and to allow the use of thicker panels in areas subjected to higher stress within the sail (Whidden and Levitt 1990). Therefore the thickness of flying squirrel skin may not necessarily be uniform throughout the patagia.

Before addressing the hypotheses described above, it is useful to review the literature on mammalian skin.

4.1.2 Physical characteristics of mammalian skin

Mammalian skin is made up of three layers, the *epidermis*, the *dermis* and the *hypodermis*. The outer layer of skin is the epidermis, which is comprised primarily of dead cells. Inside that is the dermis, about twenty times thicker and containing hair follicles, blood vessels, muscles, nerves, oil and sweat glands. The hypodermis is a very thin layer of tissue underlying the dermis. The overall behaviour of the skin can be traced to the structural properties of its main constituent, the dermis. It is effectively a composite of elastin and collagen fibres embedded in a viscous, hydrated matrix. The elasticity of the elastin fibres compliments the strength of the more prominent (60-80%) collagen fibres (Reihsner, Balogh *et al.* 1995).

Starcher, Aycock *et al.* (2005) suggested that with the exception of humans, the primary function of elastin fibres in normal mammalian skin is in the movement and/or placement of hair. In humans and bat wing skin however, which do not have fur, it seems likely that maintaining skin elasticity must be its primary function. The elastin aspect of squirrel skin dermis in particular was shown (in the same paper) to be unusually shallow, with hair follicles penetrating less than one fifth of the depth of the skin. Consequently, all of the elastin fibres are concentrated at the base of these follicles, and extend in all directions through the dermis to contact other follicles.

The skin of bat wing is uniquely different from other mammals, with elastin fibres dominating (Hollbrook and Odland 1978). Bat wing skin is used for generating lift, thrust and transmitting stresses during flight in addition to its usual protective and regulatory functions. The membrane is supported by a regular, approximately orthogonal mesh of collagen and elastin fibre bundles, with the latter dominating (Fig. 49). It is thought that these elastic components may help to keep the wing tightly folded during climbing and roosting, etc, but also facilitate passive contraction when the wings are flexed (Swartz, Groves *et al.* 1996).
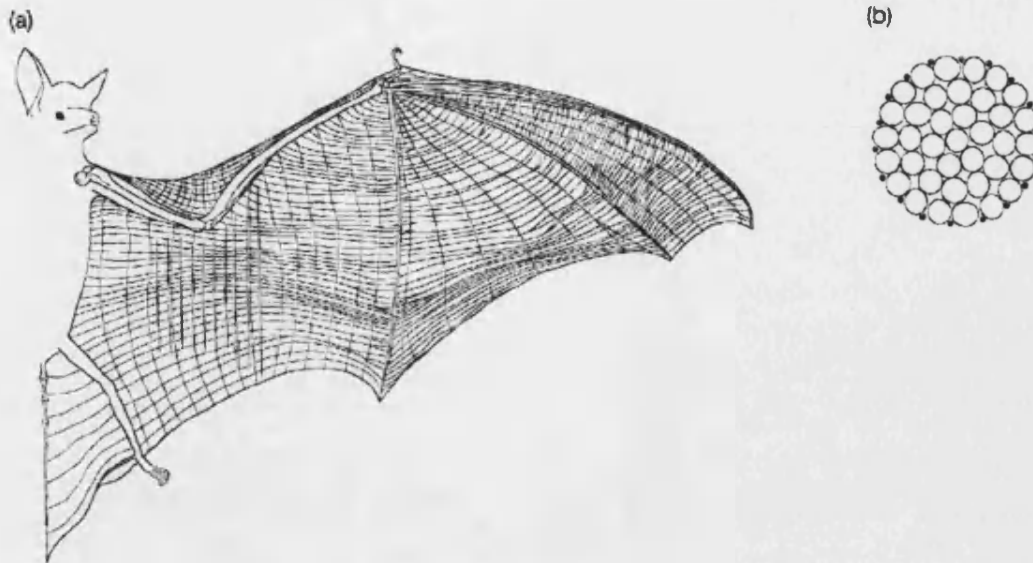
Fig. 49 – The layout of fibre bundles in a typical bat wing, (a), taken from Swartz, Groves *et al.* (1996). Also shown is a cross-section through one of these fibre-bundles, (b), showing the predominant elastin fibres (white) surrounded by collagen fibres (black).

The wing membranes of bats have been shown to be considerably thinner than what would be predicted from the regular pattern of scaling described for most mammals (Swartz, Groves *et al.* 1996). The wing membrane of bats comprises two layers of unusually thin epidermis on either side of a relatively thin dermis/hypodermis compared with the thicker, single-layered skin of the bat's body which is more comparable with other mammals. This thickness is intrinsically linked to the mechanical properties of the bat wing, controlling the 3D shape characteristics of the membrane during flight. Thinner skin also reduces the overall mass to be transported during flight, which would allow a superior lift/drag ratio and consequent range for a glider.

The properties of skin are dependent on direction. Langer (1861) investigated the elliptical wounds formed by piercing skin with small circular holes. By joining up the major axes of these ellipses over the whole body, he was able to demonstrate the lines of tension on the skin surface (Langer's lines, Fig. 50). The practical effects of these lines of tension were further explored by Ridge and Wright (1966), who showed that one-inch-square sections of skin would shrink when cut out due to the removal of this tension. There was more shrinkage in the direction of Langer's lines as a consequence of the relaxation of greater tension. Surgeons were already aware of this effect, recognising that incisions made along Langer's lines are naturally pulled together, thus healing more quickly and minimising scarring (Gibson, Stark *et al.* 1971). Simple load vs extension graphs showed that specimens taken parallel to Langer's lines would not

extend as far as those taken perpendicularly (Ridge and Wright 1966). Strain hardening, where deformation causes an increase in resistance to that deformation, occurs at lower strains when parallel to Langer's lines. Therefore, mammalian skin must be considered as an *orthotropic* material, a material which has contrasting properties in two orthogonal directions.
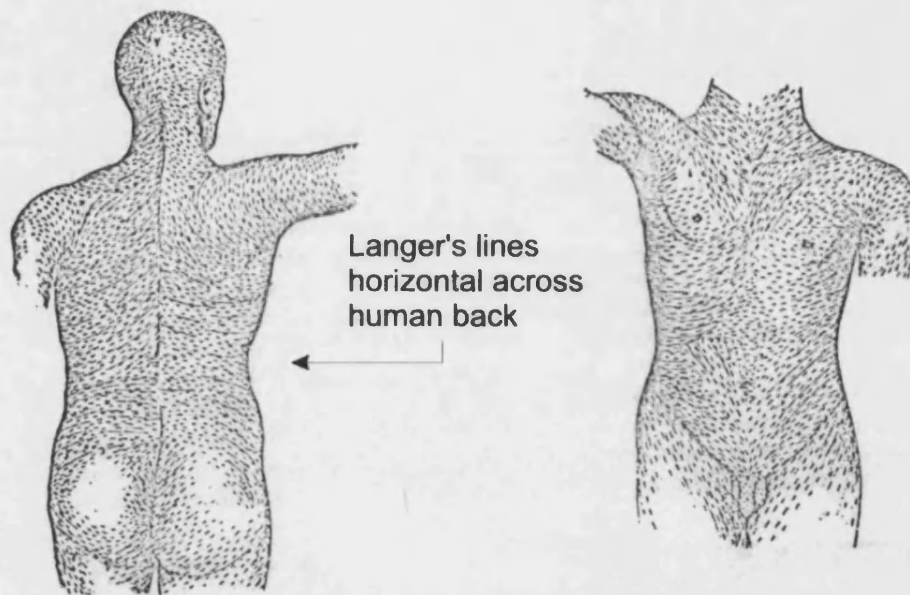
Fig. 50 – Langer's lines are the lines of principal tension around the skin surface, shown here on a human. This figure was modified from Gibson, Stark *et al.* (1971).

The reason for the orthotropic nature of skin depends on the preferential direction of its collagen fibres, which were shown through histological testing to follow Langer's lines (Cox 1942). Ridge and Wright (1966) confirmed this and further explained the resulting skin properties by modelling it as a simplified 2D lattice structure (Fig. 51), although in reality it would be a 3D matrix. The mean fibre angle is less than 45° in the direction of Langer's lines, and hence samples taken in this direction will require relatively less extension (than for a higher fibre angle) before all fibres begin to line up parallel to one another. Further extension will require the fibres to be strained, requiring more force than fibre reorientation. It can also be seen that extending specimens taken across the Langer's lines will result in a smaller fibre area (i.e. the number of fibres available at each end of the sample) and greater orientated length, all of which contributes towards the orthogonal differences in the resulting load-extension graphs observed.
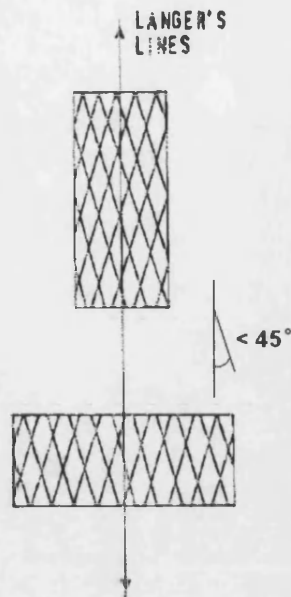
Fig. 51 – Simplified 2D lattice model of skin proposed by Ridge and Wright (1966) to explain how the primary orientation of collagen fibres can produce the orthogonal difference between mechanical properties of skin. This diagram is a modification of two diagrams from the same paper.

4.2 Modelling the structure of flying squirrel skin

It is generally considered that mammalian skin does not vary much between species, with the exception of bat skin, for which Swartz, Groves *et al.* (1996) concluded that the structural design of these soft tissues is influenced by selective forces in the same way as the harder skeletal elements and overall wing shape are. It is probable that flying squirrel skin would be similarly specialised for its unique role.

It has been shown that in normal mammalian skin, collagen fibres are predominantly orientated close to the direction of Langer's lines, the lines of primary tension in the skin. Therefore in order for flying squirrel patagia to have higher longitudinal stiffness than lateral, as was proposed to be advantageous for aerodynamic control, Langer's lines would be expected to run primarily from head to foot.

The fact that bat skin is known to have higher elastin content than normal mammalian skin suggests that flying squirrel skin too may have relatively more elastin fibres, which would be advantageous both to the wing aerodynamics, and in keeping their patagia tightly folded away during walking and running. The particularly shallow network of

elastin reported for squirrel skin may have afforded flying squirrels the opportunity to evolve a thinner, and highly elastic membrane structure. Thinner skin would seem a highly likely specialisation for flying squirrel skin, which would advantageously reduce the total mass of the animal and yet still provide sufficient insulation because it would normally be bunched up (when the limbs are not abducted in the gliding posture), effectively acting as a thicker insulating layer.

Considering the ideal properties of high longitudinal stiffness, and high lateral elasticity, it is proposed here that the flying squirrel membrane may resemble a bi-directional composite of two different types of fibre, as demonstrated in Fig. 52. The higher stiffness fibres (most likely collagen) would primarily be oriented longitudinally, with some much more elastic fibres (perhaps but not necessarily elastin) running orthogonal to them in a matrix. The resultant composite behaviour would be similar to that of a weave of the two fibres. This suggested structure would suppose that flying squirrel skin is composed of proportionally much more elastin than is found in other normal mammalian skin.

Fig. 52 – Demonstration of cross matrix proposal for the primary orientation of fibres in flying squirrel skin, in the gliding position, when all the fibres are extended. The black lines represent fibres with higher stiffness, perhaps collagen, predominantly parallel to the long axis of the animal. The red lines indicate the principle direction of the more elastic fibres, perhaps elastin, orientated transversely so as to elastically collect in the longitudinal fibres towards the body when the arms are not abducted.

The additional springiness in the lateral direction of the proposed structure would be advantageous to the animal, because the direction of this elastic behaviour acts to pull the patagia in tight towards the body from the sides during normal quadrupedal locomotion. This amount of skin would otherwise present a tripping hazard. When walking or bounding, all four legs move forwards and backwards with respect to the body axis with very little sideways motion. In this way, the skin is being stretched slightly along the length of the squirrel. Only the deliberate abduction of the flying squirrel's limbs for gliding would stretch the membrane against the direction of elasticity described, which would become conveniently stiffer at high strains. At this point only a much smaller protraction of the limbs away from each other (towards the head and tail respectively) is necessary to stiffen the membrane in the longitudinal direction, which should enable the animal to precisely control the camber of its wing. Finally, the proposed bi-directional matrix structure should ensure a rapid retraction of the membrane again on landing owing to the high elasticity of the elastin fibres.

The gliding lizards, *Draco volans*, also have highly specialised patagia, with high elasticity. On stretching these into the erect gliding position, these naturally retract back to their original state even on preserved specimens (Russell and Dijkstra 2001). It was shown in the same paper that the accurate folding in of the flight membranes is aided by the elastic properties of its skin, together with bands of elastin running transverse to the protracted ribs. Bands of collagen connect the distal ends of the ribs and are pulled taut during gliding, giving the patagia a prominent rim, and the bands of elastin are simultaneously placed under tension. The architecture of collagenous networks within the membrane is said to result in regional differences in mechanical properties, which improve the aerodynamics of the wing (Russell and Dijkstra 2001). Such specialisation of the membrane towards gliding in Draco adds credibility to hypothesis in this chapter that flying squirrel skin would be similarly optimised.

4.3 Experimentation

In order to briefly test the credibility of the patagial skin structure hypothesis developed above, a southern flying squirrel, *Glaucomys volans*, was obtained so that mechanical testing could be performed to look for evidence of an orthogonal difference in skin

stiffness. A mouse, *Mus musculus*, was also obtained in order for a direct comparison of skin thickness.

4.3.1 Introduction to mechanical testing of skin

Mechanical testing of skin is of great interest, particularly in the field of plastic surgery, but it is subject to many difficulties and as such there is much variation in both the methods and results. *In vitro* testing refers to skin which has been removed from the body. In theory, this allows more option when choosing the test method, and testing to destruction can be carried out. However, the mechanical properties of skin are highly dependent on water content, which is likely to alter soon after removal from its natural environment. *In vivo* testing ensures that the skin behaves normally, but is subject to ethical restrictions. Standard equipment cannot be used, as the measurements are influenced by other structures the skin is attached to, not least itself. Consequently, the range of reported measurements for the Young's modulus of human skin, which have been achieved using commercially available *in vivo* systems, has varied considerably, between 0.01 and 100 MPa (Wan Abas and Barbenel 1982; Rodrigues 2001).

Lanir and Fung (1974) developed an experimental system for two-dimensional testing of soft tissues for use on rabbit skin. Biological tissues were assumed to be incompressible like a liquid, meaning that three-dimensional mechanical properties could be obtained from these 2D tests. However, this required a complex arrangement of sensing equipment and feedback cameras in order to accurately control the strain applied to both axes of the square test-pieces. For this brief investigation, *in vitro* uniaxial tensile testing of flying squirrel skin samples was performed for convenience. This method is commonly used and perfectly valid for determining materials properties, but it cannot account for the affect of surrounding tissues (Lanir and Fung 1974). Dog-bone shaped samples are used for uniaxial tensile testing to minimise the effects of stress concentrations in the grip-contacting region of the material. The middle segment of the sample has uniform cross-sectional area, which is assumed to undergo a uniform reduction as the sample is subjected to tension. This shape also allows materials properties to be calculated based on changes in geometry, because it can be assumed that loads will act directly on the relatively long and narrow central section.

4.3.2 Procedure

4.3.2.1 Animals

The test animal was a male southern flying squirrel, Glaucomys volans, of unknown age that had been imported from a colony at SouthEast Missouri State University. This animal had died naturally and been frozen within 24 hours of death. It had been packaged in a cool box full of dry ice to prevent defrosting during transit, and then kept frozen and only allowed to thaw overnight before the day of testing. It was weighed to be 62.5 g immediately prior to testing.

In order for a comparison of skin thickness, a mouse, *Mus musculus*, was also obtained from the Department of Pharmacy at the University of Bath, frozen after use in another experiment which had not affected its skin. This was also allowed to thaw overnight prior to testing, and it weighed 29.5 g.

4.3.2.2 Uniaxial Tensile Tests

Initial visual inspection of the southern flying squirrel obtained for experimentation revealed that there were many clear striations or folds orientated along the length of the squirrel (Fig. 53). It was possible to pull open these folds completely, which approximately doubled the width of the original sample. Langer's lines of strain could not be oriented perpendicular to such folds or they would naturally be pulled apart, so it is likely that the majority of the collagen fibre bundles making up the flying squirrel skin are oriented parallel to its main axis. Interestingly, this finding is opposite to the primary direction of Langer's lines reported in other mammals such as humans and mice (Gibson, Stark *et al.* 1971). This is also evident in Fig. 50, which shows the horizontal Langer's lines across the human back. Consequently, uni-axial mechanical tests were only carried out on dog-bone-shaped test samples cut parallel to, and perpendicular to the spine.

Fig. 53 – View of a longitudinally oriented test sample of southern flying squirrel skin, approximately 20 mm long and 6 mm wide, looking at the ventral side. The image looks blurry owing to the white fur, but horizontal striations are still clearly evident, as highlighted.

Standard test strips were cut from the skin, some oriented along the length of the animal, and others at 90° to its long axis using the cutter described below. The ends of these were glued to plastic mounts with cyanoacrylate adhesive. The mounts were clamped vertically within an Instron 4202 tabletop tensile test machine. All the tests were carried out at the same strain rate, 5 mm/min, to ensure that the results would not be affected by strain rate sensitivity. At high strain rates in particular, ultimate tensile strength has been shown to increase with strain rate (Haut 1989; Dombi, Haut *et al.* 1993; Shergold, Fleck *et al.* 2006). A consistent method for mounting the samples in the testing machine was used to avoid issues arising from differences in l_0, the length at zero strain. Problems would arise if the samples were subjected to differing amounts of pre-straining in the machine prior to calibration and testing, so the top pneumatic clamp was applied first, and then the sample lowered vertically into the jaws of the second clamp, hanging only under its own weight. Given that the size of both the sample and the plastic mounting tabs were both consistent, it is reasonable to assume that any error in l_0 should also be consistent, if not negligible.

4.3.2.3 Cutting test samples

A scalpel was not sufficient to cut the standard dog bone shape test pieces required for tensile testing (Edsberg, Cutway *et al.* 2000). Instead a custom made cutter was made

by heating Stanley-knife blades to soften them, then bending them in a milled die using a vice. Two such blades, bent in symmetrically opposite directions, were then bolted to a block of mild steel against a thin, machined flat on each side (Fig. 54). This allowed repeatable, accurately sized dog bone shaped test-pieces to be punched out cleanly using a hammer. Blades could be easily changed to avoid blunting, which would pre-strain the samples.
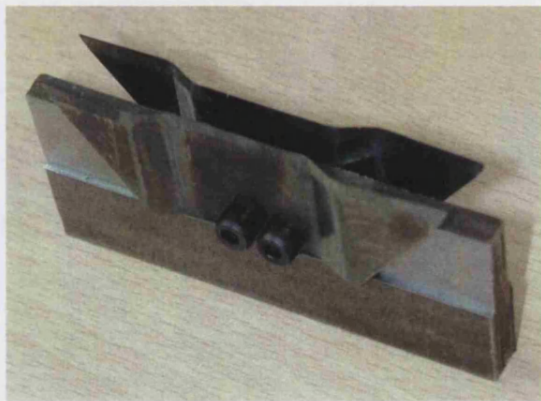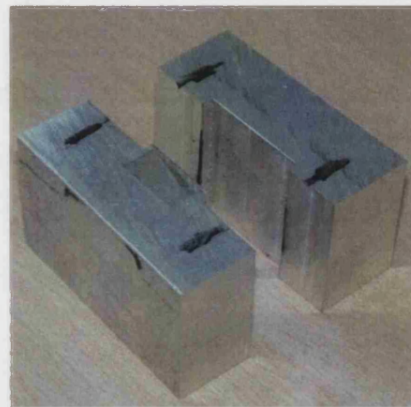
A　　　　　　　　　　　　　　　　**B**

Fig. 54 A – Punch for accurately cutting dog-bone-shaped test samples from the skin. B – Simple die used to shape the Stanley knife blades used in the cutter.

The dimensions of the dog bone test shapes are shown in Fig. 55. The effective length of the sample is 20mm, and width is 5.5mm. The flying squirrels were pinned out in a gliding posture prior to cutting, once again to try to keep l_0 as similar as possible between tests.

5.5

10

20

30

60
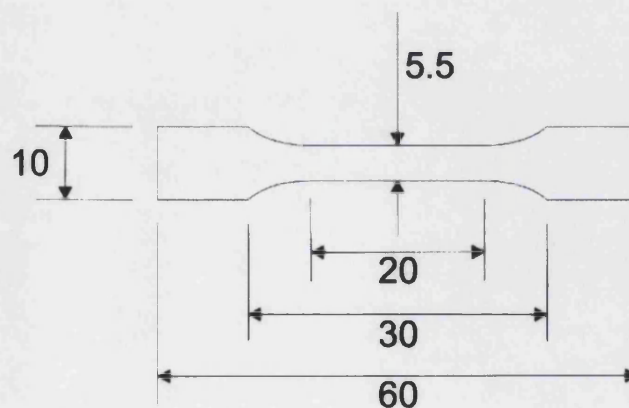
Fig. 55 – Dimensions of dog bone test pieces used in all experiments in mm.

After ensuring that the animal was completely defrosted by lightly manipulating the limbs, it was pinned out face-up and with its limbs spread to approximate a gliding posture. Test samples were cut through both surfaces of the skin simultaneously, after which the newly created edges were quickly smeared with petroleum jelly to minimise any exposure to the air. The size of the dog-bone test shapes was chosen so that it was possible to cut skin samples through both the ventral and dorsal skin simultaneously, either longitudinally or laterally, and these two layers of skin would remain firmly held together throughout the test procedure. This method is based on an assumption that there would be no difference in tensile properties between the two layers (ventral and dorsal) of skin.

4.3.2.4 Dehydration prevention

The decision to carry out experiments on flying squirrel skin *in vitro* required a means of preventing dehydration prior to or during testing. Vaseline™ petroleum jelly was gently smeared onto both sides of the skin immediately prior to removal from the body following Hepworth, Gathercole *et al.* (1994), who employed a similar method successfully to prevent the dehydration of egg capsules after removal from dogfish for tensile testing. The petroleum jelly coating acts as an oily barrier, preventing water from passing to or from the skin. It was important to keep this layer thin, to minimise the increase in pre-loading on the sample.

4.3.2.5 Data Analysis

Stress strain curves were drawn by calculation from the force-extension data from the Instron tensile tester. This required the dimensions of the dog bone test shape as described in Fig. 55 in conjunction with the thickness of the skin, measured to the nearest 0.01mm using a micrometer. The stress and strain were determined using Equation 16 and Equation 17 below:

$$\sigma = \frac{F}{A}$$

Equation 16

Where σ is engineering stress, F is the measured force and A is the original cross-sectional area of the test piece. True stress would require that the instantaneous area be used in place of the original cross-sectional area in the above equation.

$$\varepsilon = \frac{\partial l}{l_0}$$

<div align="right">Equation 17</div>

Where ϵ is the engineering strain, δl is the change in length of the test sample and l_0 is its original length. In order to measure true strain, instantaneous length would need to be substituted for the original length in this equation.

Engineering stress and strain are only accurate for small extensions, and the consequence of using these approximations in tensile testing is that stiffness will be underestimated. However, it is assumed that the error introduced will be negligible in comparison to the existent experimental uncertainty, owing to the high compliance of the test material.

4.3.3 Results

4.3.3.1 Skin thickness

In order to draw stress-strain curves, the thickness of skin samples was measured. The skin from flying squirrels was thinner (approx. 0.25mm) than that of mouse skin (approx. 0.35mm). These measurements are likely to be an overestimate because they were made without first shaving the animals. However, the comparison should be fair owing to the use of the *spring-loaded ratchet thimble* on the micrometer, which slips at a certain torque ensuring that the fur is compressed to the same degree for both animals. This method was used because it was feared that damage might be caused to the skin if shaved prior to testing, but there would be no value in measuring the thickness after stretching it. Therefore, all values of stress calculated in this study might be slightly

conservative, but this will not affect the direct comparisons between the different flying squirrel test samples.

4.3.3.2 Mechanical properties

It was possible to cut out six test samples from the southern flying squirrel using the cutter decribed, three oriented longitudinally and three laterally. Fig. 56 shows all the resulting stress against strain curves on one pair of axes to enable visual comparison. All have the characteristic J-shape associated with mammalian skin, and for an equivalent amount of strain, the longitudinal samples are subjected to higher stress than the equivalent lateral samples, hence the steeper curves. The lateral samples, in contrast, can tolerate much larger strains before failure.
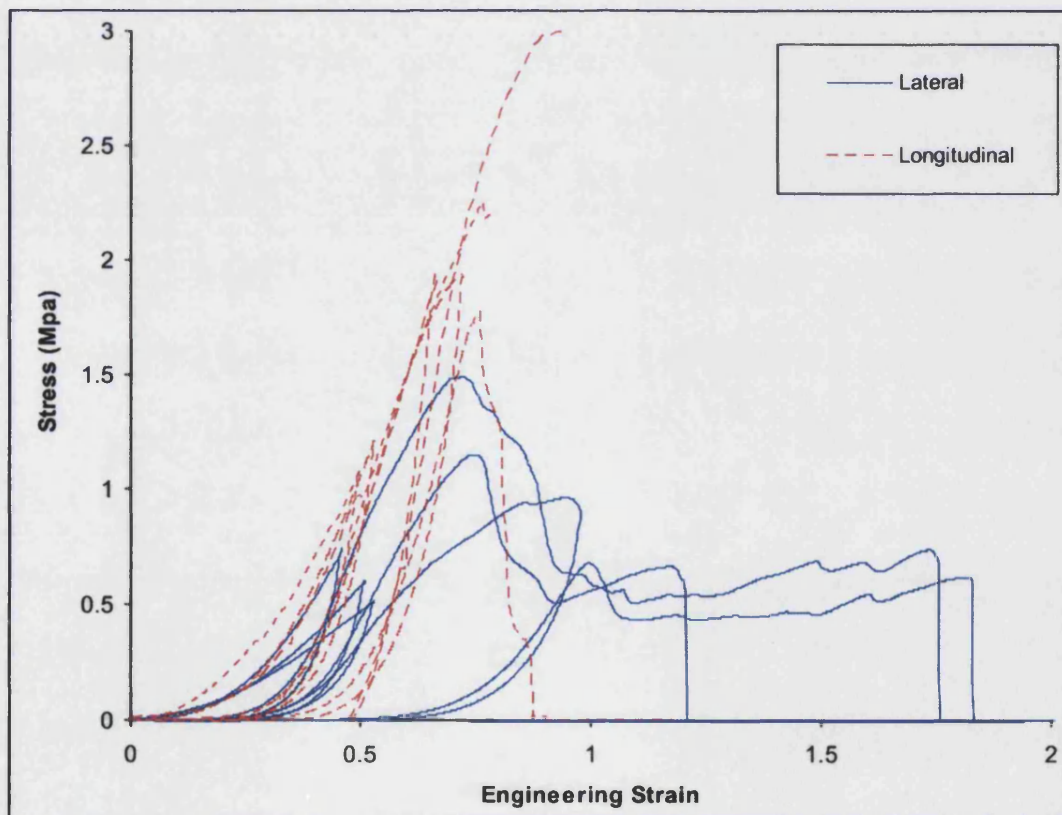
Fig. 56 – Graph showing stress against strain for all six samples of southern flying squirrel skin. It is clear that the three longitudinal samples represented by dashed lines have the steepest curves and reach the highest values of stress. In contrast, the three lateral samples can cope with much larger stains before failure.

Fig. 57 shows the data for the longitudinal samples separately for clarity. A straight line was overlaid by hand to demonstrate that all three curves strain harden to a linear region of approximately the same gradient, when the strain is more than 0.4. The gradient of this line is the Young's modulus, also referred to as the stiffness of the skin, and is estimated to be 4.8 MPa for these longitudinal samples. The ultimate tensile strength (UTS) and failure strain can be read from the graph as indicated by the arrows. The UTS ranges from 1.93 to 3.00 MPa, and all samples fail catastrophically while the strain is between 0.7 and 0.9.
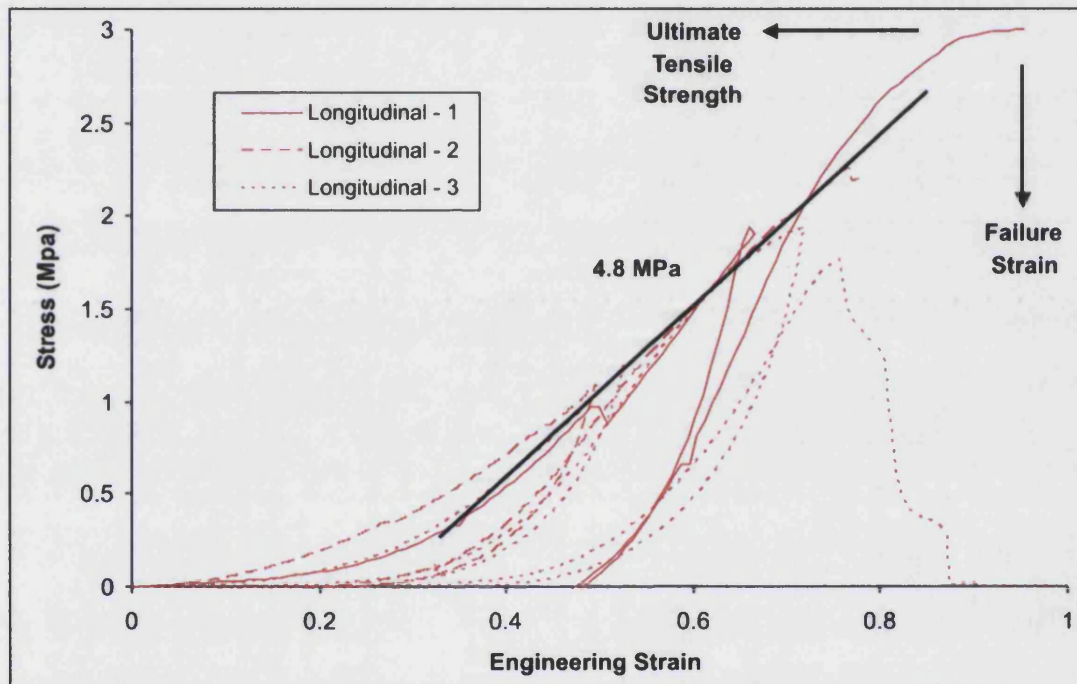
Fig. 57 – Stress Strain graph showing only the three longitudinal samples. It can be seen that the stress on each test sample increases when strain is applied, and some permanent deformation is present when the strain is taken back down again. The curve then continues from approximately the same point when the strain is reapplied again. A straight line has been added to show that the strain hardened section of all three curves has approximately the same gradient. This gradient is equivalent to the Young's modulus or stiffness of the skin samples in this region of the curve, which is approximately 4.8 MPa. The arrows indicate how the Ultimate Tensile Strength and Failure Strain can be easily read from the graph.

Similarly Fig. 58 shows the stress against strain graph for the laterally orientated samples of skin. Initially, the typical J-shaped curve can be seen although the stiffness of the strain hardened section of these curves is between approximately one third and two thirds of the value for the longitudinal samples. In all cases, the UTS is reached when the strain is between 0.7 and 0.9, although the values range from only 0.95 to 1.47, lower than the longitudinal equivalents. Instead of complete failure though, these lateral samples continue to extend considerably further with a new, much lower stiffness

value. The resultant failure strains are between 1.2 and 1.8, up to double those achieved by the longitudinal test pieces.
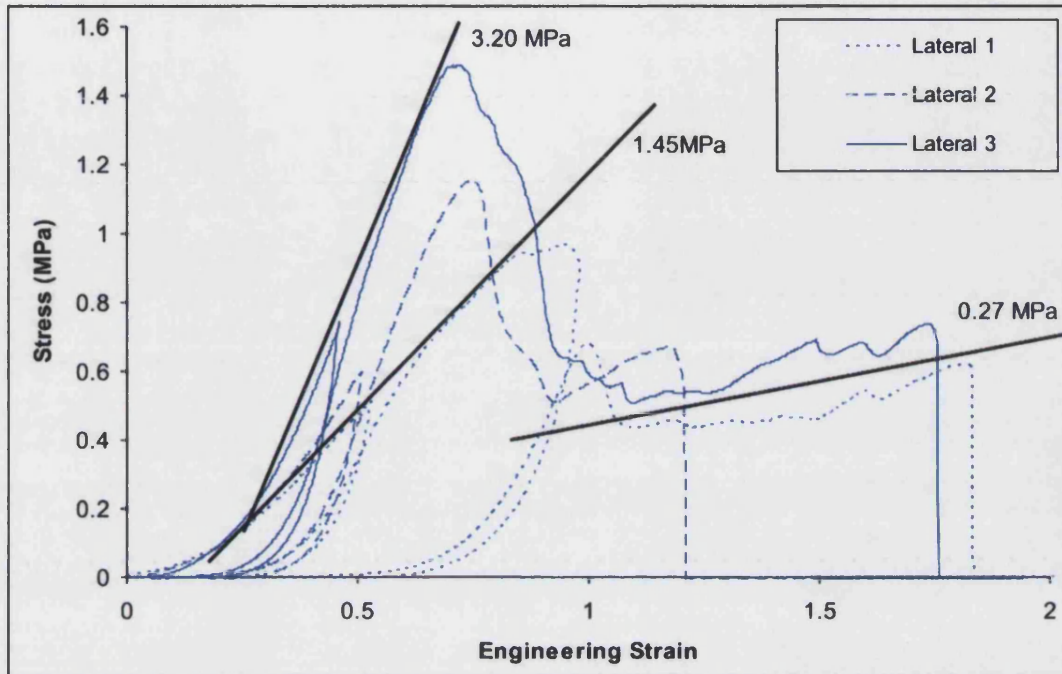
Fig. 58 – Graph showing stress against strain for the laterally orientated samples of skin. The lines show how the stiffness (Young's modulus) of the strain hardened linear sections of these curves changes with increasing strain.

Another interesting result is demonstrated in Fig. 59. This shows the middle example stress against strain curve for the two orientations, zoomed in to show its behaviour at low values of strain in more detail. The longitudinal sample visibly yields during its extension but the lateral one does not. This observation is consistent with data from the other four test pieces, although these are not included in the figure for clarity.

This suggests that the physiological strain range for the southern flying squirrel is less than 0.3 when stretching its patagia longitudinally. However, it should be able to stretch its skin much further in the lateral direction (by limb abduction) without causing damage.
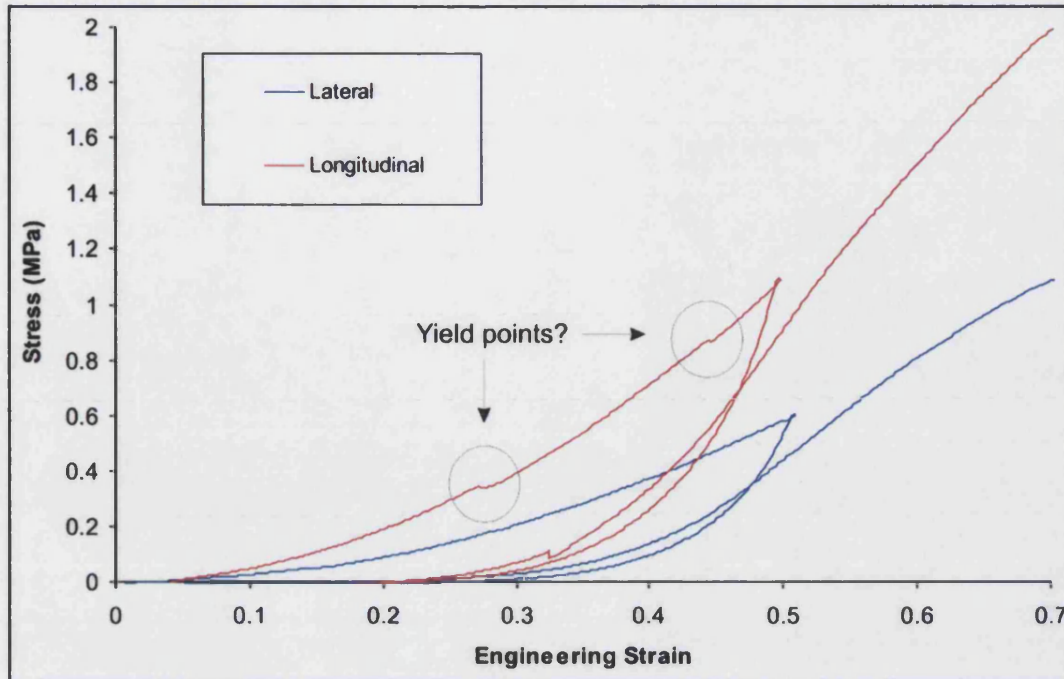
Fig. 59 – Close up showing only the early section of the stress strain graph for the skin of a southern flying squirrel. Only the middle curve for each of the two sample orientations is displayed for clarity. There is evidence that the longitudinal sample starts to yield as the engineering strain approaches 0.3 (circled), which is not evident in the lateral equivalent. This observation is also consistent with respect to the other four curves not displayed in this figure.

4.3.4 Discussion

This study set out to investigate whether or not flying squirrel skin differs from normal mammalian skin as a result of its integral function as a membranous wing. Unfortunately though, there is little or no value in comparing the specific values of stiffness, strength and failure strain measured here with equivalent results obtained for other types of mammalian skin in other studies. This is due to the difficulties in measurement and the consequent wide variation discussed previously. It is, however, acceptable to make comparisons within just this data set derived from a consistent test procedure.

The data presented here demonstrates a clear difference in mechanical properties between the two orthogonal orientations of the skin. The values of stiffness and ultimate tensile strength measured for the longitudinal samples were all higher than those measured from lateral test pieces, although these could all tolerate a higher strain before failure. In fact, the longitudinal samples were seen to yield at strains of less than 0.3,

with no similar yielding seen for the lateral equivalents. This is consistent with the observation that flying squirrel skin remains tight into the sides of the animal during normal arboreal locomotion. Therefore this would be subjected to relatively higher strains when the limbs are fully abducted for gliding than the largest likely for longitudinal skin, which would be when the forelimbs and hindlimbs are moved away from each other.

An observation was made during this experimentation that lateral samples sprang in on themselves more after removal from the squirrel. It was shown in the theory introduced in section 4.1.2, (page 116), that most shrinkage would occur in the direction of Langer's lines for normal mammalian skin, implying therefore that these ran laterally across the animal. Skin stiffness is normally highest parallel to the Langer's lines, so patagia must consist of some fundamentally different material in order for it to be higher in the longitudinal direction, which it was predicted would be more useful during gliding flight. More shrinkage would thus be expected in the direction of these lines (contrary to the actual finding). However, this observation could be explained by the bi-directional composite structure proposed in this chapter (Fig. 52).

The stress-strain curves in Fig. 58 add weight to the argument that the majority of collagen fibres would likely be orientated transversely to these laterally cut skin samples. The first peak would thus be the catastrophic failure of some of the stiffer collagen fibres in the composite acting against the strain direction, but the remaining material, with its lower stiffness, is able to absorb much larger strains until it finally breaks. This occurs at a much lower UTS than that required to break the primary fibres, so perhaps this is the breaking of more elastic secondary fibres, possibly elastin, after which the matrix material of the composite no longer holds together.

Considering the bi-directional composite model proposed for flying squirrel skin, the folds observed running along the length of the animal (Fig. 53) could be explained by it having a high quantity of pre-strained elastic fibres running across them perpendicularly in a flat piece of material. Thus relaxing the more elastic fibres would cause the bunching together of the stiffer fibres oriented orthogonally to them.

Using an identical procedure for each, the skin of the southern flying squirrel was measured to be thinner than that of a mouse, even though the latter was less than half the size. This is consistent with the prediction that thinner skin would be an ideal morphological attribute for a flying squirrel. However, there would likely be a trade-off between the associated aerodynamic advantages of a lighter weight material, and its strength and damage tolerance.

4.4 Tips for future researchers on this subject

This chapter was only a brief diversion into the important field of materials science in search of inspiration for the development of an autonomous jumping robot, the main objective of this thesis. However, it should provide a solid platform for any future research in the area, as the experimental procedure described details some useful, inexpensive solutions to the many obstacles presented by such *in vitro* mechanical testing of skin.

Importantly, a novel and inexpensive solution is presented for cutting out the dog-bone shaped test pieces preferred for mechanical testing without pre-straining the soft, biological material. The design is comparable to a pastry cutter in operation, and constructed from replaceable Stanley knife blades to keep it sharp.

One of the most critical aspects of the design of soft tissue tensile testing experiments is determining the point of zero strain for each test sample, l_0. It is virtually impossible to set up samples of such a compliant material as skin such that they are under zero load in the relatively large and cumbersome tensile testing machine. This is calibrated after each sample is loaded, so any pre-strain will have a direct consequence on that measurement and subsequent calculations. A consistent and reliable test procedure must therefore be adopted to ensure that genuine differences can be detected when comparing samples against each other. In this study, the arbitrary length of l_0 was chosen to be the length of the dog bone shaped test piece suspended under its own weight, plus that of the plastic tab at the free end. By clamping the top end into the machine first, this could be raised and lowered until the bottom tab sat between the jaws of the lower clamp, which were then closed pneumatically. The cutting tool used allowed good repeatability

of shape, and the plastic tabs were all of identical size and material. Therefore the total weight, and hence the load which pre-strains each sample should be consistent so long as the layer of petroleum jelly on each side of the skin was of equal thickness in all experiments.

It has been shown that females have higher wing loading than males (Thorington and Heaney 1981) and therefore it would be necessary to separate the sexes in any mechanical testing.

Age effects are also likely to be important. The elasticity of skin decreases with age as the elastic fibres degenerate owing to relatively poor repair and regenerative capacity of elastin fibres (Starcher, Aycock et al. 2005). The squirrel tested here was of unknown age, but were this study to be repeated in future, care should be taken to investigate the behaviour of skins from animals of a variety of known ages.

4.5 Conclusions and implications for the jumping robot

It was thought likely that the skin of flying squirrel patagia would be highly specialised owing to the unique physiological requirements. A model was proposed for the structure and composition of patagial skin, based on observed physical characteristics, accepted theory regarding mammalian skin and consideration of the ideal mechanical behaviour. It was predicted that this skin would be thinner than would be expected by scaling from other similar mammals, and combine high longitudinal stiffness with high elasticity in the lateral direction. Uni-axial tests carried out on a single southern flying squirrel produced results which were consistent with these hypotheses, and so this research is presented as a useful starting point for future research into this question. Although it would have been interesting to develop this brief experimentation into a full study on the mechanical properties of flying squirrel skin, it was considered too much of a diversion from the main objective of the thesis, which was to develop an autonomous robot. In order to confidently test the proposed model, such an investigation should include a histological test to determine the elastin content of flying squirrel skin, together with its primary fibre direction. These are likely to differ both from other small mammals, and in different areas of the patagia. During this research, a novel and inexpensive technique for cutting out test samples of biological tissue such as skin was successfully demonstrated.

Much can be learnt from this study and applied to the design of the jumping and gliding robot discussed in the following chapter. The robot will similarly require a gliding membrane that is damage tolerant, puncture resistant, and can deploy rapidly during the high-power jump cycle. Making this membrane as thin as possible with respect to the properties mentioned above would also clearly be an advantage. Flying squirrels are able to walk, run and climb in addition to jumping and gliding, so when designing this robot, it would be advantageous to avoid prohibiting any other form of locomotion if such were to ultimately become integrated into the design. Therefore, a gliding membrane with an elastic element which naturally folds it away during the longer, winding-in cycle of the robot would be ideal.

4.6 References – Chapter 4

COX, H. T. (1942). "The cleavage lines of the skin." Brit. J. Surg. **29**: 234.

DOMBI, G. W., HAUT, R. C. and SULLIVAN, W. G. (1993). "Correlation of High-Speed Tensile Strength with Collagen Content in Control and Lathyritic Rat Skin." Journal of Surgical Research **54**(1): 21.

EDSBERG, L. E., CUTWAY, R., ANAIN, S. and NATIELLA, J. R. (2000). "Microstructural and mechanical characterization of human tissue at and adjacent to pressure ulcers." Journal of Rehabilitation Research and Development **37**(4): 463-471.

GIBSON, T., STARK, H. and R.M.KENEDI (1971). The significance of langer's lines. Transactions of the 5th International Congress of Plastic Reconstrutive Surgery, Australia, Butterworth - Heinemann.

HAUT, R. C. (1989). "The Effects Of Orientation And Location On The Strength Of Dorsal Rat Skin In High And Low-Speed Tensile Failure Experiments." Journal Of Biomechanical Engineering-Transactions Of The Asme **111**(2): 136-140.

HEPWORTH, D. G., GATHERCOLE, L. J., *et al.* (1994). "Correlation Of Ultrastructure And Tensile Properties Of A Collagenous Composite-Material, The Egg Capsule Of The Dogfish, Scyliorhinus Spp, A Sophisticated Collagenous Material." **112**(3): 231-240.

HOLLBROOK, K. and ODLAND, G. F. (1978). "A collagen and elastin network in the wing of the bat." J. Anat **126**: 21-36.

JOHNSON-MURRAY, J. L. (1977). "Myology of the gliding membranes of some petauristine rodents (Genera: Glaucomys, Pteromys, Petinomys, and Petaurista) " Journal of Mammalogy **58**(3): 374-384.

JOHNSON-MURRAY, J. L. (1987). "The comparative myology of the gliding membranes of Acrobates, Petauroides and Petauras contrasted with the cutaneous myology of Hemibelideus and Pseudocheirus (Marsupialia: Phalangeridae) and with selected gliding Rodentia (Sciuridae and Anamoluridae). ." Austr. J. Zool. **35**: 101-113.

LANGER, K. (1861). "Zur Anatomie und Physiologie der Haut. 1. Über die Spaltbarkeit der Cutis." Sb.Akad.Wiss. Wien **44**: 19-46.

LANIR, Y. and FUNG, Y. C. (1974). "2 Dimensional Mechanical Properties of Rabbit Skin Part 1 Experimental System." Journal of Biomechanics **7**(1): 29-34.

LANIR, Y. and FUNG, Y. C. (1974). "2 Dimensional Mechanical Properties of Rabbit Skin Part 2 Experimental Results." Journal of Biomechanics **7**(2): 171-182.

LASHER, W. C., SONNENMEIER, J. R., FORSMAN, D. R. and TOMCHO, J. (2005). "The aerodynamics of symmetric spinnakers." Journal of Wind Engineering and Industrial Aerodynamics **93**(4): 311-337.

REIHSNER, R., BALOGH, B. and MENZEL, E. J. (1995). "Two-dimensional elastic properties of human skin in terms of an incremental model at the in vivo configuration." Medical Engineering & Physics 17(4): 304-313.

RIDGE, M. and WRIGHT, V. (1966). "The directional effects of skin. A bio-engineering study of skin with particular reference to Langer's lines." J Invest Dermatol 46: 341-346.

RODRIGUES, L. (2001). "EEMCO guidance to the in vivo assessment of tensile functional properties of the skin - Part 2: Instrumentation and test modes." 14(1): 52-67.

RUSSELL, A. P. and DIJKSTRA, L. D. (2001). "Patagial morphology of Draco volans (Reptilia : Agamidae) and the origin of glissant locomotion in flying dragons." Journal of Zoology 253: 457-471.

SAVILE, D. (1962). "Gliding and flight in the vertebrates." American Zoologist 2: 161-166.

SHERGOLD, O. A., FLECK, N. A. and RADFORD, D. (2006). "The uniaxial stress versus strain response of pig skin and silicone rubber at low and high strain rates." International Journal Of Impact Engineering 32(9): 1384-1402.

STARCHER, B., AYCOCK, R. L. and HILL, C. H. (2005). "Multiple Roles for Elastic Fibers in the Skin." J. Histochem. Cytochem. 53(4): 431-443.

SWARTZ, S. M., GROVES, M. S., KIM, H. D. and WALSH, W. R. (1996). "Mechanical properties of bat wing membrane skin." Journal of Zoology 239: 357-378.

THORINGTON, R. W. and HEANEY, L. R. (1981). "Body Proportions and Gliding Adaptations of Flying Squirrels (Petauristinae)." Journal of Mammalogy 62(1): 101-114.

WAN ABAS, W. A. B. and BARBENEL, J. C. (1982). "Uniaxial Tension Test Of Human-Skin Invivo." 4(1): 65-71.

WHIDDEN, T. and LEVITT, M. (1990). The art and science of sails : a guide to modern materials, construction, aerodynamics, upkeep and use. New York, St Martins Press.

Chapter 5

Robot Design

The aim of this research set from the outset was to design a small, autonomous and inexpensive jumping robot for traversing irregular terrain, using a low power, locally-available energy resource. This chapter will begin with the design requirements specification which was drawn up after consideration of the broad range of jumping specialisations that have evolved in nature. Perhaps the first key design decision for the robot was to choose between the two distinct jumping strategies observed in nature, 'pause and leap' or 'continuous hopping', introduced in Chapter 2. Of these, the 'pause and leap' strategy would seem much better suited to an autonomous jumping robot, where absences and irregularities in the power supply could be accommodated during the 'pause' phase. Hopping requires a more sophisticated level of control, and continuity, demonstrated by the fact that animals with more primitive cognition (including all the insect jumpers) utilise the 'pause and leap' approach. Furthermore, at the outset of this research project a 'jumping and gliding' robot was proposed, due to its relative prominence over 'jumping and rolling' in the natural world. However, the advantage of gliding would be a reduction in impact forces, which would directly reduce the amount of energy that could be recycled by a hopping mechanism, so a 'pause and leap' robot was be developed.

5.1 Design Requirements Specification

Table 3 shows the final design requirements specification for the jumping and gliding robot to be developed, together with the biological inspiration for each item.

Biological Inspiration	Design Requirement
Animals must eat in order to convert and store the energy required by its muscles for locomotion. The food resources available are generally of a lower than necessary energy density. It was shown in the introduction that power is the performance limiting factor in small jumping animals and insects, for which the specific energy available from muscle contraction alone is insufficient. Power amplification is achieved by operating their muscles at lower than maximum speed, and storing the energy for rapid release.	In order to be fully autonomous, the robot must be able to ready itself for a jump using a locally available energy source.
Different animals store energy in different ways. For example, fleas and leafhoppers store energy in resilin, a rubber-like material, in compression. Larger mammals, such as humans and dogs, store energy in tension in tendons, primarily made from collagen. Locusts, however, store their energy in stiffer skeletal cuticle, in bending.	Energy should be stored somehow, ready for a jump when instantaneous release is required.
Most jumpers have relatively long jumping limbs.	A long leg length (relative to overall robot size) should be chosen for further power amplification.

The large jumping (metathoracic) legs of the locust, for example, are held in the flexed position by a natural catch caused by a belt of tendon becoming hooked around a lump of cuticle (see Section 2.1.3.1.1, page 28). Fleas also rely on a mechanical catch.	A catch mechanism is required to ensure that the robot can remain in the charged condition until its next jump without requiring additional energy to hold it there.
Even the most primitive insects are able to orientate themselves prior to jumping to ensure that they jump away from the ground. Locusts, for example once again, were shown in Appendix 1 to display little or no control on landing, frequently landing on their heads. However, they can quickly find their feet and jump again almost immediately if necessary.	The robot must jump upwards no matter which orientation it lands in.
For an organism to jump, a suitably massive element of its body needs to be accelerated away from the remaining mass. By considering conservation of momentum and neglecting losses, greatest jump height is achieved by maximising the ratio of the accelerated mass to trailing mass which directly increases take-off velocity.	During jumping, the robot must maximise the ratio of the accelerated mass to trailing mass.
Most animals deliberately jump in the direction that they would like to travel.	The robot must be able to orientate itself prior to jumping.

All animals, irrespective of size can jump to approximately the same height as shown in the Literature Review, but the additional mass of the required payload will have less detrimental effect on the peak height of larger animals.	The robot must be able to carry a useful payload, such as an environmental sampling device.
In all animals, it is essential to the preservation of life that delicate organs are protected from excessive impact during locomotion. Connections are not rigid, so forces are damped by these softer tissues. Some animals, such as flying squirrels, are able to glide, enabling them to reduce their landing impact forces aerodynamically.	The robot must be able to carry any sensitive electronic equipment without it sustaining any damage during the jumping and landing cycles.
Flying squirrels were observed to fully abduct their limbs during take-off, deploying their gliding membranes, (patagia), in the process. This behaviour occurred even during leaps when it was demonstrated that the squirrels achieved no resultant advantage in landing altitude.	The robot should have membranous wings to enable gliding, and these should deploy automatically and fully during take-off.

It was shown in Chapter 3 that flying squirrels choose to pitch upwards, rapidly increasing their angle of attack, immediately prior to landing in order to reduce impact forces. Similarly, flying fish deliberately employ air braking to slow themselves down prior to re-entering the water, by positioning their pelvic fins forwards, and angled against the motion.	The robot should have the ability to control its angle of attack during the gliding phase to enable effective air braking as it lands.
In nature, all components must be manufactured following a group of natural rules during embryo development.	Industrial designers do not have this limitation but it must be possible to create and assemble the required components according to what current technology permits.

Table 3 – Table presenting the design requirements specification for the jumping and gliding robot to be developed.

One final requirement was specified, which has no particular biological source:

- The robot should be constructed from materials that could be adapted for use in space applications.

5.2 Design Detail – Glumper

During this research, a number of prototype jumping mechanisms were created along the way to reaching a satisfactory design solution for a robot which can both jump and then glide. Descriptions of these early prototypes can be found in Appendix 2, but a photograph of the final robot design for this thesis is shown in Fig. 60. It has been called

Glumper, so named because it is a merge of the two relevant descriptive words, 'Gliding' and 'Jumper'. In the following section, the design details of Glumper will be introduced with respect to the requirements outlined previously.
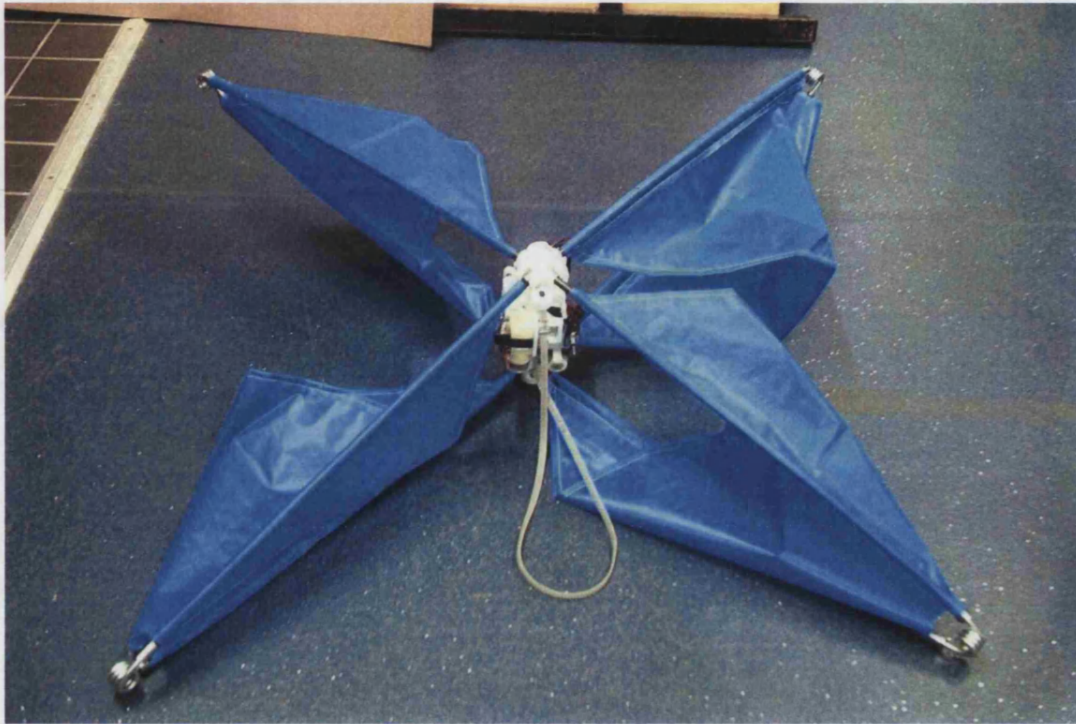
Fig. 60 – Photograph of Glumper winding itself in immediately prior to take-off.

The photograph of Glumper (Fig. 60) shows its four long legs, each with a torsion spring "knee" at its midpoint, distributed perpendicularly between a "head" and an identical "foot". A triangular shaped membrane mounted between each leg element and along the axis of the robot acts as its gliding wings. By way of introduction to some of the more complex design solutions, an overview of the discrete steps required for Glumper to jump is given in Fig. 61.
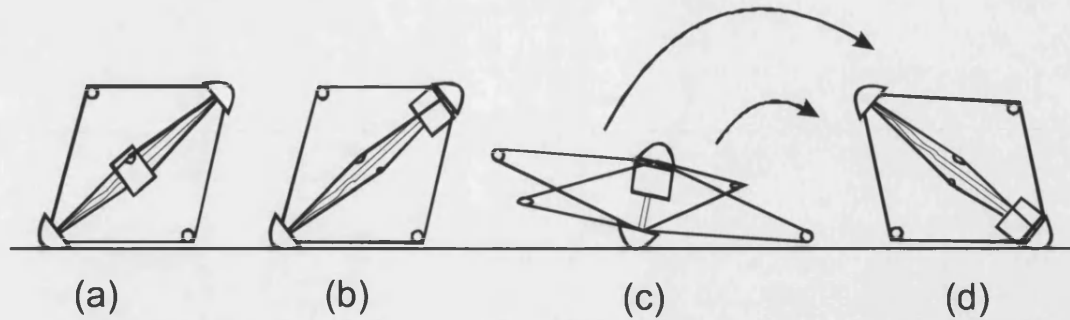
Fig. 61 – A sketch to introduce the steps required for compression and release of Glumper, showing: (a) A mechanism is freely suspended on a cord between the head and the foot, which can wind in the cord to compress the robot. (b) This compression mechanism can be attached to whichever end of the robot is uppermost. (c) When the robot becomes fully compressed a clutch releases the cord and the robot jumps upwards. (d) After landing the clutch requires resetting and the process can repeat. The gliding membranes are omitted from this figure for clarity.

The first requirement specified for this robot was that it must be able to ready itself for a jump using a low grade energy source. Glumper is able to achieve this using a small 3 V motor, but this low power motor can still generate relatively high torques simply by gearing it down sufficiently. As a consequence, the time taken to charge the jumping mechanism increases, but this is only of secondary importance for applications requiring complete autonomy, where the maximum lifetime of the robot takes precedence.

Next it was specified that energy should be stored somehow and instantaneously released into a jump. Energy could be stored by extending or compressing rubber-like materials, such as the high-performance elastics used in modern catapults. Fleas, for example, store energy by compressing resilin pads and so the early prototype jumpers were built using elastic bands and silicon rubber, as described in Appendix 2, (page 210). However, these demonstrated that energy is lost with time in the loaded state due to stress relaxation. Locusts, by contrast, store energy in the bending of more rigid, structural elements, such as their semi-lunar processes which act as leaf springs. Another requirement, however, was that the robot should be constructed from materials that could be adapted for use in space applications. Although rubbers have the capacity to store a lot of energy, this property is severely affected by temperature and time. At cold temperatures, rubber-like materials become hard and brittle, causing them to fail before much energy has been absorbed. The time taken to charge the robot is likely to be slow, and extreme environments present the most useful applications for a jumping robot. Therefore storing energy in bending should provide a more suitable approach,

and Glumper stores energy in the rotation of four heavy-duty steel torsion springs. These are made from 3.75 turns of 4 mm diameter spring steel rod, which are mounted in the knee-like hinge-joints of four legs and constrained symmetrically between the two ends of the robot.

A long leg length (relative to overall robot size) was specified to amplify the power produced by releasing these compressed torsion springs. Glumper's legs are each made from two hinged carbon-fibre reinforced plastic (CFRP) rods, 0.5 m long with an 8 mm outside diameter, and a 4 mm internal diameter. These rods have very high specific stiffness and are reinforced by two steel rings, one at each end, allowing the legs to fully compress the torsion springs. If the legs were less stiff they would themselves bend before the springs were fully compressed, reducing the total jump energy. However, although the low specific stiffness of carbon-fibre was ideal for this prototype, this would not be a suitable material for space applications. Carbon is something that instruments are searching for when looking for evidence of life on other celestial bodies, so it is important to avoid transporting some from earth. However, glass-fibre reinforced plastic (GFRP) offers even higher stiffness to weight ratio, as can be seen in the selection charts produced by Ashby, (Fig. 62), which were created specifically for choosing the optimum materials for engineering design (Ashby 1992).
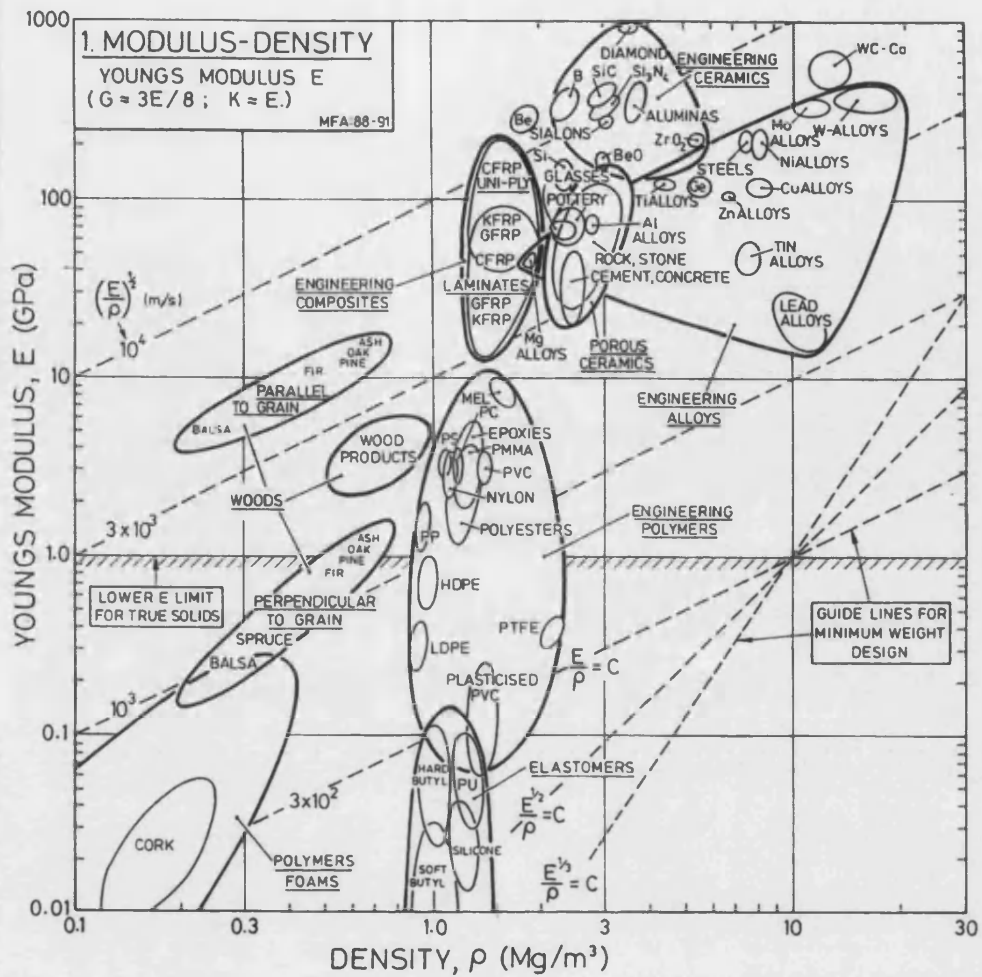
Fig. 62 – Ashby chart showing Young's modulus against density for most common engineering materials. It can be seen that both GFRP and CFRP combine high Young's modulus and low density. Chart reproduced courtesy of Ashby (1992)

The reinforcement rings are made from 2 mm thick mild steel, and are stuck to the surface of the rods using both an epoxy resin based glue, and an interference fit. Their primary function is to strengthen the legs by preventing the carbon-fibre rods from splitting. Where the legs connect to the two ends of the robot, the ring is just 6 mm long (to keep the weight to a minimum), and has a through hole to enable rotation around an M3 mounting bolt (see Fig. 63 below). The other ring is longer at 14 mm, which incudes a 6 mm thicker-walled section beyond the length of the underlying carbon-fibre rod. Here the internal diameter of the steel ring is 4 mm rather than 8 mm, giving a total thickness of 10 mm. A tapped through hole allows for the insertion of two M3 grub screws into each, which tighten down onto the torsion springs.

A   B
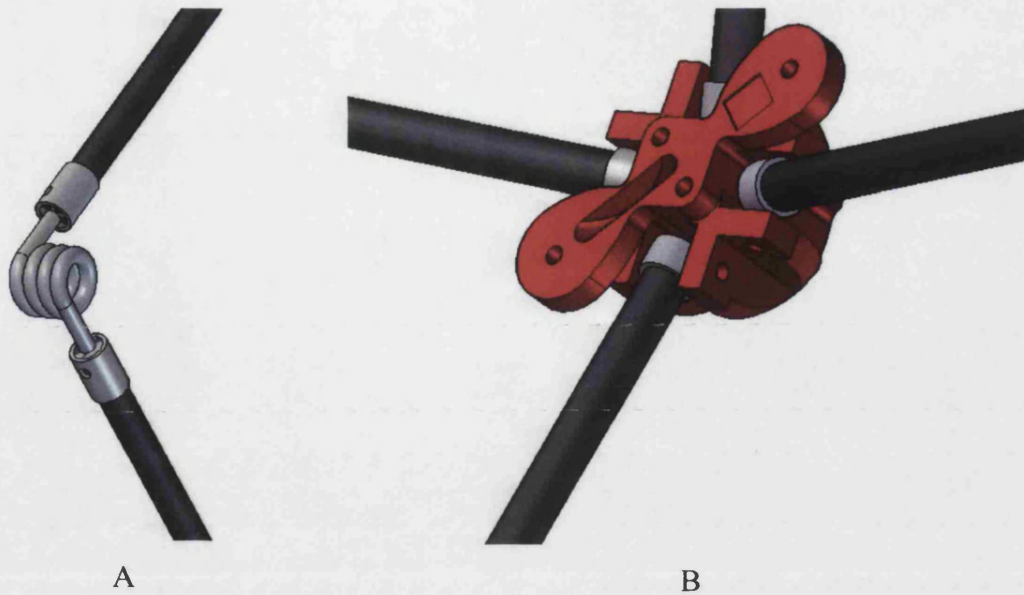
Fig. 63 – Rendering from Solid Edge V.17 showing the two types of reinforcement rings used at each end of the carbon-fibre leg pieces. A – At the knees, the steel extends 6 mm further than the carbon-fibre leg, with this section of the tube having a thicker wall diameter and a tapped through hole. This allows the spring to be held in place by grub screws from both sides. B – At the ends of the leg the reinforcement ring is only 6 mm long, and has a through hole allowing the leg to rotate about an M3 bolt mounted through the holes in the head/foot piece as shown.

It was specified that the robot must jump upwards no matter which orientation it lands in, which seems a superior solution to simply incorporating a self-righting mechanism because this adds dead weight to the system (weight that does not contribute towards the jump). Glumper folds down flat as its torsion spring knees are compressed, and consequently can be in only one of two orientations prior to take-off, in the same way that a coin can only land 'heads' or 'tails'. By making the robot symmetrical such that its head and foot are identical, and by separating the compression mechanism (together with any other mass, such as the payload) from the energy storing frame, bi-directional jumping can be achieved. Prior to each jump, the decoupled mass must be rigidly connected to whichever of these end pieces is determined to be uppermost.

Another important specification to be inspired by nature was the requirement for a catch mechanism to ensure that the robot can remain in the charged condition until its next jump without requiring additional energy to hold it there. A neat design solution for this design problem developed for Glumper was the incorporation of a worm gear into the compression mechanism. This has the dual advantage of increasing motor torque, while preventing energy stored in the system from acting directly against the motor's stall torque in the event of complete power loss. Such a design is essential when considering

using solar power, which would obviously be subject to large variations at different hours of the day, reducing to nothing during the night. The compression mechanism will be housed in a control box, which will be described more fully in the following section.

It is clear that in order to be useful, this jumping robot must be able to carry a useful payload, such as a camera and transmitter. Therefore, sizes should be chosen for the best compromise between the low weight and small final volume preferred for space applications, and the payload requirements, given the current technological limits on necessary components. The current evolution of Glumper weighs 700 g, and has a maximum standing height of 0.5 m. The performance of this robot, including an investigation into the effects of increasing and decreasing weight to the resultant clearance height, will be detailed later in this chapter.

Of similar importance regarding the payload, the robot must also be able to carry any sensitive electronic equipment without it sustaining damage during the jumping and landing cycles. Landing impacts are likely to be the most damaging. Therefore Glumper's compression mechanism and potential payload will not be rigidly connected to the extremities of the robot, which contact the ground first on landing. Instead, compression will be achieved by the winding around a capstan of a cord connecting the two end pieces of the robot, (full details of this winding mechanism are given in the next section). By choosing a suitable cord length, it will be slack when released at take-off, and hence absorb some of the landing impulse due to the slight increase in force duration. The flying squirrel research in Chapter 3 has also shown that landing forces can be further reduced by equipping the robot with membranous wings to enable gliding, which should deploy automatically and fully during take-off. Deployment of the gliding membranes during take-off avoids any complications that would otherwise be caused by the need to conserve angular momentum in mid-air. Glumper naturally adopts this behaviour because it has four triangular-shaped gliding membranes spanning the gap between its legs and the mid-line between the two identical end pieces. Section 5.2.3 on page 156 details the selection of membrane material, how it is attached and its folding and deployment.

The robot should have the ability to control its angle of attack during the gliding phase to enable effective air braking as it lands. Given that the mass of Glumper's

compression mechanism for this jumping robot is localised in a box which is free to move between its two end pieces, it would be possible to control the pitch angle by incorporating one additional motor. This drives a pulley quickly along a toothed belt, loosely attached (to avoid excessive strain during jumping) between the head and foot of the robot, thus moving the centre of mass either forwards or backwards during gliding flight depending on motor direction. This particular design was chosen because it can also serve as the mechanism by which the control box attaches itself to the top of the robot between jumps.

A   B
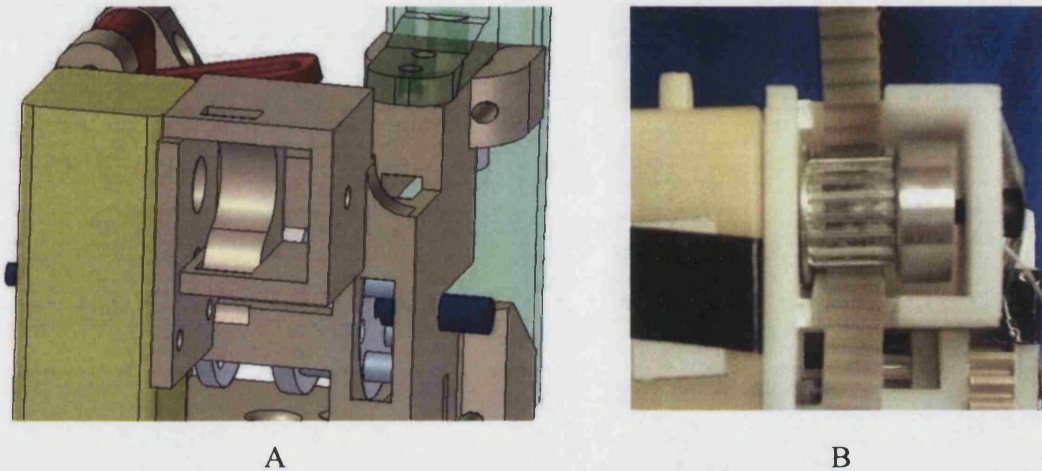
Fig. 64 – Pitch-up and foot attachment mechanism. A – Solid Edge rendering to show how the control box was designed with a profiled curve included to guide the toothed belt tightly around the pulley. B – Photograph showing the pulley and toothed belt in place. The pulley was bored out to allow the interference fit of an 8 mm rapid prototyped insert, which mates with the motor output shaft at one end and the M3 locating bolt at the other.

Finally, the robot must be able to re-orientate itself prior to jumping. An additional motor or a complex gear selection arrangement would allow an eccentric mass, such as a battery, to rotate horizontally around the control box by up to 180° in either direction from its natural position. The slight protrusion of the end pieces from the legs means that Glumper naturally rests on only two legs, giving it eight possible resting states, four one way up and four the other. The rotation should cause the centre of mass to shift sufficiently to rock it from one pair of legs to an adjacent pair, such that the resulting take-off direction changes by 90°. Unfortunately time did not permit such a mechanism to be designed for Glumper, although details of how this will function are given in the future work section of this thesis (Section 6.2, page 184).

5.2.1 Winding mechanism

The control mechanism to compress and release Glumper is housed in a small box made, like many of its components, from ABS, (acrylonitrile butadiene styrene), the plastic output from a Stratasys rapid prototyping machine. A small 3 V motor with a gear ratio of 1:200 is used to drive a worm-gear arrangement which slows it by another 50:1 ratio. The driven gear has four holes in it, which locate four small aluminium locating rods protruding from a capstan that is held against it on the same shaft by a compression spring. Fig. 65 shows a diagram of this capstan, showing how the aluminium bars are located in an additional wall to ensure no skew, and hence allow clean transition in and out of the drive gear. The drive shaft running through the capstan is stepped such that the capstan can be pushed away from its drive gear with a linear movement of the shaft, compressing the 'return spring' in the process. This compression spring, which normally keeps the capstan engaged on the drive gear, is not acting directly against the capstan but against a circlip approximately 1 mm away. This means that the capstan is able to freewheel on the shaft (when away from the drive gear).

A	B
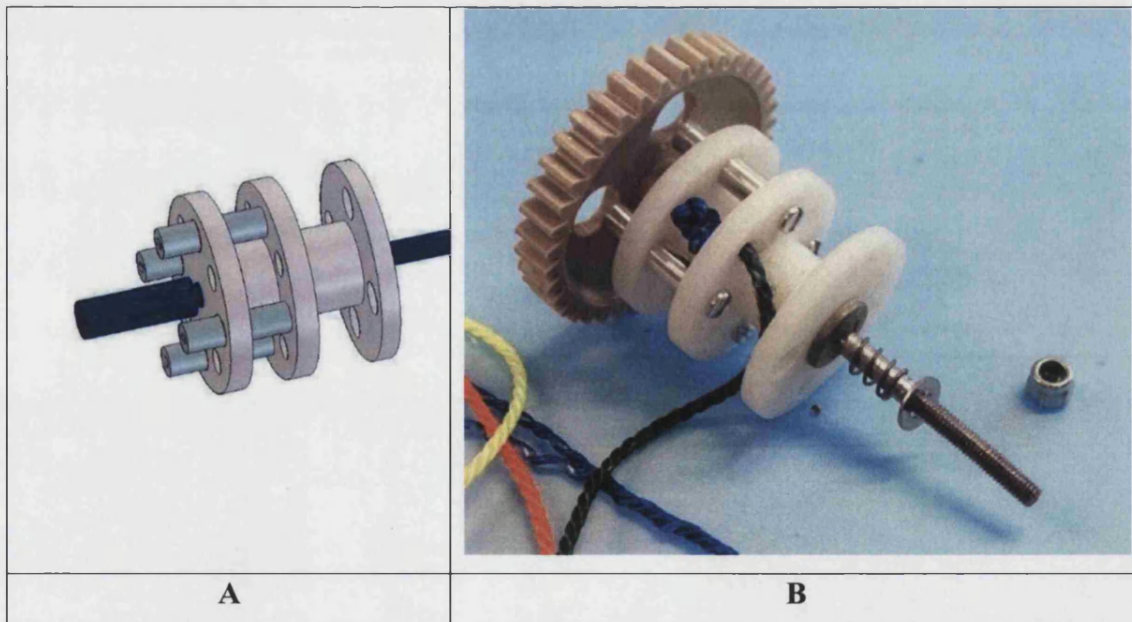
Fig. 65 A – Rendering of an assembly drawing showing how the capstan sits on a stepped shaft, and how the four aluminium drive rods are located in an additional wall to prevent skew. B – Photograph showing how additional holes in the capstan walls make it possible to secure these rods, which have a tapped internal thread, using M2 screws. The location of these drive rods into holes in a driven gear, which sits adjacent on the wider section of the stepped shaft, enable the capstan to wind in a cord, (shown as secured by a large knot), and hence compress the robot. The circlip, compression spring and washer which normally hold the capstan located in the drive gear are also shown.

The two free ends of a length of high-strength nylon fibre cord are attached to the capstan by pulling them each through a hole in the middle wall of the capstan, (using a small hook crafted from a paperclip), and tying a large knot in them so that they cannot return through the same hole. From here, this cord loops around smooth, non-rotating pulleys in one of the two end pieces, back through a guide hole in the control box and around the identical pulley at the other end of the robot. Thus winding in the string around the capstan causes the robot to compress. This would subject the ABS capstan to a significant torque at the attachment point of the cord, but the design is such that it is the much stronger aluminium rods which absorb this loading.

The friction acting against the required linear movement of the stepped shaft to push the capstan away from the drive gear is very high when the robot is highly compressed, such that separate linear actuation would require high force. However, this design avoids the need for any such device, by using a hinged lever to pull the shaft out when both ends of the robot are pulled in against the control box. The end of the stepped capstan shaft has actually been threaded using an M3 die. The hinged lever has a slot in it which this shaft passes through, and an M3 nylon locking nut can be tightened to any position along the thread. By turning this nut one way or the other, the exact linear movement of the capstan shaft on depression of the hinged lever can be accurately controlled.

In order to make sure that the robot doesn't jump until fully compressed, this hinged lever is constrained by a latch, held closed by a small torsion spring, which is only released when the other end of the robot is pulled tight against the opposite side of the control box. At this moment, the capstan disengages from the drive gear, freewheeling as the cord unwinds rapidly and causing the robot to jump into the air. Fig. 66 shows a view of the partially complete control box to clarify how the vertically compressing robot can pull the capstan shaft only when the blue latch is moved away from the end of the red hinged lever.

Fig. 67B and C are photographs showing the hinged lever in the closed and open position respectively, and the nylon locking nut which drags the shaft with it is clearly visible in both images.
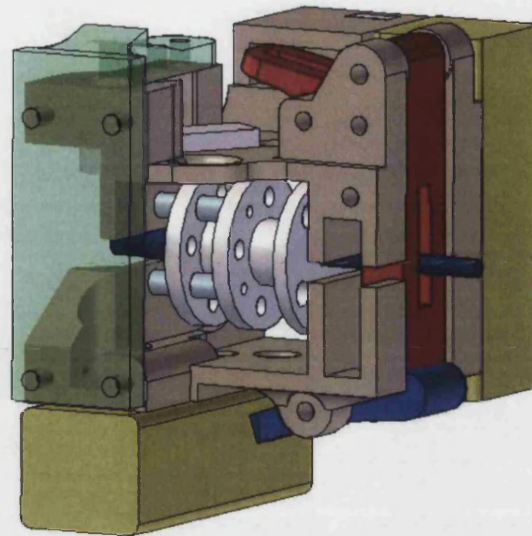
Fig. 66 – Rendering from Solid Edge v.17 of the control box showing the red hinged lever and its blue retaining clip. Some components, such as the over-centre mechanism, the worm and drive gears, have been omitted for clarity. There would also be an M3 nylon locking nut sitting close to the hinged lever on the capstan shaft, causing it to be pulled sideways when the latter rotates.

An over-centre mechanism on the hinged lever prevents premature re-engaging, which would otherwise happen as soon as the robot left the ground (due to the compression spring on the capstan shaft).

Fig. 67A shows the components added to the control box to make the over-centre mechanism. There is an M3 bolt with its top sawn off and replaced by an approximately hemi-spherical blob of solder, with a small but very stiff compression spring around it. (It was necessary to add this solder blob at very high temperature to ensure strong adhesion.) The spring acts against a nut on this solder bolt when the mounting piece is fixed in place with two additional M3 bolts, which screw into nuts recessed so that flush in the opposite wall of the control box to avoid interference with the hinged lever. Adjustment of the nut on the solder bolt allows control of the force with which it is held protruding into a hole in the side of the closed hinged lever. Opening of this lever requires significant initial force but once overcome, it moves quickly to the fully open position and is held open by the returning sprung solder bolt. It is thus important that the compression spring used for the over-centre mechanism is stronger than the one on the capstan shaft.
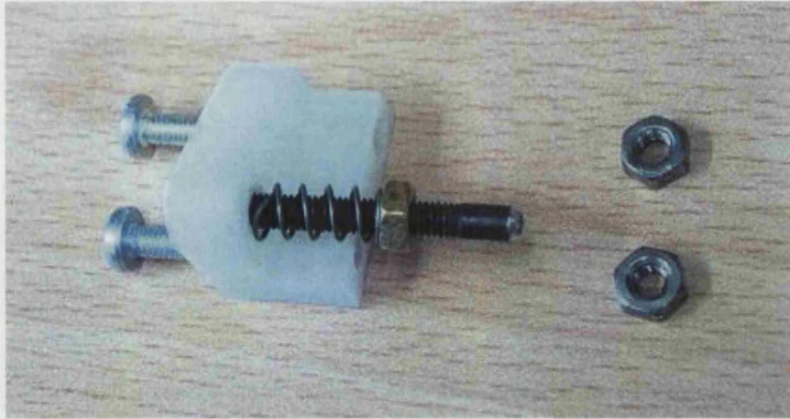
A
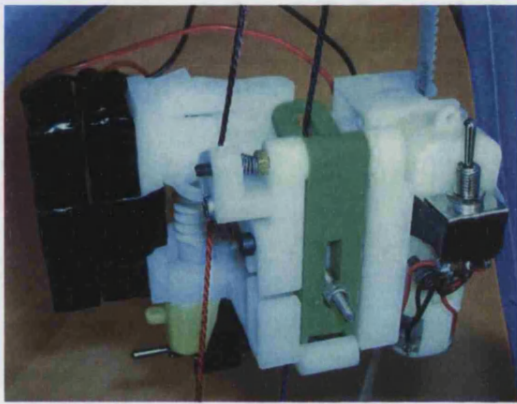
B
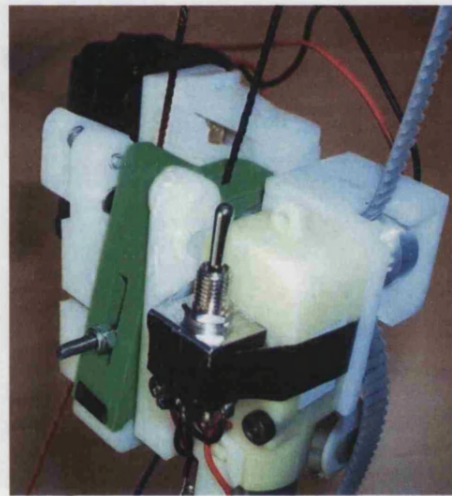
C

Fig. 67 – Photographs showing: A – The individual components making up the over-centre mechanism. These are an M3 bolt with the top sawn off and replaced by an approximately hemi-spherical solder blob, an M3 nut, a small but very stiff spring, and a mounting piece containing holes for the sprung solder bolt, and two additional mounting M3 bolts, which screw into nuts recessed so that flush in the opposite wall of the control box to avoid interference with the hinge. B – This photograph shows the hinge in the closed position, when the rounded end of the bolt is located in a hole in the side of the hinge. C – This shows the same hinge being held in the open position by the assembled over-centre mechanism.

After a jump, the hinged lever needs to be reset past the over-centre spring again in order that winding can be re-initialised. This is achieved without the need for a separate actuator thanks to the design of the worm drive. Rather than directly coupling the worm gear to the motor output shaft, the motor instead drives a piece of ABS which holds a brass square-section bar of 4 × 4 mm. Glumper's worm gear has a slightly larger brass square-section hollow bar of 5 × 5 mm mounted through its centre, allowing it to float freely along the other square bar. Driving the motor in one direction will cause the worm gear to inch itself along the driven gear (on the capstan shaft) until it presses against the RP piece driven by the motor, after which continued rotation turns the driven

gear and hence the capstan. By reversing the direction of the motor, the worm inches itself back along the driven gear away from the motor, and pushes a follower (sitting in a recess to guide it) towards the hinged lever. On contact, this has sufficient force to flip it back up past the over-centre spring ready for the next jump. This design requires high friction on the gear driven by the worm, which is achieved by mounting it in a tight fit against the side wall of the control box.

A

B
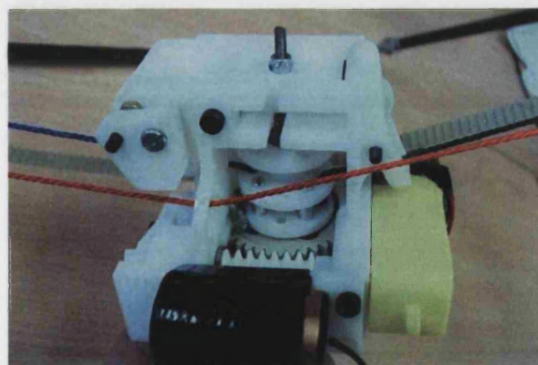
C

Fig. 68 – Floating worm gear 'hinged-lever reset' design. A – Photograph of components showing, (from top), a piece of RP with a grub screw in it to couple the motor to the square-section drive bar below. The worm gear has a mating square-section tube running down its centre enabling it to float along the drive bar, and push the follower at the bottom of the picture in the process. B – Photograph demonstrating how these components assemble together. C- Photograph showing this mechanism as it looks in Glumper's control box.

5.2.2 Head/foot pieces

The two ends of the robot are of the same design, as shown in both a Solid Edge rendering (Fig. 69A) and photograph (Fig. 69B). They are each constructed of two pieces in order to facilitate Glumper's assembly and construction. The outer parts have a rounded base which will allow Glumper to roll from one pair of legs to another prior to a jump simply by moving its centre of gravity once the orientation mechanism to do this has been developed. They also contain four perpendicular recesses with bolt holes to enable Glumper's legs to be mounted here, each free to rotate in one plane only. Each of the two mating parts has a fixed pulley shape which fits into a recess in the outer part, (seen on the left hand side of Fig. 69A), constraining a cord which runs smoothly over it between the top and bottom of the robot, and through the conical protrusion to the capstan in the control box. The mating parts on the head and the foot also have some indentations which help to grip the slightly slack toothed belt which runs from the head to the foot of the robot. The two mating pieces are clamped tightly together by M3 bolts as shown in Fig. 69B. This photograph also shows a square of high friction material which has been glued to the base to reduce slippage during take-off.
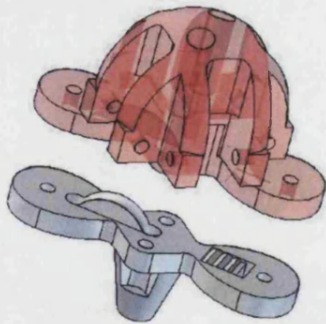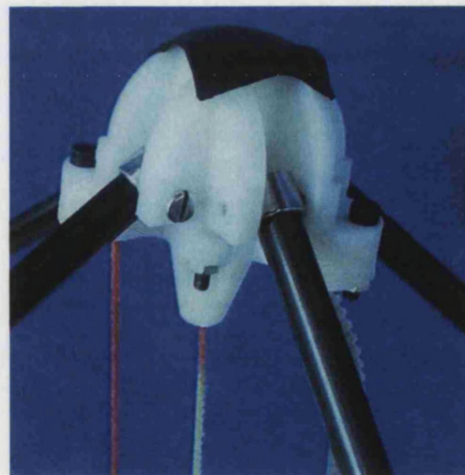
A   B

Fig. 69A – Rendering of an assembly drawing showing a head or foot piece for Glumper. It is essentially two pieces of rapid prototyped ABS, bolted together using M3 nuts and bolts. On the right hand side of the lower piece in this drawing, indentations can be seen which grip the end of the toothed belt, which runs between this and another identical assembly. The cord which winds around a capstan to compress the robot runs over the fixed pulley shape (seen on the left hand side of the lower piece in this figure) and down through the centre of the conical protrusion at the base. This is naturally guided towards the hinge lever, which the cord is pulled through to get to the capstan, eventually pushing it open for take-off. B – Photograph showing this assembly on in position on Glumper. This also shows a small patch of black rubber, attached with cyanoacrylate, which reduces the likelihood of slippage during take-off.

The depth of these end pieces determines the take-off angle of the robot, such that making them deeper would cause a shallower trajectory. For the prototype of Glumper presented in this Thesis, relatively small end pieces were chosen so that the robot jumps approximately vertically when launched automatically from a flat horizontal surface. It was shown in the literature review that the impressive jumping performance of frogs is helped by their unique knee joints, which enable the feet to be brought further under the body and prolong the duration of the impulse. In vertical jumping, the take-off force exerted by Glumper on the ground acts approximately perpendicularly, minimising the risk of slippage. It would be worthwhile for any future researchers to consider adding some frog-inspired articulation to the eventual end pieces, the size and design of which would need to be chosen accordingly in order to enable Glumper to take-off effectively at a specific angle.

5.2.3 Gliding membranes

Four individual membranes are conveniently fitted to fill the triangular shaped spaces between Glumper's four articulated legs and the central axis of the robot. Consequently, there is a gap in the gliding membrane along this central axis, which is necessary to enable the compression and pitch control mechanism to move freely between the two ends of the robot when required. Secondarily this also simplifies the selection of materials, which would otherwise need to be highly deformable because these wings are naturally pulled outwards as the robot changes shape during compression. However, the resultant gap between the membranes should not prohibit gliding from taking place, just as the horizontally flattened, s-shaped body of the flying snake is capable of impressive gliding even with relatively large gaps in the resulting surface (as can be seen in Fig. 21, page 53).

During a typical jump, it is expected that Glumper will naturally roll (rotate around its central axis) once airborne so that it is gliding on any two opposite wings, in order to balance an otherwise inevitable pressure difference. The geometry of Glumper is such that the resulting aspect ratio of the wings during such a glide is approximately one. This means that Glumper should (in principle) be able to glide at much higher angles of attack without stalling than would be possible for higher aspect ratio wings, as

discussed in the literature review (Section 2.2.3, page 54). This is an essential factor in the design because Glumper will naturally launch at a relatively high angle of attack in order to gain sufficient altitude during a jump. In the same section, it can be seen from work by Torres and Mueller (2004) that an elliptical wing gives superior performance than rectangular, Zimmerman or Inverse Zimmerman shapes when the A.R = 1. The diamond shape formed between two opposite wings on Glumper more closely resembles an ellipse than any of the other shapes tested in that work.

It was also shown in the literature review that bird wings are made from feathers which are more porous to air flowing through from the top surface (Section 2.2.2.1, page 47). However, it is not possible to incorporate any such material specialisation to positive effect with Glumper, owing to the fact that it is equally likely to be gliding on any two of its four wings, and either way up.

Glumper's gliding membranes are made from rip-stop nylon, the same fabric used in parachutes and kites due to its ideal high strength, tear resistance and low weight properties. Four triangular pieces were cut out to fit the space between the head, foot and each torsion spring knee of Glumper's legs. All three sides of these triangular sheets were folded over and a seam added using a sewing machine. This allowed the creation of tubular sections to fit over the carbon-fibre leg pieces, and acted solely as a strengthening device down the centre of the robot, where the edge of the membrane might frequently contact the moving control box. This design keeps the membranes in place without hindering compression of the robot. During compression, the membranes naturally fold out gradually to one side or the other, well away from any of the moving parts of the jumping mechanism and hence are unlikely to catch on anything that could cause damage.

5.2.4 Design for Assembly

Due to the high force required to turn the capstan in order to compress Glumper's relatively stiff torsion springs, it was important to ensure that the worm gear could not work itself away from the drive gear. The simple solution would be to mount both the worm drive shaft and the driven capstan shaft in fixed holes in the control box.

However, this is not possible because the circlip (which allows a compression spring on the shaft to keep the capstan engaged without preventing free rotation) needs to be pushed on from the end using a tool and a vice. Therefore, slots of the same diameters as the stepped shaft were cut in one half of the control box to allow the capstan shaft assembly (Fig. 70) to be slid in from the side. The control box thus constrains the shaft vertically, and the assembled components restrict forwards and backwards movement to compression of the spring only. The motor and worm gear can only be mounted afterwards, as these are located to push against the driven gear from the open side of the mounting slot, so that slippage at this end is impossible.
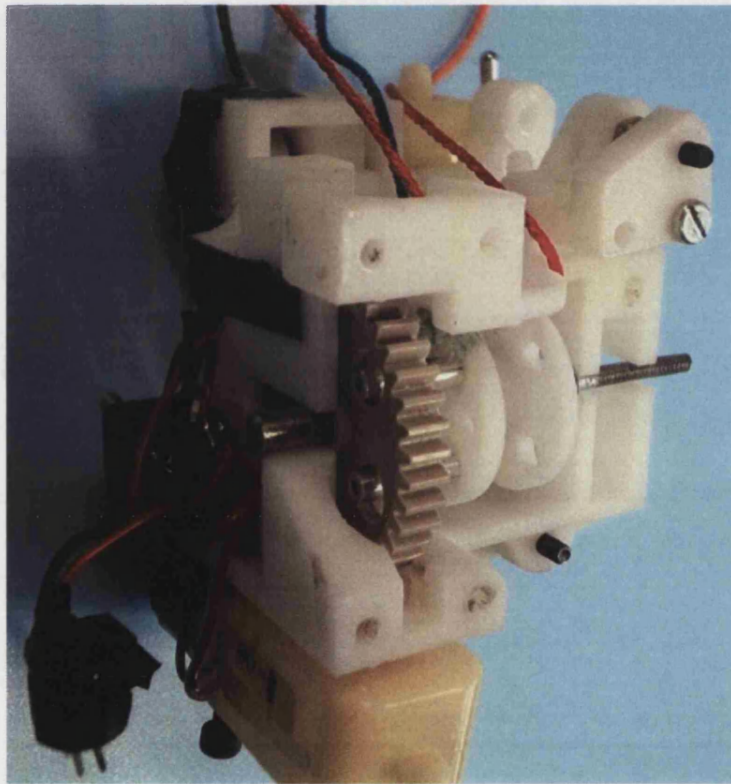
Fig. 70 – View of control box with worm shaft assembly removed to reveal the slots that make it possible to slide in the pre-assembled capstan shaft (including drive gear).

The distant end of the capstan shaft is also constrained to move only linearly thanks to the subsequent mounting of the hinged lever. This has a slot in it which can easily be passed over the end of the shaft before its location around a pivot bolt in the control box.

5.3 Robot performance

It is slightly problematic to determine whether or not a robot is performing well without reference to a specific application. Glumper was designed with thought to several potential applications, but suitability for use in space exploration became a design requirement so it would seem suitable to consider this when analysing its performance. Surface exploration of other planets requires that the vehicle is able to move across completely irregular terrain. Therefore, for optimal performance the robot should be able to jump over the largest possible obstacle, whilst being of the smallest possible volume and mass to minimise the cost of transport.

5.3.1 Jumping performance

In order to capture the peak height of Glumper during jump testing, a *Redlake Images Motionscope* high-speed camera was used at a frame rate of 125 Hz to film each jump. Every fifth frame of an example sequence is shown in Fig. 71 below.
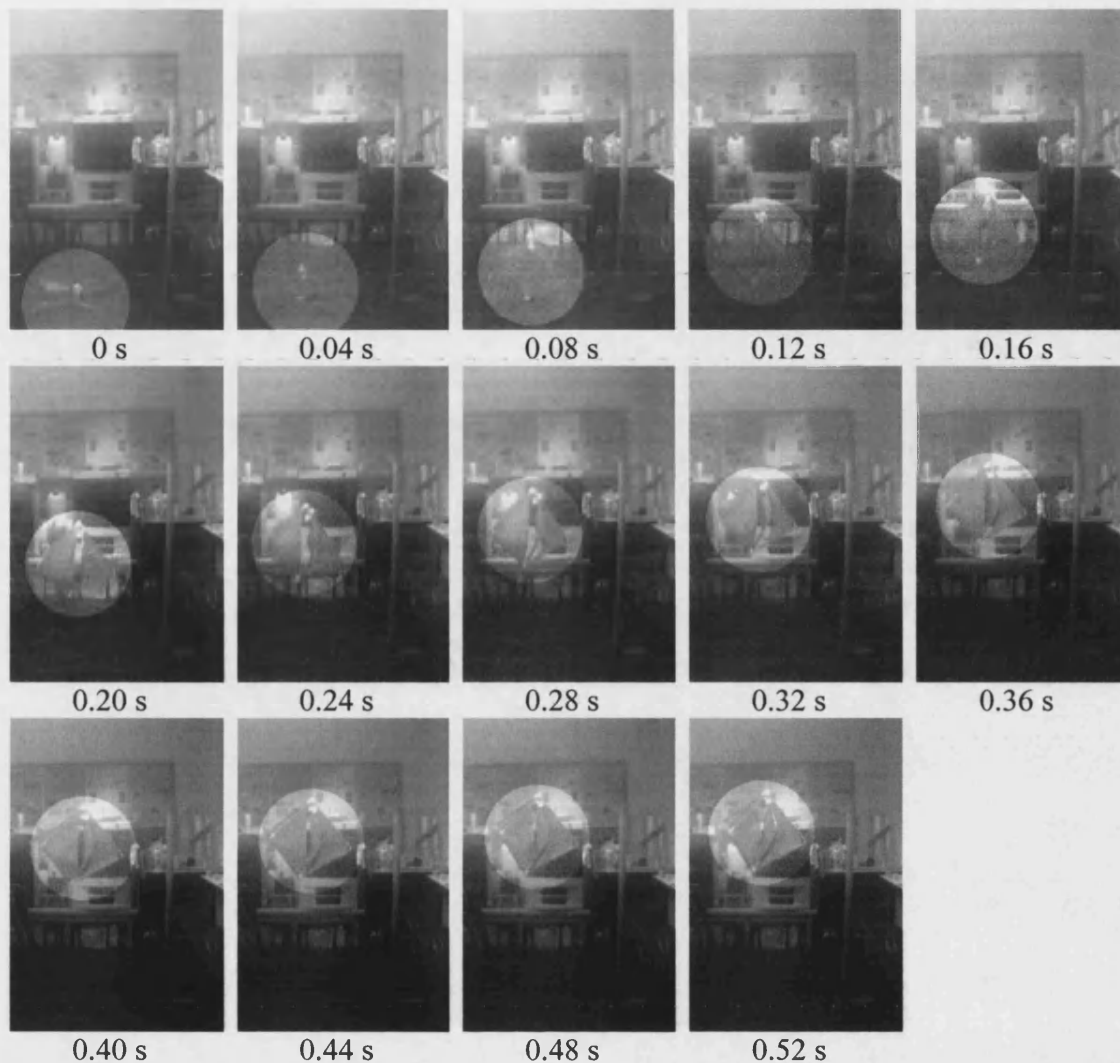
Fig. 71 – Example sequence of images showing Glumper jumping vertically.

Scion Image is useful internet freeware that can handle sequences of images, and output the pixel co-ordinates of all the points clicked on by a user in order, (www.scioncorp.com). The software was used to determine the height of the head and the foot of the robot in each frame of each image sequence captured during testing. In order for this method to be valid, the robot was placed such that it jumped in a plane parallel to the camera lens, and a graded cardboard tube was arranged in line with it for calibration purposes.

Thus Table 4 was produced detailing both the peak height and mean clearance height reached by Glumper during four consecutive vertical jumps, launched automatically and powered by its two onboard lithium cells.

Jump number	Peak height – head (m)	Peak height – foot (m)
1	1.89	1.26
2	1.82	1.19
3	1.72	1.10
4	1.72	1.13
Average (m)	1.79	1.17
Standard Deviation (m)	0.08	0.07

Table 4 – Measured peak heights of Glumper launching itself approximately vertically, powered by two onboard rechargeable lithium cells. The total mass of Glumper (complete with its membranous wings) was weighed on the day of testing and found to be 700 g.

5.3.2 Efficiency of the jumping energy storage mechanism

In order to determine the efficiency of Glumper's energy storage and release mechanism, it was necessary to determine how much energy it is capable of storing. This could be demonstrated by measuring the force required to fully compress the robot, and plotting a force-displacement graph. The area under this graph (Fig. 72) is equivalent to the energy stored. It can be seen that some energy is lost due to hysteresis, but this graph was made by compressing and releasing the robot at 50 mm/min when the robot would actually release instantaneously. Nonetheless, the minimum amount of energy stored in a fully compressed Glumper can still be approximated by estimating the area under the lower curve on this graph. This curve is almost linear, so the area of the triangle made between this line and the axis becomes:

$$\text{Energy} = \tfrac{1}{2} \times F_{max} \times x_{max}$$

(where F_{max} and x_{max} are the maximum values of measured force and displacement respectively).
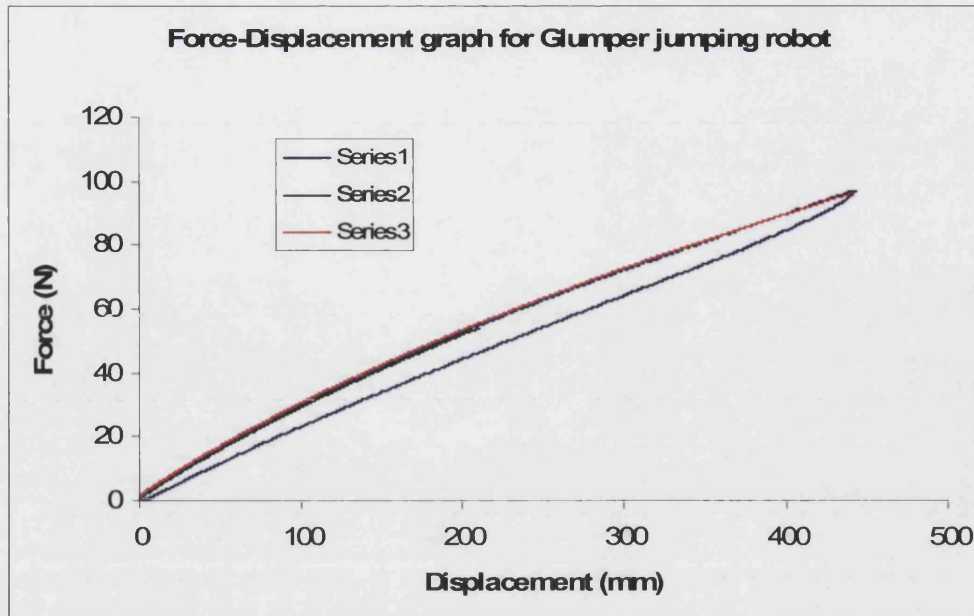
Fig. 72 – Graph showing Force against Displacement for Glumper when compressed using an Instron table-top compression testing machine at a speed of 50mm/min. Series 1 shows the hysteresis in the system as the machine compresses and then releases the robot, and Series 2 and 3 show that the results are repeatable.

Using the output data from the Instron machine, F_{max} = 97 N at x_{max} = 443 mm, meaning that approximately 21.5 joules of energy is stored when Glumper is fully compressed. From this figure, the maximum height that Glumper could reach can be calculated by assuming that all this energy would be converted to potential energy at the peak of a vertical jump if it was 100% efficient. From the potential energy equation below, and the known mass of Glumper without any additional payload (700 g during testing), it follows that the centre of mass of a 100% efficient Glumper jumping vertically would reach 3.1 m on Earth. In testing, the top of Glumper reached an average peak height of only 1.8 m. A large concentration of its mass is in the control box which is physically attached to the top of the robot when it jumps. Consequently its centre of gravity has been estimated to be 15 cm beneath this peak, which would equate to an efficiency of 53%.

$$PE = mgh$$

Equation 18

5.3.3 Effect of mass reduction.

The parasitic mass of the robot, (the mass of the skeletal structure including the foot, legs and springs) is 0.414 kg with the gliding wings attached, compared with 0.395 kg without. Experiments were performed to measure the peak height cleared by the robot both with and without these wings by adding various weights to the top end piece before manually compressing it and launching it vertically. A ruler was used to ensure that the robot was always compressed such that there was a 10 cm gap between the head and the foot, which is equivalent to the amount of compression it would be subjected to if launching autonomously with its control box. A high-speed camera was used to film the jumps, and it was expected that there would be an optimum weight for the eventual control box. (At very small masses, air resistance would adversely affect the peak height achieved). Scion Image was used to determine the maximum distance from the ground of the lowest extremity of the robot in each frame. The results are plotted in a graph (Fig. 73) and it can be seen that the optimum total mass of the robot is less than the current frame weighs, whether or not the wings are attached. Therefore, there is no momentum advantage gained by the additional mass of the control box accelerated away from the foot of the robot. A similar experiment was performed using Glumper Mk1, and the same results can be seen in Appendix 2 on page 210.
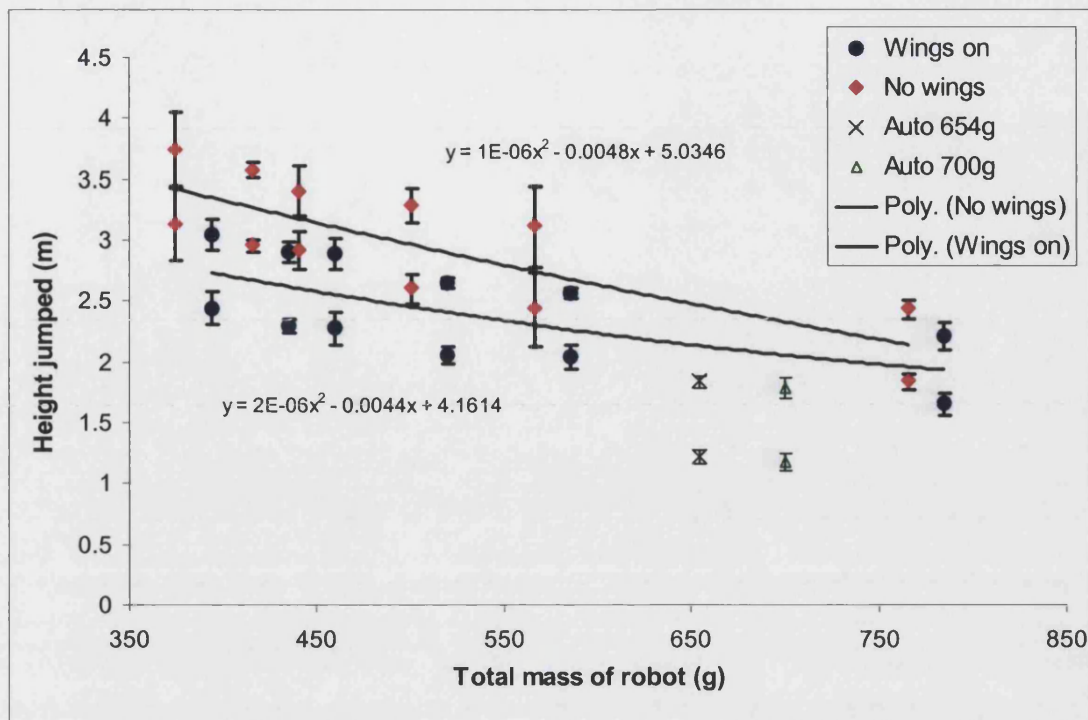
Fig. 73 – Graph showing that adding mass to Glumper's basic frame reduces its peak clearance height both with and without its wings attached. There must be an optimum value of weight to achieve maximum clearance, but this cannot be quantified because it occurs at a lower mass than that of the present frame structure alone. The graph was produced by measuring the peak height of both the head and foot of the robot repeatedly for every given condition, and plotting the average values. Microsoft Excel was used to plot a polynomial trendline through the centre of these head and foot points for both the winged and non-winged measurements, and the respective equations of the resulting curves are displayed. Finally, the average measured peak height of Glumper's head and foot for automatic launches is shown for comparison, firstly powered by one and then with two onboard lithium cells, the latter setup proving to be more consistent and reducing the winding time, but adding 50 g to the weight. The error bars represent plus and minus one standard deviation from the means in all cases.

Fig. 73 allows the efficiency of Glumper's launch mechanism to be calculated in relation to the manually released jumps. The triangles labelled 'Auto 700 g' represent the jump height data presented in Table 4, corresponding to an automatically releasing Glumper with its wings fitted and operating from its two onboard Lithium cells connected in Series. The total time for wind-in using this power source is 435 seconds. The equations of the two curves can be used to predict the height reached by the centre of the robot, either with or without its nylon wings attached, for a given mass. In this way, it is possible to show that the mid-point of (the winged) Glumper should have reached a height of 2.06 m if manually released, when it actually peaks at 1.48 m due to energy losses during automatic launching. This equates to a relative efficiency of 71.7%, with the losses likely to be primarily due to friction in the rapidly unwinding of the string from the capstan (as it passes through locating holes and around the pulley shaped pieces on the head and foot). It should be noted that even the manually released

launches are only 66.5% efficient when compared with the total energy storage capacity measured for the torsion springs, as discussed in Section 5.3.1 on page 159. Some of this energy loss can be attributed to vibration in the torsion springs causing the top and the bottom of the robot to oscillate towards and away from each other during its climb away from the ground. There will also be some loss of energy through friction and conversion to sound.

5.3.4 Gliding performance

It can be seen from Fig. 73 that the presence of its wings cause a reduction in Glumper's peak jump height, even when making an allowance for the increased weight. This is presumably the result of the drag force caused by air resistance acting against the membranes, both during and after unfolding, although the design is such that these are in plane with the direction of motion which should minimise this drag force. Experiments were carried out to test what effect the presence of gliding membranes has on the peak clearance height and total range of a forwards jump. Up until now, all the data presented has been concerned with approximately vertical jumping, but in order for Glumper to be able to make useful progress, the depth of its end pieces will ultimately need to be increased such that Glumper is angled forwards when in its compressed state. For the purposes of these experiments, a fixed take-off angle of 63° to the vertical was used, established by launching Glumper from an inclined ramp. The use of this ramp rather than deliberately developing deeper end pieces to adjust the take-off angle of the robot was both less time consuming, and minimised the likelihood of the foot slipping during take-off from the artificially smooth surfaces in the laboratory (though these could have been roughened, of course).

Graphs are presented showing the trajectories followed by the two end points of Glumper, (labelled head and foot where the foot was the end in contact with the ground), during six jumps launched automatically at an angle of 63° to the horizontal and powered by its onboard rechargeable lithium batteries. In the first three jumps the wings were present (Fig. 74), and for the second three they were removed (Fig. 75). Considering the mean peak height reached by the robot in these tests, the presence of the wings reduces this by 4 cm from 1.77 m (SD = 3 cm, n = 3) to 1.73 m (SD = 9 cm, n

= 3). Likewise, the mean peak clearance height falls from 1.17 m (SD = 5 cm) to 1.10 cm (SD = 9 cm).

Fig. 74 –Graph showing the trajectories followed by Glumper's head and foot during three jumps launched automatically at an angle of 63° to the horizontal and powered by its onboard rechargeable lithium batteries. [Colours hard to distinguish]
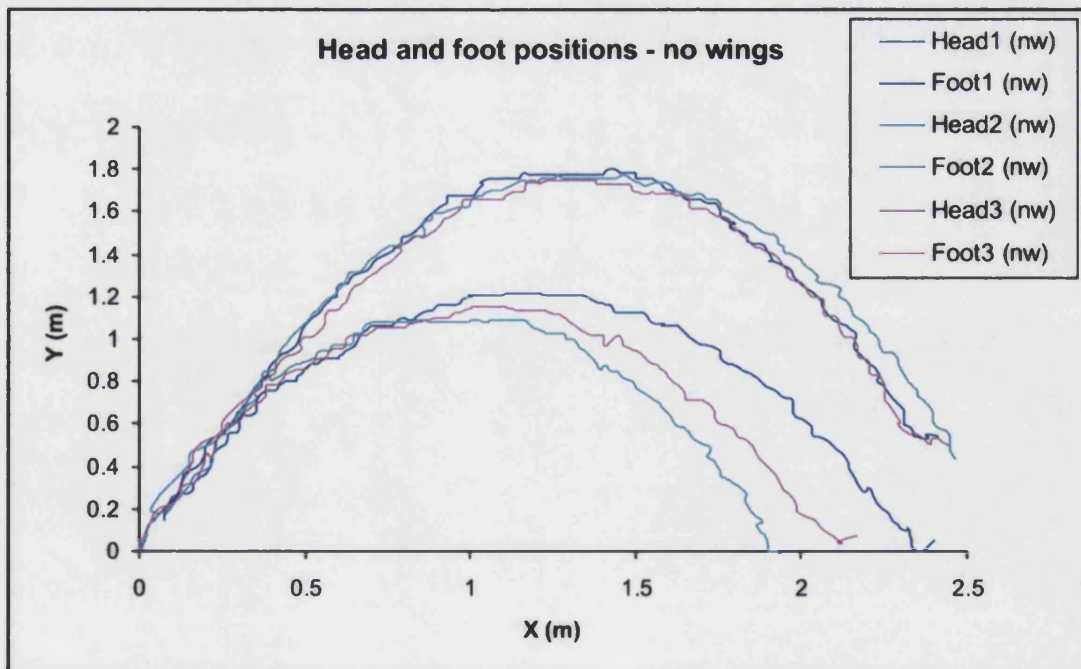
Fig. 75 – Graph showing the trajectories followed by Glumper's head and foot during three jumps launched at an angle of 63° to the horizontal. These jumps were powered by the onboard rechargeable lithium batteries, but the membranous wings had been removed from the robot.

Fig. 76 plots the trajectories followed by the mid-point between the two ends of Glumper for these six jumps. It is clear that the presence of the wings actually reduces the total range of the jump rather than extending it as was intended, presumably owing to the additional mass and drag force noted previously. With regard to impact force reduction, the other role of the gliding membranes, evidence is provided in Appendix 3 (page 225) that the wings do reduce the vertical velocity of the robot even over the short trajectories presented above. Likewise, they reduce the total velocity at the moment of impact, but this is also a direct consequence of the resultant reduction in horizontal range. This result can be related directly to the flying frog, introduced during the literature review (Section 2.2.2.3, page 50), which is able to gain some aerial control and slow itself while falling but is not so successful at increasing its horizontal range travelled.
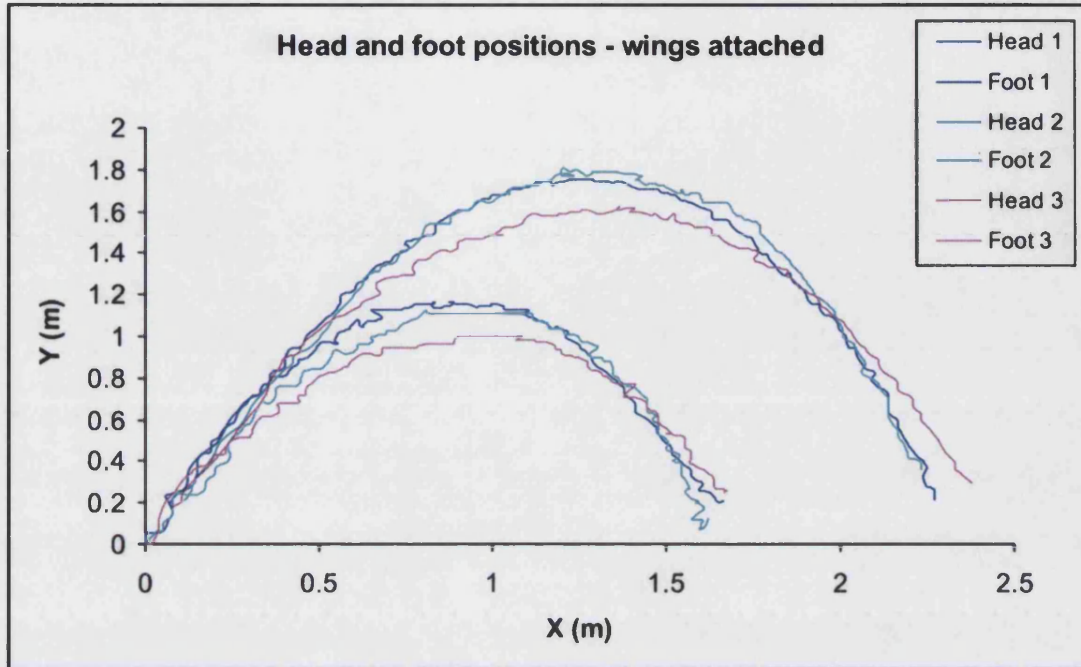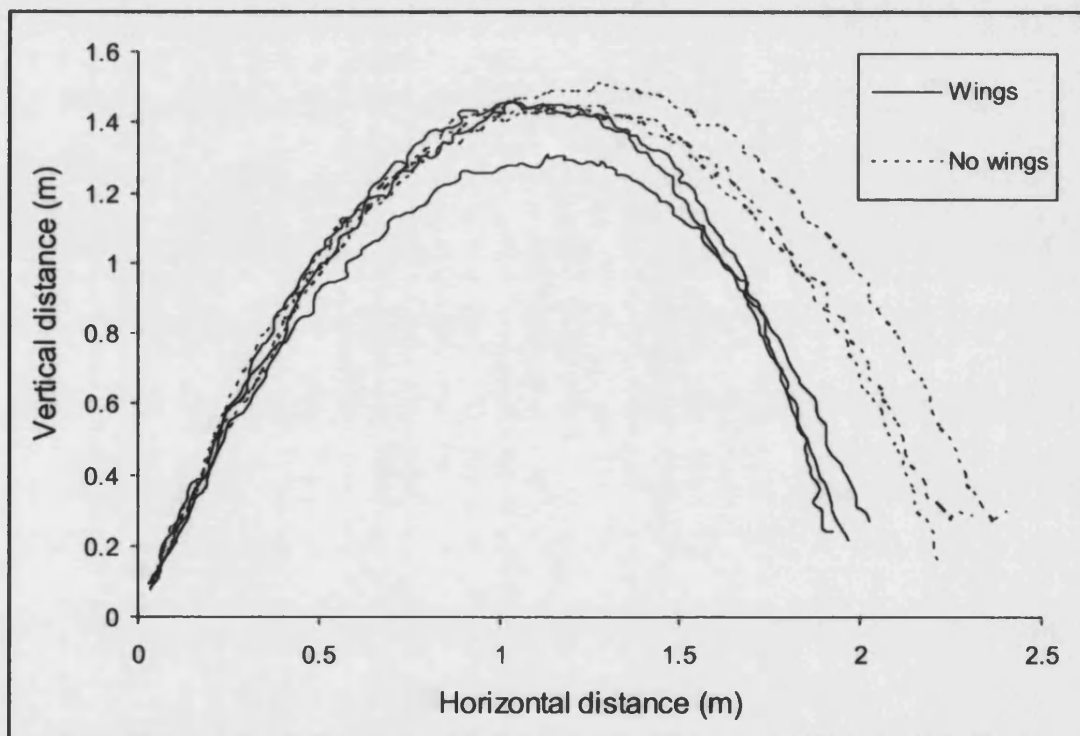

Fig. 76 – Graph showing the trajectories followed by Glumper's centre position during six jumps launched automatically at an angle of 63° to the horizontal, three with and three without its membranous wings attached. Unfortunately, under these conditions, the presence of the wings actually reduces the total range of the jump rather than extending it as was hoped. (This is presumably due to air resistance and increased weight). It can be seen that in all but one of the jumps, the centre of the space occupied by Glumper reaches a clearance height of 1.4 m, with the exception being a winged launch peaking approximately 15 cm lower.

Drop tests were set up to prove that the wings were successfully reducing Glumper's impact velocity, over a mandatory distance of 3.6 m, chosen because it seemed a height

which might reasonably be achieved with successful weight reduction on the basis of Fig. 73. The results are shown in Table 5 and it can be seen that the wings both prolong the jump and reduce the impact velocity, independent of the orientation of the wings or the position of the compression mechanism.

How released?	Time taken to drop 3.6 m (s)	Final velocity (m/s)	As % of ballistic
Wings flat, mechanism central	0.92	6.7	66.3%
Wings flat, mechanism at end	0.99	7.5	74.3%
Wings diagonal	0.98	8.1	80.2%
No wings	0.81	10.1	100%

Table 5 – Table showing the time taken for the robot to fall 3.6 m, with and without the wings and with the control mechanism located centrally in all cases except where specified. This table also shows the final velocity reached by Glumper in each of the various drop tests. All values shown are the average of two measurements.

Therefore, Glumper's gliding membranes should start to have a more positive effect on performance if sufficient weight can be removed from the robot, which should also simultaneously improve peak jump height and the lift to drag ratio during gliding. This principle is clearly demonstrated in Fig. 20, (page 52), which shows that the smaller of two otherwise similar species of gliding lizard, (Draco), achieves a much superior glide angle. Hypothetically, however, reducing the weight too much could also lead to a reduction in performance, owing to air resistance against the wings which would cause a relatively larger drag force against the ascending robot. Additionally, an increase in horizontal velocity would improve the ultimate glide angle of the robot. This is demonstrated by the fact that soaring birds and flying fish achieve the shallowest glide angles in nature owing to their respective abilities to propel themselves to relatively high horizontal velocities immediately beforehand. A slight improvement in gliding performance might therefore be achieved by launching Glumper at a shallower angle, although this would have negative implications to its peak clearance height and so the appropriate compromise would need to be found by experimentation.

Considering the flying squirrel once again, it was stated in Chapter 3 that although these animals protract and abduct their forelimbs during the launch, full gliding posture is only adopted once airborne by extension of the wrists and elbows. Perhaps therefore, Glumper might benefit from the incorporation of a delay in the full deployment of its

gliding membranes, thus reducing drag while it attempts to gain altitude. All the modifications discussed in this section are central to the suggestions for further work in the next chapter, as would be the development of a method for altering Glumper's pitch angle (while gliding) to the resultant trajectory by a suitable control system.

5.4 Power requirement

Throughout the initial trials of Glumper, it was powered using a small, laboratory bench power supply capable of delivering several Amperes of current. A digital multi-meter was used to measure the voltage and current drawn by Glumper every 30 seconds during its compression and release. Therefore, from Equation 19 below, it was possible to plot a graph of electrical power against time (Fig. 77). The results were used to select two rechargeable lithium ion cells, weighing 50 g each, which were mounted on board the Glumper control box for use in the performance testing. These were wired in series to give a theoretical operating voltage of 7.4 V, (although this was actually measured to be 8.05 V during compression) and a maximum rated current dissipation of 2 A, five times the maximum requirement measured at the moment of take-off to be 0.4 A. These batteries were deliberately over-specified to ensure consistent and repeatable usage during testing. Fig. 77 demonstrates that Glumper can compress itself ready for jumping much more quickly using the batteries than the bench top power supply, owing to the higher operating voltage. In both cases, the peak electrical power required for Glumper to jump is approximately 3.2 W. The simple equation for deriving electrical power output (P) from the measured voltage (V) and current (I) is:

$$P = V \times I$$

<div align="right">Equation 19</div>
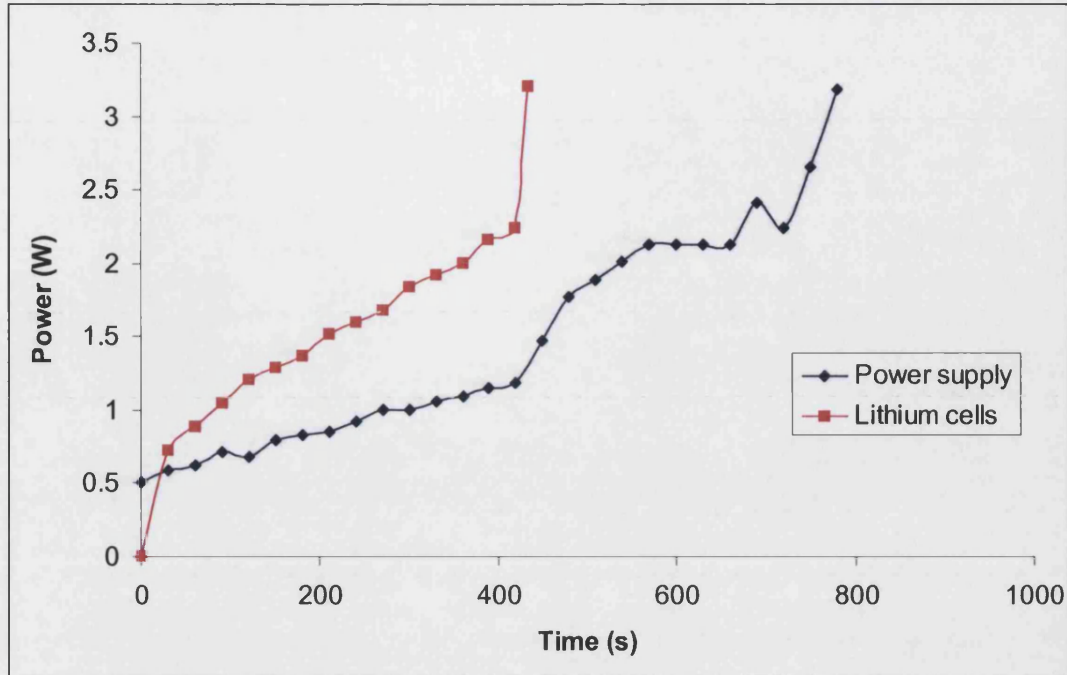
Fig. 77 – Electrical power consumed by Glumper's compression mechanism against time, calculated from the voltage and current measured throughout its entire compression cycle. The graph shows that the peak power requirement is the same (approximately 3.2 W) whether driven by the bench top power supply at a continuous voltage of 5.89V, or the two rechargeable lithium cells wired in series (which have a measured output voltage of 8 V).

5.4.1 Flexible solar cells

At the outset of this research, solar panels were proposed as a potential source of energy for an autonomous jumping robot. Solar panel technology has developed to a very high level, largely as a result of their use in space applications. On Earth the Sun's radiation is diffused and scattered by the environmental conditions, but in space it delivers a constant power of 1370 W/m^2 at the radius of the Earth's orbit. If considering using solar panels for exploration of a planet or moon further from the sun, then the available power will reduce according to Newton's inverse square law. The use of solar panels in space applications has created a need for increasingly stronger and lighter solar panels that can be protected during launch and deployed once in orbit. As a result thin-film photovoltaic cells are increasingly more available, and the prices are reducing. These thin-film technologies use layers of semiconductor materials only a few micrometers thick, attached to an inexpensive backing such as glass, flexible plastic, or stainless steel.

On Earth, the intensity of the Sun's radiation varies enormously and solar panels are capable of producing very high voltages, so loads are generally not connected directly (to avoid damage to sensitive electronics). Instead, it is usual to integrate a charge controller (or regulator) and a battery. This also allows energy to be generated during hours of sunlight, and stored for use at other times. The charge controller prevents the solar panel or array from overcharging the battery, which itself serves to store energy for the system. The quality of power is also improved, because the battery can be discharged as required to supply a variable electrical load.
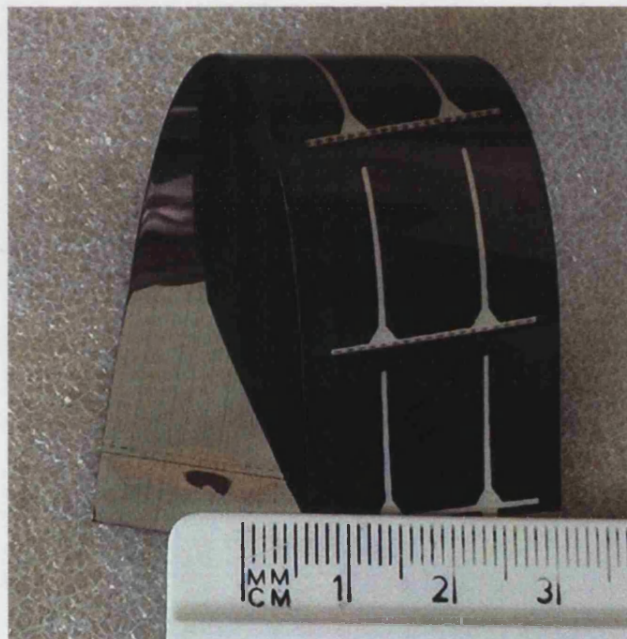
Fig. 78 – Photograph showing one of the Photon Technologies Powerfilm® flexible solar modules rolled and held under a ruler to demonstrate its flexibility and size.

Fig. 78 shows a flexible panel manufactured by Photon Technologies. A number of these flexible solar panels were bought in order that experiments could be performed to evaluate the feasibility of using them to power Glumper. In principle, these solar panels could be easily attached to Glumper's gliding membranes owing to their light weight and flexibility. The panels would need to be connected together into an array, with the maximum voltage and current preset by connecting them in series or parallel as required (see Fig. 79). However, another thing that must be taken into account when making the relevant calculations is that it is only possible for ¼ of the panels to be directly pointing

at the sun, assuming that equal numbers are mounted on each of the membrane wings. The results from these solar panel experiments will be detailed in the following section.

| Connection in parallel increases the current | Connection in series increases the voltage |
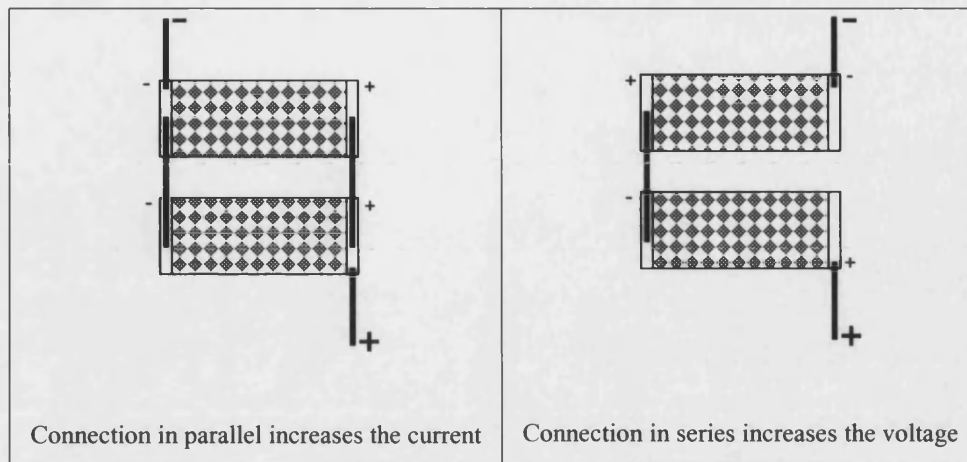
Fig. 79 – Demonstration of how to connect up the Solar Array to generate the required output (Photon Technologies).

5.4.2 Solar power experiments

Photon Technologies Powerfilm® flexible solar modules are specified as generating 0.15 W each of power in bright (Earth) sunlight for a panel of 15 × 3 cm (Photon Technologies, Colorado Springs, CO, USA.) Their flexibility, lightweight and size would make them ideally suitable for mounting on Glumper's membrane wings. Importantly, only two wings could ever be directly pointing at the sun irrespective of robot's orientation, which is enough area for 45 panels. Hence, a maximum power of 6.75 W is theoretically available and Glumper's control mechanism thus satisfies the requirement that it should be able to ready itself for a jump using a locally available energy source. From the plot of electrical power against time for the rechargeable lithium cells (Fig. 77), the total electrical energy required to power a jump, (the area under this curve), was estimated to be 643.8 joules. Therefore, the efficiency of the conversion of electrical energy into strain storage energy is approximately 3.3%, with some of this deficit clearly being converted into heat.

In order to verify that it would indeed be possible to connect these particular flexible solar panels (in series and in parallel as necessary) to drive the measured load required by Glumper's compression mechanism, some experiments were set up to test them. The

open circuit voltage measured for a single solar panel was approximately 4 V, slightly higher than the manufacturer's rating which was given to be 3 V. Thus two of the flexible solar panels were soldered together in series, giving them an open circuit voltage of 7.84 V together, approximately equivalent to the output from the rechargeable lithium batteries currently fitted to Glumper. Together these solar cells could be considered as a battery, which was then connected across a range of load resistors in turn, while positioned on a flat horizontal surface in direct sunlight. It is important to note that for these experiments, no attempt was made to try and achieve the best possible power output from these cells, which would require them to be oriented perpendicular to the direction of the sunlight during the mid-afternoon when the available solar power is highest. Instead the intention was to prove that these particular flexible solar cells could be used together, to reliably generate enough power from a non-optimal position on a normal day. These experiments were conducted at 3 pm in Bath in the UK, on a slightly hazy but sunny day in April 2007.

While voltage measurements were recorded with the two solar cell battery connected across each load resistor, the voltage through a larger array of 10 of these solar panels was simultaneously measured to ensure that the sun's intensity was consistent between tests. These voltages were measured using two channels of a Measurement Computing 'PMD 1208 LS' Analogue to Digital converter, at a sampling rate of 10 Hz. The output from each channel could be stored simultaneously, and the two solar panels connected in series, and the ten panel parallel array were positioned side-by-side on a flat horizontal surface (as shown in Fig. 80) to ensure a fair comparison.

Fig. 80 – Photograph showing solar cell experimental apparatus in use

From the closed circuit voltages measured, the current could be determined using Ohm's Law (Equation 20 below):

$$V = IR$$

Equation 20

Fig. 81 is a plot showing how the measured output voltage from the two solar cells (connected in series) increases with the load resistance, while Fig. 82 shows that the resultant current falls, as would be expected.
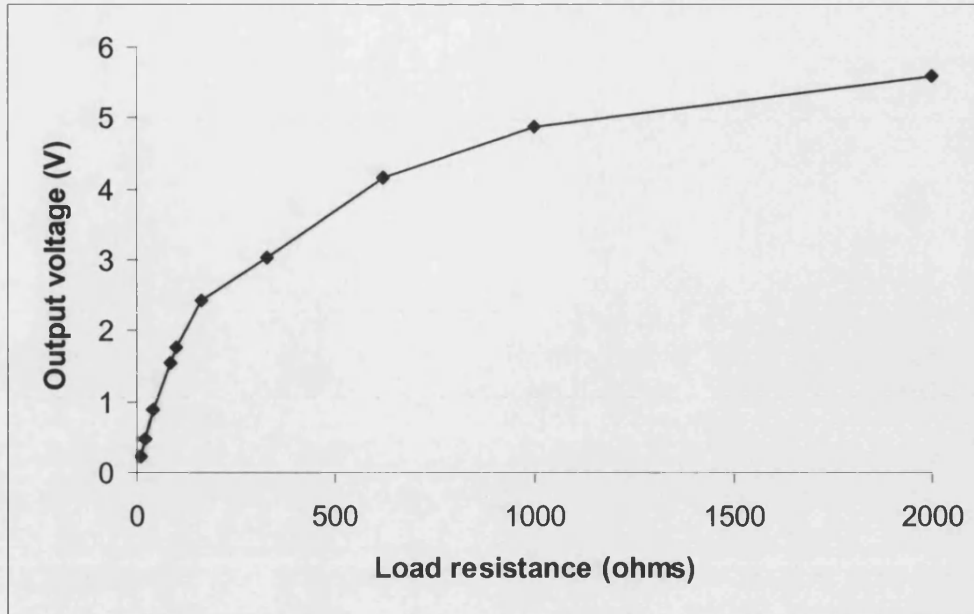
Fig. 81 – Graph showing how the measured output voltage of the solar cell increases with the value of the load resistor across it.
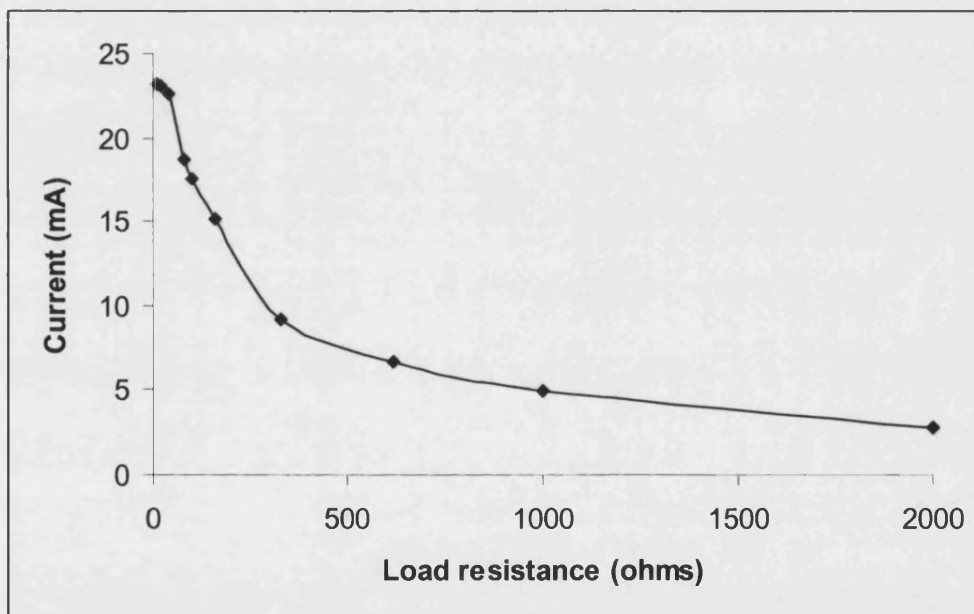
Fig. 82 – Graph showing how the current flowing through the load resistor drops as its resistance increases.

The effective load of Glumper's compression mechanism could also be found from Equation 20. Therefore, using the measured maximum value of current drawn by the motor, at the moment immediately prior to jumping, 0.4 A, and the known output voltage, 8 V, this equates to a load of 20 ohms. By considering the two solar cells as one battery, it was possible for every data point to determine the number of such batteries that would need to be connected in parallel in order for the effective load resistance felt

by all together to be 20 ohms. In each instance, the total current produced should be equal to the measured current at the respective data point multiplied by that total number of batteries. Hence it is possible to calculate the total electrical power that would be generated by a given number of the Photon Technologies flexible solar cells, (under these specific conditions), and the results were plotted in Fig. 83. By definition, this graph assumes that all the individual solar cells are divided into two equally sized parallel arrays, both of which are then connected together in series to generate the desired operating voltage of approximately 8 V. The additional lines on the graph show that 45 panels, (equivalent to one quarter of the maximum number that could be fitted to the area of Glumper's membrane wings, which allows for the fact that the others would be shaded from the sun to varying extent), could only produce 0.63 W if used to power the robot's compression mechanism.
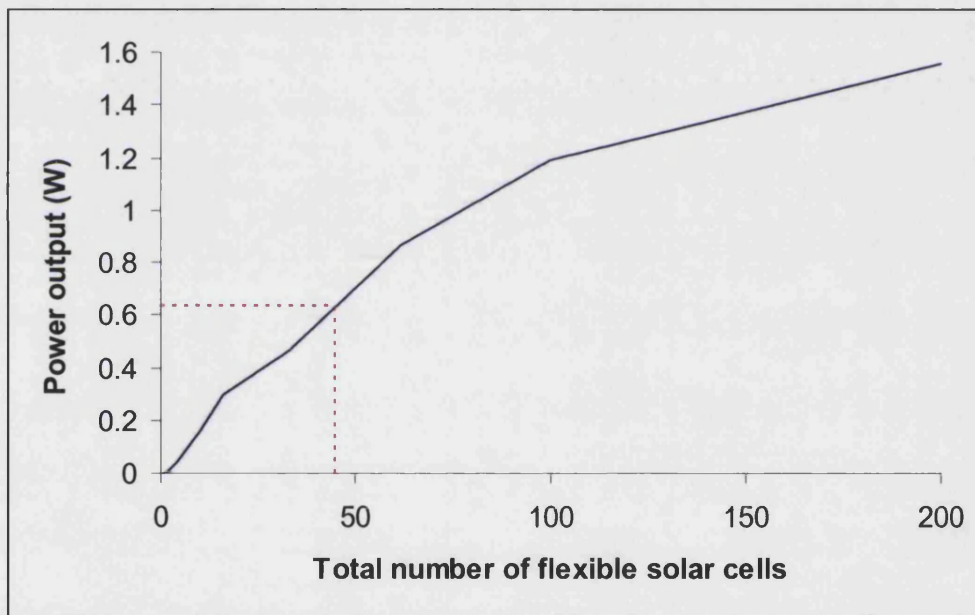
Fig. 83 – Graph showing how the electrical power (W) available for the Glumper compression could be increased by adding more panels. An assumption is made that all these flexible solar cells are divided into two equally sized parallel arrays which are then connected together in series to give the desired operating voltage of approximately 8 V.

However, it was stated previously that Glumper's compression mechanism requires approximately 3.2 W at the instant of take-off. Therefore these 45 small panels would only be able to produce 25% of the maximum power requirement, although this does not take into account the fact that most of the other solar cells on Glumper's wings, though shaded, would likely still be able to contribute some power to the system.

Although this is a disappointing result, the consequence is not critical because the power requirement of Glumper can easily be reduced with more gearing.

A simple experiment to demonstrate the effect of increasing the gearing of Glumper's compression mechanism to its power requirement was carried out. This was effected by removing one end of the cord from the capstan, and tying it instead straight to the housing just beneath. Consequently, the capstan is only winding in one end of the cord instead of both, more or less doubling the time taken to compress the system. Fig. 84 shows the resulting current against time graph. The time taken to compress and release Glumper has increased from 7.25 to 13.5 minutes, while the maximum power requirement has decreased to 1.84 W. This approximately demonstrates the expectation that doubling the gear ratio would halve the power needed. It has been stated from the outset that the speed of the robot is unimportant in comparison with the requirement that it should be fully autonomous, and hence able to power itself from a locally available power source. Although the power requirement determined by this experiment was still marginally too high for an area of the flexible solar cells equivalent to the size of Glumper's wings, it can be seen that by choosing a suitable gear ratio, they should become sufficient. Throughout the testing, the motor driving Glumper's compression mechanism had a total gear ratio of 10000:1, and from these experiments it seems likely that this would need to be increased to about 40000:1 in order to effect a reliable transition from batteries to the flexible solar cells.
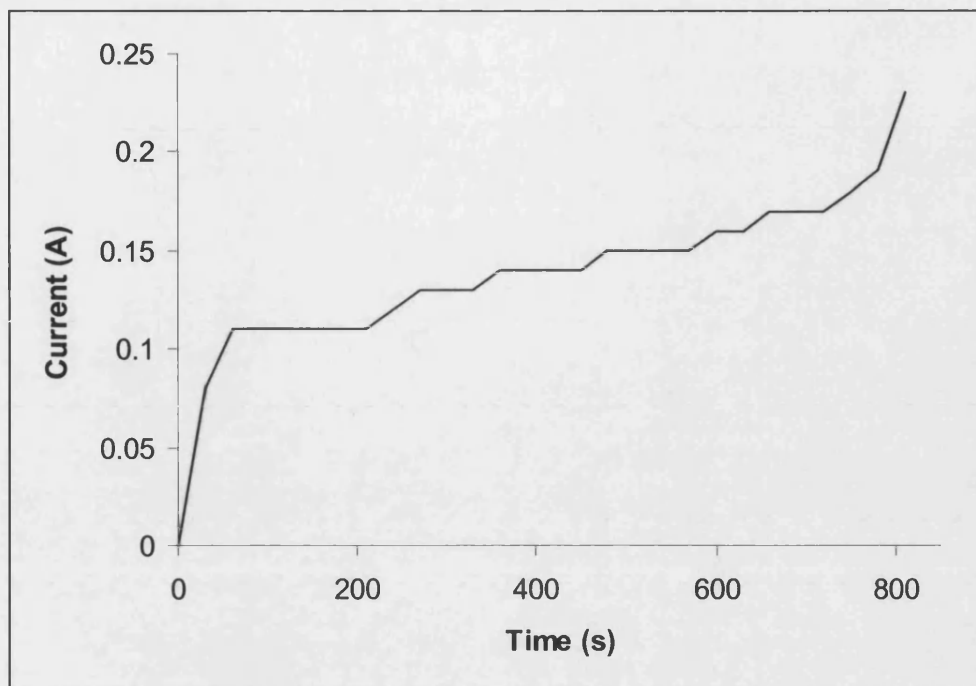
Fig. 84 – Current against time graph for Glumper after modification to reduce the gear ratio further. At the instant of release, after 810 seconds (13.5 minutes), the current drawn was 0.23 A, equating to a maximum power requirement of 1.84 W.

5.5 Discussion of performance

When launched at an angle of 63° to the vertical, Glumper has an approximate horizontal range of 2 m with the wings attached, and 2.4 m without, excluding any additional distance that might be travelled as it bumps and rolls to a complete stop. If Glumper was modified to be powered by flexible solar panels, with a total gear ratio of 40000:1, then its total winding in time should be 29 minutes. Therefore, left to operate continuously for 24 hours, it would average 94.8 m per day with wings, and 119.2 m per day without (on Earth and assuming it could orientate itself to continue a straight path and was uninfluenced by external factors such as wind). This is dependent on the robot choosing a path with no obstacles greater than approximately 1 m in height. On Mars, both the range and clearance height of the robot would be significantly higher owing to the smaller gravitational force acting on the robot. Even without taking this into account however, the data compares very well with NASA's planetary rovers currently exploring Mars, Spirit and Opportunity, which are averaging 6.3 m and 9.3 m per

Martian day. (Note, this also includes the Martian night when no solar power is available).

It has been shown that Glumper's gliding membranes do not increase jumping range in its present design state, but they do help to reduce the landing impact force.

5.5.1 Jump height - comparison with nature

Glumper's performance is directly compared with some suitable jumping animals in Fig. 85, which shows jump height against object length for each. This figure also displays equivalent data for all the existing jumping robots introduced in the literature review (Section 2.3.2, page 59). The animal data was taken directly from Bennet-Clark (1977). The horizontal lines show energy density and the sloping lines are a measure of power per unit weight, derived from Equation 21 below which relates power (P), mass (m) and leg length (s) to maximum height, h, for a vertical jump where g is the acceleration due to gravity (Bennet-Clark 1977):

$$h = \left(\frac{2sP}{m}\right)^{\frac{2}{3}} \times \frac{1}{2g}$$

Equation 21

The power to weight ratio of direct muscle action in animals has a practical limit of 100 W/kg (Bennet-Clark 1977). Hence, all the animals above that line in Fig. 85 are producing more power than their muscles can deliver, requiring some additional energy storage mechanism. In fact, all the animals shown are above that line, demonstrating that power amplification is usual for animals when jumping.
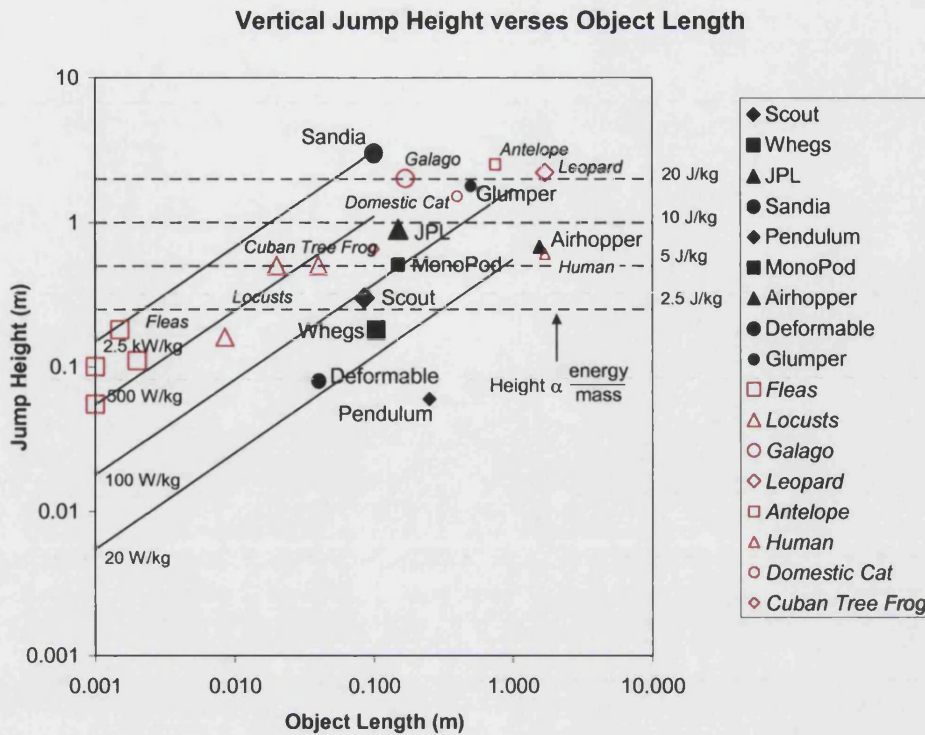
Fig. 85 – Height of jump versus length of a selection of animals (outlined markers) and robots (solid markers). The graph also shows required specific energy and specific power to produce a jump assuming that the objects accelerate through their own body length and that there is no air resistance. This graph was compiled by Rhodri Armour in a joint paper (Armour, Paskins et al. 2007).

At the outset of this chapter, optimal performance of a jumping robot for use in planetary exploration was declared to require maximisation of height together with minimisation of mass and volume to reduce the cost of space transport. Considering Fig. 85 the closer the robot sits to the top left corner of the chart, the better. This is equivalent to a maximisation of power density, represented by the diagonal lines, which is consistent with the finding in the principles of jumping section of the literature review (page 21) which proved that decreasing size demands increased power to achieve equivalent height.

Looking parallel to these lines of power density in Fig. 85, Glumper performs rather well compared to the animals that would not be considered to be specialised jumpers, sitting directly between the domestic cat and the antelope (and thus producing equivalent specific power). The jump heights recorded by specialised jumpers, such as fleas, frogs and the lesser galago demonstrate a superior power density.

5.5.2 Jump height – comparison with previous jumping robots

A number of prototype jumping devices are introduced in Appendix 2, (page 210), which were built to demonstrate design ideas throughout this research process. However, none of these were capable of fully automatic compression and release meaning that valid performance comparisons with Glumper (or any of the existing jumping robots reviewed in Chapter 2) could not be made.

From Fig. 85 it can be seen that in terms of both energy density and power density, Glumper outperforms all the existing jumping robots reviewed in Section 2.3.2 of this thesis, (page 59), with one exception. This was the Sandia robot, which is propelled by the combustion of propane and this superior performance would be expected because the energy density of hydrocarbons is much higher than that of springs. Interestingly, the author can think of no comparable biological transport modes. The use of combustion to power jumps was not considered in this research, due to the primary requirement of autonomy. Other potential applications are also prohibited by this design. In confined areas, for example, exhaust gases could pose a problem and on other planets, the lack of oxygen in the atmosphere would prevent the burning of fuel (though high explosives could obviously be used, and in a reducing atmosphere oxygen could be used as a fuel). The robots with either helical or bending springs as their energy storage medium, including Glumper, outperform the remaining devices. This does not even take into account that those devices, Airhopper, Pendulum and Deformable all rely on external power giving them an immediate weight advantage. It is not clear from this sample whether one type of metal spring consistently outperforms any other, although no difference was expected. The only elastomer-based jumping robot does not jump particularly high, and the absence of other published devices storing energy in elastomers might be confirmation of their unsuitability for slow pause-and-leap jumping devices owing to stress relaxation.

Power density can be increased by either increasing power or reducing mass. More power can be produced by generating higher force or reducing its time of action over a given distance. In animals this is limited by the maximum power output of muscle resulting in the use of energy storage. Therefore the performance limiting factor for a

jumping robot is its energy storage and release mechanism. The mass reduction experiment conducted demonstrates clearly the advantage of reducing unnecessary weight. It is possible to eliminate mass from engineering systems through optimisation techniques such as FEA and by changing materials, whereas nature's jumpers are already highly optimised as a result of natural selection. The Sandia robot has already proved that it is possible to outperform nature's jumpers by using a hydrocarbon based energy storage and release mechanism, which requires the use of high performance materials in its construction. Such materials are unavailable to natural organisms due to their additional practical constraints, such as the need for reproduction.

One compromise that is faced when designing a rover for space exploration is that it needs to carry a useful payload, such as a vision system, or scientific data collection equipment. This mass has to be allowed for when choosing the optimum size of the robot, because a set payload will have a greater implication on the clearance height of smaller, lighter designs. Glumper's total mass was 700 g, including its four wings. Fig. 85 demonstrates that it could absorb the additional weight of a small payload, perhaps 100 g, without a large decrease in jump height.

The overall performance of the biomimetic jumping and gliding robot Glumper, freshly developed for this Ph.D research, is good. It has been shown to achieve most of its design requirements successfully, and is able to jump higher and further in a single leap than all but one of the comparable robots found in the literature search, and to jump as well as some good but non-specialised, jumping animals such as cats and antelope.

5.6 References – Chapter 5

ARMOUR, R., PASKINS, K., *et al.* (2007). "Jumping robots: a biomimetic solution to locomotion across rough terrain." Bioinspiration & Biomimetics **2**: S65-S82.

ASHBY, M., F. (1992). Materials Selection in Mechanical Design, Pergamon.

BENNET-CLARK, H. C. (1977). Scale Effects in Jumping Animals. Scale Effects In Animal Locomotion. T.J.Pedley. London, Academic Press**:** 185-201.

PHOTON TECHNOLOGIES, I. "Solar Panels and Solar Cells for Rechargeable Battery Powered Products."   Retrieved 12/12/03, from *http://members.aol.com/photontek/1/photon2a.html*.

TORRES, G. E. and MUELLER, T. J. (2004). "Low-aspect-ratio wing aerodynamics at low reynolds numbers." AIAA **42**(5): 865-873.

Chapter 6

Future Work

The scope of this research was broad ranging and interesting to the author. This section will briefly introduce some of the work which he feels should be undertaken to best further this research. It will be split into two categories, depending on whether it concerns the biology of flying squirrels, or the development of the jumping robot, Glumper.

6.1 Further study recommended on flying squirrels

It would be useful to repeat the study described in Chapter 3 using larger sample sizes, and if possible, across a greater range of distances.

It would also be useful to study flying squirrel skin under a suitable microscope in order to identify the proportion and orientations of collagen and elastin fibres within its matrix structure. A similar method to that reported in Chapter 4 could then be used to fully evaluate the hypotheses determined in the same chapter for the structure of skin in flying squirrel patagia.

6.2 Further development work required on Glumper

A mechanism for orientating Glumper prior to take-off could be developed; this would be essential in enabling the robot to choose its destination. This could be achieved by rotating an eccentric mass around the middle of the box housing Glumper's compression mechanism using a small additional motor and a suitable gear arrangement.

It was shown theoretically that Glumper should be able to power itself for jumping using 45 of the flexible solar cells according to their maximum specification supplied by the manufacturer, Photon Technologies. It was shown experimentally that, on a normal April day in Bath at least, covering both sides of all Glumper's gliding membranes with flexible solar cells should provide sufficient power for the robot to jump if the gear ratio was increased to 40000:1 for the motor driving the compression. It would be interesting and worthwhile to obtain the required number of cells and prove this experimentally. Such an experiment should verify that Glumper does achieve the original requirement of converting locally available solar energy into jumping locomotion, and also under what weather conditions. If this did not work for some reason, then the gear ratio of the compression mechanism could be adjusted accordingly. The time taken to compress the robot could thus be re-evaluated for estimating its average speed in an exploratory mission. Further experiments should be performed to determine whether or not the motors can be run directly from the solar panels, or if a charge controller is required. In this way it might also be possible to store some of the energy in super capacitors, an emerging electrical energy storage technology.

Flying squirrels are able to quickly switch between locomotion modes, and it was demonstrated in Chapter 4 that their patagia naturally retract away to avoid hindering the animal when it is not gliding. Glumper's gliding membranes naturally fold out to the sides as the robot compresses, and it should not be possible for them to catch on anything as they straighten unless an object somehow moved into the middle of a folded wing once the robot was mostly compressed. Unlike flying squirrels, Glumper was only capable of two forms of locomotion, jumping and gliding. In future, it would be highly advantageous for additional transport modes to be incorporated into this robot to improve its versatility. The use of wheeled rolling where possible, for example, would likely increase the life of the robot because it is subjected to relatively high impact loading during jumping. Assuming it had sufficient power, Glumper could save time by compressing its jumping mechanism while in motion, and hence it would be vital that its gliding membranes were out of the way. A flying squirrels inspired solution would thus be to incorporate an elastic element into the robot's wings to pull them tightly together while the robot compresses. However, such a solution would cause a small opposing force slowing the resultant acceleration of the robot away from the ground

during take-off. It must be added that this same force would therefore be helping the winding motor slightly during compression.

It is essential for flying squirrels to be able to swiftly change between several transport modes, so that they can quickly cover a sufficient distance in order to escape a predatory attack. A jumping robot is not necessarily faced with exactly the same time pressure, and hence trying to imitate the patagia may not be the optimum solution. The elastic element to the membranes proposed in the previous paragraph could be replaced instead with an additional mechanism to deliberately fold the gliding membranes away after a jump, and release them again immediately prior to the succeeding one. For example, a small motor could be used to draw fitted cords through each of the wing panels to bunch them together. It would be worthwhile for future research to include experimenting with such a design, which should facilitate the integration of other useful locomotion systems into the jumping and gliding robot presented in this thesis.

6.3 Design issues

In this section, the design issues that became apparent during the performance testing of Glumper will be highlighted, together with suggested improvements which could be implemented in the future. One obvious outstanding design issue is that Glumper lacks an orientation mechanism, although it is not thought that this would pose a significant design problem.

While testing the final version of Glumper, it also became clear that the toothed belt and winding cord should be arranged differently to improve the balance of the suspended control box. Specifically, the toothed belt should be clamped directly in the centre of both the head and the foot, while the fixed pulley (that the cord follows through the mating pieces to the head and foot) should be repositioned such that the free ends of the cord are symmetrically located either side of this belt. Improved balance should have the additional advantage of reducing the friction on the cord during winding, meaning that it might be possible to use a smaller, faster motor for the pitch-up/attachment mechanism.

(a)   (b)
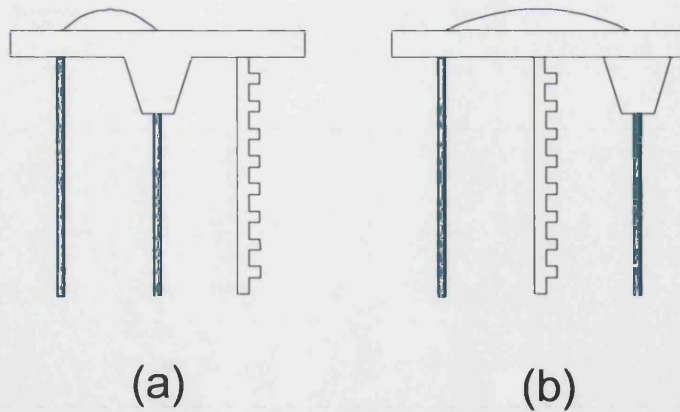
Fig. 86 A – Sketch of an end connecting piece showing how the force acting on it by pulling on the loop of cord, (coloured green here), is not currently acting through its centre. B – Proposed resolution, with the toothed belt mounted down the centre-line of the robot instead, and the cord passes either side of this so that the force caused by winding this cord around a capstan acts down the centre line of the robot.

The following weaknesses are more critical, because they were all responsible for catastrophic failures of the robot at some point during testing:

Glue joint between leg and spring holding steel reinforcement ring

<u>Reason:</u> Araldite breaks away from both surfaces due to shear forces.

<u>Solution:</u> Use better adhesive and tighter fit. Rough up the edge of the carbon-fibre before applying glue.
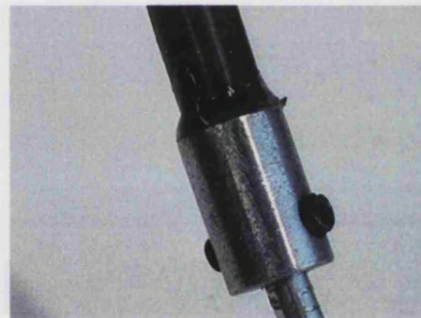
Worm gear with square-section tube insert

<u>Reason:</u> Forces are too high for this low-spec plastic.

<u>Solution:</u> Use more suitable material such as aluminium and machine in one piece.

Toothed belt.

Reason: Prone to snapping due to the sudden high tensile forces.

Solution: leave some slack in the system during assembly.

End pieces

Reason: These components are made as small as possible (to minimise mass) from the low quality ABS that the Rapid prototyping machine uses, but then subjected to repeated high impact loading.

Solution: Make a mould (using vacuum moulding for example) so that this component can be made from a stronger plastic such as reinforced epoxy.
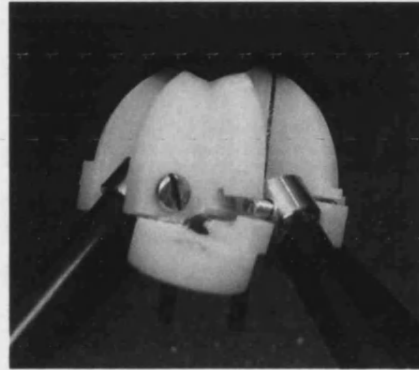
6.4 Potential for weight reduction

It is clear from Fig. 85 that mass reduction will have an immediate positive impact on the peak height reached by Glumper when it jumps. It was also discussed in the literature review that heavier gliders must glide faster in order to achieve a given glide angle, so mass reduction is doubly advantageous towards an improvement in robot performance (Section 2.2.1, page 43). Table 6 below shows a complete list of Glumper's components together with a photograph for each, their role in the structure or mechanism, and corresponding masses. This information was collated in order to highlight where these important weight savings could be made. Suggestions for how weight could be reduced are given in the right hand column.

Robot frame structure:

Description	Photo	Total mass (g)	Ideas for weight reduction
Torsion springs QTY – 4		118.2	Difficult. Requires springs with a higher energy density.
Carbon fibre tubes used for the legs QTY – 8		128	
Large steel reinforcement rings to hold springs QTY – 8		56	
Small steel reinforcement rings QTY - 8		21	
Head and foot (identical design) QTY - 2		37.1	A reduction in size, and hence weight, is feasible if using a material with superior mechanical properties to the ABS from the RP machine.
Head and foot mating pieces QTY - 2		9.6	
Nuts and bolts for head and foot assemblies.		12.9	Use nylon rather than steel if sufficient.
Screws to locate the legs in the head and foot pieces. QTY - 8		9.4	Use nylon rather than steel if sufficient.
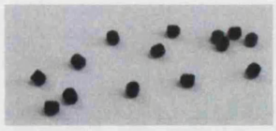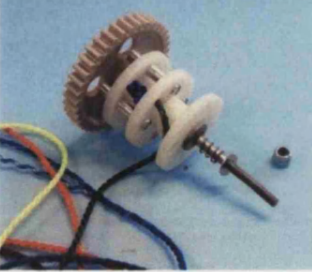
Grub screws to fix torsion springs into the robot legs QTY - 16		2.8	
Wings		19.0	

Table 6A – Breakdown of all the components comprising Glumper's frame structure including its wings. The total mass of all these parts is 414 g.

Compression mechanism:

Description	Photo	Total mass (g)	Ideas for weight reduction
Small box for compression mechanism including sprung retaining clip QTY - 1		47.3	This component is quite large in order to get the required structural rigidity from low quality ABS.
Small motor complete with internal gearbox, switch and associated wires QTY - 2		81.8	It might be possible to reduce the number of motors to one, by using ratchet gearing.
Two rechargeable lithium cells connected in series with mounting piece and associated bolts.		109	Replace with as few flexible solar panels as necessary for the robot to jump.
Drive gear QTY - 1		3.8	
Shaft, circlip and capstan assembly		12.4	
Compression spring, washer and lock nut		1.8	
Cord QTY - 1		1.2	
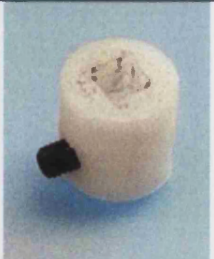
Bi-stable spring assembly		4.2	
Hinge lever QTY – 1		6.5	
Hinge lever bolt QTY – 1		2.1	
Toothed belt QTY - 1		4.1	
Drive pulley with insert for motor mounting QTY - 1		5.0	
Pulley locating bolt		0.9	
Follower to reset hinge lever		1.4	
Worm gear		2.1	
Square section drive shaft		2.0	
Motor coupling and grub screw		0.7	

Table 6B – A breakdown of how much all the individual components parts of Glumper's compression mechanism weigh. The total mass of compression mechanism = 286.3 g.

The largest mass contributor to this prototype jumping robot, Glumper, were its 8 steel reinforced CFRP leg pieces, which make up 29.3% of its total mass. Next are the four heavy duty torsion springs, which comprise a further 16.9% of the total mass. These springs are able to store a large amount of energy by bending them a short distance, and so consequently they must be subjected to large forces. It is for this reason that the leg pieces needed to be so strong and stiff in order to compress them sufficiently, driving their weight up in the process. Thus future optimisation should enable the compromise to be addressed, between reducing the size and weight of these related components, while still maximising the amount of energy storage capacity of the robot.

The next heaviest components of the robot were its rechargeable lithium cells, which made up 15.6% of the total mass. However, it has been shown that it might be possible to power Glumper from some lightweight flexible solar cells attached to its gliding membranes. These weigh 0.76 g each, so the maximum number of panels that could feasibly be added, 180 (which does not take into account the area lost due to the shape of the cells not fitting the geometry of the wings) would weigh 136.8 g, one third more than the weight of the lithium cells. It may be better not to attach the maximum number of cells possible, but rather to adjust the gear ratio of the compression motor sufficiently so that fewer cells are necessary, and thus the robot would have the potential to jump higher and further when ready, albeit less frequently.

Finally, it was suggested throughout the table that further weight reductions should be possible by using materials with superior specific mechanical properties, allowing size reduction. This would begin a domino effect, enabling the size of the numerous connecting nuts and bolts to be reduced also.

In summary, significant size reduction of Glumper's control box could be made by selecting materials with higher specific strength and stiffness. This has the two-fold advantage of weight reduction, and allows additional compression of the robot body so that more energy is stored before release. Clearance height could also potentially be improved by adjusting the attitude of the robot during flight, in much the same way as a human high-jumper chooses to pass the bar horizontally.

6.5 Materials selection for space design

The majority of Glumper's components were made from ABS using a Stratasys rapid prototyping machine. The poor mechanical properties of the ABS used determined the sizes and shapes used in many of the structural components but ultimately, however, these could be redesigned for manufacture from higher performance materials chosen depending on final application. Space applications in particular have demanding materials requirements, which will be highlighted below. Using materials with superior specific properties will allow weight reduction to be achieved, the importance of which will be discussed in the following chapter about Glumper's performance and suggestions for future work.

Spacecraft materials are typically subjected to large temperature variations. Satellites, for example, go into and out the earth shadow region as they orbit, leading to a change in their surface temperature in the range of −160 to 180 °C (Dunn 1997). To some extent, however, an exploratory robot could be protected slightly from such extremes during transit if stored carefully well within the craft, perhaps close to on-board electronics which are particularly sensitive to temperature changes. On arrival, the robot would only be subjected to the relatively milder range of surface temperatures on the planet or moon being explored. These temperatures will still be extreme relative to earth, causing the materials to become more brittle, so these would need to be specified so that fracture toughness would be acceptable for both the destination and transport conditions.

Extremes of temperature are not the only difficulty facing spacecraft designers. The materials also need to be able to perform under vacuum conditions, and could be subjected to an atmosphere quite different to that of Earth. Vacuum conditions reduce the likelihood of corrosion, which normally requires oxygen to be in the atmosphere, but materials with low out-gassing properties would be essential because some polymers and metals would decompose or sublimate respectively. The rate at which atoms and molecules leave the surface of a material in a vacuum increases with temperature. Radiation does not affect metallic materials considerably, but organic materials can be damaged by ionisation as a result of the various protons and electrons

freely travelling through space from cosmic rays, solar emissions and radiation belts (Dunn 1997). An additional general point of note for the designer is that it must be possible to pack the robot very carefully for transit to its final destination in order to prevent fatigue damage caused by excessive vibration during launch. The launch craft must also be able to discharge any electrical potential built up on its journey, (which can reach tens of thousands of volts), so that any sensitive electronics in the robot are never subjected such large potential differences.

Focussing specifically on Glumper's design, its moving parts such as the long legs, and the hinged-lever, capstan and stepped shaft in the control box would be subject to the additional problems resulting from friction and wear. On earth, binding between moving surfaces is prevented by an oxide layer, and friction can be reduced by using a lubricant. In a vacuum, however, this layer can be disrupted by outgassing unless special lubricants are used such as molybdenum disulphide (Dunn 1997). All Glumper's moving components contain interfaces between different types of material, so testing would be required to ensure that those selected finally do not encounter problems due to their different coefficients of expansion. This problem is also particularly relevant to the choice of composite material for Glumper's long jumping legs.

Reinforced epoxy based composites, such as the GFRP and CFRP have been proposed for use in Glumper's legs due to their high specific strength and stiffness properties. Some composites of carbon fibres and epoxy resin are already used on structural components such as antennas, solar cell panels and truss structure in spacecraft (Gao, He *et al.* 2005). However, the thermal expansion coefficient of carbon fibres can be an order of magnitude lower than that of the epoxy matrix causing thermal stresses. Consequently, much vacuum thermo-cyclic testing work is being carried out to develop improved structural composite materials for use in spacecraft (Gao, He *et al.* 2005).

6.6 Control System

Glumper has been carefully designed in order to try and minimise the quantity of actuators and sensors required, without increasing complexity. Although it was not possible to develop a fully functioning autonomous control system with the time and

resource available, the requirements are shown in a function block diagram, Fig. 87. This would control Glumper's two lightweight, low power DC motors using four sensory inputs, as described below.

Firstly, a mechanical push sensor is required to detect whether or not the hinged-lever is in the closed position prior to compression taking place. If not, the capstan would not be located in the drive gear, so rotating the motor would not compress the robot. The design of Glumper is such that the motor driving this capstan, (Motor 1 in Fig. 87), need never be switched off, running whenever it has power available with the direction determined by the output of this mechanical push sensor. A simple contact sensor would be sufficient, with one part mounted on the hinged-lever, and the other mounted on the wall of the control box which it rests against while in the closed position.

A gravity sensing switch is also required to determine which way up Glumper is, such that Glumper's second motor (Motor 2 in Fig. 87) can be driven to whichever is uppermost prior to take-off. A suitable example for this task would be a mercury gravity switch, which generally consist of liquid mercury in a sealed tube with electrical contacts at one end. When the one end is higher than the other, gravity will pull the mercury down to complete the electrical circuit through these contacts. Otherwise, (when the robot is upside down), the mercury will move away from the contacts, breaking that circuit. Such a solution would be adequate on Earth, but not if the robot was being intended for space applications, because mercury freezes at -38.83°C. However, a mechanical switch could be created to work in exactly the same way, only using a solid conducting cylinder instead of the mercury. The exact size and materials would need to be chosen carefully such that the conductor would slide easily to and from the contact depending on robot orientation.
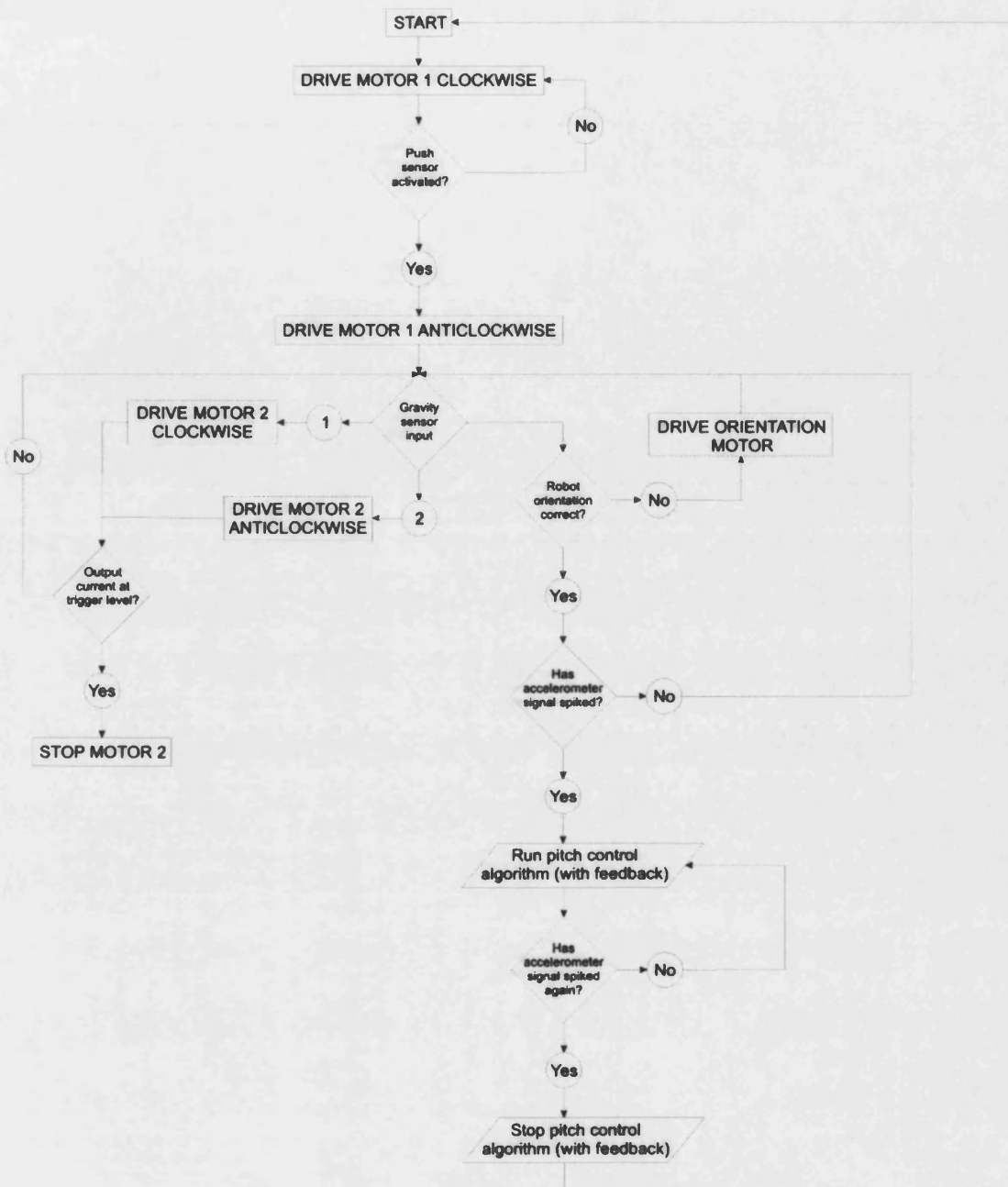
Fig. 87 – Control Diagram illustrating the simple control system required for a fully autonomous version of Glumper to operate successfully. I take it all the boxes are legible when printed.

An accelerometer could also be used to detect which way up the robot is, in place of such a gravity switch. This could also detect the sudden acceleration that would occur during take-off, and a second spike in the accelerometer signal would be detected soon afterwards during landing. Fig. 87 shows how the control system is designed such that Glumper continues to monitor its vertical and horizontal orientation until it receives a positive input from the accelerometer to indicate that it is airborne. At this point the diagram includes reference to a pitch control algorithm that has not been explored in

great detail. This would need to determine the angle of attack of the airborne Glumper, (perhaps through sensors mounted on its extremities), and adjust it accordingly by moving the control box rapidly between the head and the foot to shift the centre of mass. This can be achieved by driving Motor 2, which drives a pulley along a toothed belt that spans between the two ends of the robot, dragging the control box along it in the process.

It is beyond the scope of this thesis to decide how this exploratory robot would determine for itself where to go, but clearly it would need the ability to re-orientate in between leaps. A simple solution would involve the mounting of an additional motor on the control box to rotate this eccentric mass on its axis and thus cause the robot to lean accordingly. Fig. 87 shows when the control system would have to choose whether the orientation was correct, and if not, drive this orientation motor in response. Future development work should attempt to implement this control system, and experiments should be set up to observe how Glumper copes in different environments with various obstacles.

6.7 References – Chapter 6

DUNN, B. D. (1997). Metallurgical assessment of spacecraft parts, materials and processes Chichester, Wiley.

GAO, Y., HE, S., et al. (2005). "Effect of vacuum thermo-cycling on physical properties of unidirectional M40J/AG-80 composites." Composites Part B: Engineering 36(4): 351-358.

Chapter 7

Conclusions

The primary aim of this Ph.D research was to design a small, autonomous and inexpensive jumping robot for traversing irregular terrain using a locally-available energy source. Such terrain poses problems for traditional wheeled, tracked and legged designs and the incorporation of jumping was deemed a useful addition to the repertoire of existing locomotion systems available to robots owing to the diversity of jumping mechanisms found in nature. Suitable example organisms were sought and investigated throughout the biomimetic design process, inspiring the prototype solution, Glumper, which was presented in this thesis.

Two distinct patterns of jumping were observed in natural systems, 'pause and leap' which refers to single jumps followed by a rest period to recharge and re-orientate, and 'continuous hopping' where energy is recovered during landing and used in the following jump. The 'pause and leap' strategy, prevalent in insects and small animals such as frogs, was selected for the development of this biomimetic jumping robot because 'continuous hopping', although efficient, is more energy intensive and relies on sophisticated control and a continuous, reliable power source.

7.1 Conclusions on experimental methods

In the flying squirrel study the use of compliant poles in the determination of take-off and landing force measurements facilitates the simulation of real life test environments, which is important in comparative biology, but it is essential that the variation in compliance along the length of such poles be taken into consideration. In the case of the cantilever beam discussed in Chapter 3, this begins to behave more like a rigid instrument towards its fixed end. Valuable comparisons should only really be made between forces measured at known points of equal compliance. Given that this will not

always be possible, then sample sizes should be chosen to ensure a random scattering of landing positions.

While experimenting with procedure for performing tensile testing experiments on soft biological tissues in Chapter 4, a novel and inexpensive means of cutting dog-bone shapes from such material was successfully demonstrated.

7.2 Conclusions on the robot

Choosing the appropriate robot size was also an important decision with regard to Glumper's potential for use in space exploration. The "Size-Grain Hypothesis" was introduced which points out that with decreasing body size, a moving object becomes more likely to meet an obstacle of similar or larger size to itself which it must negotiate in order to continue in that direction. However, the economic cost of transport is a significant factor in space missions, so ideally any exploratory robot would be of minimum volume and mass. It was demonstrated from first principles in Chapter 2 of this thesis that with decreasing body size, power amplification becomes essential in enabling the smallest animals to jump well due to the limits imposed by the operating speed of the actuator, which is muscle. This can be observed in the variety and sophistication of the power amplification mechanisms found in insects. Examples of each were presented under three broadly defining categories of catapult mechanisms, bi-stable designs and flippers, although it was also shown that larger animals, which employ direct actuation of muscles in order to jump, are also able to amplify this power generated to improve their jumping. Therefore it became clear that a biomimetic jumping robot should be able to store energy somehow, and the principle of the catapult mechanisms seemed most suitable for the task. These are so called because energy is pre-loaded slowly into a quick release mechanism in much the same way as the catapult elastic is pulled back and then released, causing it to accelerate at a much higher speed than could be achieved by the arm that was operating it.

Glumper was developed with no one specific application intended, although the additional requirements associated with space exploration were deliberately considered owing to the obvious suitability for this task. This is reflected in the decision not to use

elastomers as an energy storage material, owing to their degradation in performance at extreme temperatures. Instead Glumper stores the majority of its jumping energy in four steel torsion springs and takes inspiration from the power amplification mechanisms found in insects. Springs are also better suited for this role than elastomers owing to the highly detrimental effect of stress relaxation, as demonstrated in the early prototype jumping robot, JHB (see Appendix 2, page 210). As in the catapult mechanisms described for locusts and fleas, a physical catch was incorporated into the design to hold the catapult mechanism ready for a jump without the need for additional power. This is necessary owing to the original requirement that the robot should be able to use a locally available energy source, which may therefore be intermittent in addition to having a low power output. Glumper's catapult release mechanism is slowly engaged by driving a capstan which winds in a cord causing the robot structure to compress and store energy in the springs. The capstan is driven by a worm gear, which both increases the torque provided by the motor, and acts as the catch to prevent the robot from releasing itself prematurely in the event of a loss of power (because the resulting force acts against the teeth of the worm gear rather than directly against the motor stall torque). Rapid release of the system relies on a dog clutch to quickly disengage the capstan from its drive gear, which was a process requiring more power than available from the small winding motor. Thus the increased torque available through this motor's gearing is utilised by designing Glumper to auto-release when fully compressed. Further inspiration was drawn from the insect jumpers when developing this release mechanism, which incorporates a bi-stable component to ensure that the dog clutch fully disengages and cannot reengage during take-off. It was also demonstrated from first principles in Chapter 2 that maximising leg length (relative to body size) also amplifies the power generated by the jumper. Glumper is of octahedral shape, with four legs that each comprise of two 0.5 m lengths of CFRP tube articulating around torsion spring "knees". The standing height of the robot is also about 0.5 m owing to the fact that it rests on two of these knees and the torsion spring forms a right angle when not compressed. With these sizes, Glumper's peak clearance height during approximately vertical jump tests averaged 1.17 m (n = 4, SD = 0.07 m). This means it can clear objects of more than twice its own height, which compares favourably with wheeled robots, which can generally only pass obstacles of up to half their wheel diameter.

Conclusions

Above a certain size, being able to safely land a jump becomes as important as the take-off. It was shown that a locust will land on its head with no obvious ill-effects, in contrast to cats, which are well known for their ability to try and re-orientate themselves and spread the impact force over their extended limbs and arched back. Part of the objective for this Ph.D research project was to investigate the biological approaches to jumping, including consideration of what strategies are adopted to maximise range and/or minimise damage. This naturally led to the consideration of gliding flight as a means to control the jumping robot while airborne. In the introduction to gliding in Chapter 2, it was shown that this can increase the range of a jump while also allowing for active selection of landing site.

In Chapter 3, a study was carried out on flying squirrels, selected as an ideal case-study animal to inspire this research owing to the fact that they regularly jump and glide through a difficult arboreal habitat. The study aimed to clarify why these animals developed their unique gliding ability, and diverged evolutionarily from normal squirrels, through the observation and measurement of take-off and landing forces. The results showed that take-off and landing forces generated by northern flying squirrels were both positively correlated with horizontal range, at least up to 2.5m. The maximum take-off force measured was 9.57 bodyweights, although the squirrels would occasionally produce close to this force when jumping only short distances, most likely a natural behavioural response to alarm. Take-off forces were not significantly different to the corresponding landing forces on these similarly compliant substrates. They were shown to be able gliders, abducting all limbs to create a wing-like surface which is held at a low angle of attack for maximum lift/drag ratio. Glide angle increased rapidly with horizontal range up to approximately 4 m, before progressively improving suggesting that gliding in northern flying squirrels is optimised for significantly longer ranges than were possible in this study.

This study could not reject the hypothesis that gliding evolved in flying squirrels to reduce their energetic cost of transport, even though they were observed to make deliberate aerial manoeuvres, which would increase the drop in altitude during the jump. The measured take-off angles provide evidence that the individuals in this study may well have been adopting optimum trajectories.

It seems less likely that gliding evolved primarily to improve the predatory escape response of flying squirrels, owing to the fact that they did not attempt to make either unplanned or deliberately unpredictable take-offs in this study.

It was concluded that gliding might have evolved to maximise the foraging area that could be reached in a given time. High glide speeds were measured and this velocity increases with range. However, the development of improved landing control becomes increasingly important with faster flight and evidence was provided that if northern flying squirrels could not slow themselves aerodynamically prior to landing, they would have to be able to sustain impact forces of more than 28 times their bodyweight.

Therefore, the major conclusion from Chapter 3 is that at divergence, small glide producing surfaces were developing in flying squirrels allowing mid-air adjustments in pitch and roll, and improving their resilience during high speed arboreal transport. Supporting evidence comes from the fact that these animals seem to innately adopt a gliding posture on take-off, even during leaps of less than a metre when it was shown that no vertical advantage was gained. However, this posture has the advantage of allowing them superior aerial control, and this was reflected in a consistent landing strategy over these distances. These northern flying squirrels were able to spread their landing impact force over all four limbs and their arched back, thanks to a dramatic pitch upwards immediately prior to contact with the pole. It was concluded that this rapid increase of their angle of attack immediately prior to landing is likely a behaviour evolved to enable rapid deceleration by stalling, something that would have had a greater effect at higher speeds.

Several features of the prototype jumping robot presented were inspired by flying squirrels as a consequence of the study. Most obviously, membranous wings were incorporated into the design to enable gliding, which always deploy automatically and fully during take-off. Attempting to deploy these once airborne would cause detrimental mid-air rotations and their actuation would have additional energetic cost, where as incorporation into the take-off utilises the already amplified power of the release mechanism. In order to reduce their landing forces, flying squirrels attempt to control their angle of attack such that their membranous wing is parallel to the landing surface. A mechanism to enable pitch control was thus incorporated into Glumper, which served

an additional purpose of enabling its compression mechanism to attach to either end of the robot. This means that whichever way round Glumper lands, it can ready itself for the next jump without having to turn over.

It was demonstrated in Chapter 5 that Glumper did not manage to benefit from the potential increase in range which it was hoped that the addition of gliding membranes would provide. The lift to drag ratio of the gliding robot would have been greater, and hence gliding performance improved, if the total mass of Glumper was less. Apart from weight reduction, a useful piece of future work would be to explore the effect of launching Glumper at various take-off angles, because there should be an optimum angle allowing sufficient height in the jump to be reached, while maximising forward velocity which has a direct influence on the glide ratio achieved.

Glumper's wings were made from rip-stop nylon, chosen because of its light weight and damage resistance. Further investigation into flying squirrels in Chapter 4 of this thesis suggested that their skin might be highly specialised to improve flight performance. It seems likely that the skin of southern flying squirrels is thinner than would be expected by scaling from other similar mammals, which would give an overall reduction in weight, and hence, improved gliding performance. It was suggested that elastin fibres could potentially play a crucial role in facilitating the stretching of the membrane when limbs are abducted and protracted for gliding flight, while causing it to fold away neatly again on landing. A structural model was proposed for flying squirrel skin which explained how it could be optimised for a range of transport modes including running, jumping, gliding and climbing, and able to quickly change from one to another. This supposes that patagial skin is a composite material comprising of two different types of fibre, arranged orthogonally to one another. The fibres running primarily along the length of the animal would have higher stiffness, enabling flying squirrels to precisely control the camber of their wings with small adjustments of their limbs. Unless its limbs were abducted in the gliding posture, much more elastic fibres oriented laterally would relax causing the stiff, longitudinal fibres to bunch together side-by-side and close to the body of the squirrel. Without such a specialisation, the additional skin required by flying squirrels for gliding would be a tripping hazard, and the presence of highly elastic fibres in the proposed skin structure improves its damage tolerance.

Glumper's wings naturally fold out to the side as its legs are compressed ready for jumping. They did not catch on anything or present a trip hazard to the robot during testing, but this prototype was only designed to jump and glide. It would be advantageous in future to integrate this technology with alternative transport modes such as walking or wheeled rolling, in which case it might be useful to incorporate an additional mechanism to keep the wings safely tucked away until required. However, this would present a compromise between facilitating the additional transport modes, and the maximum area of each membrane that would still be available for collecting solar energy when the robot was not gliding.

A critical requirement for the robot was that it should be able to carry sensitive electronic equipment without it sustaining any damage during the jumping and landing cycles. Glumper was designed so that its electronic components would all be housed centrally with its compression mechanism. This is connected to the external frame of the robot only by cord and a toothed belt, neither of which are held rigidly in tension during the landing impact, and so the impulse is reduced slightly. Although no particularly sensitive electronic components were ever used during testing, the fact that no motors, batteries, switches or connectors were damaged during the numerous impacts was a good sign. In contrast, damage was sustained by other structural components and the toothed belt during the same tests, owing to under specification of the materials for these parts. The presence of Glumper's gliding membranes was shown in Chapter 5 to cause a decrease rather than the expected increase in horizontal range, although they did reduce the resulting landing impact velocity, and hence force sustained by the robot. It would be useful to carry out optimisation experiments for these wings, which could potentially improve the resultant lift to drag ratio of the gliding robot. The wings also have an important secondary function, providing the necessary area for collecting solar energy (were this power resource to be adopted).

The requirement that this jumping robot should be constructed from materials that could be adapted for use in space applications was fulfilled. Although the actual materials used would not be suitable, (for example the many ABS components used to make the compression mechanism would be subject to outgassing under vacuum conditions), the avoidance of elastomers in the design means that high performance materials intended for use in space could be substituted easily.

Two rather self-explanatory requirements for the jumping robot were that it must be designed for manufacture, and that it should also be as simple and cheap as possible, to satisfy all the stated requirements. It was possible to put Glumper together on a relatively modest budget, within the bench fees awarded to this Ph.D project (approximately £750 was spent in total). Although many of the component parts were fabricated in a rapid prototyping machine, these were not generally highly complex, and so could also have been machined using more conventional cutting technology such as saws, mills and drills. A lathe was required to produce the stepped shaft and the worm gear, and a soldering iron to connect the motors and switches, but otherwise assembly was simple, requiring only the bolting together of components using a screwdriver, a spanner and an Allen key.

In vertical jump tests, the average change in Glumper's estimated centre of mass between the pre-launch state and the peak height was 1.6 m (n = 4, SD = 0.07 m). It was shown using an Instron compression testing machine that Glumper can store 21.5 joules of energy, meaning that its energy storage and release mechanism is 52% efficient.

The efficiency of the two lithium cells used to power Glumper during the performance tests was only 3.3%. It was also shown that it should be possible to make Glumper fully autonomous with respect to its power source, through experimentation with some commercially available flexible solar panels. This would however require a reduction in the gear ratio of the motor which currently drives Glumper's compression mechanism.

It was also demonstrated, based on the experimental data for launches at an angle of 63° to the vertical, that Glumper should be able to travel much larger distances each day than NASA's Martian exploratory rovers Spirit and Opportunity. It would be necessary to incorporate path planning algorithms into any such control system, to ensure that Glumper navigate around any obstacles that were too large, or could position itself such that it reaches other large obstacles when its peak clearance height is at a maximum.

Mass reduction was shown to be critical to both the jumping and gliding performance of Glumper. It was also shown that almost half of the total mass of the robot is shared between its legs and the torsion springs that they compress. Therefore, optimisation of

the compromise between maximising the amount of energy storage, while minimising the mass of these components should enable a large amount of weight reduction. Likewise, choosing superior materials would enable the various components of the compression mechanism to be reduced in size, having the twofold advantages of reducing the mass and increasing the distance through which the springs can be compressed.

Appendix 1 – High speed camera filming of jumping insects

In the early stages of this research, a *Redlake Images Motionscope* high-speed camera was used by the author to film two species of jumping insect: Desert locusts, *Schistocerca gregaria,* and leafhoppers, from the family Cicadellidae, the exact species of which used is unknown (there are over 20,000 species of leafhopper).

Locusts

Both adult locusts (which jump into flight) and their nymphs (which are wingless) were filmed and it was clear that both were able to generate the impressive jumping impulse as a result of the high velocity of their leg movement. Quantitative measurements have shown that the locust energy storage mechanism is very efficient, with approximately 80% of the stored energy converted into kinetic energy during the jump. The impulse lasts 25-30 ms and in this time, the locust can reach a take-off velocity of 3.2 ms^{-1} thanks to a peak acceleration of 180 ms^{-2}. This is equivalent to a peak power output of 0.75 W (Bennet-Clark 1975).
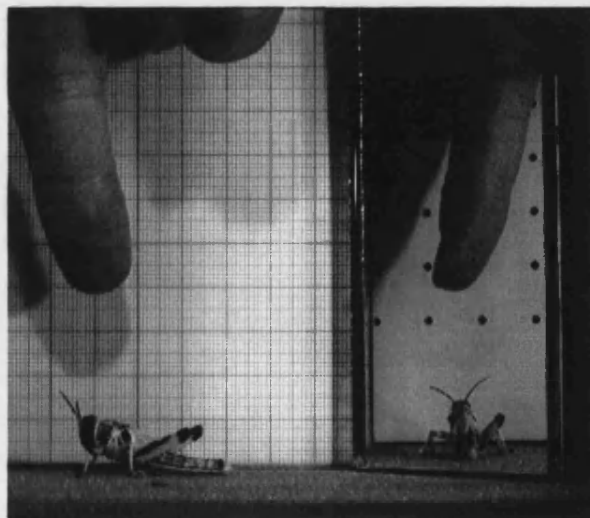
Fig. 88 – High-speed camera footage of a locust nymph being prompted to jump.

Another observation of the high-speed filming work was that the locusts did not attempt to control their landing and were even observed landing headfirst, before immediately righting themselves (Fig. 89). However, perhaps this is because they are sufficiently light that even landing at their terminal velocity would not be enough to damage their hardened cuticular exterior. Terminal velocity is the limiting velocity a free falling body can reach, when its drag force equals the gravitational force acing on it and this can be approximated using the following equation:

$$V_T = \frac{\sqrt{2mg}}{C_d \rho A}$$

C_d is the coefficient of drag, ρ is the density of air and A is the cross-sectional area; so by modelling the falling locust is a flat plate against the motion of the air, of $1cm^2$, and using the standard equation for kinetic energy (Equation 2, section 4.1), the locust has an absolute worst-case kinetic energy of 0.29 joules on impact.
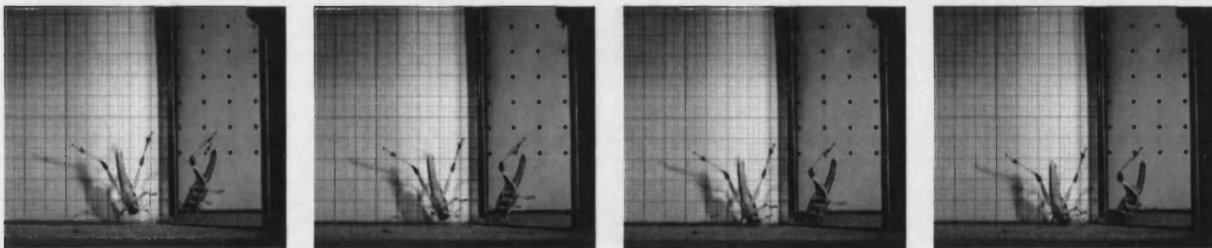
Fig. 89 – High-speed camera sequence of a locust nymph landing a small jump head first.

Leafhoppers

Burrows (2003) showed that froghoppers are out-jumping fleas relative to their body size. He reported accelerations of between 2800 and 4000 ms^{-2} on jumps captured with a high-speed camera at 2000 fps. These lead to an average take-off velocity of 2.8 ± 0.1 ms^{-1}: impressive considering the leg length is only approximately 3 mm. Leafhoppers are closely related to froghoppers, and have a similar ecology, so this work was

reproduced at the same maximum frame rate of 2000 fps for comparison. A sequence of images showing one such take-off is shown in Fig. 90.
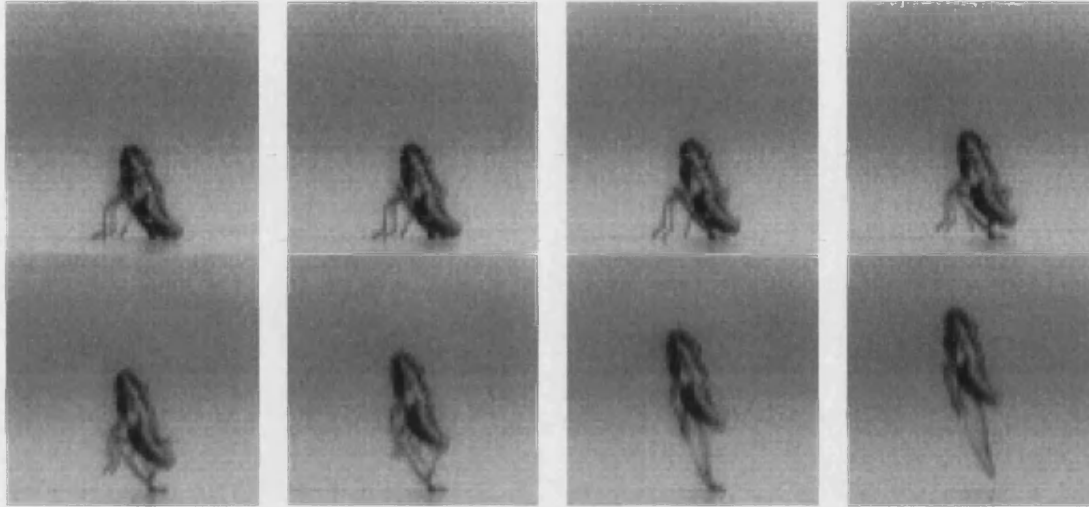
Fig. 90 – High-speed camera sequence of a leafhopper taking off (2000fps). The length of the hard cuticular body was measured as 6.1mm.

Digital Vernier callipers were used to measure the length of the leafhopper after the experiments. With this information, Scion Image (useful internet freeware that can handle sequences of images, and output the pixel co-ordinates of all the points clicked on by a user in order, www.scioncorp.com) was used to determine the total distance moved by the leafhopper between each frame. In order for this method to be valid, the leafhopper needs to be jumping in a direction parallel to the camera lens, which unfortunately reduces our sample size to just 2 usable jumps. It seems that although still impressive, leafhoppers do not jump quite so well as froghoppers. The take-off velocity measured from the clearest recording was 2.5 ms^{-1} (SD = 0.3ms^{-1}), achieved due to a peak acceleration of approximately 2200 ms^{-2} (SD = 190 ms^{-2}).

References – Appendix 1

BENNET-CLARK, H. C. (1975). "The energetics of the jump of the locust Schistocerca Gregaria." Journal of Experimental Biology **63**: 53-83.

Appendix 2 – Previous prototype jumping robots

In this Ph.D research, biomimetic principles were applied to develop an autonomous robot capable of jumping and gliding in order to traverse rough terrain. Only the final prototype design, Glumper, was described fully in the Thesis but this contains many design features that were tested and developed in earlier prototypes which will be introduced in this Appendix.

Jumping devices storing energy in elastomers

The underlying principle derived from successful insect jumpers was to use an elastic energy storage mechanism for power amplification. Fleas and leafhoppers store energy in resillin, an elastomer, in contrast to locusts which primarily store energy by bending hard cuticular elements. Owing to the high performance of both fleas and leafhoppers relative to their body length (reported in Section 2.1.3.1, page27), the first prototype employed an elastomer based energy storage mechanism. The basic concept was to accelerate a portion of its mass away from the ground as quickly as possible by instantaneously releasing energy stored in a normal elastic (rubber) band. It is only necessary for a portion of the total mass to be accelerated, so long as this is travelling fast enough for its momentum to carry the remainder of the mass with it.

A model was built from balsa wood and plasticine to prove the principle (Fig. 91). This prototype stands 150 mm tall, and was able to consistently make jumps of 1 m, approximately 7 times its own height using a mass ratio of 3:4 (frame:payload).

Fig. 91 – Simple balsa model to prove the catapult jumping design.
The model is 150mm tall, and was released from rest on the wooden table-top.

This first prototype had successfully demonstrated the jumping principle, and so the design was developed to improve its performance. This was achieved by simultaneously enhancing the energy storage capacity and reducing the weight. Stiff, lightweight materials were selected allowing multiple elastic bands to be extended over a greater distance before release. Fig. 92 is a photograph of the resulting device, which travels several metres when pulled back and released (manually). The body is a 5 mm diameter aluminium tube which has a shorter, heavier tube around it attached using elastic bands.

This can be pulled down to the ground, extending the elastic bands, and then released to launch.
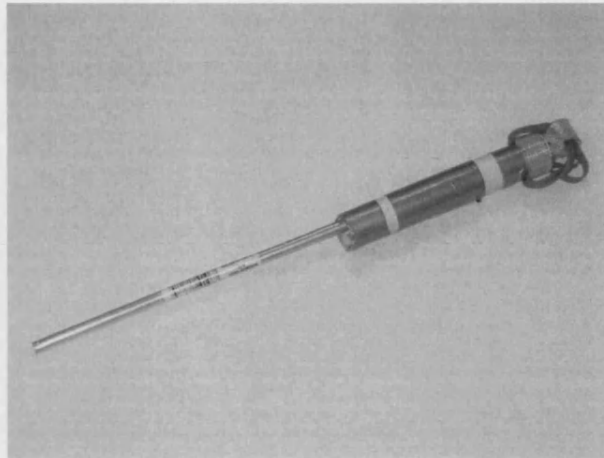
Fig. 92 – Photo of successful elastic jumping mechanism

Having engineered these two naturally inspired catapult jumping mechanisms, the next step was to try and develop something capable of carrying a payload and launching itself automatically. The resulting prototype was called JHB, which stands for jumping hanging basket, because an actual horticultural hanging basket was used for the hemispherical base.

JHB prototype

Fig. 93 shows a sketch of the JHB prototype, which like the previous devices is a monopod. Energy is primarily stored in the extension of silicon rubber tubes, although some additional energy is stored in stiff, vertical, bow-shaped spars. The idea for that aspect of the design comes from the false stick insect, described in the literature review (Section 2.1.3.1.1, page 28), which gains a further 7% recovery of elastic energy through flexion of its tibia. A launch mechanism would need to pull the mass into the foot of the robot, stretching the rubber and bending the spars back as shown. On release, the stored energy in the elastic and the spars launch the mass upwards, carrying the frame behind it.
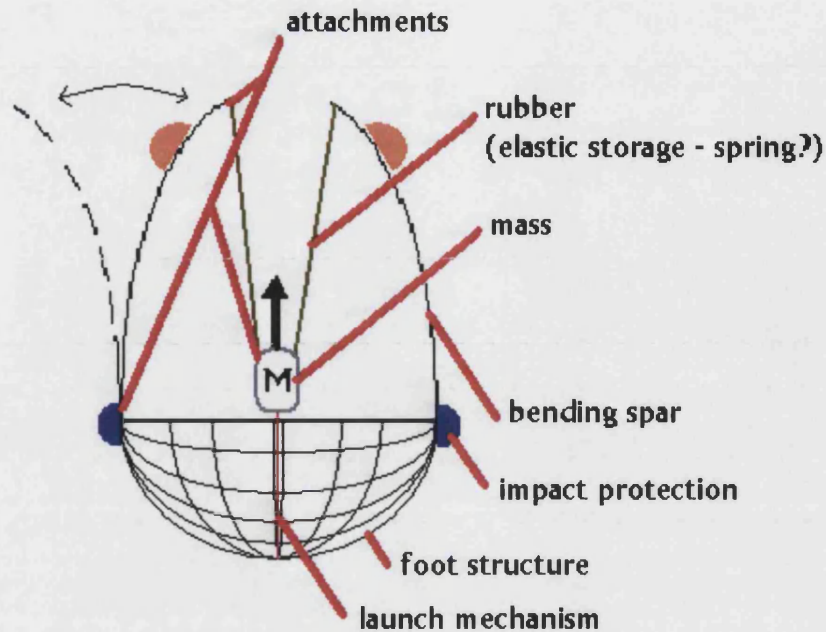
Fig. 93 – Labelled sketch of the JHB prototype

The launch mechanism winds in the mass into the foot of the robot, stretching the rubber and bending the spars back in the opposite direction of their natural bow shape (for extra stiffness). On release, the stored energy in the elastic and the spars launch the mass upwards, carrying the frame with it as it travels.

Construction detail

Composite materials were chosen for the stiff bow-shaped spars of the design, and the lay-up process of the GFRP required the pre-preparation of moulds in the required bow shape. These were prepared using 2mm thick sheet-steel, cut and shaped to the chosen curve using a roller-bender. It was then necessary to prepare the surface thoroughly, by smoothing the surface with beeswax to eliminate any potential surface roughness before lay-up could begin. After making the resin, layers of glass-fibre sheet were laid down, and more resin applied using a roller to force it into any spaces. Extra stiffness along the length of the bows was obtained by using bi-directional glass-fibre webbing for the external surfaces. It was also possible to make the bows progressively less stiff along the length, by interweaving gradually shorter lengths of the glass-fibre matt during the lay-up process. Not including the bi-directional external surfaces, six and nine pieces of multidirectional glass-fibre matt were laid up to make the bottom half of the spar thicker

than the top. The spars were arranged so that they would be bent in the *recurve direction,* meaning that more force would be required to pull them a given displacement, and hence more energy is stored in the process.

At the top of the GFRP spars, holes were drilled and long bolts put through, facing inwards, and fixed with soft washers and a nut. The protruding ends of these bolts were then covered with tight fitting plastic covers. The elastic part of the design, silicon rubber tubes were initially intended for use in a slingshot and hence likely to have favourable energy storage properties. These were ideal because two tubes came pre-connected via a leather thong, allowing for two of these thongs to be connected at right angles to the central mass leaving four free ends of elastic at 90° to each other as required. These tubes were easily forced over the protruding bolt ends at the top of each spar, but due to the effect of the high negative Poisson's ratio of rubber, pulling them off again under tension was not possible. (A negative Possion's ratio means that straining a material in the longitudinal direction causes a negative lateral strain so in this case the internal dimension of the tube is decreasing.) The spars were then mounted onto a hemispherical foot, and foam padding added all over the external surfaces of the structure to limit damage from the uncontrolled landings.

Jumping performance

Unfortunately, the GFRP bows constructed were found to be both too heavy, and yet still not stiff enough. Too much bending in the bows meant that the elastic was not being stretched as far as it usefully could be. It was considered that the specific stiffness of these spars could potentially be increased by laying up an I-section beam if this did not make the structure too vulnerable to buckling. Further improvements might have been made to the properties by laying up custom composites using high-quality fibres (such as Kevlar fibres for example) and resins. As a consequence of the high weight of JHB frame, another heavy mass was required in the middle to generate the launching momentum. The total mass of the prototype was 3.5 kg when a launch mass of 0.5 kg was used.
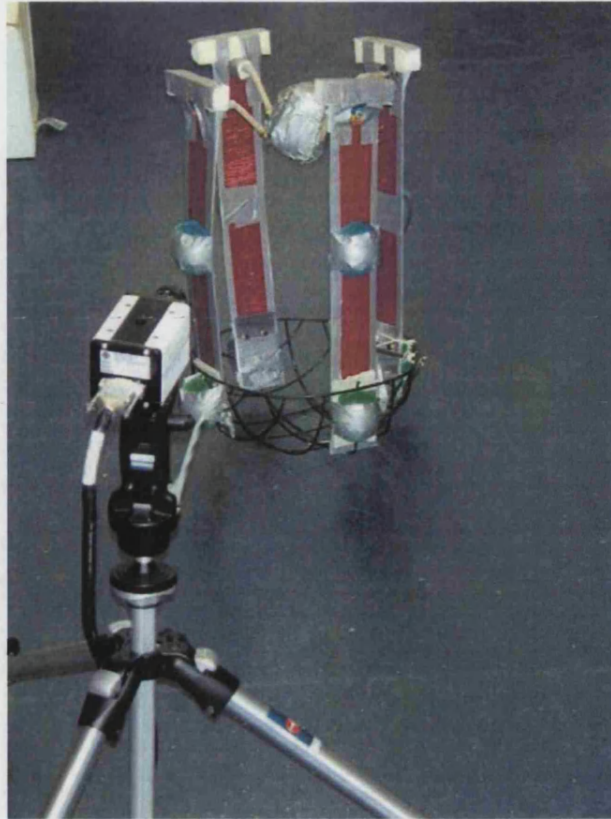
Fig. 94 – The high-speed camera was used to film the prototype jumping.

While designing a self-winding mechanism for autonomy, it was observed that unless the load and release of the elastic storage mechanism was immediate, the performance was considerably reduced. A Motionscope high-speed camera was used to record the prototype in action for direct comparison with various parameters of biological subjects and those of future prototypes. An interesting hovering effect was seen as the two masses sprung back and forth relative to each other, occasionally meaning that the initial height reached was not actually the peak height of the jump. Altering the stiffness of the spars, the elastic or the ratio of the masses would enable the tuning of this effect, which otherwise may reduce the maximum height achievable in the jump.

Fig. 95 shows both the first peak and maximum vertical clearance height of each jump of this prototype, when subjected to different conditions. These heights were measured by digitising the high-speed camera images using the method described in Section 5.3.1, (page 159), of this thesis. Calibration was achieved by measuring known lengths that were in a plane perpendicular to the camera. The accuracy of this method is limited because it doesn't account for any movement of the prototype in the dimension away

from or towards the camera, but this should be a negligible error since the jumps were approximately vertical. The different conditions applied to the prototype included varying the weight of the launch mass (the mass that is accelerated upwards to begin the jump) during manual launches, restricting circumferentially the amount of outward flexion possible by the spars and or coupling the mass to the frame rigidly such that take-off happens earlier. The potential advantage of this last idea is to avoid energy being absorbed by the elastic which would otherwise have to pull the rest of the frame with it at the moment of take-off.
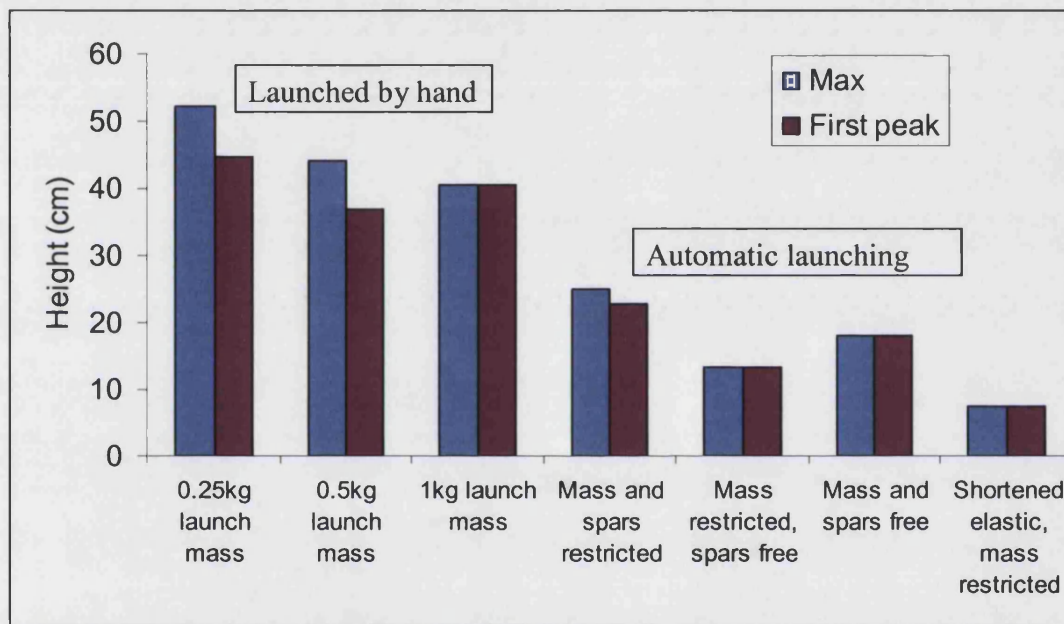
Fig. 95 – Initial and peak heights of Prototype 2 jumping under different conditions.

All the automatically launched jumps used a launch mass of 0.5 kg. In the hand-launched jumps, the mass and spars were free, so a direct comparison with the automatic launcher reveals as suspected, that energy is being lost with time spent in the loaded position. Within the hand-launched tests, it can be seen that the best result came from the lightest launch mass, peaking at just over 0.5 m. Further reduction may improve performance up to a critical point where the momentum will become insufficient. Comparison of the automatically triggered jumps shows that best results were achieved by restricting circumferentially the amount of outward flexion possible by the spars and simultaneously coupling the mass to the frame rigidly. Much more testing could have been carried out to converge on the optimum strategies for the jumping design presented in this section. However, it was felt that the deterioration of

properties with temperature and time (associated with elastic materials) would limit potential applications, such as planetary exploration, so this work was never undertaken.

Tri-legged torsion spring jumper

Experiments conducted with JHB demonstrated that elastic rubbers were not an appropriate energy storage mechanism and that weight reduction would be key to a successful jumping robot. Locusts store most of their energy in the bending of stiff, cuticular elements and so springs (which also store energy in bending) were the natural alternative. In a comparison of mechanical energy storage systems, a spring was shown to be more efficient in torsion than in compression (Alexander 1990). Therefore this prototype uses torsion springs as articulating knee joints between six 0.5 m long steel-reinforced carbon fibre rods. The robot stands at approximately 0.7 m tall before compression, which takes it down to less than 10 cm before release.
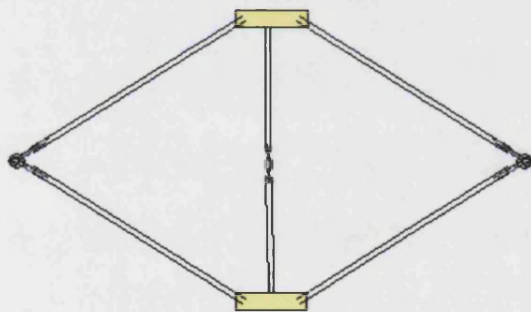
Fig. 96 – Crude sketch of the third prototype and a photograph of the reinforced carbon fibre-rods connected by a torsion spring

An automated winding mechanism was successfully added this time, although in order to keep the mass to a minimum a small, heavily geared motor was chosen increasing the time taken for compression. The design consisted of a cord fixed to the centre of the top-piece of the robot and fed through a loop in the centre of the foot. Winched in the cord on a motorised pulley mounted in the top-piece caused the robot's legs to bend, storing energy in the springs. Having the additional weight of the motor and associated components at the top of the robot is an advantage when considering the underlying conservation of momentum principle behind the design, but the cost is a reduction in

stability. Additionally, careful design of the foot would be required to enable the robot to right itself as the winching takes place.

Ideally, the contact time with the substrate should be maximised during the thrusting contact phase of the cycle. The longer impulse allows the force-time distribution curve to reduce architectural and material problems associated with peak forces for any given energy transfer. This would also reduce the likelihood of the point-of-contact slipping in non-vertical jumping.

Performance of torsion spring jumper Mk1

During the development of this robot it became apparent that four legs rather than three would facilitate the incorporation of gliding membranes into the design. Work begun on a four legged device before a release mechanism was ever successfully tested on the tri-legged design, and hence the only performance data available comes from manually launched jumps.

Fig. 97 – The third jumping prototype in action, taken with the high-speed camera. The base of the mechanism clears a height of approximately 1.5 m when manually released.

Fig. 98 shows the vertical displacements plotted against time for 3 consecutive jumps, released manually by pushing down and letting go. They were measured by digitising the images by hand, using the technique described previously in section 5.3.1 (page 159). Once again, calibration was achieved by measuring known lengths and the accuracy of this method is dependant on jumps not moving away from or towards the camera.
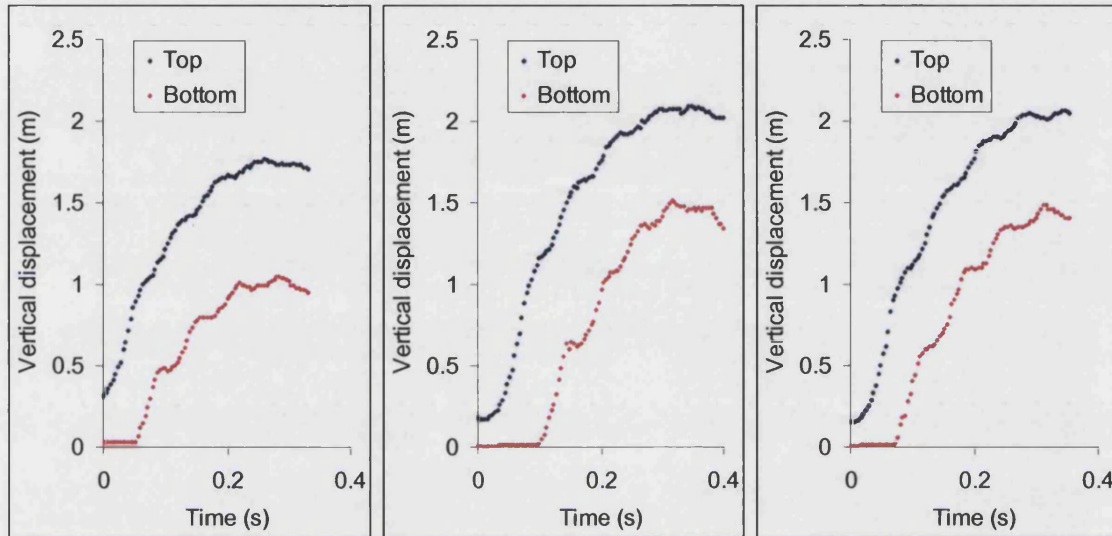
Fig. 98 – Vertical displacement against time for 3 consecutive, manually released jumps of Prototype 3.

There will be some losses associated with this launch method due to friction and the difficulty of removing hands quickly enough during the launch. However, in 2 of the 3 jumps analysed here, the base of the robot clears 1.5 m, with the top piece over 2 m from the ground for over a tenth of a second. This could be a useful height to reach were a camera to be mounted here.

In the key area of weight reduction, a significant improvement has been made from its predecessor. Each carbon fibre leg weighs 56.5 g and this figure includes the steel reinforcing connecting pieces mounted around each end. The mass of each spring is 29.5 g, and the total mass of this tri-legged jumper tested was 650 g including the motor and gears necessary for the winding mechanism. The potential energy of the system can be calculated for its maximum jumps using the standard equation (**Equation 18**), which is approximately 10 joules. A quick back-calculation shows us that this design would still able to make a vertical jump of 1 m with an additional payload of 325 g attached.

Glumper – Mk1

Glumper Mk1 is the predecessor to the robot discussed in this Thesis. It will be seen that Glumper Mk1 shares many of the same principles as the final Glumper design, and that many of the differences in construction between the two were changes that became necessary when upgrading to larger springs. The larger springs have much greater energy storage capacity, but require the application of higher force to load them. As a result, weak points in the design were continually discovered and improved, finally resulting in the reliable solution described in the thesis.

The design stores energy in four torsion springs that allow a maximum torque of approximately 1.8 Nm each. These are mounted in the hinge-joints of four legs, constrained symmetrically between a head and foot (actually identical). The legs are each made from two hinged carbon-fibre rods, 0.5 m long and 4 mm in diameter (see Fig. 100 below).

The control mechanism to compress and release the robot is housed in a small box made, like many of its components, in a rapid prototyping machine. A small 3 V motor with a gear ratio of 1:200 is used to drive a worm-gear, (thus slowing it by another 50:1). The driven gear has two M3 bolts protruding from it, which turn a capstan that is held against it on the same shaft by a compression spring. This spring is not acting directly against the capstan but against a circlip approximately 1 mm away. This means that the capstan is able to freewheel on the shaft (when not located on the bolts of the drive gear). The two ends of a length of high-strength nylon fibre cord are fixed to the capstan and looped around bars in both the head and foot, such that rotation causes these to be pulled together. This design is favourable because the control box is freely suspended within the central space surrounded by the robot's legs, meaning that landing impact forces are partially absorbed by the cord.

The drive shaft running through the capstan is stepped such that the capstan can be pulled away from its drive gear with a linear movement the shaft. The friction acting against this movement is very high when the robot is highly compressed, such that separate linear actuation would require high power. However, this design avoids the

need for any such device, by using a hinged lever to pull the shaft out when one end of the robot is pulled in against the control box. In order to make sure that the robot doesn't jump until fully compressed, this hinged lever is constrained by a latch, held closed by a small torsion spring, which is only released when the other end of the robot is pulled tight against the opposite side of the control box. At this moment, the capstan disengages from the drive gear, freewheeling as the cord unwinds rapidly and causing the robot to jump into the air.

Capstan located on drive gear by a spring

Forcing lever over-centre pulls capstan shaft away
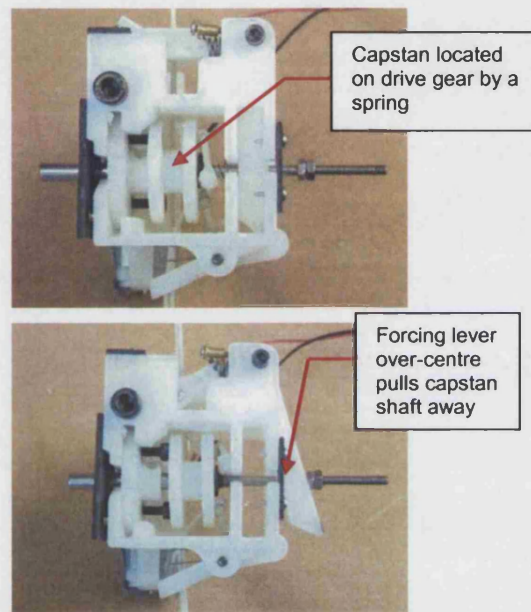
Fig. 99 – Side view of control box showing how the hinged lever pulls the capstan away from its drive gear.

An over-centre mechanism on the hinged lever prevents premature re-engaging, which would otherwise happen as soon as the robot left the ground (due to the compression spring on the capstan shaft). It is important that the compression spring used for the over-centre mechanism is stronger than the one being compressed on the shaft. Fig. 99 shows two side views of the control box, showing the hinge (with its over-centre spring) in each of the stable positions. After a jump, the hinged lever needs to be reset past the over-centre spring again in order for winding to begin again. This is achieved by reversing the direction of the motor as the worm gear is free to float along the square-section drive shaft that it is driven by. In this reverse direction, a conical shaped piece behind the worm is driven towards a guide on the hinged lever, flipping it back up past its spring ready for the next jump. This design requires high friction on the gear driven

by the worm, which is achieved by mounting it in a tight-fit against the side wall of the control box.
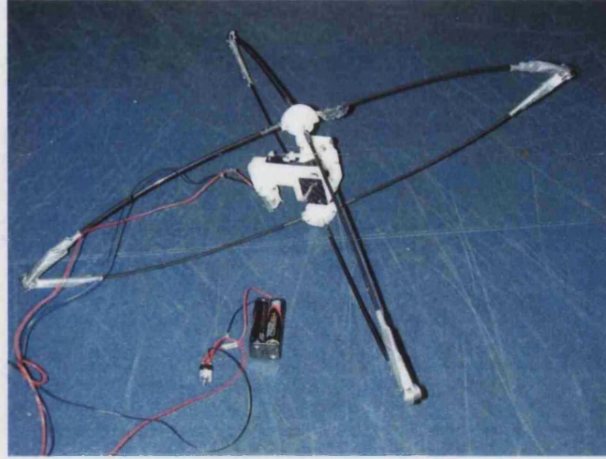
Fig. 100 – Photograph of the robot winding itself in shortly before jumping.

In order for the robot to jump upwards, a gravity hook was to be developed to ensure that, whichever way up the robot lands, the control box always attaches itself to the top side prior to take-off. However, the flying squirrel study demonstrated the advantage of pitch control during flight, which inspired the combined pitch control and attachment mechanism described for Glumper in this thesis (section 5.2.1, page 150). For the purposes of obtaining performance data for this prototype, the control box was simply tied to the top of the robot using cord.

Jumping performance

The parasitic mass of the robot, (the mass of the skeletal structure including the foot, legs and springs) is 0.169 kg at present. Experiments were performed to measure the peak height cleared by the robot with various weights added to its head before manually compressing it fully and launching it vertically. A high-speed camera was used to film the jumps, and it was expected that there would be an optimum weight for the eventual control box. (At very small masses, air resistance would reduce the peak height achieved). Scion Image was used to determine the maximum distance from the ground of the lowest extremity of the robot in each frame. The results are plotted in a graph

(Fig. 101) and it can be seen that the optimum total mass of the robot is less than the current frame weighs. Therefore, there is no momentum advantage gained by the additional mass of the control box accelerated away from the foot of the robot.
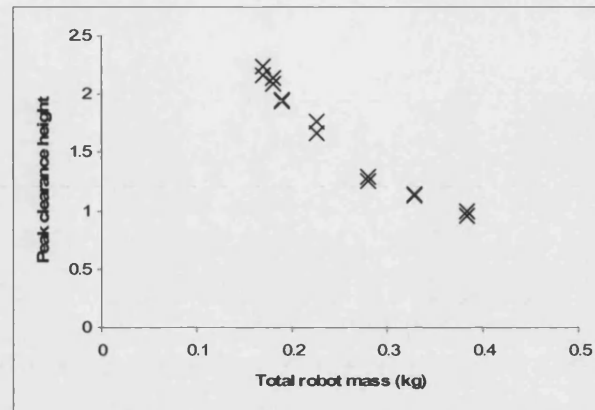
Fig. 101: Graph showing that adding mass to the basic frame of the robot reduces its peak clearance height. There must be an optimum value of weight to achieve maximum clearance, but this cannot be quantified because it occurs at a lower mass than the frame alone.

An Instron table-top machine was used to compress the robot body to investigate the energy storage potential of the current design. Fig. 102 shows the resulting force-displacement graph from compressing the robot by 350 mm. Around 400 mm displacement would have been possible, but this would not be an accurate reflection of the robot's capabilities because the position of the control box will prevent full compression.
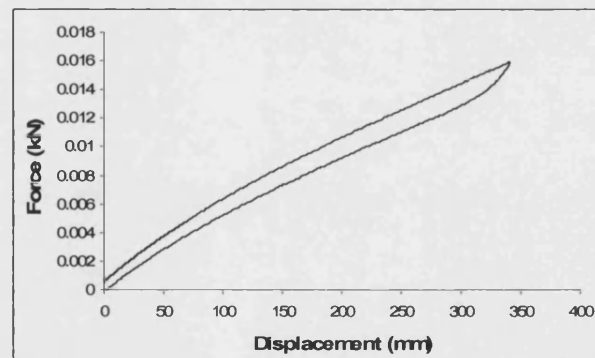
Fig. 102: Force – displacement graph for robot body under compression.

The energy stored in the robot's springs and body is equivalent to the area under this force-displacement curve, which is approximately 2.8 joules. Using the potential energy equation, P.E = mgh, and neglecting losses, a prediction can be made for the height that the centre-of-mass of our automated design described above ought to be able to reach.

Table 7 shows this prediction to be approximately 1 m. Visual inspection of repeated jumps against a vertical, extended tape-measure demonstrated that the approximate clearance height of the bottom of this robot was 0.6 m. The height reached by the centre-of-mass of the robot is actually much higher, approximately 0.9 m, because the control box (more than a third of the mass) was fixed to the top of the robot during these performance tests. This extra height could be useful if a camera was mounted on the control box, for example.

Total mass (kg)	Accelerated mass (kg)	Predicted height of C.of.G (m)	Approx height of C.of.G (m)	Approx clearance height (m)
0.284	0.115	1	0.9	0.6

Table 7: Performance data for prototype jumping robot

A more accurate method of measuring the jump height could not be used because this prototype winding mechanism was irreparably damaged during preliminary testing and this was never rebuilt.

References – Appendix 3

ALEXANDER, R. M. (1990). "3 Uses for Springs in Legged Locomotion." International Journal of Robotics Research 9(2): 53-61.

Appendix 3 – Additional performance data

This appendix contains some additional graphs relating to the performance of Glumper's gliding membranes during the jump tests launched at an angle of 63° to the horizontal, which were introduced in Section 5.3.4, page 165. Six jumps were recorded in total, three normal and three more after the removal of Glumper's nylon wings. The trajectories of the mid-point between the head and foot of the robot were determined by manually digitising a sequence of images recorded by a high-speed camera, and these are compared for all six jumps in Fig. 76 on page 167. Given that the recordings were captured at a known frame rate, it was possible to determine the velocity of this robot centre between neighbouring frames (Fig. 103). The noise is a consequence of human error during the manual digitisation of the image data, caused by low resolution. It can be seen in all cases that the robot accelerates quickly to around 6 ms^{-1} before slowing down as it reaches the peak of its jump (although it does not reach 0 ms^{-1} because it is still travelling forwards at this moment). Afterwards the robot accelerates again due to it dropping under gravity until it lands. The trendline function in Microsoft Excel was used to fit a best fit line to the section of each curve where Glumper is freely dropping under gravity, as highlighted in red in Fig. 103. This was carried out to try and establish whether or not the nylon wings were reducing the impact velocity under the given experimental conditions. The three graphs on the left hand side show that the winged Glumper tended to impact at just above 4 ms^{-1}, marginally slower than the wingless launches when impact velocities reached almost 6 ms^{-1}.
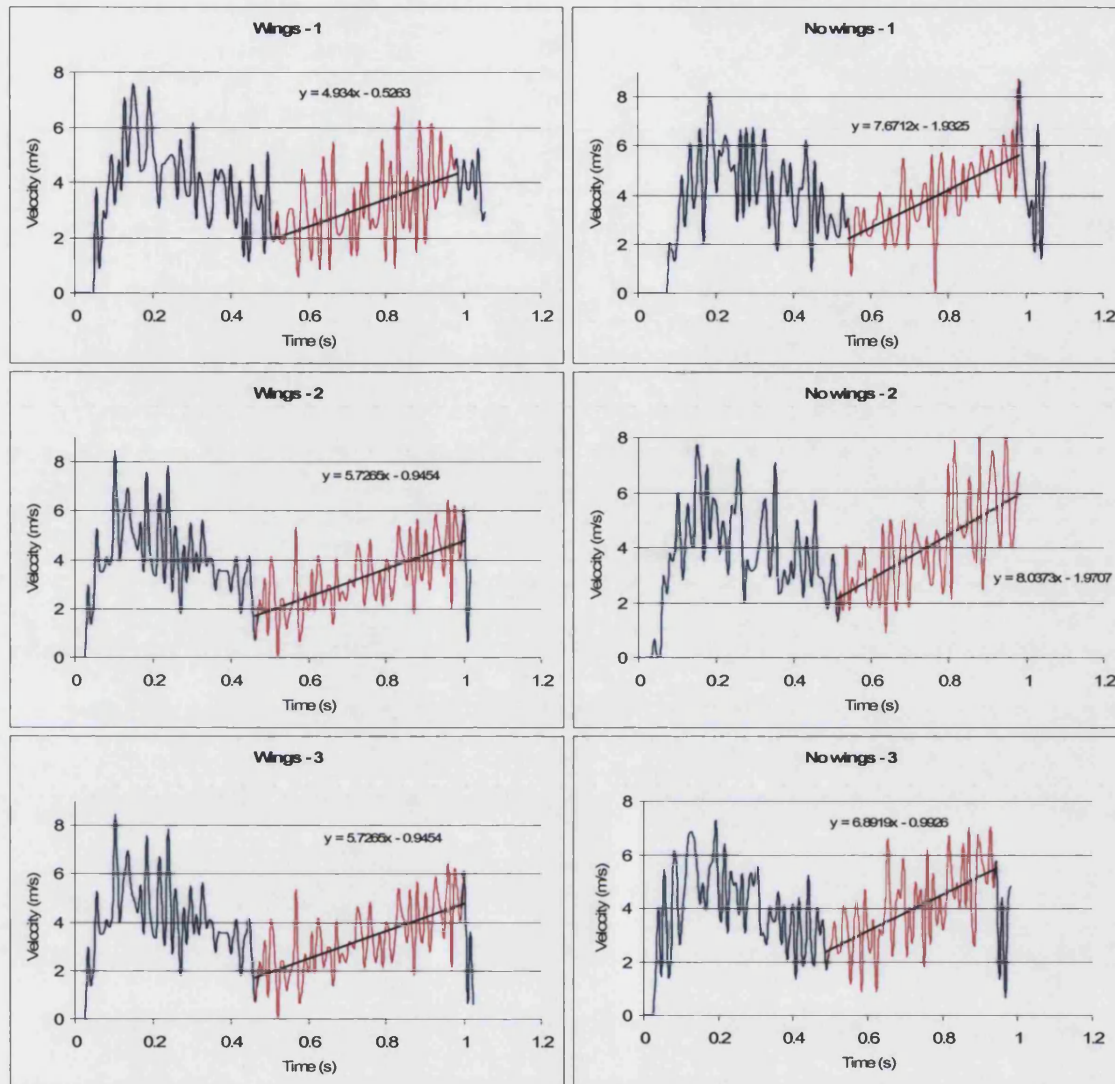
Fig. 103 – Graphs comparing the measured velocity against time for each of the six jumps of Glumper when launched at an angle of 63 degrees to the horizontal.

Although Fig. 103 would appear to suggest that Glumper's landing impact force is reduced by the presence of its wings, it does not take into account the fact that these increased its weight and restricted its movement slightly, resulting in a reduction in range. Therefore the apparent reduction in impact velocity may be due entirely to the fact that the initial horizontal velocity was smaller so Fig. 104 compares only the vertical drop velocity against time during landing for each of the six jumps. This would seem to be reasonable, because the central point of Glumper peaked at approximately the same height of 1.4 m in all but one of the tests. Once again the trendline function (Microsoft Excel) is used to help distinguish between the curves, this time using a polynomial equation. In spite of the noise, there does seem to be a clear levelling off of these curves for the winged Glumper, reaching a vertical impact velocity in all cases of

approximately 3.5 cms^{-1}. The non-winged equivalent curves are marginally steeper, all reaching vertical impact velocities of more than 4 cms^{-1}.
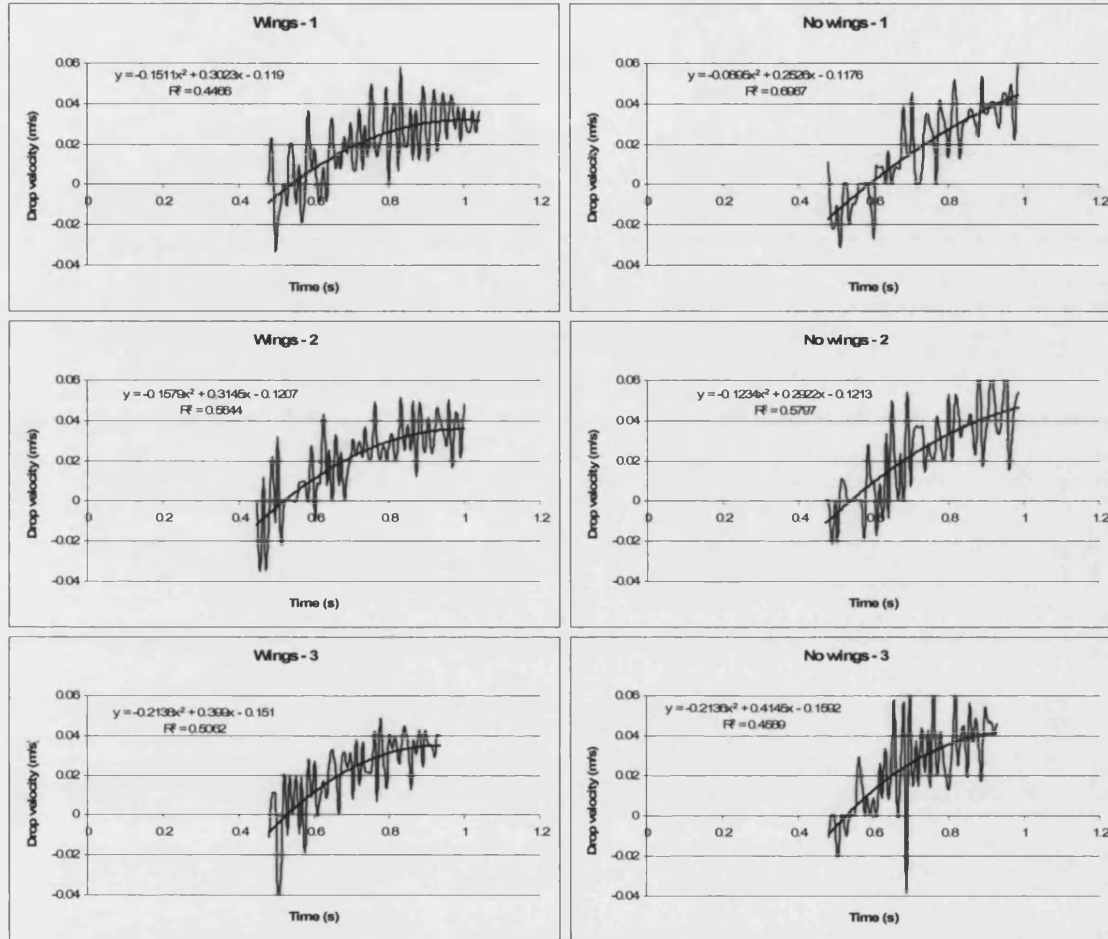
Fig. 104 - Graphs comparing only the vertical drop velocity against time for each of the six jumps of Glumper when launched at an angle of 63 degrees to the horizontal.

Appendix 4 – Published articles

Two articles were published during the course of this Ph.D project, which are included unaltered in this final Appendix. The first is titled "Take-off and landing forces and the evolution of controlled gliding in northern flying squirrels, *Glaucomys sabrinus*", and is published in the Journal of Experimental Biology. The latter is titled "Jumping robots: a biomimetic solution to locomotion across rough terrain", and is published in Bioinspiration and Biomimetics, a relatively recent journal from the Institute of Physics.

Take-off and landing forces and the evolution of controlled gliding in northern flying squirrels *Glaucomys sabrinus*

Keith E. Paskins[1,*], Adrian Bowyer[1], William M. Megill[1] and John S. Scheibe[2]

[1]*Centre for Biomimetic and Natural Technologies, Department of Mechanical Engineering, University of Bath, Bath, BA2 7AY, UK and* [2]*MS 6200, Department of Biology, Southeast Missouri State University, 1 University Plaza, Cape Girardeau, MO 63701, USA*

*Author for correspondence (e-mail: K.E.Paskins@bath.ac.uk)

Summary

Flying squirrels are well known for their ability to glide between trees at the top of a forest canopy. We present experimental performance and behavioural evidence that flight in flying squirrels may have evolved out of a need to control landing forces. Northern flying squirrels were filmed jumping from a horizontal branch to a much larger vertical pole. These were both slightly compliant (less than 1.9 mm N^{-1}), and instrumented using strain gauges so that forces could be measured. Take-off and landing forces were both positively correlated with horizontal range between 0.5 and 2.5 m ($r=0.355$ and $r=0.811$, respectively, $P<0.05$), but not significantly different to each other at each range tested. Take-off forces ranged from 1 to 10 bodyweights, and landing forces were between 3 and 10 bodyweights. Glide angles increased rapidly with horizontal range, approaching 45° at 3 m, above which they gradually decreased, suggesting that northern flying squirrels are optimised for long distance travel. We show that northern flying squirrels initiate full gliding posture at ranges of less than 1 m, without landing any higher than an equivalent ballistic projectile. However, this gliding posture enables them to pitch upwards, potentially stalling the wing, and spreads the landing reaction force over all four extended limbs. At steeper approach angles of close to 45°, flying squirrels were unable to pitch up sufficiently and landed forelimbs first, consequently sustaining higher impact forces. We investigate four hypotheses to explain the origin of flight in these animals and conclude that the need to reduce landing impact forces was most likely to have stimulated the development of aerial control in flying squirrels.

Key words: flying squirrels, *Glaucomys sabrinus*, jumping, gliding, kinetics, substrate reaction forces, biomechanics.

Introduction

There are three principal hypotheses to explain the divergence of flying squirrels from other types of squirrel. The first suggestion (Norberg, 1985) is that gliding may have evolved as a means of reducing the energetic cost of foraging. The squirrel can jump and glide from one tree to the next, enabling it to cover greater distances within the canopy more quickly than would be possible by climbing down and moving across the forest floor. An alternative suggestion was that, rather than reducing cost of transport, gliding may offer a means of foraging over a larger area in a certain time, making flying squirrels better able to exploit a patchy food resource than non-gliders of similar size (Scheibe et al., 2006). The third hypothesis is that gliding evolved primarily as an escape mechanism (Scheibe et al., 1990; Keith et al., 2000). Tree squirrels react to disturbances by moving to the opposite side of their tree, whereas flying squirrels climb upwards and then glide to another tree. However, this behaviour may increase susceptibility to attack from their most likely predator, owls

(Scheibe and Robins, 1998). We propose a fourth hypothesis: that the patagia, the flexible membranes that squirrels stretch by fully extending their forelimbs and hindlimbs, evolved to reduce or control landing forces. There is published evidence to support this (Caple et al., 1983), where it was calculated that increasing the amount of lift available to a body from 0 to 5% would not noticeably lengthen the jump nor allow much turning, but would give the animal significantly improved control around the pitch and roll axes. Of course, none of these four hypotheses are mutually exclusive.

This paper will investigate these hypotheses through experimental determination of the performance and behaviour of these animals. By measuring take-off and landing forces, we propose to quantify the advantage flying squirrels can achieve as a result of their unique morphology. The outcome of these measurements will be directly affected by substrate compliance. The majority of previous studies measuring ground reaction forces used rigid force measuring devices, while others investigated the effects of substrate compliance on

ground reaction forces (Demes et al., 1999; Bonser, 1999). Demes et al. found that take-off forces were higher than landing forces when testing seven primate species of varying body sizes using compliant apparatus, contradicting previous studies based on rigid platforms (Demes et al., 1999). Some of the take-off force is used in bending the compliant branch before toe-off, whereas the reaction force on landing is damped as the substrate yields in the direction of motion, allowing more time for deceleration. Likewise, Bonser showed that the magnitude of landing forces for starlings was lower than their take-off forces (Bonser, 1999). He proposed both that the birds used their wings to decelerate during landing, and that additional energy is dissipated in deflecting their compliant perch during take-off.

In arboreal locomotion, flying squirrels must generate higher take-off forces when jumping from narrow (and hence compliant) tree branches, and encounter their highest impact forces when landing on rigid tree trunks. Compliant substrates have been instrumented for this study, and so we expect take-off forces to exceed landing forces over short distances. At higher ranges, the squirrels will have accelerated due to gravity and their landing force will likely increase unless the squirrel can use its morphology to slow itself aerodynamically. Therefore our hypothesis that gliding in the squirrel evolved primarily to enable aerodynamic control of its landing speed can be rejected if measured landing forces continually rise at high ranges.

It is possible for animals to utilise stored elastic energy within a branch by timing their take-off with its motion. However, primates do not seem to take advantage of this (Demes et al., 1995), which supports the proposition (Alexander, 1991) that they would not intentionally recover this energy. Therefore, we do not expect flying squirrels to take advantage of the recoil of our instrumented branch either. However, they have been observed using a bounding gait before launching with both fore- and hind-feet together at the end of a platform just before take-off (Keith et al., 2000). It is probable that this bounding is used to maximise take-off velocity and hence increase range.

The northern flying squirrel *Glaucomys sabrinus* is the larger of two species of North American flying squirrel, although still much smaller than some species found in SE Asia (Ando and Shiraishi, 1993). Flight is made possible by the presence of patagia, a morphological feature which has evolved independently several times in vertebrates, the earliest known being from the Mesozoic era (Meng et al., 2006). By manipulating their limbs, flying squirrels are able to actively modify the shape of this lift-generating surface during flight. The body proportions of flying squirrels were compared with those of tree squirrels to determine what morphological changes might be attributed to gliding (Thorington and Heaney, 1981). Increased leg length allows more energy to be expended during take-off, offering superior horizontal range. In comparison with other similar-sized squirrels, the forelimbs of flying squirrels are significantly longer, a trait that has almost certainly evolved to improve aerodynamics during gliding

(Essner, 2002). This is further improved by the styliform cartilage, which is a flexible projection from the wrist held upward from the rest of the lift surface during gliding. This combines with the manus (or hand, which points ventrally towards the mid-line of the squirrel) to form a wing tip very similar to a NASA designed winglet (Thorington et al., 1998), who proposed that it reduces induced drag by diffusing and directing vortices away from the patagia. Smaller flying squirrels tend to have greater manoeuvrability and agility, whereas the larger species must glide faster to achieve the same glide ratio.

Materials and methods
Animals

Study animals came from a laboratory colony of northern flying squirrels *Glaucomys sabrinus* (Shaw 1801) housed in the Department of Biology at Southeast Missouri State University. Two young females and a young male were chosen because they had been consistent performers in previous kinematic work. All animals were born in the same week and approximately 27 months old. The mass, wing span and wing area of each animal is given in Table 1. Other members of the colony were required for other projects and were not available. The colony has been maintained for 5 years on a diet of pecans, walnuts, sunflower seeds, mushrooms and birdseed in a large, temperature-controlled room (20°C). The room is on a continuous 12 h:12 h light:dark cycle. There are various branches and sufficient space for jumping and gliding to take place. Initially, measurements were made in the squirrel lab, but longer glides were measured in a 7 m×14 m×7 m barn on the university farm.

Apparatus

As flying squirrels often land on tree trunks, allowing vertical variation in contact point, we used a vertical landing pole based on the design of Demes et al. (Demes et al., 1995; Demes et al., 1996; Demes et al., 1999). The squirrels were acclimated to it for several months prior to experimentation and used it regularly. It was constructed in two pieces: a 1.52 m long PVC tube (114 mm o.d.) covered in carpet and marked at 10 cm intervals (for calibration and image analysis), mounted 80 cm of the way up a 2.41 m long galvanised steel tube (23 mm o.d.). A concrete base secured this steel tube, which had four strain gauges (FLA-2-11-3L, TML, Tokyo, Japan) equally spaced around its circumference and aligned vertically (Fig. 1). A half-bridge circuit was used for each tension/compression pair so that force parallel and perpendicular to the squirrel's direction of motion could be determined. The compliance of the pole was measured to be 1.5 mm N^{-1} at the free end, gradually decreasing down the pole, reducing to 0.2 mm N^{-1} close to the fixed end and the resonant frequency was 2.2 Hz.

For the take-off branch, a horizontal cantilevered beam was designed to mimic a tree branch because northern flying squirrels predominantly launch from a crouched, horizontal

Table 1. *Summary table of all the measured forces generated by northern flying squirrels during leaping and landing*

Squirrel ID	Wing span (cm)	Wing area (cm²)	Leap distance (m)	Mass on day of testing (g)	Take-off force (bw)		Landing force (bw)	
					Count	Mean ± s.d.	Count	Mean ± s.d.
YF1	28.0	511	0.5	272	9	3.70±1.99	–	–
			1	274	6	4.64±1.17	6	3.47±0.37
			1.5	267	10	4.36±1.64	10	4.88±0.35
			2	256.5*	7	5.57±1.53	7	7.58±0.96
			2.5	256.5*	5	5.91±1.49	5	6.16±0.54
YF2	27.5	500	0.5	200	8	2.56±1.28	–	–
			1	201	10	5.21±2.47	10	3.56±0.30
			1.5	198	11	3.30±1.70	11	4.28±0.21
YM	25.9	554	0.5	259	9	3.38±0.96	–	–
			1	260	4	6.97±1.23	4	3.79±0.44

YF, young female; YM, young male; bw, body weight.

There are 79 take-offs but only 53 corresponding landings because no landing force data was obtained for the shortest range jumps of 0.5 m. Only one individual, YF1, performed in the barn but it would not land on the force pole at distances greater than 2.5 m. Unfortunately, for reasons beyond our control, YF2 only cooperated at 0.5, 1 and 1.5 m and YM at 0.5 and 1 m.

*Squirrels seemed to lose a considerable percentage of their weight before testing at this distance. The reason for this is unknown but it could have been caused by the change of environment as these tests were carried out in a barn, which was very hot and humid compared to the temperature-controlled lab.

position (Vernes, 2001). Four standard linear strain gauges (CEA-13-240UZ-120, Vishay, Basingstoke, UK) were mounted in two pairs, 50 mm from the fixed end of the 10 mm square aluminium bar (Fig. 1) and connected in a half-bridge circuit. Alignment was simplified because the chosen gauge width was almost as large as the 10 mm width of the aluminium bar, but not critical because any cross-talk was eliminated during calibration. The aluminium branch was covered by tightly wound rope to simulate the surface of a tree branch. The strain gauges were protected using polystyrene foam, which

was itself covered by plastic. A length of 4 cm×9 cm timber was fixed vertically to the wall, and drilled with mounting holes every 10 cm to allow height adjustment of the launch branch. The design of the branch was such that the compliance was similar to that of the landing pole, measured to be 1.9 mm N⁻¹ at the free end and decreasing as would be expected towards 0.0 mm N⁻¹ at the fixed end. The resonant frequency of the take-off branch was 17.3 Hz. The signal outputs from the strain gauges on both instruments were amplified using AD524 chips or equivalent and the sampling rate was 250 Hz. There was no need to acclimatise the squirrels to the take-off pole as, unlike the landing pole, they had no choice over whether or not to use it.

Experimental design

The take-off branch was raised as the experimental range increased such that the angle between the tip of the branch and the base of the landing pole remained consistent at approximately 55°. This configuration was chosen because it was not possible with our equipment, and in the locations available, to set up short jumps at high altitudes, and the
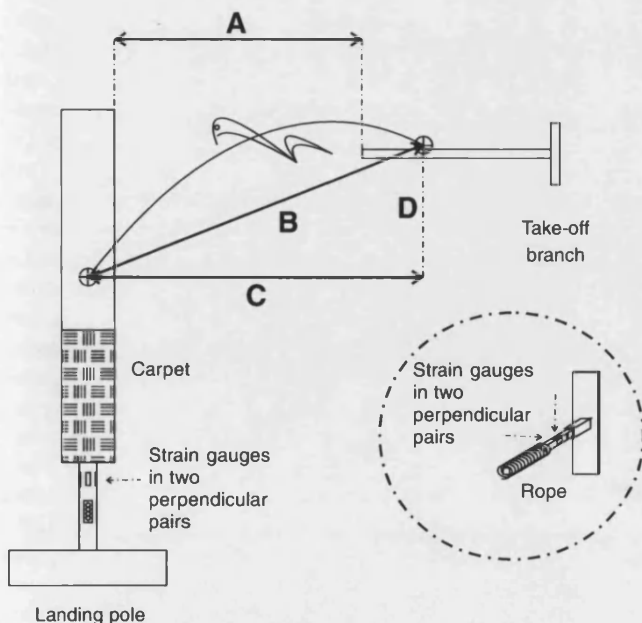
Fig. 1. A diagrammatic representation of the experimental set-up, showing the instrumentation used to measure take-off and landing forces including the carpet-covered landing pole, the rope-covered take-off branch and the location of the strain gauge pairs on each. Also shown are the measurements used to analyse the results, relative to an approximate squirrel trajectory. (A) The controlled horizontal distance between the end of the take-off branch and the vertical landing pole, (B) the total distance covered in the glide calculated from the exact horizontal distance (C) and the drop (D).

squirrels were unable to reach the landing pole unless given sufficient starting height. Animals were released individually on the instrumented branch and responded by running along the branch, usually pausing and then leaping to the instrumented landing pole. The horizontal range was increased progressively from a low distance of 0.5 m, to capture the leap-to-glide transition point, below which squirrels merely leap around, and above which the flying squirrels achieve aerodynamic advantage over other types of squirrel. Analysing this range of arboreal locomotion was considered to be more critical for investigating the initial divergence of flying squirrels.

Three digital video cameras (Canon GL2, Sony TRV 108, and Panasonic NV-DS55B) were used to film jumps. The first was positioned to capture take-off angle, the second to capture lateral landing angle and the third to capture a ventral view of landing. In the large squirrel barn it was not possible to mount a camera level horizontally with the take-off branch, so the resultant images represent frames perpendicular from the known camera angle. A minor trigonometric correction was therefore necessary to adjust all vertical distances measured from this take-off footage.

Calibration

With strain gauges, large changes in the external environment are potentially significant, so a record of temperature was kept using two I-buttons (Maxim Integrated Products, Sunnyvale, CA, USA), fixed to the top and bottom of the 4 cm×9 cm timber stud, respectively. These recorded temperature every hour. This daily verification of calibration was particularly important because testing was carried out in two contrasting environments; a temperature-controlled laboratory, and a hot and humid metal barn.

Only the landing forces were measured by converting the output from strain gauges into force, for which a static calibration was performed daily by applying forces to different points along the pole. Resultant steady signals were used to draw calibration graphs that established the force constant, k, where $F=kx$; F is force (N) and x is the measured strain signal (V). Forces equivalent to between 1 and 10 body weight units (bw) were applied, producing good linearity across the full range of marking points on the pole. (On average, the square of the Pearson product moment correlation coefficient $r^2=1.00$ in line and 0.99 transverse to the expected direction of motion.) Position of the animal along the instrumented poles was taken into account and a linear equation allowed the correct calibration to be used at any point. The cross-talk magnitudes were 13% and 17%, respectively, for parallel and transverse forces. Cross talk, in this context, is the unwanted output signal measured on one pair of strain gauges for a force applied perpendicularly. The frequency response of our equipment is sufficient to measure impulses generated by the squirrels. The effect of temperature on the calibration was found to be unimportant, as although it varied considerably between the two test areas, calibration graphs remained consistent throughout the study.

Results processing

Although both could measure force in two directions, neither the take-off branch nor the landing pole were capable of measuring forces along their long axes. To overcome this limitation, video footage from laterally positioned cameras was recorded to determine the angle of action of the force, which allowed the force vector to be resolved in 3D from the two measured force components. This was an acceptable procedure for the landing forces because the squirrels were arriving at angles perpendicular to the pole. For the median data point at medium range, 1.5 m, a trigonometric calculation showed that a 5° shift in measured landing angle would cause a 10% change in the resultant force. During take-off the squirrels were consistent in their behaviour, always choosing to move towards the free end of the branch and jump away in the same direction. However, the resulting shallow take-off angles mean that a 5° measurement error leads to an unacceptable 39% change to the median resultant force at 1.5 m. Hence, resultant take-off forces had to be calculated by integrating the output from the strain gauges with respect to time, so that measured take-off velocity could be used to determine the acceleration. This was multiplied by the known mass of each flying squirrel for all jumps to calculate the resultant force. The frame rate of the lateral take-off camera was 30 frames s^{-1} so an estimate of velocity between the first two consecutive frames after toe-off could be obtained by measuring the change in position of the centre of mass. The resultant force calculated by this method is the total force required to accelerate the squirrel to its actual take-off velocity based on its known acceleration profile. This method does not take into account losses caused by deforming the branch, but is completely independent of the accuracy in measurement of take-off angle.

The video records were digitised using edge-detection software, which tracked the outline of the squirrel in each frame of a sequence of images from the laterally positioned camera (LabView – National Instruments, Austin, TX, USA). The tail was deliberately excluded from this outline, because it constitutes only a small percentage of the total weight of the animal and was often dorsally flattened and moving at high velocity outside the plane of the images. The centre of the region enclosed by the lateral outline of the squirrel was used as an approximation for its centre of mass and could be tracked from frame to frame, enabling both the landing point on the pole, and the angle of impact to be determined. Hence the resultant reaction force for each landing squirrel could be calculated.

To measure the take-off angle of the squirrel, principal components analysis was applied in the LabView squirrel tracking program to find the best-fitting ellipse to the outline detected in each frame. The take-off angle was taken to be the angle between the major axis of this ellipse and the axis of the branch in the final frame before toe-off. This program was also used to estimate the change in pitch during the landing sequence shown in Fig. 2C. Another program was written in NI Labview to determine the wing span and wing area of each
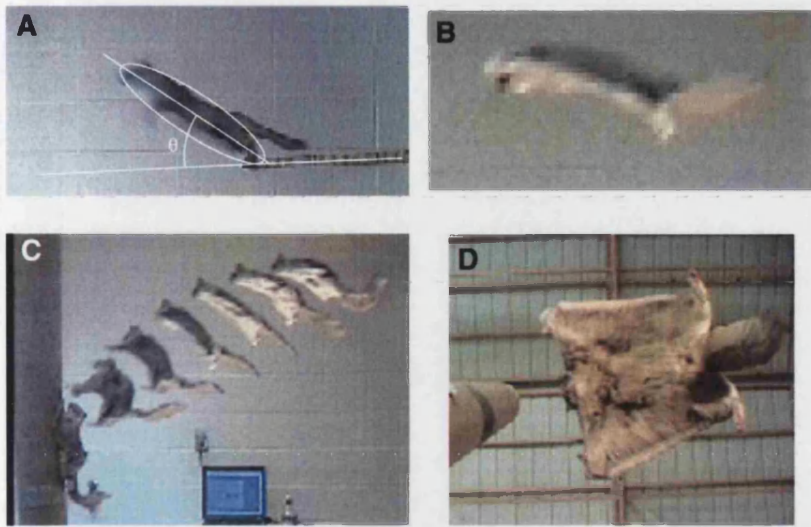
squirrel from ventral images of a glide. Lateral images were used in conjunction with these to ensure that only frames in which the squirrels were in plane with a calibration bar were used for these measurements.

A calculation was performed to determine the percentage of body weight supported during each measured glide, relative to the equivalent ballistic trajectory (that is the trajectory of an object with the same take-off velocity and angle subject to no drag or lift). For a simple free-falling mass, the gravitational force acting downwards is opposed by any lift generated. The resultant force acting on the body is hence:

$$F = M_b a = M_b g - L, \qquad (1)$$

where M_b=mass (kg), a=resultant acceleration (m s^{-2}), g is gravitational acceleration (9.814 m s^{-2}) and L is the lift force (N). The percentage weight supported is simply this lift force divided by the animal's weight. Measured take-off angle, θ, velocity, v (m s^{-1}), and jump duration, t (s), are sufficient to calculate the vertical drop, y (m), from the resultant acceleration using the standard kinematic equation below:

$$y = (v\sin\theta)t - \tfrac{1}{2}at^2. \qquad (2)$$

Therefore, by combining Eqn 1 and Eqn 2 we get an expression for the overall lift force generated during the glide:

$$L = M_b[g - (2tv\sin\theta - y)/t^2]. \qquad (3)$$

Jumps observed, general mixed model, and other statistics

We measured 79 take-offs and 53 corresponding landings with the number of jumps of each animal at each range specified in Table 1. No landing force data were obtained for the shortest range jumps of 0.5 m, but with this exception, all measured take-off forces have a corresponding landing force. Only one squirrel, young female 1, performed in the barn but it did not leap to the force pole at distances greater than 2.5 m, landing instead on the ground beyond the instrumented pole.

This was the only animal to perform at all ranges tested. Unfortunately, young female 2 only cooperated at 0.5, 1 and 1.5 m and the young male at 0.5 and 1 m. Owing to the number of missing data points, the typical multivariate ANOVA could not be applied to our data, and so a general mixed model (Krueger and Tian, 2004) was applied to both take-off and landing forces, with range as a fixed factor and squirrel ID a random factor. Unless otherwise stated, all correlation statistics use Pearson's product moment correlation.

Results

Video stills from the lateral camera illustrate the consistent take-off, gliding and landing postures of the squirrels (Fig. 2). During take-offs, the forelimbs were abducted prior to toe-off enabling the squirrel to immediately adopt gliding posture. During gliding all limbs were abducted creating a cambered wing surface held at a small positive angle of attack. The tail was dorsally flattened, presumably to generate lift. Prior to landing, the squirrel pitched upwards keeping its body and tail in line and flattened against the direction of motion. Immediately prior to landing, the head tilted backwards while the limbs were all pushed forwards with the tail simultaneously rotated back so that it was parallel with the ground. In the example landing sequence (Fig. 2C), the pitch angle of the body changed from approximately 22.5° relative to the horizontal, towards 90° immediately prior to landing.

In the barn, the squirrels tended to have a steeper approach and did not pitch up very much prior to landing. The head still tilted backwards but the tail was rotated forwards towards the vertical. As a consequence of the lower angle of attack, the forelimbs contacted the pole first, causing the body to rotate around rapidly onto the hindlimbs due to the conversion of linear to angular momentum. Occasionally the tail was cambered such that the inside of the curve faced the landing pole. In some jumps, the squirrels were clearly banking or
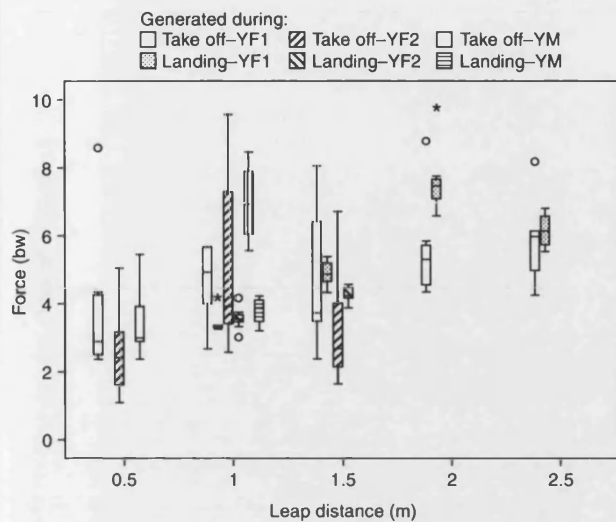
Fig. 3. A box plot directly comparing the landing forces with the corresponding take-off forces for three of the flying squirrels (young females YF1 and YF2, and young male YM) at each horizontal range (from the end of the take-off branch to the landing pole). Asterisks and circles show values that were outside the interquartile range, the former being statistically significantly far away.

Fig. 4. A graph showing the output from the mixed model statistics of mean take-off and landing forces at each horizontal range. The error bars represent the 95% confidence intervals. By ignoring the few jumps at 2 m, when the squirrel consistently landed at the more rigid base of the pole, the square of the Pearson product moment correlation coefficient (the r^2 value) improves from 0.61 to 0.99.

turning in the penultimate frames to correct misalignment with the pole and in one instance, a subject landed on the side of the pole. As it was simple to calculate the forces for these jumps too, these results were included in our analysis.

A summary of take-off and landing forces recorded as a multiple of body weight is shown in Table 1. There was considerable variation between take-off and landing forces measured for each squirrel at each distance. Take-off forces normalised by body weight increased significantly with leap distance (Fig. 3; $r=0.323$, $P=0.004$). The same box plot also shows the positive correlation between landing forces and horizontal range ($r=0.816$, $P<0.001$).

The general mixed model introduced above provides statistical verification that normalised take-off forces were significantly dependent on range ($F_{5,11.5}=45.182$, $P<0.001$) but not squirrel identity ($P=0.602$). Likewise, landing forces were dependent on range ($F_{4,9.5}=409.341$, $P<0.001$) but independent of the particular squirrel ($P=0.548$). The means and 95% confidence intervals produced by the mixed model are plotted in Fig. 4.

All landing and take-off forces are not correlated to one another ($r=0.094$, $P=0.507$). A paired sample t-test comparing landing force with its corresponding take-off force for each jump was not statistically significant ($t_{51}=0.374$, $P=0.710$). The standard deviations of the mean forces for each animal at each distance are shown in Table 1. Standard deviation in take-off forces at each range is clearly larger than that for landing forces. Excluding the 0.5 m range, for which there is no landing force data, the standard deviation ranges from 1.37 to 6.10 bw

for take-off force, compared with only 0.04 to 0.92 bw for landing.

Landing force is positively correlated with angle of descent ($r=0.740$, $P<0.001$).

The outputs from all strain gauges were recorded simultaneously, enabling the duration of each glide to be measured. There is, unsurprisingly, a strong positive correlation ($r=0.923$, $P<0.001$) between glide distance and glide duration. Mean glide velocity based on the linear distance from take-off to landing position and not the actual trajectory, was strongly positively correlated ($r=0.951$, $P<0.001$) with horizontal range. This reached 4.5 m s^{-1} across a horizontal range of 2.5 m.

Average take-off angle for each squirrel at each distance was negatively correlated with range ($r=-0.684$, $P<0.001$) (Fig. 5).

Fig. 6 shows the percentage of bodyweight supported by lift during gliding, as a function of horizontal range. The average value for each squirrel at each range is plotted against horizontal range and the error bars represent plus and minus one standard deviation. At ranges of 1.5 m and above, the squirrel was able to support the equivalent of approximately 40% of its weight by gliding, but none when jumping smaller distances. The advantage gained by gliding increases with range ($r=0.609$, $P<0.001$).

Landing force was found to be significantly correlated to the position of impact on the pole ($r=-0.713$, $P<0.001$).

Glide angles increased steeply with horizontal range until they reached approximately 45° beyond 2.5 m (Fig. 7), the angle at which gliding is distinguished from parachuting, after which they gradually improve as seen by a strong, negative correlation between the 17 longest jumps ($r=-0.816$, $P<0.001$). At this point, only one animal was still performing but it did not land on the pole, and instead glided past it and landed on the floor.

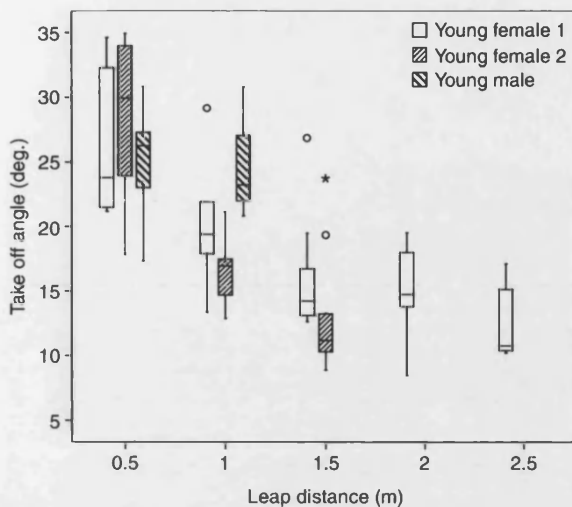Fig. 5. Average take-off angle for each individual flying squirrel as a function of the horizontal distance travelled in the jump (labelled C in Fig. 3). This implies that the squirrels are planning ahead, which in turn may imply that they are considering their landing. Asterisk and circles, see Fig. 3.

Discussion

In this study, take-off and landing forces were measured for northern flying squirrels traversing various distances between compliant substrates. Extensive analysis of video recordings of their movements was also carried out. To our knowledge no such data has been published before and we believe our results provide more insight into the evolution of gliding in these mammals. We link our observations, where possible, to the following four hypotheses for the divergence from other tree squirrels: (1) to reduce energetic cost of foraging; (2) to maximise the potential foraging area in a given time without thought to transport cost; (3) to improve predation escape capability; and (4) to enable superior control of landing.

Take-off, landing and gliding performance are discussed separately.

Take-off

Flying squirrels generated take-off forces ranging from 1.08 to 9.57 bw. The amount of force was proportional to the distance the animal travelled (Fig. 3). It is logical that squirrels generate a larger take-off force to go further, as ballistic theory dictates they require a higher velocity in order to cover the distance. However, there must be a maximum force the squirrel can generate. Our results suggest this might be approximately 10 bw, which is equivalent to occasional high jump forces at shorter ranges. (These occasional jumps support the idea that flying squirrels jump more forcefully when startled, incidentally.)

The highest take-off angle recorded was 35° and this occurred at the shortest range of 0.5 m, which was short enough that landing position was often higher than take-off position. Take-off angle decreased as range of the jump increased
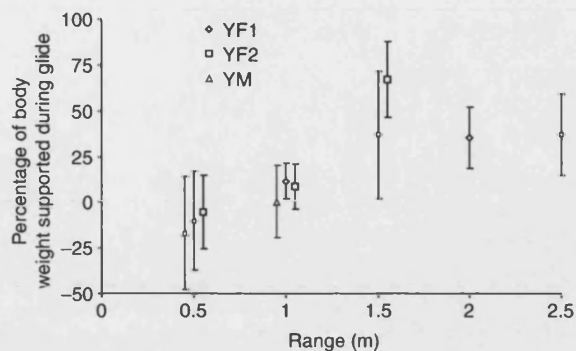

Fig. 6. Percentage of body weight supported by lift during gliding as a function of horizontal range in flying squirrels (young females YF1 and YF2, and young male YM). Values are means for each squirrel at each range ± 1 s.d.

(Fig. 5) but this may have been influenced by a confounding factor, the height of the branch. With sufficient height the animal can afford a shallower take-off angle, allowing it to generate a higher horizontal velocity.

Overall velocities of the squirrels increased with range. The animals usually ran and jumped immediately after release onto the branch, but occasionally it was necessary to startle them. It is unknown if the apparent levelling off of glide angle that we observed for longer jumps is a general trend because we did not obtain results for longer leaps.

Gliding performance

Squirrels used lower glide angles in the lab, but angles near 45° (parachuting) for the longer ranges of 2 m and above in the barn. This may have been a behavioural change due to unfamiliarity, and is based on only one squirrel at these ranges. In a study describing the kinematics of two southern flying squirrels *Glaucomys volans*, glides from both animals were shorter and significantly steeper after moving to a new test arena (Bishop, 2006). However, our measured glide angles improved with increasing range (Fig. 7) and are comparable with similar distance results from two field studies of northern flying squirrels (Vernes, 2001; Scheibe et al., 2006), so it is more likely a consequence of the need for this species (the larger of the two North American species) to reach a higher velocity before it is able to exhibit superior aerodynamic performance. Average glide velocities measured in this study increased with range as would be expected. Observations of the Japanese giant flying squirrel on long glides (Ando and Shiraishi, 1993) sometimes showed an initial steep descent with the glide angle decreasing with increasing velocity, until both became constant. Likewise, northern flying squirrels dropped steeply prior to gliding, and often even managed to gain altitude slightly, just before landing (Vernes, 2001). The squirrels in this study may have initiated a similar behaviour, but the possible ranges were too short for the effect to be noticed. This would help to explain why field observations of northern flying squirrels have reported significantly better glide
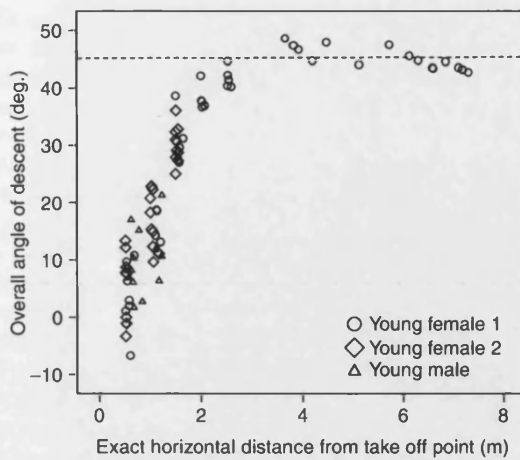
Fig. 7. Scatter plot showing how the glide angle increases with horizontal range until it reaches approximately 45°, represented by a broken line, after which the glide ratio begins to improve slightly. High take-off angles and limited time spent in the air are the factors responsible for the low vales of glide angle across low ranges. Glide angle is strongly negatively correlated with range above 4 m ($r=-0.816$, $P<0.001$) where higher glide speeds enable northern flying squirrels to exhibit superior lift to drag ratios.

ratios. In Alaska, USA, Scheibe et al. evaluated 168 glides from 82 different squirrels with mean glide distances of 12.46 m and 14.39 m in successive years, and corresponding mean glide angles were 41.31° and 36.31° (Scheibe et al., 2006). Vernes reports a mean angle of descent of just 26.8° for glides which were longer, averaging 16.4 m (Vernes, 2001). Gliding behaviour is therefore likely to be optimised for significantly longer ranges than were possible in this study.

Flying squirrels use their patagium as a low-aspect-ratio wing, which has good aerodynamic stability at the relatively low speeds involved, generating lift at high angles of attack of up around 40° without stalling (Torres and Mueller, 2004). This shape allows the squirrel to overcome any detrimental rotational momentum that it might have generated during take-off. In the present study, full gliding posture was always initiated before the hindlimbs left the substrate, allowing the angular momentum produced by forelimb abduction to be transmitted directly to the branch, even over the shortest leaps of just 0.5 m. It has been argued (Essner, 2000) that this behaviour enabled the squirrel to begin gliding earlier, resulting in a flatter trajectory with more immediate manoeuvrability and control. We quantified the gliding performance of each squirrel by calculating the percentage of its bodyweight supported during each glide and showed that flying squirrels exploited their unique morphology to generate lift at ranges greater than 1.5 m (Fig. 6). However, these values were negative over 0.5 m, implying that the squirrels generated down-force. It could be that the combination of steep take-off angles with immediate initiation of gliding results in their large patagial surface area working against the squirrels on these steeper take-

off angles. Alternatively our estimate for the percentage body weight supported could be slightly conservative. In any case, we have established that the transition from leaping to gliding occurs at a horizontal range of 1.5 m for northern flying squirrels. They are not able to benefit from gliding over distances of less than 1 m, so although the resultant glide angles may appear to be superior at these ranges, this is only a consequence of the higher take-off angles and limited time in the air.

Landing

Landing forces varied between 3.01 and 9.52 times body weight. The impact force on the landing pole was proportional to the range of the leap. This is expected because the measured gliding velocity increased with horizontal distance, reflecting the effects of gravitational acceleration.

The correlation of measured landing force with the contact position of the animal on the pole is due to the compliance decreasing towards the fixed end. Higher forces were experienced by squirrels landing lower down on the pole, where it was relatively stiffer and did not deflect so far. This is inevitable because the kinetic energy of the squirrel becomes the product of reaction force and deceleration distance – proportional to the deflection of the pole given that leg length remains constant. This has an important implication for the use of compliant substrates when quantifying forces for comparison. Ideally, only forces measured at points of equal compliance should be compared directly, or there should be a random scattering of landing positions. This was the case for our results, with the exception of the 2 m range, at which the squirrel consistently landed at the base of the pole. The reason for this is unknown, because the angle between the base of the landing pole and the tip of the take-off branch was consistent at 55° for all ranges. However, by removing the data from the 2 m range (7 data points out of 53), a strong linear relationship can be observed between the means of the other 46 jumps where more compliance was available (Fig. 4). The square of the Pearson product moment correlation coefficient (the r^2 value) improves from 0.61 to 0.99 when the 2 m data is ignored. Such a good linear fit means that the flying squirrels adopt a consistent landing technique. On stiffer substrates, we would expect a similar, but steeper, linear increase in landing force with range.

Over short leaping distances, take-off forces are not significantly different from landing forces (Fig. 3; t-test). This fits with the expectation (see Introduction) that landing forces would not be higher than take-off forces on compliant substrates, as they are on rigid platforms (Demes et al., 1995).

Landing force was correlated with angle of descent, suggesting the squirrels are better able to absorb landing impacts with a flatter approach. Some of the impact force is likely absorbed as a result of the consistent landing posture observed, which it seems the squirrels were unable to accomplish with steeper approaches. During shallower glides the squirrels are able to increase their drag force by transforming the patagia and distichous tail from a cambered

surface with low angle of attack, high lift and low drag, to a more parachute-like surface orientated against the direction of motion. Additionally, this posture enabled the squirrel to absorb the remaining impact forces more evenly over its four extended limbs on contact. Aerodynamically, the flying squirrel has a low aspect ratio (close to 1) and glides at low speed so an angle of attack in excess of 40° would be required for it to stall in flight (Torres and Mueller, 2004). The squirrel has additional aerodynamic implications associated with its morphology, such as its fur, so it is not possible to measure whether or not they are actually stalling from our video footage. However, it is clear from the example landing sequence shown in Fig. 2C that the pitch angle of the body has increased to effectively 90° immediately prior to landing, supporting the theory that they deliberately stall themselves (Alexander, 1995).

Caple et al. stated that the vector sum of angular momentum must be conserved during any mid-air movement of a body with no lift or drag (Caple et al., 1983). Although flying squirrels will also be able to generate some external force from their patagium, this could help explain the origin of some of the consistent landing movements observed. For example, the rotations of the head and tail backwards would directly counteract the thrusting of the limbs ventrally, although it is equally likely that the head tilt may be for defence against accidental impact. A falling cat also uses counter-rotations in order to right itself when falling from an upside-down position (McDonald, 1960). Caple's calculations (Caple et al., 1983) also show that some of the morphological features of flying squirrels, such as long forelimbs with dense, distally located mass (hands and feet) and a lightweight tail that can produce lift, are optimisations for controlling pitch and roll. We show that the squirrels were able to reduce landing forces by pitching upwards as they approach, and it is this behaviour which may have applied selective pressure to these morphological features rather than glide range, which increases negligibly in comparison. Increasing forelimb length allows the landing energy to be absorbed over a larger distance. Likewise, the flexed back on impact should further reduce the peak landing force. A falling cat also tries to land with its back arched and all four limbs outstretched towards the ground (McDonald, 1960).

Unfortunately the squirrels could not be persuaded to land on the pole above the relatively small horizontal range of 2.5 m, compared to their normal arboreal glide distances (Vernes, 2001; Scheibe et al., 2006), choosing instead to deliberately manoeuvre past the landing pole and land on the floor. It is possible that the squirrels may have a sense for a maximum speed at which they can safely or comfortably land on a stiff or unknown substrate for a given approach angle. Glide angles achieved at ranges between 3 and 6 m exceeded 45° (Fig. 7), which would normally be defined as parachuting rather than gliding (Oliver, 1951), and we speculate that this is likely to be the most difficult distance for northern flying squirrels to land. The steeper approach angles inhibit their ability to pitch up and absorb the landing across all four limbs simultaneously, and

there is more energy to dissipate due to the inevitable increase in velocity with range. Velocity continues to increase above the proposed awkward range but this also improves the flying squirrel's aerodynamic ability, allowing a progressive improvement in approach angle and consequent landing posture. It is likely that these animals would try to avoid making hard landings on tree trunks at this unfavourable range. Vernes reported that in 21% of his 100 glides observed (Vernes, 2001), northern flying squirrels landed on the ground or in dense undergrowth. The other landings were on trees and it should be noted that the mean glide distance was much higher in the Vernes study than ours. Likewise, Scheibe et al. noted that sometimes squirrels released onto a tree trunk at breast height did not climb and glide, choosing instead to jump to the ground and run to a nearby tree (Scheibe et al., 2006). Future experimental designs should consider that northern flying squirrels might be more likely to land on an instrumented pole positioned at a high rather than medium horizontal distance from the take-off position, but this would necessitate an arena allowing sufficient take-off height.

The equation for the linear relationship between landing force and range on the compliant part of the pole is shown on Fig. 4 and can be used to predict the landing force at longer ranges than we were able to measure. However, the squirrels would not keep accelerating indefinitely during long glides; rather their speed would stabilise as they approach terminal velocity. Maximum glide velocities of close to 12 m s^{-1} have been reported (Scheibe et al., 2006), although the weighted means were 6.26 m s^{-1} and 8.11 m s^{-1} in two consecutive years. These values are much higher than our highest observed speed of 4.5 m s^{-1}, although this was measured across a relatively much shorter horizontal glide distance. With more time in the air, squirrels must be able to control their trajectories, otherwise they would be subject to extremely high impact forces. Depending on substrate compliance, we can use the equation from Fig. 4 to calculate that squirrels trying to land from an ordinary 16 m glide would be subject to impact forces of upwards of 28 bw if they did not slow themselves, as we have shown, by pitching up and employing air braking.

Evolution of gliding

Hypothesis 1

Hypothesis 1 that gliding developed to reduce the energetic cost of foraging supposes that the squirrels' primary objective should be to maximise range in every jump while minimising the loss in altitude. Therefore, from ballistic theory we would expect the squirrels to jump at close to the optimum take-off angle of 45°, but they did not. As expected, the advantage gained by gliding increases with range. This vertical advantage achieved relative to the ballistic trajectory enables flying squirrels to reach trees beyond normal jumping range, or reduces the amount of climbing required after a glide is completed, thus saving energy. However, during this study flying squirrels did not try to take off at 45°, which would be expected for maximising range, and take-off angle decreased

with range. However, the non-optimum take-off angles and frequently observed range-reducing aerial manoeuvres are evidence to suggest that energetic transport cost is not of primary importance to flying squirrels.

Hypothesis 2

If gliding evolved to maximise the foraging area that could be reached in a given time, as proposed by Hypothesis 2, then we would expect the squirrels to glide at high velocities. We have shown that velocity increases with range, and that flying squirrels can generate higher lift forces when travelling further, so we cannot reject the hypothesis that gliding is an optimisation to maximise speed and potential foraging area.

Hypothesis 3

Hypothesis 3 is that gliding evolved primarily to facilitate escape from predation. One might expect that an escaping squirrel would jump horizontally, or downwards given sufficient altitude, in order to ensure that it did not decelerate due to gravity. Bonser and Rayner proposed that starlings may deliberately vary take-off trajectory for predator avoidance (Bonser and Rayner, 1996), but we have shown a negative correlation of the take-off angle with range, suggesting that during this experimentation at least, flying squirrels choose a take-off trajectory to suit their intended destination. Caple et al. stated that all gliders pre-select a landing site, which must be large enough to allow some vertical variation in the contact point (Caple et al., 1983). Vernes also observed that flying squirrels appeared to think about their intended flight path before launching and we saw no evidence to suggest otherwise (Vernes, 2001). Given that the squirrels seem to exhibit this behaviour even during the jumps that were initiated by startling, it seems unlikely that gliding evolved primarily for escape, at least not from high-speed chases.

The ability to make sudden aerial direction changes could potentially help to lose a predator. However, their most likely aerial predator is the owl (Scheibe et al., 1990), and it is unlikely that such sophisticated fliers would be troubled by the relatively clumsy swerving squirrel.

Hypothesis 4

Hypothesis 4 relates the development of flight to the control of landing. Even at the relatively short ranges in this study, we observed direction changes being introduced by rapid beating of the tail from side to side. Additionally, last-second manoeuvres were observed, such as banking and using the tail as a rudder, implying that flying squirrels are able to make precise adjustments to improve their landing. As range increases, any error in take-off trajectory would become more significant without aerial control; in this case squirrels could face serious consequences for misjudging long leaps at the top of the forest canopy.

Flying squirrels choose to initiate a full gliding posture even though they do not produce significant lift during glides of less than 1 m, suggesting that this behaviour is innate. It might be that the squirrel is simply throwing its arms out conveniently

widely for rapid rotation of the joint in order to gain forward momentum during take off. They do exhibit a consistent landing behaviour at these distances, with the gliding posture enabling them to pitch upwards as they approach and spread the landing reaction force over all limbs. It is likely that the squirrels deliberately stall themselves by this quick increase of their angle of attack immediately prior to landing.

Landing control of pitch and roll improves much more rapidly than range for the same incremental improvements in forelimb length and tail surface area. Increasing forelimb length simultaneously reduces the landing force further by increasing the deceleration distance. Landing force was correlated with angle of descent, suggesting flying squirrels were unable to pitch up sufficiently to execute the evenly distributed four-limbed landings when approaching steeply, demonstrating the utility of aerial control in longer jumps. Given the reported values of terminal velocity for flying squirrels, and the measured landing forces on compliant substrates that increase with range, we know that if the squirrels could not slow themselves or improve landing posture aerodynamically prior to landing, they would have to sustain impact forces of upwards of 28 bw.

Evolution of gliding in flying squirrels has undoubtedly reduced their energetic cost of transport, while improving potential foraging area and response to predation, but we conclude that the selective pressure for their divergence from ground squirrels was the improvement of landing control.

Conclusions

Take-off and landing forces generated by northern flying squirrels are both positively correlated with horizontal range, at least up to 2.5 m. The maximum take-off force measured was 9.57 bodyweights, although the squirrels would occasionally produce close to this force when jumping only short distances, most likely a natural behavioural response to alarm. Take-off forces were not significantly different to the corresponding landing forces on these similarly compliant substrates. They are able gliders, abducting all limbs to create a wing-like surface, which is held at a low angle of attack for maximum lift/drag ratio. Glide angle increased rapidly with horizontal range up to approximately 4 m, before progressively improving, suggesting that gliding in northern flying squirrels is optimised for significantly longer ranges than were possible in this study.

Any compliant force-measuring device will likely have some variation in its compliance along its length. In the case of a cantilever beam, this begins to behave more like a rigid instrument towards its fixed end. Valuable comparisons can only be made between forces measured at known points of equal compliance. If this is not possible, then sample sizes should be chosen to ensure a random scattering of landing positions.

It seems unlikely that gliding evolved in flying squirrels to reduce the energetic cost of transport even though the measured lift generated would lessen the amount of climbing required. Take-off angle decreased with range without getting close to 45°, the value for maximum ballistic range, and further height

would be lost to the aerial manoeuvres occasionally observed. The flying squirrels in this study did not attempt to make either unplanned or deliberately unpredictable take offs, casting doubt on the theory that gliding might improve predatory escape response.

Gliding might have evolved to maximise the foraging area that could be reached in a given time. High glide speeds were measured and this velocity increases with range, but the development of improved landing control is a necessary consequence of faster flight. We provide evidence that if northern flying squirrels could not slow themselves aerodynamically from terminal velocity, prior to landing, they would have to try and sustain impact forces of upwards of 28 bw. Flying squirrels seem to innately adopt a gliding posture on take off, even during leaps of less than 1 m when no vertical advantage is gained, but this leaves them better prepared for aerial control. At these low distances, a consistent landing strategy was exhibited by flying squirrels, allowing the impact force to be spread over all four limbs and their arched back, thanks to a dramatic pitch upwards immediately prior to contact with the pole. This rapid increase of their angle of attack immediately prior to landing is likely a behaviour evolved to enable rapid deceleration by stalling, although this would have greater effect at high speeds. We conclude that at divergence, small glide producing surfaces were developing in flying squirrels allowing mid-air adjustments in pitch and roll, and improving their resilience during high-speed arboreal transport.

List of symbols and abbreviations

a	resultant acceleration (of centre of gravity)
bw	body weight
F	force
g	gravitational acceleration
k	force calibration constant
L	lift force
M_b	body mass
r^2	the square of the Pearson product moment correlation coefficient
t	jump duration (time between take off and landing)
v	velocity
x	strain gauge signal voltage
y	vertical drop
θ	take-off angle

References

Alexander, R. M. (1991). Elastic mechanisms in primate locomotion. *Z. Morphol. Anthropol.* **78**, 315-320.

Alexander, R. M. (1995). *How Animals Move.* Fareham: Maris Multimedia, Discovery Communications.

Ando, M. and Shiraishi, S. (1993). Gliding flight in the Japanese giant flying squirrel *Petaurista leucogenys. J. Mammal. Soc. Jpn.* **18**, 19-32.

Bishop, K. L. (2006). The relationship between 3-D kinematics and gliding performance in the southern flying squirrel, *Glaucomys volans. J. Exp. Biol.* **209**, 689-701.

Bonser, R. H. C. (1999). Branching out in locomotion: the mechanics of perch use in birds and primates. *J. Exp. Biol.* **202**, 1459-1463.

Bonser, R. H. C. and Rayner, J. M. V. (1996). Measuring leg thrust forces in the common starling. *J. Exp. Biol.* **199**, 435-439.

Caple, G., Balda, R. P. and Willis, W. R. (1983). The physics of leaping animals and the evolution of pre-flight. *Am. Nat.* **121**, 455-476.

Demes, B., Jungers, W. L., Gross, T. S. and Fleagle, J. G. (1995). Kinetics of leaping primates. *Am. J. Phys. Anthropol.* **96**, 419-429.

Demes, B., Jungers, W. L., Fleagle, J. G., Wunderlich, R. E., Richmond, B. G. and Lemelin, P. (1996). Body size and leaping kinematics in Malagasy vertical clingers and leapers. *J. Hum. Evol.* **31**, 367-388.

Demes, B., Fleagle, J. G. and Jungers, W. L. (1999). Take-off and landing forces of leaping strepsirhine primates. *J. Hum. Evol.* **37**, 279-292.

Essner, R. L. (2000). Comparison of takeoff kinematics in gliding and nongliding squirrels. *Am. Zool.* **40**, 1010-1011.

Essner, R. L. (2002). Three-dimensional launch kinematics in leaping, parachuting and gliding squirrels. *J. Exp. Biol.* **205**, 2469-2477.

Keith, M. M., Scheibe, J. S. and Hendershott, A. J. (2000). Launch dynamics in *Glaucomys volans.* In *The Biology of Gliding Mammals* (ed. R. Goldingay and J. S. Scheibe), pp. 185-198. Fürth, Germany: Filander Press.

Krueger, C. and Tian, L. (2004). A comparison of the general linear mixed model and repeated measures ANOVA using a dataset with multiple missing data points. *Biol. Res. Nurs.* **6**, 151-157.

McDonald, D. D. (1960). How does a cat fall on its feet? *New Sci.* **7**, 1647-1649.

Meng, J., Hu, Y., Wang, Y., Wang, X. and Li, C. (2006). A Mesozoic gliding mammal from northeastern China. *Nature* **444**, 889-893.

Norberg, U. M. (1985). Evolution of vertebrate flight – an aerodynamic model for the transition from gliding to active flight. *Am. Nat.* **126**, 303-327.

Oliver, J. (1951). Gliding in amphibians and reptiles. *Am. Nat.* **85**, 171-176.

Scheibe, J. S. and Robins, J. H. (1998). Morphological and performance attributes of gliding mammals. In *Ecology and Evolutionary Biology of Tree Squirrels* (ed. M. A. Steele, J. F. Merritt and D. A. Zegers), pp. 131-144. Martinsville, VA: Virginia Museum of Natural History.

Scheibe, J. S., Figgs, D. and Heiland, J. D. (1990). Morphological attributes of gliding rodents: a preliminary analysis. *Trans. Mo. Acad. Sci.* **24**, 49-56.

Scheibe, J. S., Smith, W. P., Bassham, J. and Magness, D. (2006). Locomotor performance and cost of transport in the northern flying squirrel *Glaucomys sabrinus. Acta Theriol.* **51**, 169-178.

Thorington, R. W. and Heaney, L. R. (1981). Body proportions and gliding adaptations of flying squirrels (Petauristinae). *J. Mammal.* **62**, 101-114.

Thorington, R. W., Darrow, K. and Anderson, C. G. (1998). Wing tip anatomy and aerodynamics in flying squirrels. *J. Mammal.* **79**, 245-250.

Torres, G. E. and Mueller, T. J. (2004). Low-aspect-ratio wing aerodynamics at low Reynolds numbers. *AIAA* **42**, 865-873.

Vernes, K. (2001). Gliding performance of the northern flying squirrel (*Glaucomys sabrinus*) in mature mixed forest of eastern Canada. *J. Mammal.* **82**, 1026-1033.

Jumping robots: a biomimetic solution to locomotion across rough terrain

Rhodri Armour, Keith Paskins, Adrian Bowyer, Julian Vincent and William Megill

Centre for Biomimetic and Natural Technologies, Department of Mechanical Engineering, University of Bath, Claverton Down, Bath BA2 7AY, UK

E-mail: R.H.Armour@bath.ac.uk, K.E.Paskins@bath.ac.uk, A.Bowyer@bath.ac.uk, J.F.V.Vincent@bath.ac.uk and W.M.Megill@bath.ac.uk

Abstract

This paper introduces jumping robots as a means to traverse rough terrain; such terrain can pose problems for traditional wheeled, tracked and legged designs. The diversity of jumping mechanisms found in nature is explored to support the theory that jumping is a desirable ability for a robot locomotion system to incorporate, and then the size-related constraints are determined from first principles. A series of existing jumping robots are presented and their performance summarized. The authors present two new biologically inspired jumping robots, Jollbot and Glumper, both of which incorporate additional locomotion techniques of rolling and gliding respectively. Jollbot consists of metal hoop springs forming a 300 mm diameter sphere, and when jumping it raises its centre of gravity by 0.22 m and clears a height of 0.18 m. Glumper is of octahedral shape, with four 'legs' that each comprise two 500 mm lengths of CFRP tube articulating around torsion spring 'knees'. It is able to raise its centre of gravity by 1.60 m and clears a height of 1.17 m. The jumping performance of the jumping robot designs presented is discussed and compared against some specialized jumping animals. Specific power output is thought to be the performance-limiting factor for a jumping robot, which requires the maximization of the amount of energy that can be stored together with a minimization of mass. It is demonstrated that this can be achieved through optimization and careful materials selection.

M This article features online multimedia enhancements

1. Introduction

The aim of the research reported in this paper is to produce a small, autonomous and inexpensive jumping robot for traversing irregular terrain. It will use a locally-available energy resource. Given the breadth of successful jumping organisms present in nature, biomimetics will deliberately be used to aid the design and development.

The majority of robot locomotion utilizes wheels, which are very efficient at covering smooth terrain, but these vehicles are unable to pass obstacles of greater than half their wheel diameter. One exception is Shrimp, a space rover designed for improved mobility which has its wheels mounted on high, articulating bogeys, enabling it to climb obstacles of up to twice its wheel diameter (Estier *et al* 2000). Wheeled robots tend to have good manoeuvrability and could skirt around some obstacles, but others, such as a flight of stairs, walls or perimeter fences, would still halt progress completely.

Walking robots are better able to cope with rough terrain, but generally rely on more complex control systems. The multiple degrees of freedom required for each leg demand several actuators to control them, meaning that the power and computational requirements are likely to be large. There are some novel 'legged' robots with very few actuators such as RHex (Altendorfer *et al* 2001) and Whegs™ (Quinn *et al* 2002), which combines the simplicity of wheels with the adaptability of legs. However, although legged vehicles have a surprising ability to clamber over rough terrain, they are

unlikely to get past obstacles of higher than double their leg length.

Tracked vehicles are often chosen for traversing rough terrain but there are still limitations on the maximum obstacle height that can be overcome. This height is dependent on various factors including the dimensions of a tracked unit, the positioning of its centre of gravity and the friction between the track and the terrain. Tracked robots are typically dimensioned specifically for the terrain requirement and therefore it is difficult to determine a generic maximum obstacle height. Lui (2005) presents a useful analysis of the stair-climbing ability of a simple tracked robot which results in a maximum obstacle height but this is representative of a specific case only. Obstacles that are taller than half the length of a tracked robot are likely to be impassable unless the centre of gravity is far from the geometric centre of the device.

In summary, traditional ground robot locomotion techniques seem to be limited to traversing obstacles of a similar order of magnitude as their size. Jumping robots may be able to traverse obstacles an order of magnitude larger than their own size.

As the size of a moving object decreases, it becomes more likely to meet an obstacle of similar or larger size to itself, and therefore it will encounter rough terrain more often. This is called the 'size-grain hypothesis' (Kaspari and Weiser 1999) which is defined as an 'increase in environmental rugosity with decreasing body size'. So a small robot, whether it walks, rolls or jumps will need the ability to cover rough terrain more frequently than a larger robot.

The most effective way of travelling over rough terrain would be to fly over it. Micro-air vehicles are not hindered by obstacles on the ground, but are energetically expensive, resulting in limited power-source life or power requirements that cannot be met continuously from the surroundings, and are hence unsuitable for some applications. The periodic nature of jumping allows time for recharging energy from the surroundings, making it a more sensible approach to designing a fully-autonomous rough-terrain robot.

Looking at nature, we find that many animals employ jumping as a tactic for traversing obstacles. Some jump to escape predators or capture food, while for others, such as kangaroos, it is the favoured method of locomotion. There are two distinct jumping patterns that can be observed. Locusts, for example, travel using single jumps followed by a rest period to recharge and re-orientate (Bennet-Clark 1975). This can be categorized as the 'pause and leap' method and is common in insects and other small animals such as frogs. The alternative approach is continuous hopping, where energy is recovered during the landing and used in the following jump, a technique employed by kangaroos in order for them to travel large distances across the bush (Alexander and Vernon 1975). Continuous hopping requires a higher level of sophistication in control, and this, combined with the lack of recoverable kinetic energy due to insects small mass means that all the insect jumpers are in the 'pause and leap' category. They tend to have little or no control in the air, landing ungracefully before getting back to their feet and sometimes launching again.

In order for a biological system to achieve its largest jump, it needs to produce the maximum amount of energy in a single event. In nature, muscles are the most common means of initiating locomotion. These have the ability to either shorten or generate tension and if they do both simultaneously, they can perform mechanical work (Bennet-Clark 1976). (It is also possible to store muscular energy for jumping in spring-like structures; this will be covered below.) Neglecting air resistance and losses due to the slipping of the feet on the ground, all the work done by the animal will be converted directly into kinetic energy:

$$KE = \tfrac{1}{2}mv^2 \qquad (1)$$

where m is the mass of the animal, and v is its take-off velocity. The kinematic equations for calculating the maximum height and range of ballistic projectiles ignoring wind resistance are well known.

Peak height, h:

$$h = \frac{(v \sin \theta)^2}{2g}. \qquad (2)$$

And maximum range, x:

$$x = v^2 \frac{\sin 2\theta}{g} \qquad (3)$$

where g is the acceleration due to gravity and θ is the take-off angle. These equations and all subsequent kinematic equations can be found in any elementary physics text book. It is clear from (3) that the maximum horizontal range is achieved when the take-off angle is 45°. Likewise, in order to maximize the height of a jump, the ideal take-off angle is 90°. By combining either equation (2) or (3) with equation (1), we see that both the maximum height h, and the maximum range x, are proportional to the energy, or work done by the muscle, divided by the total mass. Therefore, by assuming that the amount of mechanical work done by a muscle is proportional to its mass (Gabriel 1984), then the jumping performance is dependent on the percentage of the body that is muscle directly involved in the jump. It follows then that if the proportion of the body mass taken up by jumping muscle is consistent across a range of animal sizes, and neglecting other factors such as air resistance, all animals should in theory be able to jump to the same height (Hill 1950). However, Henry Bennet-Clark suggests that larger animals are limited by the maximum amount of mechanical work which their jumping muscles are capable of developing, whereas the performance of smaller animals is limited by high power requirements (Bennet-Clark 1977). What the first half of this statement means is that larger animals would have to dedicate a higher proportion of their total mass to jumping muscles. Looking in more detail at this latter point, the energy required for a jump is usually applied to the ground through extension or rotation of the legs, and the take-off force can only act while these are in contact with the ground. Therefore, the length of the leg also has a direct influence on jumping performance and in order to overcome this many insects and small animals use 'biological catapults'—energy storage mechanisms—as a means of generating higher power from their muscles. The proof that shorter leg length requires higher power actuation is given below.

The equation for an accelerating body is

$$v^2 = u^2 + 2as \qquad (4)$$

where u is the initial velocity, a is the acceleration and s is the distance through which it is accelerating, which in biology is typically directly proportional to the leg length. Therefore, from equations (2), (3) and (4), again we can see that the height and range will improve directly with increased leg length.

The power output, P, can be related to either energy or force using the standard equations (5) and (6):

$$P = \frac{energy}{time} \qquad (5)$$

$$P = Fv = mav. \qquad (6)$$

Therefore, for an animal jumping from rest, (4) and (6) can be combined to give

$$P = \frac{mv^3}{2s}. \qquad (7)$$

Hence, the smaller the leg length, the higher the specific power requirement to reach a given take-off velocity, and therefore range and height.

By combining (2) and (7), we get the following equation which relates power, mass and acceleration distance to height, h, for a vertical jump (Bennet-Clark 1977). This equation will be used later on to evaluate jumping robot performance:

$$h = \left(\frac{2sP}{m} \right)^{\frac{2}{3}} \times \frac{1}{2g}. \qquad (8)$$

Owing to their small size, an insect's leg length is limited and on top of this, insects are more affected by air resistance so power amplification is essential for jumping. As a result, many different specializations have evolved in insects to enable effective jumping, some of which have even developed so far as to hinder simple walking (Bennet-Clark 1977). Grasshoppers and locusts have metathoracic legs that are only used for jumping and that are very much larger than the other pairs of legs that are primarily used for walking and stability. It was shown by Bennett-Clark (1975) that locusts are able to achieve a large jumping impulse by moving these legs at a velocity much higher than is possible by direct muscle action by pre-loading energy into a quick-release mechanism. Energy is stored in spring-like cuticular elements by the extensor leg muscles after a physical catch has been engaged (Heitler 1974). This elastic energy storage is comparable with a catapult, which is pulled back slowly against a high force, and then travels much faster when released. Other examples of such catapult mechanisms include fleas (Bennet-Clark 1975, Bennet-Clark and Lucey 1967, Rothschild et al 1975) and froghoppers (Burrows 2003), both of which are very small but can jump more than 100 times their body length. Bi-stable mechanisms inherent in their structure are also used by some insects to store energy for jumping including springtails (Brackenbury and Hunt 1993) and click beetles (Evans 1973).

Power amplification is by no means restricted to the insect jumpers. Even larger animals, such as dogs, which use direct actuation of muscles to jump, can generate more power by storing energy in tensile elastic elements during a counter-movement immediately prior to jumping (Alexander 1974).

Another point to consider is that in order to maximize either distance or height, the energy-to-mass ratio must be as large as possible (equations (1)–(3)). The physical size has no effect on the jump unless air resistance is considered. Increased energy requires stronger structures to react the higher forces, but improving strength generally increases the mass thus negating some of the benefit of higher energy levels. To minimize the requirements on the structure, the force should remain constant, below a threshold, throughout the time of the jump rather than peak. Constant force would imply constant acceleration, and hence velocity and power would rise linearly with time to a maximum at take-off.

Owing to the low density energy availability specified for our jumping robots, the 'pause and leap' strategy will be much more suitable than 'continuous hopping'. This allows a robot as much time as necessary to recharge and re-orientate itself between jumps. In principle, jumping robots should be able to clear obstacles much larger than themselves with simple construction and direction control. This could enable a jumping exploration robot to be smaller and cheaper than the equivalent wheeled or walking robot, which would be particularly desirable for space applications where volume and mass are at such a premium. There is also potential for many simple jumping robots to be employed together, in place of a single conventional robot, allowing a semi-sacrificial team mission strategy to be employed.

2. Existing designs

This section highlights a series of existing pause-and-leap jumping robots, grouped by energy storage medium and the capabilities of each are summarized later in table 4. Most existing jumping robots can operate under earth gravity, but there is an important range of microgravity jumping robots that are not discussed here since their application is specifically for very low gravity environments such as surface exploration of asteroids and other interstellar bodies (Nakamura et al 2000, Raibert 1986, Shimoda et al 2002, Yoshimitsu et al 2003). Other 'jumping' robots not described here include a series of hopping robots which continuously jump (Brown and Zeglin 1998, Okubo et al 1996, Paul et al 2002, Raibert 1986, Wei et al 2000). This is because of different design problems which include active balancing and dynamic stability.

2.1. Coil spring based designs

Researchers at NASA Jet Propulsion Laboratories (JPL) and Caltech have developed a series of jumping robots called 'Hoppers' (Fiorini and Burdick 2003)—one of which is pictured in figure 1(a). Of the coil spring designs mentioned here, these robots jump the highest. Each is based around a six-bar linkage and coil spring leg mechanism and it is this that is the most interesting feature. The force–displacement profile of this leg system results in a nonlinear spring profile that has been produced from a linear coil spring. This gradual increasing release force rises to a peak before it reduces, ensuring that the acceleration of the device rises for as long as possible until take-off. This is in contrast to a typical spring where the force
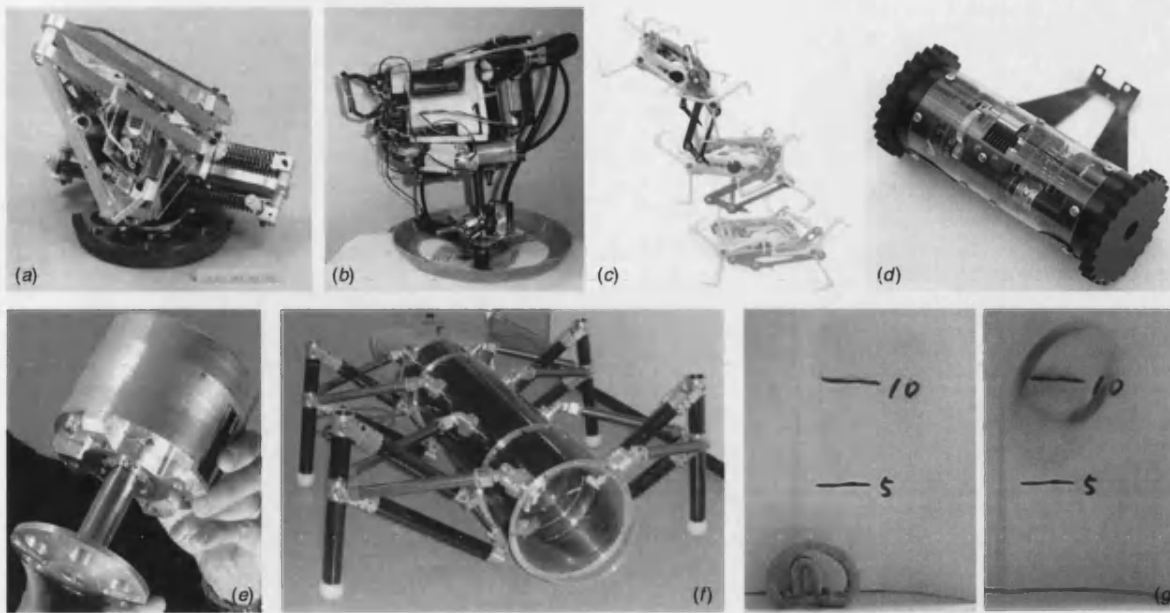
Figure 1. Existing jumping robots: (*a*) JPL Hopper (prototype 2) courtesy NASA/JPL-Caltech, (*b*) Monopod hopper courtesy of James Allison, (*c*) Jumping Mini-Whegs™ courtesy of Case Western Reserve University, (*d*) Scout robot courtesy of University of Minnesota, (*e*) Sandia Hopper courtesy of Sandia Corporation, (*f*) Airhopper courtesy of Tokyo Institute of Technology, (*g*) Deformable Soft Robot courtesy of Ritsumeikan University.

would be highest at the start. This is very important for light weight jumping robots which may undergo premature lift-off (Hale *et al* 2000) where the device jumps before all of the energy is released.

The coil spring based robot that achieved the second greatest leap is the Monopod robot developed by Allison (2002) at the University of Utah—a photograph of which is presented in figure 1(*b*). Unlike the JPL hopper, here the coil spring is compressed, but again a motor driven lead screw is used to input the energy into the system. The compressed spring fires a piston attached to the head of the main chassis of the robot upward and away from the foot.

The final coil-spring-based jumping robot was not originally designed as a jumping robot at all, rather it was designed as a simple 'walking' robot. Named Mini-Whegs™ after the hybrid of wheels and legs it has at its corners, that combine 'simplicity, robustness and reliability to provide a desirable combination of speed, mobility and versatility' (Morrey *et al* 2003). The 9J version of the robot, depicted in figure 1(*c*), is powered by a motor which rotates all four of the 'whegs' at the same time at a single speed. The jumping capability was added to improve its ability to get over larger obstacles. Jumps are achieved by employing a four-bar linkage and coil spring. The spring is stretched using a second motor within the chassis and releases automatically when the spring is fully extended.

2.2. Bending spring based designs

The Scout robot (Stoeter *et al* 2002) was developed as a platform for distributed robotic systems where multiple devices would work in conjunction to achieve a common

mission goal. The basic robot is cylindrical with a wheel at each end allowing motion on smooth surfaces and is shown in figure 1(*d*). For jumping, a steel spring foot is bent by a winch and cable, thus storing energy for a subsequent jump.

2.3. Fluid powered designs

Researchers at the Sandia laboratories developed the Sandia hopper (Weiss 2001) pictured in figure 1(*e*). Utilizing the combustion of liquid propane to fire a piston into the ground, jumps can be achieved through the acceleration of the heavier upper body. The device jumps semi-randomly making general progress in the required direction rather than accurate progression from one point to another. The hopper adopts a weighted self righting system (not pictured) and a steering system that takes a bearing from an internal compass before moving an off-centre control mass which tilts the device in the intended direction of the jump.

The second fluid-based jumper uses the expansion of compressed air to rapidly fill and extend pneumatic cylinders. The Tokyo Institute of Technology 'Airhopper' (Kikuchi *et al* 2003), shown in figure 1(*f*), has a tubular body with four widely-spaced legs providing a stable platform. Each leg consists of a four bar linkage driven by a pair of pneumatic cylinders.

2.4. Momentum-based designs

At the time of writing only one robot uses momentum to initiate a jump. When a human jumps vertically, as well as compressing the legs which release most of the jumping energy, the arms are also swung upwards in a pendulum fashion
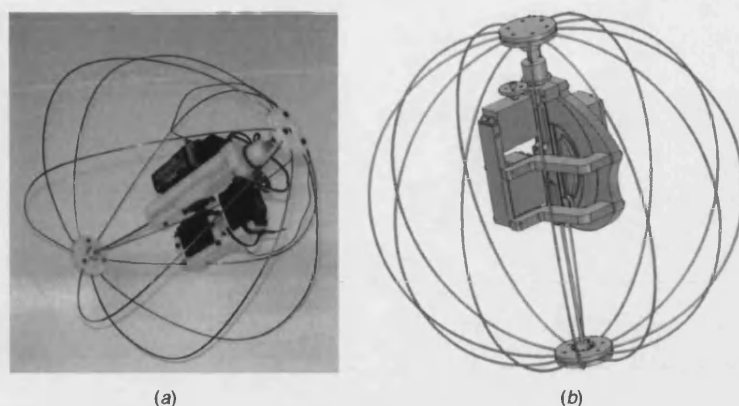
Figure 2. (*a*) Photograph of Jollbot, (*b*) CAD model of Jollbot.

to improve the jump height. A number of papers suggest that the arm swing improves vertical jumping performance in humans by around 10% (Vanezis and Lees 2005). The team at Kagoshima university have used this phenomenon to develop a pendulum jumping machine (Hayashi and Tsujio 2001). By swinging a servomotor actuated arm, the machine is able to make a small vertical jump. A forward jump has been difficult to reproduce with a single pendulum, but a robot with multiple counter-rotating pendulums has successfully climbed small steps.

2.5. Elastomer-based designs

The department of robotics at Ritsumeikan University in Japan has developed a 40 mm diameter tethered deformable robot that can roll and jump using shape memory alloy (SMA) spokes within a soft rubber shell (Sugiyama and Hirai 2004). When a voltage is applied to the SMA spokes they contract, moving the centre of mass of the robot towards the rubber hoop. By controlling which SMA actuators contract and when, the entire robot is able to roll along. The rubber element acting as the tyre for this wheel-like structure is integral to its ability to jump. To jump, the SMA actuators contract on one half of the wheel causing the rubber wheel to buckle. As the SMA actuators begin to extend, the rubber wheel rapidly returns to its original form launching the device into the air as shown in figure 1(*g*). A spherical robot is also being developed to experiment with the possibility of three-dimensional motion.

3. Requirement specification

In addition to the typical engineering requirements, such as manufacturability and cost minimization, several specific requirements for a biomimetic jumping robot are highlighted in table 1, together with their biological justification.

4. New designs

The two designs presented below were developed by the authors of this paper as potential approaches to traversing

irregular terrain. In each case, a novel jumping mechanism has been developed based on the biomimetic design requirements specification given above, although both store energy in their respective forms of metal springs for instantaneous release.

4.1. 'Jollbot'

The main skeletal structure of this robot comes from the metal semi-circular hoops. These hoops are the springs that provide the energy for jumping and make up the outer rolling surface. By compressing the sphere along a central axis joining the nodes/mounting points of the hoops, energy is stored within this outer structure. If this energy is rapidly released then the device will jump in the direction of the axis assuming that there is no slipping at the ground contact point. Direction control of the jump is achieved by adjusting the centre of gravity (CofG) of the device slightly leaning the axis over before launch. A photo and CAD model of the device is shown in figure 2 and the jumping procedure for the device is shown pictorially in figure 3.

Rolling is achieved by orienting the central axis parallel to the ground, and adjusting the centre of gravity of the sphere. Direction control of rolling is possible by moving the centre of gravity out of line with the ground contact area. This is summarized in figure 4. Having an entirely driven outer surface of the device would help it cover uneven terrain and the low ground contact pressure would enable it to traverse soft surfaces such as sand, snow or brush.

The combined jumping and rolling motion results in its name—Jollbot.

4.1.1. Additional requirements. In addition to the general design requirements for an autonomous jumping robot (table 1), the design of this robot considers those requirements relating specifically to rolling, which are shown in table 2.

4.1.2. Design detail. The first design requirement is that the robot must be able to ready itself for a jump using a locally available energy source. Jollbot is powered by a 4.8 V 600 mA h battery pack which supplies two 4.8 V standard model servos and a radio control receiver. The servos,

Table 1. Requirement specification based upon biological inspiration.

Biological inspiration	Design requirement
Animals must eat in order to convert and store the energy required by its muscles for locomotion. The food resources available are generally of a lower than necessary energy density. It was shown in the introduction that power is the performance limiting factor in small jumping animals and insects, for which the specific energy available from muscle contraction alone is insufficient. Power amplification is achieved by operating their muscles at lower than maximum speed, and storing the energy for rapid release.	In order to be fully autonomous, the robot must be able to ready itself for a jump using a locally available energy source.
Different animals store energy in different ways. For example, fleas and leafhoppers store energy in resilin, a rubber-like material, in compression. Larger mammals, such as humans and dogs, store energy in tension in tendons, primarily made from elastin, another material with rubber-like properties. Locusts, however, store their energy in harder skeletal cuticle, in bending.	Energy should be stored somehow, ready for a jump when instantaneous release is required.
Most jumpers have relatively long jumping limbs.	A long leg length (relative to overall robot size) should be chosen for further power amplification.
The large jumping (metathoracic) legs of the locust, for example, are held in the flexed position by a natural catch caused by a belt of tendon becoming hooked around a lump of cuticle (Bennet-Clark 1975, Brown 1967, Heitler 1974). Fleas also rely on a mechanical catch.	A catch mechanism is required to ensure that the robot can remain in the charged condition until its next jump without requiring additional energy to hold it there.
Even the most primitive insects are able to orientate themselves prior to jumping to ensure that they jump away from the ground. Locusts, for example display little or no control on landing, and were frequently observed landing on their heads by one author (Paskins 2007). However, they can quickly find their feet and jump again almost immediately if necessary.	The robot must jump upwards no matter which orientation it lands in.
For an organism to jump, a suitably massive element of its body needs to be accelerated away from the remaining mass. By considering conservation of momentum and neglecting losses, greatest jump height is achieved by maximizing the ratio of the accelerated mass to trailing mass which directly increases take-off velocity.	During jumping, the robot must maximize the ratio of the accelerated mass to trailing mass.
Most animals deliberately jump in the direction that they would like to travel and naturally it would be useful if the robot could do likewise.	The robot must be able to orientate itself prior to jumping.
The additional mass of the required payload would be relatively less detrimental to the peak jump height of larger animals.	The robot must be able to carry a useful payload, such as an environmental sampling device.
In animals, such as humans, it is essential to the preservation of life that delicate organs are protected from excessive impact during locomotion. Connections are not rigid, so forces are damped by these softer tissues. Some animals, such as flying squirrels, are able to glide, enabling them to reduce their landing impact forces aerodynamically.	The robot must be able to carry any sensitive electronic equipment without it sustaining any damage during the jumping and landing cycles.

which have been modified to allow continuous rotation, have integral gearboxes allowing sufficient torque to be developed for storing the jump energy within the hoop springs, and for rotating the slightly off-axis centre of gravity for jump steering and powered rolling control. As jump energy is stored in the hoop springs, it is possible to compress them slowly using a low power source. Jollbot cannot be powered by a locally available energy source as it is currently designed but it may be possible to use photovoltaic cells incorporated into a skin covering the device.

The second requirement states that jump energy should be stored, ready for instantaneous release when required. The metal hoop springs allow energy to be stored in a stable material that is unaffected by stress-relaxation. The spherical form of the robot allows pre-stressed spring elements to be used thus enabling more energy to be stored for a given displacement than would be possible to standard unstressed springs. Jump energy is stored in the hoop springs by a centrally mounted compression mechanism. The compression mechanism sits on a chassis which is fixed to the top or
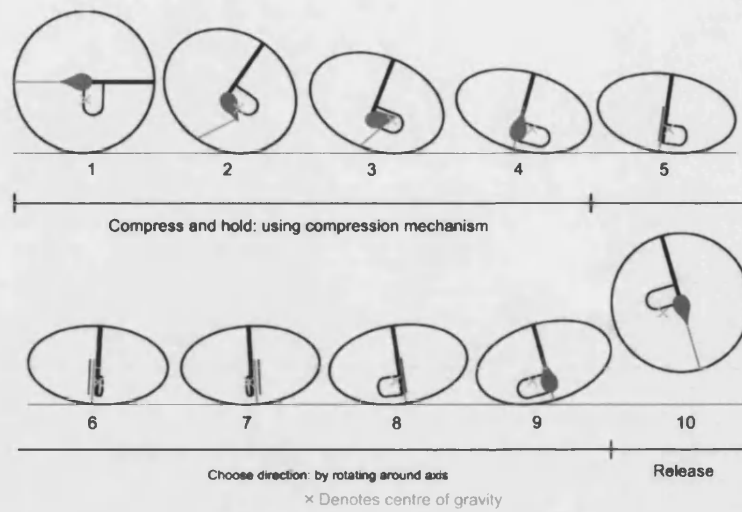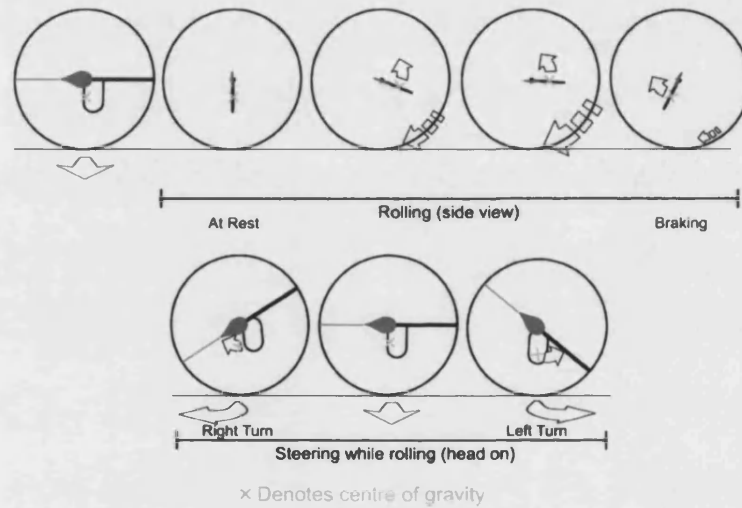
Figure 3. Jumping methodology for Jollbot.

Figure 4. Rolling methodology for Jollbot.

Table 2. Additional design requirements based upon biological rolling.

| Biological inspiration	Design requirement
The Web-toed Salamander (Garcia-Paris and Deban 1995) and Namib Golden Wheel Spider (Henschel 1990) form wheel-like shapes to enable them to roll passively down sloping surfaces more quickly than would be possible by running. Tumbleweed (Antol *et al* 2003) is able to cover many miles of comparatively flat surfaces being driven solely by the wind. The slight bouncing motion caused by its off-centre centre of gravity (CofG) enables it to roll over small obstacles.	Robot should be able to roll passively.
Only two animals are able to 'roll' using their own physiology for power—the Mother-of-Pearl Moth caterpillar (Brackenbury 1997), and the stomatopod shrimp, Nannosquilla decemspinosa, (Caldwell 1979, Full *et al* 1993)—both of which can semi-continuously roll along flat and upward sloping surfaces by adjusting their centre of gravity within a wheel-like form.	Robot should be able to roll actively.
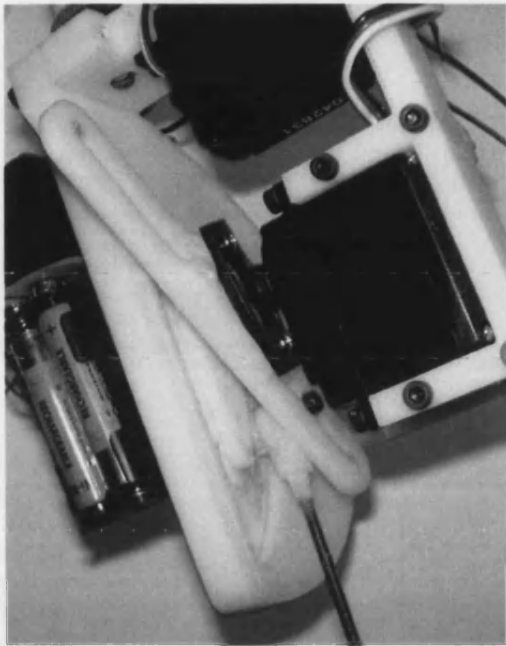
Figure 5. Photograph showing detail of guide, face cam and slider roller in Jollbot.

'head' of the robot, and consists of a model servo rotating a continuously variable length crank connected directly to the 'foot' at the opposing side of the sphere. As the servo rotates, the head and the foot of the robot are pulled together storing energy in the springs.

The variable length crank mechanism was developed after initial testing with a simple fixed length crank with an over running one-way clutch mechanism. To maximize the stored energy, the compression system, powered by a constant-torque motor, should adapt to the required compression force. As the hoop springs are compressed, the force required increases with

displacement. Therefore, when using a fixed length crank the required rotary torque increases as the deflection increases. By introducing a crank that varies in length as it rotates, the output force can vary while the input torque remains constant. This has been achieved by using a guide, face cam and slider roller as shown in figure 5. This revised mechanism outperformed the fixed length crank mechanism since it is able to compress more hoop spring elements using the same model servo. Unfortunately, the mechanism substantially increased the overall weight of the device; however, it is not yet fully optimized.

As the motor rotates the guide, the face cam ensures the slider roller moves in a specified path and therefore at a variable crank length around the servo axle. The face cam was designed to be replaceable for tuning purposes. The cam that finally worked the best kept the slider roller at a constant radius for a short time slowly compressing the sphere. As the guide rotates towards 90°, the radius of the cam reduces slightly, and between 90° and 180° rotation the radius reduces further to ease the loading on the motor. As soon as the 180° position is reached, the slider roller is free to move in the axial direction because of the cam profile and the slot along the guide. This straight axial release of the spring energy ensures that none is wasted unnecessarily as would be the case with a rotating fixed length crank. The guide then continues to rotate beginning another energy storage phase. Figure 6 shows a pictorial representation of the compression phase of Jollbot, illustrating how the crank length continuously varies throughout the rotation of the servo. This whole process takes 1.44 s which is comparatively slow compared to the release phase which takes only 0.24 s as shown in figure 7.

The third requirement relates to maximizing leg length to further improve power amplification. Although Jollbot has no 'legs' in the traditional sense, the effective leg length is approximately one quarter of the diameter of the sphere since that is the length through which the robot travels before takeoff. With optimization, it should be possible to increase this length to around half the diameter of the sphere but without
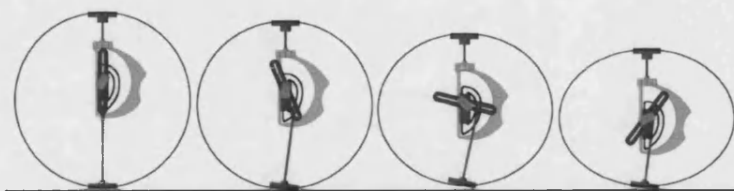

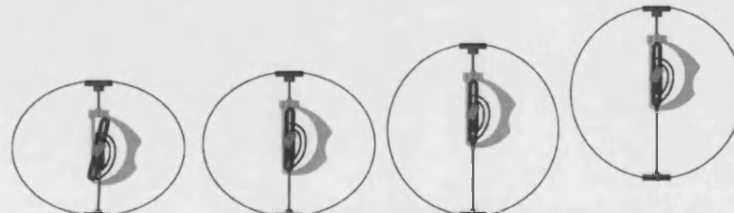**Figure 6.** Pictorial representation of the compression phase of Jollbot.

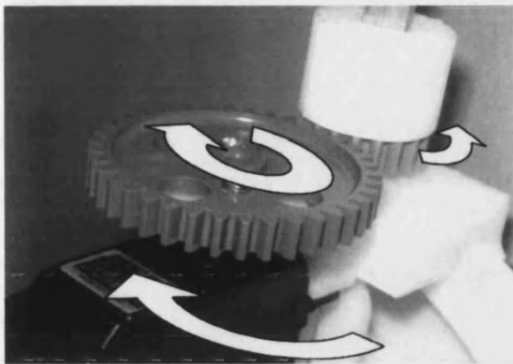**Figure 7.** Pictorial representation of the jumping phase of Jollbot.

Figure 8. Jollbot jump direction and rolling mechanism.

significant re-design of the compression mechanism, this 'leg' length cannot be increased further.

The fourth design requirement states that a catch mechanism is required to ensure that the robot can remain charged until its next jump without requiring additional energy to hold it in that position. Jollbot has a simple catch mechanism which relies on an unstable equilibrium point at complete compression and just before release. With the current manual remote control system, it proved very difficult to stop the mechanism at the required point on the cam.

The fifth design requirement says that the robot must jump upwards no matter which orientation it lands in. This is only achievable with careful control and positioning of the centre of gravity within the spherical shape of Jollbot. The centre of gravity was estimated by suspending the device on threads secured at various points. The CofG is inline and below the thread, so by combining images of the device hanging in different orientations the CofG can be found. In its current iteration, Jollbot's centre of gravity lies slightly towards the

'head' of the robot which results in toppling upon landing, from which it is not possible to recover. If the centre of gravity was slightly below the equator line, perhaps by adjusting the position of the battery pack, then Jollbot would always roll onto its 'foot' after a successful jump.

The sixth requirement states that the ratio of accelerated mass to trailing mass should be maximized. This is achieved by attaching the relatively heavy main chassis, consisting of the compression and steering mechanisms and motors, directly to the head of the robot.

The seventh design requirement relates to the direction control of jumps. By releasing jump energy at an angle to the vertical, it should be possible for Jollbot to make projectile jumps. Jump direction is controlled by rotating the slightly off-axis centre of gravity around the head-foot axis using a second model servo. The servo is mounted onto the main chassis and drives itself around a gear fixed to the spherical shell of the robot as displayed in figure 8. This enables the entire central chassis and its associated components to twist, adjusting the centre of gravity and therefore the lean of the main jumping axis. The semi-spherical form of the foot and hoop springs when compressed allows the robot to lean in any direction as shown in the video stills in figure 9. Full testing of this jump steering mechanism was not undertaken since it proved difficult to control both servos accurately to ensure the 'compress and hold', 'choose direction' and 'release' stages occurred in series. The absence of a stable catch, as discussed above, was the main contributing factor.

This same jump steering mechanism is also intended as the powered rolling mechanism for travelling along level surfaces, over small obstacles, and even up sloped surfaces. Since the centre of gravity does not lie exactly along the head-foot axis, rotating the chassis around the axis should move the centre of gravity outside the area of contact of the hoop springs with the ground. This mechanism did not perform as anticipated since the area of contact was too large with the few hoop springs
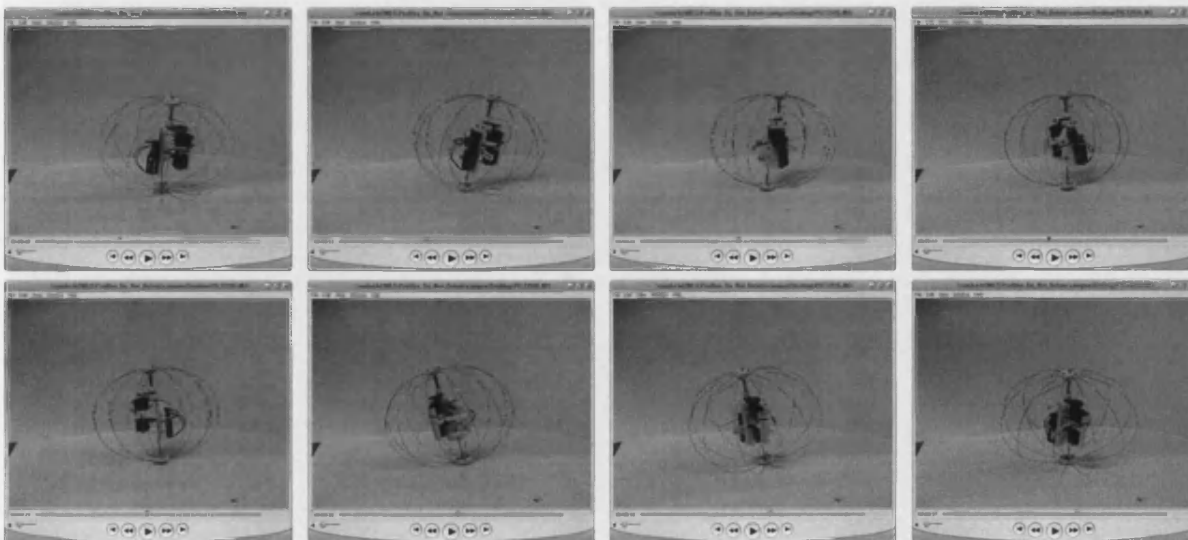

Figure 9. The jump direction control of Jollbot.

on the device. The axial location of the centre of gravity also meant that keeping the axis horizontal for rolling was very difficult.

The presented Jollbot device does not have any provision for direction control whilst rolling because steady-state rolling was initially more important. Tilting the internal axis from its normal horizontal position would cause the robot to lean over and make gentle turns in the direction of the axis tilt.

Due to the spherical shape of the robot, Jollbot will passively roll down surfaces, and bounce off obstacles, particularly after a jump. The spherical form also ensures that there are no body extremities that can get caught on obstacles. The springs on its outer surface will also absorb much of the impact energy from collisions and landing, thus protecting sensitive equipment from damage. However, if the robot were to land directly on its 'head' then the chassis would take much of the impact force but it is felt that that would be an uncommon occurrence. If the robot were covered with a suitable skin, then complete environmental protection may be achievable for all internal components. These internal components would include the electronics and control system required for autonomy consisting of elements such as position and ranging sensors, a vision system, environmental energy recovery system, data logging or transmitting equipment, amongst others. A stable non-rolling platform is possible at the transition between rolling locomotion and a jumping one for assessment of the area surrounding the robot. Jollbot could carry additional payloads with an expected reduction in jumping performance, but it has the benefit that they will be enclosed within a safe structure.

4.1.3. Robot performance. In order to measure the jumping performance of the robot, a Redlake Images Motionscope high-speed camera was used to film each jump at pre-selected frame rate. Scion Image (useful internet freeware that can handle sequences of images, and output the pixel coordinates of all the points clicked on by a user in order, www.scioncorp.com) was used to determine the height of the different components of the robot in each frame. In order for this method to be valid, the robot was always placed such that it jumped in the plane parallel to the camera lens, and both a horizontal and a vertical calibration performed using graduated markers.

The jumping performance of the 0.3 m diameter Jollbot is illustrated in the high speed camera images in figure 10 taken at a rate of 50 Hz. From the images, it was determined that the robot raises its centre of gravity by 218 mm through the course of the jump, which is approximately 2/3 its entire height. It can clear a height of 184 mm.

The efficiency of various mechanisms within the robot can be determined by comparing the energy of the device in different states. A comparison between the electrical energy consumed and the energy stored within the system gives a conversion efficiency for the compression mechanism. Comparing the energy stored with the potential energy of the robot at peak height illustrates the efficiency of the release mechanism.
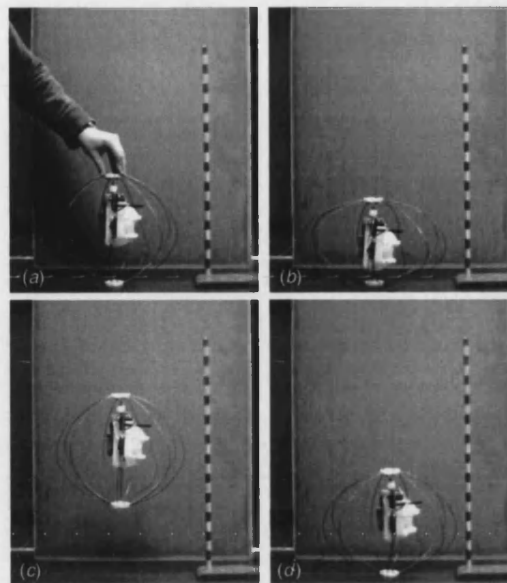

Figure 10. High speed camera images illustrating the jumping performance of Jollbot: (*a*) resting state of Jollbot, diameter = 294 mm, (*b*) 1.44 s later, Jollbot is ready to jump after compressing 65 mm, (*c*) 0.24 s later, Jollbot is at its peak jump height, clearing 184 mm, (*d*) 0.22 s later Jollbot hits the ground and absorbs impact energy in the slight compressing of the sphere.

The electrical energy consumed is found from (9):

electrical energy(J) = voltage(V) × current(A) × time(s).

$$(9)$$

The potential energy stored in the jumping system is equivalent to the area under a force-displacement curve.

The potential energy stored in a mass suspended at a height is defined in (10) where; m = mass (kg), g = acceleration due to gravity (m s^{-2}), h = change in height of CofG (m).

$$PE = mgh. \qquad (10)$$

In Jollbot's case, the servo draws a peak current of ~1.2 A from the 4.8 V battery pack over the 1.44 s compression. From (9), this gives a total energy consumption of 8.3 J. Since the current increased throughout the compression, it is felt that this is far larger than the actual energy consumption and logging of the current values throughout the short compression time would give a more accurate value.

The energy stored within the robot's spring system was estimated from the area under a force displacement curve produced through testing on an Instron compression testing machine. This resulted in approximately 1.1 J of stored energy.

The potential energy of the device was determined using (10), where the mass of the robot is 0.465 kg and the change in height of the CofG is 0.218 m. This results in 1 J of potential energy.

Comparing the first two energy measurements with one another, results in a conversion efficiency of 14% for the compression mechanism. Comparing the second two energy measurements results in a mechanism release efficiency of 91%.

Table 3. Additional design requirements based upon biological gliding.

| Biological Inspiration	Design Requirement
Flying squirrels have been observed to fully abduct their limbs during take-off, deploying their gliding membranes, patagia, in the process. This behaviour occurred even during leaps when it was demonstrated that the squirrels achieved no resultant advantage in landing altitude (Paskins *et al* 2007).	The robot should have membranous wings to enable gliding, and these should deploy automatically and fully during take-off.
Flying squirrels choose to pitch upwards immediately prior to landing, rapidly increasing their angle of attack in order to reduce impact forces (Paskins *et al* 2007). Likewise, flying fish deliberately employ air braking to slow themselves down prior to re-entering the water, by positioning their pelvic fins forwards, and angled against the motion (Davenport 1994).	The robot should have the ability to control its angle of attack during the gliding phase to enable effective air braking as it lands.
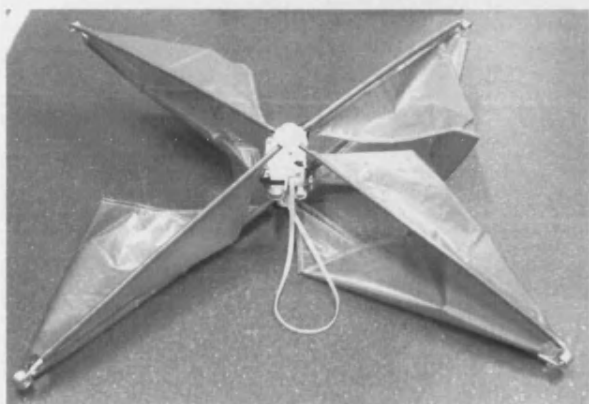
Figure 11. Photograph of Glumper winding itself in, taken immediately prior to take-off.

4.2. 'Glumper'

The concept behind Glumper was for a robot which would jump and then glide, in the hope that this would simultaneously extend range and reduce impact forces. As such, two further biomimetic requirements specifications are shown in table 3 as they are only relevant to Glumper.

The photograph of Glumper (figure 11) shows its four long legs, each with a torsion spring 'knee' at its midpoint, distributed perpendicularly between a 'head' and a 'foot'. A triangular shaped membrane mounted between each leg element and along the axis of the robot acts as its gliding wings. By way of introduction to some of the more complex

design solutions, an overview of the discrete steps required for Glumper to jump is given in figure 12.

4.2.1. Design detail. The first requirement specified for this robot was that it must be able to ready itself for a jump using a locally available energy source. Small motors can still generate relatively high torques with sufficient gearing, which is ideal for autonomous applications where the time taken to charge the jumping mechanism is of secondary importance to the maximum achievable performance. Next it was specified that energy should be stored somehow and instantaneously released into a jump. Although elastomers have the capacity to store a lot of energy, this property is severely affected by temperature and time. In the loaded state, energy is lost with time due to stress–relaxation and at cold temperatures, rubber-like materials become hard and brittle, causing them to fail before much energy has been absorbed. The time taken to charge the robot is likely to be long, and extreme environments present the most useful applications for a jumping robot, so storing energy in bending should provide a more suitable approach. Therefore, Glumper stores energy in the compression of four heavy-duty torsion springs, made from $3\frac{3}{4}$ turns of 4 mm diameter spring steel rod, which are mounted in the knee-like hinge-joints of its four legs.

A long leg length (relative to overall robot size) was specified to amplify the power produced by releasing these compressed torsion springs. Glumper's legs are each made from two hinged carbon-fibre reinforced plastic (CFRP) rods, 0.5 m long and with very high specific stiffness so that they almost fully compress the torsion springs without bending themselves. If it required less force to bend the legs than to
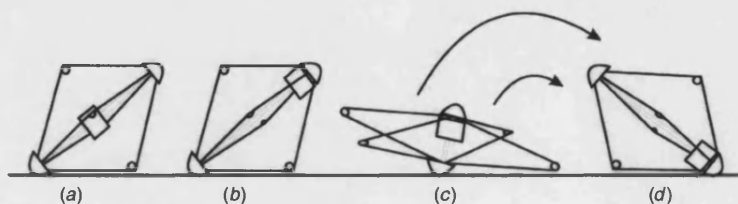
Figure 12. A sketch to introduce the steps required for compression and release of Glumper, showing (*a*) a mechanism is freely suspended on a cord between the head and the foot, which can wind in the cord to compress the robot. (*b*) This compression mechanism can be attached to whichever end of the robot is uppermost. (*c*) When the robot becomes fully compressed a clutch releases the cord and the robot jumps upwards. (*d*) After landing the clutch requires resetting and the process can repeat. The gliding membranes are omitted for clarity.

Figure 13. (*a*) Photo of the capstan shaft assembly, showing how it is driven by locating bolts through the drive gear on the left of the image, and the compression spring against which it can be released by pulling on this stepped shaft. (*b*) Rendering from Solid Edge v.17 of the control box showing the hinged lever (the darkest shaded component) and its retaining clip beneath (highlighted in a slightly lighter shade). So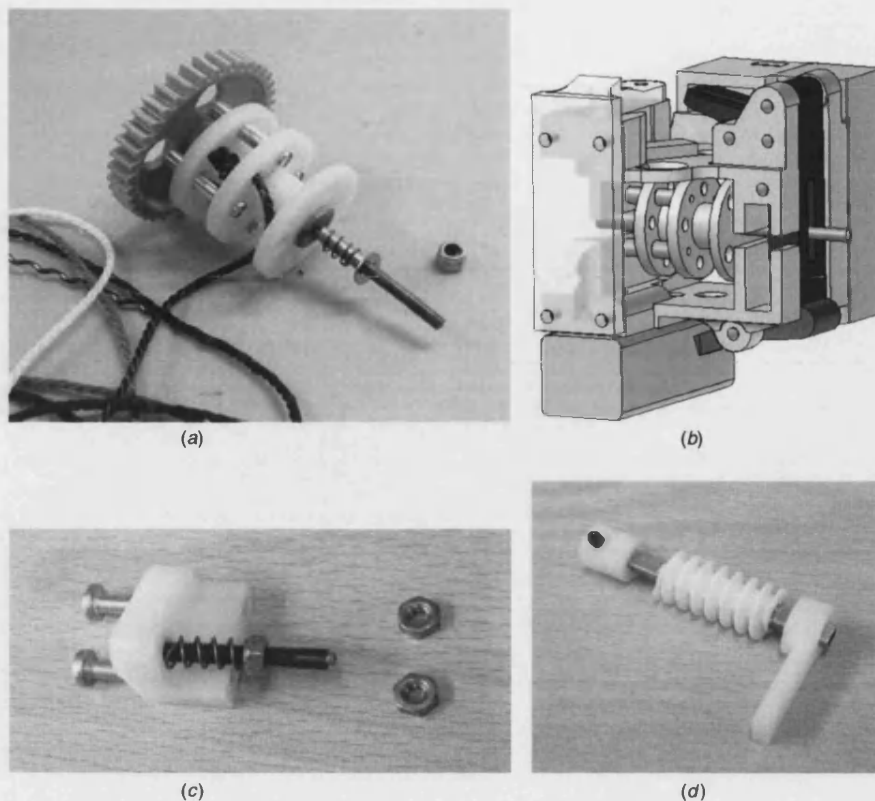me components, such as the bi-stable mechanism and the gears have been omitted for clarity. (*c*) The bi-stable mechanism, consisting of a compression spring, a nut and bolt with a hemispherical end. (*d*) The worm gear sits on a brass square-section drive shaft, but is free to move along the axis such that rotation in one direction pushes the follower (shown on the right of the image) and the reverse direction turns the capstan driving gear shown in (*b*).

compress the springs, the total energy stored would be less once the robot had reached full compression.

The mechanism to allow steady compression and rapid release of Glumper is comparable to a dog clutch. A capstan gradually winds in a loop of cord which passes through both ends of the robot in order to compress it. The capstan is free to rotate on the narrow section of a stepped shaft, between the step and a circlip. Normally a compression spring on the shaft pushes against the circlip to keep some protruding rods from the capstan engaged with corresponding holes in its drive gear (which sits on the thicker section of the same shaft). Thus the capstan can be disengaged by linear actuation of the shaft, allowing the cord to unwind rapidly under the tension of the compressed robot. The capstan drive gear is turned by a worm gear that is forced to rotate by a small motor, but is free to float axially between two points to perform a secondary function that will be discussed shortly. Another advantage of using a worm gear to drive the capstan is that, in the event of power loss, the robot will remain in its partially compressed position because the stored energy does not act directly against the motor stall torque. Such a design is essential for irregular power sources such as solar cells.

The friction acting against the required linear movement of the stepped shaft to push the capstan away from the drive gear is very high when the robot is highly compressed, such that separate linear actuation required for release would need high power. To avoid that problem, a hinged lever automatically pulls the shaft outwards to release the dog clutch when both ends of the robot are pulled in against the control box. Figure 13(*b*) shows a view of the partially complete control box to illustrate how the vertically compressing robot can pull the capstan shaft only when a release latch is moved away from the end of the hinged lever (both components are highlighted in the figure using dark shades). An M3 lock nut must be fitted on the capstan shaft (in order for it to move at all when the hinged lever is depressed), and the position of this nut allows full adjustment of the resultant linear movement of the shaft. A bi-stable mechanism on the hinged lever was necessary to prevent premature re-engagement of the capstan before it is fully unwound. This is due to the compression spring on the capstan shaft. A hemisphere is held protruding into a hole in the side of the closed hinged lever by a stiffer compression spring, such that moving the lever requires significant initial force but once overcome, it

moves quickly to the fully open position, being held there by the returning hemisphere. This hemisphere was achieved rather crudely by depositing a solder blob on a sawn off M3 bolt, as shown in figure 13(c).

After a jump, the hinged lever needs to be reset in order that winding can be restarted. This is achieved without the need for a separate motor thanks to the ability of Glumper's worm gear to slide along its driveshaft between two physical stops depending on which direction it is driven in. Driving the shaft in one direction causes the worm gear to inch itself along the teeth of the driven gear until it reaches the motor output shaft, after which continued rotation turns the driven gear and hence the capstan. By reversing the direction of the motor, the worm inches itself back along the teeth of the driven gear away from the motor, pushing a recessed follower as it travels. This is guided towards the hinged lever and on contact, this has sufficient force to flip it back past the bi-stable catch ready for the next jump. This 'sliding worm' design requires high friction on the gear driven by the worm, which is achieved by mounting it fairly tightly against the side wall of the control box.

An important advantage of Glumper's design is that any potential payload will not be rigidly connected to the extremities of the robot. By choosing a suitable cord length, it will be slack when released at takeoff, so the time of action of the landing force on the control box increases, and hence the total impulse is lower. Thus the risk of damage to any sensitive electronic equipment within the control box is reduced during the repeated jumping and landing cycles.

This research required a robot with membranous wings to enable gliding, which should deploy automatically and fully during take-off. Deployment of the gliding membranes during take-off avoids any complications that would otherwise be caused by the need to conserve angular momentum in mid-air. Glumper naturally adopts this behaviour because it has four triangular-shaped rip-stop nylon membranes spanning the gap between its legs and the mid-line between the head and foot. The robot should have the ability to control its angle of attack during the gliding phase to enable effective air braking as it lands. The mass of Glumper's compression mechanism is localized in a box which is free to move between its head and foot, so the pitch angle can be controlled by incorporating an additional motor. This drives a pulley quickly along a toothed belt, loosely attached between the head and foot of the robot, thus moving the centre of mass either forwards or backwards during gliding flight depending on motor direction. This design also enables the control box to attach itself to whichever of the two ends of the robot is uppermost in between jumps, so the robot can jump upwards no matter which orientation it lands in, and the ratio of accelerated mass to trailing mass is maximized.

The requirement that the robot must be able to orientate itself prior to jumping could be achieved by rotating an eccentric mass, such as the battery pack, around the control box. The slight protrusion of the head/foot from the legs means that this rotation should cause the centre of mass to shift sufficiently to rock Glumper from a stable position resting on one pair of legs to a stable position on another, but unfortunately no such mechanism has yet been developed.

Although an autonomous control system has not yet been developed, only the direction of Glumper's two lightweight, low power dc motors would need to be controlled at present, and this could be achieved by using a small number of sensory inputs. Ultimately this control system would need to be expanded to include direction control and decision making.

4.2.2. Robot performance.
In vertical jump tests, the average change in Glumper's estimated centre of mass between the pre-launch state and the peak height is 1.6 m ($n = 4$, SD = 0.07 m) and its peak clearance height averages 1.17 m ($n = 4$, SD = 0.07 m). In order to determine the efficiency of Glumper's energy storage and release mechanism, the force required to fully compress Glumper was measured using an Instron compression testing machine. From the area under the resulting force–displacement curve, it is estimated that Glumper is able to store 21.5 J of energy. If the launch mechanism was 100% efficient, the maximum height that Glumper could reach can be predicted by assuming that all this energy would be converted to potential energy at the peak of a vertical jump. The total weight of Glumper during testing was 700 g, so a hypothetical vertical increase in the height of its centre of gravity of 3.1 m should be possible, meaning that its energy storage and release mechanism is actually only 52% efficient.

A multi-meter was used to measure the current drawn by Glumper every 30 s during its compression and release. The total time for wind-in using its two rechargeable lithium ion cells (wired in series with an operating voltage of 8 V) is 435 s. The current rises steadily, rising sharply just before take-off when it reaches 0.4 A, equivalent to a peak electrical power requirement of 3.2 W. Solar power is an example of a locally available energy resource for many potential robot applications. On Earth the Sun's radiation is diffused and scattered by the environmental conditions, reducing the maximum power delivered from the 1370 W m^{-2} available in space at the radius of the Earth's orbit. Photon Technologies Powerfilm® flexible solar modules are specified as generating 0.15 W each of power in bright sunlight for a panel of 15 × 3 cm (Photon Technologies, Colorado Springs, CO, USA). Their flexibility, low weight and size would make them ideally suitable for mounting on Glumper's membrane wings. Importantly, only two wings could ever be directly pointing at the sun irrespective of robot orientation, which is enough area for 45 panels. Hence, a maximum power of 6.75 W is theoretically available and Glumper's control mechanism thus satisfies the requirement that it should be able to ready itself for a jump using a locally available energy source. By plotting the electrical power against time, the total electrical energy required to power a jump (the area under this curve) was estimated to be 80.5 J. Therefore, the efficiency of the conversion of electrical energy into strain storage energy is approximately 3.3%, with some of this deficit clearly being converted into heat.

The effect of reducing mass on jump height was demonstrated in an experiment using the Glumper robot without its control box. The mass of this structure including the foot, legs and springs was 375 g. Various weights were added
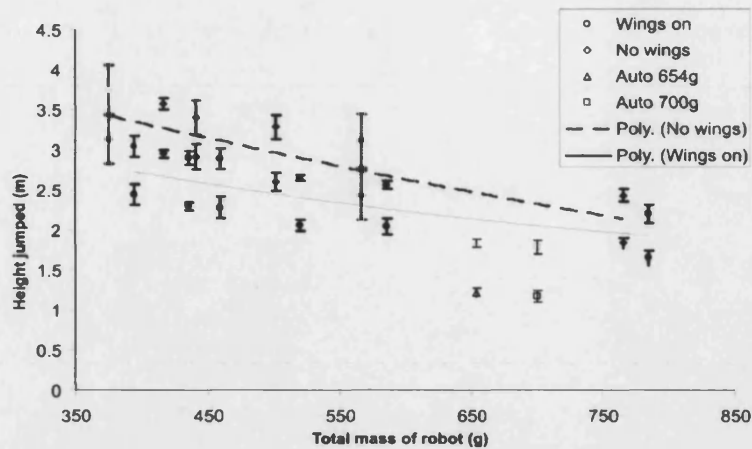
Figure 14. Graph showing that adding mass to Glumper's basic frame reduces its peak clearance height both with and without its wings attached. The graph was produced by measuring the peak height of both the head and foot of the robot repeatedly for every given condition, and plotting the average values. Microsoft Excel was used to plot a polynomial trendline through the centre of these head and foot points for both the winged and non-winged measurements, and the respective equations of the resulting curves are displayed. The average height of Glumper's head and foot for automatic launches is shown for comparison, powered by one (654 g) and then with two onboard lithium cells (700 g). The error bars represent ± 1 standard deviation from the means in all cases.
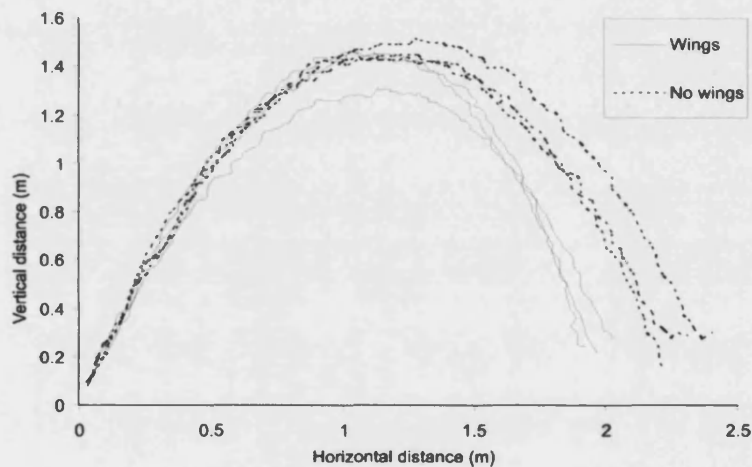

Figure 15. Graph showing the trajectories followed by Glumper's centre position when launched automatically at an angle of 63° to the horizontal, with and without its membranous wings.

to its head before manually compressing it and launching it vertically. A ruler was used to ensure that the robot was always compressed such that there was a 10 cm gap between the head and the foot, which is equivalent to how much it compresses when launched by its automatic launch mechanism. The results are shown graphically in figure 14, and it can be seen that the optimum total mass of the robot would be less than its current frame weight. No momentum advantage would be gained by adding mass to the current control box to improve the ratio of accelerated to trailing mass of the robot. Glumper's total mass was 700 g, including its four wings, which in total weigh 19 g. One of the initial requirements was that the jumping robot must be able to carry a useful payload, such as a camera and transmitter for example. Figure 14 demonstrates that it should be able to absorb the additional weight of the

example payload, perhaps 50 g, without a large decrease in jump height.

It can be seen from figure 14 that more energy is lost when Glumper launches itself automatically, which is likely due to friction as the cord unwinds from the capstan. It is also clear that the wings cause a reduction in peak jump height, presumably owing to air resistance.

Figure 15 shows the trajectories followed by Glumper's centre position during six jumps launched automatically at an angle of 63° to the horizontal, three with and three without its membranous wings attached. The presence of the wings actually reduces the total range of the jump rather than extending it as was intended. This might change with weight reduction, which should simultaneously improve peak jump height and the lift to drag ratio during gliding. However, the

reverse may also be true because air resistance against the wings would also be relatively more effective acting against the ascending robot. Unfortunately it has not been possible to test the effect of altering Glumper's pitch angle, while gliding, to the resultant trajectory because a suitable control system was never developed, and the flight time was typically short prohibiting remote control.

5. Discussion

Table 4 compares the performance data of Jollbot and Glumper with equivalent data for the existing jumping robots introduced previously in order to facilitate the evaluation of the two new designs. The maximum jump height for each robot is assumed to be the change in height of its centre of gravity between the pre-launch state and its peak height. It is important to consider that the other robots were not developed using the biologically inspired design specification presented in this paper and may have had other objectives.

The definition of the performance of a jumping robot depends entirely on the specific requirements of an application. Here we have chosen to evaluate the robots above based on a space exploration application no matter their actual intended application. Surface exploration of other planets requires that the robot is able to move across rough terrain, so the robot should jump over the largest possible obstacle, whilst also being of the smallest possible volume to ensure that it takes up as little room as possible in the launch craft. Being of small size also means that many can be sent in place of a larger exploration rover, or that one robot could be used in conjunction with other exploration devices.

Figure 16 is adapted from (Bennet-Clark 1977) and shows jump height against object length for all of the robots reviewed including some data on animals for comparison. An assumption is made that all animals and robots presented here can only accelerate through a distance equal to their leg length. Owing to the fact that all the animals and robots presented here have similar aspect ratios, body length becomes an acceptable measure of both leg length and object size. The horizontal lines show energy density and the sloping lines are a measure of power per unit weight, derived from (8). The power to weight ratio of direct muscle action in animals has a practical limit of 100 W kg^{-1} (Bennet-Clark 1977). Hence, all the animals above that line in figure 16 are producing more power than their muscles can deliver, indicating some additional energy storage mechanism.

Optimal performance of a jumping robot for use in planetary exploration was declared to require maximization of height together with minimization of mass and volume to reduce the cost of space transport. Considering figure 16, the closer the robot sits to the top left corner of the chart, the better. This is equivalent to a maximization of power density, represented by the diagonal lines, which is consistent with the statement in the introduction that decreasing size demands increased power to achieve equivalent height.

Glumper achieves a superior power density to Jollbot. The power density of approximately 20 W kg^{-1} achieved by Jollbot is also inferior to that of all the natural examples displayed.
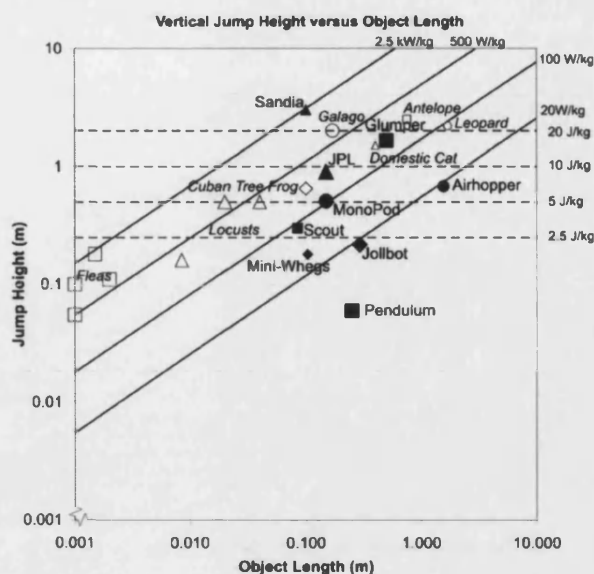

Figure 16. Height of jump versus length of a selection of animals (outlined markers) and robots (solid markers). The graph also shows required specific energy and specific power required to produce a jump assuming that the objects accelerate through their own body length and that there is no air resistance.

Looking parallel to the lines of power density in figure 4, Glumper has comparable performance to the animals that would not be considered to be specialized jumpers, sitting directly between the domestic cat and the antelope. The jump heights recorded by specialized jumpers, such as fleas, frogs and the lesser galago all demonstrate a superior power density.

In terms of both power density and energy density, Glumper outperforms all the documented jumping robots in figure 16 with the exception of the Sandia robot, which is propelled by the combustion of propane. This superior performance would be expected because the energy density of hydrocarbons is much higher than that of springs, and the authors can think of no comparable biological transport modes. The use of combustion to power jumps was not considered in this research, due to the primary requirement of autonomy. Other potential applications are also prohibited by this design. In confined areas, for example, exhaust gases could pose a problem and on other planets, the lack of oxygen in the atmosphere would prevent the burning of fuel (though high explosives could obviously be used). Springs are the next best energy storage medium, because the robots with either helical or bending springs, including Glumper and Jollbot, outperform the remaining devices. This does not even take into account that those devices, Airhopper, Pendulum and Deformable all rely on external power giving them an immediate weight advantage. It is also clear from figure 16 that Jollbot was outperformed by other robots with equivalent energy storage mediums. It is not clear from this sample whether one type of metal spring consistently outperforms any other although no difference was expected. The only elastomer-based jumping robot does not jump particularly high, but the absence of other published devices storing energy

Table 4. Robot details and jumping capability.

Robot	Energy storage medium	Jump height (m)	Jump distance (m)	Weight (kg)	Size $L \times W \times H$ (m)	Control	Power source	Jump steering method
JPL Hopper (V2)	Metal helical spring	0.9	2	1.3	$0.15 \times 0.15 \times 0.15$	Radio controlled	Onboard batteries	Rotating foot
Monopod	Metal helical spring	0.51	0.305	2.4	$0.15 \times 0.2 \times 0.3$	Autonomous (from IR sensors)	Onboard batteries	Rotating foot
Jumping Mini Whegs	Metal helical spring	0.18	Not known	0.191	$0.10 \times 0.08 \times 0.05$	Radio controlled	Onboard batteries	Turning robot before launch
Sandia	Fluid powered	3	3	2.5	$0.1 \times 0.1 \times 0.2$	Follows built-in compass	Liquid propane	Moving centre of gravity
Airhopper	Fluid powered	0.68	0	20	$1.5 \times 1.1 \times 0.5$	Remotely controlled via cable tether	External compressed air supply	(Not possible unless legs 'walk')
Pendulum	Momentum	0.06	0	0.72	$0.25 \times 0.1 \times 0.25$	Remotely controlled via cable tether	$\sim$9 V power supply	No steering possible
Deformable	Elastomer	0.08	0	0.003	$0.04 \times 0.02 \times 0.04$	Remotely controlled via cable tether	External power supply	(Not possible unless spherical)
Scout	Metal bending spring	0.3	0.25	0.2	$0.09 \times 0.11 \times 0.05$	Radio controlled	Onboard batteries	Turning robot before launch
Jollbot	Metal bending spring	0.218	0	0.465	$0.3 \times 0.3 \times 0.3$	Radio controlled	Onboard batteries	Moving centre of gravity
Glumper	Metal bending spring	1.6	2	0.7	$0.5 \times 0.5 \times 0.5$	Manually activated	Onboard batteries	Not implemented

in elastomers was unexpected. This may be due to the gradual loss of energy resulting from stress relaxation during the pause inherent in a pause-and-leap robot.

Power density can be increased by either increasing power or reducing mass. More power can be produced by generating higher force or reducing its time of action over a given distance. In animals this is limited by the maximum power output of muscle resulting in the use of energy storage. Therefore the performance limiting factor for a jumping robot is its energy storage and release mechanism. The mass reduction experiment conducted on the Glumper robot demonstrates clearly the advantage of reducing unnecessary weight. It is possible to eliminate mass from engineering systems through optimization techniques such as FEA and by changing materials, whereas nature's jumpers are already highly optimized as a result of natural selection. The Sandia robot has already proved that it is possible to outperform nature's jumpers by using a hydrocarbon-based energy storage and release mechanism, which requires the use of high performance materials in its construction. Such materials are unavailable to natural organisms due to other practical constraints, such as reproduction.

6. Future work

It has been shown that the clearance height of the robots in development by the authors could be improved by weight reduction, increasing the force or reducing its time of action.

In the case of Jollbot, although its performance could be improved by optimization of the component materials, it is probable that the performance of this evolution of Jollbot is limited by the design of its compression mechanism, which is unable to produce more force. Specifically, a revised mechanism is being designed to provide greater force and allow for greater compression of the springs. Jumping force will be improved by changing to glass-fibre springs. The poor rolling performance will be improved through the development of a new system allowing for more movement of the centre of gravity of the robot.

Significant size reduction of Glumper's control box is intended by selecting materials with higher specific strength and stiffness. This has the two-fold advantage of weight reduction, and allows additional compression of the robot body so that more energy is stored before release. Clearance height could also potentially be improved by adjusting the attitude of the robot in much the same way as a human high-jumper chooses to pass the bar horizontally. Finally, flexible solar panels should be added to see if the compression mechanism can be powered by these directly, and hence the relatively large mass of the batteries could potentially be removed.

Note. Additional videos and colour images of Jollbot and Glumper are available from the online version of this journal.

Acknowledgment

References

Alexander R M 1974 Mechanics of jumping by a dog Canis-familiaris *J. Zool.* **173** 549–73
Alexander R M and Vernon A 1975 The mechanics of hopping by kangaroos (Macropodidae) *J. Zool.* **177** 265–303
Allison J 2002 *Monopod Jumping Robot* (Salt Lake City, UT: University of Utah)
Altendorfer R, Moore N, Komsuoglu H, Buehler M, Brown H B, Mcmordie D, Saranli U, Full R and Koditschek D E 2001 Rhex: a biologically inspired hexapod runner *Auton. Robots* **11** 207
Antol J, Calhoun P, Flick J, Hajos G, Kolacinski R, Minton D, Owens R and Parker J 2003 Low cost Mars surface exploration: The Mars Tumbleweed *NASA Report* NASA/TM-2003-212411
Bennet-Clark H C 1975 The energetics of the jump of The Locust Schistocerca Gregaria *J. Exp. Biol.* **63** 53–83
Bennet-Clark H C 1976 Energy storage in jumping animals *Perspectives in Experimental Biology* ed P Spencer Davies (Oxford: Pergamon)
Bennet-Clark H C 1977 Scale effects in jumping animals *Scale Effects in Animal Locomotion* ed T J Pedley (London: Academic)
Bennet-Clark H C and Lucey E C A 1967 The jump of the flea: a study of the energetics and a model of the mechanism *J. Exp. Biol.* **47** 59–76
Brackenbury J 1997 Caterpillar kinematics *Nature* **390** 453
Brackenbury J and Hunt H 1993 Jumping in springtails—mechanism and dynamics *J. Zool.* **229** 217–36
Brown B and Zeglin G 1998 The Bow Leg Hopping Robot *IEEE Int. Conf. on Robotics And Automation (Leuven, Belgium)*
Brown R H J 1967 Mechanism of locust jumping *Nature* **214** 939
Burrows M 2003 Froghopper insects leap to new heights *Nature* **424** 509
Caldwell R L 1979 A unique form of locomotion in a stomatopod—backward somersaulting *Nature* **282** 71–3
Davenport J 1994 How and why do flying fish fly *Rev. Fish Biol. Fisheries* **4** 184–214
Estier T, Crausaz Y, Merminod B, Lauria M, Piguet R and Siegwart R 2000 An innovative space rover with extended climbing alilities *Proc. Space and Robotics 2000 (Albuquerque, NM)*
Evans M E G 1973 The jump of the click beetle (Coleoptera : Elateridae)—energetics and mechanics *J. Zool.* **169** 181–94
Fiorini P and Burdick J 2003 The development of hopping capabilities for small robots *Auton. Robots* **14** 239–54
Full R, Earls K, Wong M and Caldwell R 1993 Locomotion like a wheel? *Nature* **365** 495
Gabriel J M 1984 The effect of animal design on jumping performance *J. Zool.* **204** 533–9
Garcia-Paris M and Deban S M 1995 A novel antipredator mechanism in Salamanders: rolling escape in hydromantes platycephalus *J. Herpetol.* **29** 149–51
Hale E, Schara N, Burdick J and Fiorini P 2000 A minimally actuated hopping rover for exploration of celestial bodies *Proc. 2000 IEEE Int. Conf. Robotics & Automation (San Fransisco, CA)*
Hayashi R and Tsujio S 2001 High-performance jumping movements by pendulum-type jumping machines *Proc. IEEE/RSJ—Int. Conf. Intelligent Robots And Systems (Maui, HI)*
Heitler W J 1974 Locust jump—specializations of metathoracic femoral-tibial joint *J. Comp. Physiol.* **89** 93–104
Henschel J R J 1990 Spiders wheel to escape *South African J. Sci.* **86** 151–2
Hill A V 1950 The dimensions of animals and their muscular dynamics *Sci. Prog.* **38** 209–30
Kaspari M and Weiser M D 1999 The size-grain hypothesis and interspecific scaling in ants *Func. Ecol.* **13** 530–8

Kikuchi F, Ota Y and Hirose S 2003 Basic performance experiments for jumping quadruped *Proc. 2003 IEEE/RSJ Int. Conf. Intelligent Robots And Systems (Las Vagas, NV)*

Liu J J 2005 Analysis of stairs-climbing ability for a tracked reconfigurable modular robot *Proc. 2005 IEEE Int. Workshop on Safety, Security and Rescue Robotics*

Morrey J M, Lambrecht B, Horchler A D, Ritzmann R E and Quinn R D 2003 Highly mobile and robust small quadruped robots *IEEE Int. Conf. Intelligent Robots and Systems*

Nakamura Y, Shimoda S and Shoji S 2000 Mobility of a microgravity rover using internal electro-magnetic levitation *Proc. 2000 IEEE/RJS Int. Conf. Intelligent Robots and Systems*

Okubo H, Nakano E and Handa M 1996 Design of a jumping machine using self-energizing spring *Proc. Iros 96. IEEE*

Paskins K E 2007 The mechanics and energy economy of animal jumping and landing applied to autonomous robots (Department of Mechanical Engineering, University of Bath)

Paskins K E, Bowyer A, Megill W M and Scheibe J S 2007 Takeoff and landing forces and the evolution of controlled gliding in northern flying squirrels (*Glaucomys Sabrinus*) *J. Exp. Biol.* **210** 1413–23

Paul C, Dravid R and Iida F 2002 Design and control of a pendulum driven hopping robot *IEEE/RSJ Int. Conf. Intelligent Robots and Systems (Lausanne, Switzerland)*

Quinn R D, Offi J T, Kingsley D A and Ritzmann R E 2002 Improved mobility through abstracted biological principles *IEEE/RSJ Int. Conf. Intelligent Robots and System (Lausanne, Switzerland)*

Raibert M H 1986 Legged robots *Commun. ACM* **29** 499–514

Rothschild M, Schlein J, Parker K, Neville C and Sternberg S 1975 The jumping mechanism of Xenopsylla cheopis *Phil. Trans. Roy. Soc.* B **271** 457–520

Shimoda S, Kubota T and Nakatani I 2002 New mobility system based on elastic energy under microgravity *Proc. Int. Symp. on Exp. Robotics (Washington, DC)*

Stoeter S A, Rybski P E, Gini M and Papanikolopoulos N 2002 Autonomous stair-hopping with scout robots *Proc. IEEE Int. Conf. Intelligent Robots And Systems (Lausanne, Switzerland)*

Sugiyama Y and Hirai S 2004 Crawling and jumping by a deformable robot *Proc. Int. Symp. on Experimental Robotics (Singapore)*

Vanezis A and Lees A 2005 A biomechanical analysis of good and poor performers of the vertical jump *Ergonomics* **48** 1594–603

Wei T, Nelson G M, Quinn R D, Verma H and Garverick S 2000 A 5 cm autonomous hopping robot *IEEE Conf. on Robotics and Automation (Icra '00) (San Francisco, CA)*

Weiss P 2001 Hop . . . Hop . . . Hopbots!: designers of small, mobile robots take cues from grasshoppers and frogs *Sci. News* **159** 88

Yoshimitsu T, Kubota T, Nakatani I, Adachi T and Saito H 2003 Micro-hopping robot for asteroid exploration *Acta Astronaut.* 441–6